THE RELATIONSHIP OF IRON AND AMYLOID: INSIGHTS FROM A NEW MOUSE MODEL OF IRON LOADING AND AMYLOIDOSIS

Ritambhara Aryal

B.Sc. Biotechnology

THESIS SUBMITTED FOR THE DEGREE OF

DOCTOR OF PHILOSOPHY

MARCH 2019

FACULTY OF HEALTH

UNIVERSITY OF NEWCASTLE

This research was supported by an Australian Government Research Training Program (RTP) Scholarship

Statement of originality

I hereby certify that the work embodied in the thesis is my own work, conducted under normal supervision. The thesis contains no material which has been accepted, or is being examined, for the award of any other degree or diploma in any university or other tertiary institution and, to the best of my knowledge and belief, contains no material previously published or written by another person, except where due reference has been made. I give consent to the final version of my thesis being made available worldwide when deposited in the University's Digital Repository, subject to the provisions of the Copyright Act 1968 and any approved embargo.

Ritambhara Aryal

Acknowledgements

It is hard to believe that the four-year long roller coaster ride with my thesis has finally come to a beautiful end. Words are not enough to thank everyone who has supported my PhD journey, all this time. Firstly, I would like to express a humble gratitude to my principal supervisor, Prof. Liz Milward. The collaboration that started off with some snorkelling lessons has now resulted into the successful completion of this research project. Needless to say, Liz's supervision has been remarkable not only for my PhD project but also for my professional and personal development.

I am thankful for the financial assistantship that I received through the Australian Government Research Training Program Scholarship. I would also like to give thanks to my co-supervisor Dr Dan Johnstone, who was always willing to provide valuable suggestions regarding my project and also helped me with my lab work at University of Sydney. I am thankful to the staff of the research support unit and teaching support unit (School of Biomedical Sciences), Dr Karen Mate and Dr Sivaraman Purushothuman for their support during my PhD.

I will always cherish the brilliant camaraderie that I developed with my labmates Kristy, Jason, Seak, Will, Sam, Elvis, Moones and Ali. They have made me realise the power of teamwork in the accomplishment of our individual research goals and in the collective upliftment of our careers.

Lastly, I dedicate this thesis to my family, which means the world to me. My earnest gratitude to Ashim, who has been my pillar of strength and my motivator at times when I am filled with self-doubt and apathy. My parents (Aama and Bauji) have constantly taught me to do best in all of my endeavours and I am really grateful to them for believing in my ability, more than I do myself. I am sure that Supu, my little one will be super proud of this accomplishment, just as she has always been even in my tiniest of achievements. Lastly, I am thankful to my extended family members (Mamu, Buwa, Agya didi and Suraj bhinaju) who have always inspired me with their kind and encouraging words not to give up on my goal that I had set four years ago.

"It always seems impossible until it's done."

- Nelson Mandela

Table of Contents

LIST OF TABLES

LIST OF FIGURES

LIST OF ABBREVIATIONS

AAS	Atomic absorption spectroscopy
Aβ	Amyloid-β
AD	Alzheimer's disease
AICD	APP intracellular domain
ANOVA	Analysis of variance
APLP1	Amyloid-precursor-like protein-1
APLP2	Amyloid-precursor-like protein-2
APOE	Apolipoprotein E
APP	Amyloid precursor protein
ATP	Adenosine triphosphate
BACE1	β-site APP-cleaving enzyme 1
BBB	Blood brain barrier
CI	Confidence interval
CNS	Central nervous system
CP	Ceruloplasmin
CR	Congo red
CRISPR	Clustered Regularly Interspaced Short Palindromic Repeats
CSF	Cerebrospinal fluid
DAB	3, 3'-diaminobenzidine
Dcytb	Duodenal cytochrome b
ddH_2O	Deionised, distilled water
DMT1	Divalent metal transporter 1
DNA	Deoxyribonucleic acid
DPX	Di-n-butylphthalate in xylene
ELISA	Enzyme-linked immunosorbent assay

EOAD	Early onset Alzheimer's disease
ES	Embryonic stem
FAD	Familial Alzheimer's disease
Fe2+	Ferrous iron
Fe3+	Ferric iron
Fpn	Ferroportin
FTIR	Fluorescence
GFAP	Glial fibrillary acidic protein
GPI	Glycophosphatidylinositol
h	Hours
HAMP	Hepcidin gene
HCP1	Haem carrier protein 1
HEK293T	Human embryonic kidney 293
Heph	Hephaestin
Hfe KO	*Hfe* knockout mice
H-ferritin	Ferritin heavy chain
HH	Hereditary haemochromatosis
HJV	Hemojuvelin
HO	Haem oxygenase
H_2O_2	Hydrogen peroxide
HRP	IgG-horseradish peroxidise
IHC	Immunohistochemistry
IRE	Iron responsive element
IRP	Iron regulatory protein
KO	Knockout

L-ferritin	Ferritin light chain
LIP	Labile iron pool
LOAD	Late onset Alzheimer's disease
MAPT	Microtubule-associated protein tau
min	Minutes
MRI	Magnetic resonance imaging
mRNA	Messenger RNA
MRI	Magnetic resonance imaging
N	Experimental sample size
NFTs	Neurofibrillary tangles
nm	Nanometer
NS	Not significant
NTBI	Non-transferrin-bound iron
OCT	Optimal cutting temperature
OD	Optical density
PBS	Phosphate buffered saline
PBS-T	Phosphate buffered saline-Tween
PHFs	Paired helical filaments
PS/PSEN	Presenilin
PS1	Presenilin 1
PS2	Presenilin 2
p-tau	Phospho-tau
RNA	Ribonucleic acid
RNAi	RNA interference
ROS	Reactive oxygen species
rpm	Revolutions per minute

RT	Room temperature
s	Seconds
SEM	Standard error of the mean
sAPPα	Soluble APPα
STEAP	Six transmembrane epithelial antigen of the prostrate
TBI	Transferrin-bound iron
Tf	Transferrin
TFR	Transferrin receptor
TFR1	Transferrin receptor 1
TFR2	Transferrin receptor 2
Tfr2mut	*Tfr2* mutant
TUNEL	Terminal deoxynucleotidyl transferase dUTP nick end labelling
TX-100	Triton X-100
UTR	Untranslated region
WT	Wildtype control mice

Abstract

Alzheimer's disease (AD) is a neurodegenerative disease which has been proposed to be associated with brain iron abnormalities, although this remains contentious. To investigate the broad hypothesis that increased brain iron levels may exacerbate Alzheimer's amyloid pathology, this project studied a novel mouse model (the 'Aβ+Iron model'). This model was developed by cross-breeding the APPswe/PS1ΔE9 mouse model of amyloidosis (the 'Aβ model') with the *Hfe*$^{-/-}$*xTfr2*^{mut} mouse model of the iron loading disorder haemochromatosis (the 'Iron model') and backcrossing onto the AKR background strain to maximize iron loading.

Brain iron content by non-haem iron assay of homogenised brain hemispheres at 6 months of age showed substantial iron loading in Aβ+Iron mice compared to age-, gender- and strain-matched Aβ mice (fold change ≥ 1.8, p<0.0001, n ≥11 mice/group, with ≥4 per sex in each group). Likewise the relative intensity of 3,3'-diaminobenzidine-4HCl (DAB)-enhanced Perls' staining for iron was significantly increased in Aβ+Iron mice compared to Aβ mice (fold change 1.7, p<0.0001, n=4 mice/group).

Since the Iron model does not express human Aβ, it would not be generally predicted to have classical amyloid. This model was used to assess whether abnormal mouse Aβ deposition could be induced by the presence of increased brain iron levels even though this model does not contain any human Aβ sequence. As expected, classical amyloid with Congo red birefringence under polarised light was not observed in the Iron model. These mice produce only endogenous murine Aβ which is not likely to aggregate and form plaques (i.e model does not express human Aβ), suggesting increased brain iron levels alone are not sufficient to induce amyloid formation in the absence of amyloid-related mutations. Histological labelling with Congo red stain for amyloid alone or in combination with DAB-enhanced Perls' stain for iron was used to examine whether increased brain iron levels altered amyloid deposits in the Aβ and Aβ+Iron transgenic models. No differences were observed for mean counts and size distribution of amyloid deposits, amyloid burden or amyloid density across matched Bregma (-2.46 to -3.16) in Aβ+Iron compared to Aβ mice (all p>0.05, n=4 mice/group). This Bregma range includes hippocampal and entorhinal cortex regions strongly affected in AD.

An increased proportion of amyloid plaques had observable iron labelling in the Aβ+Iron model, in which 99.25% of detected plaques co-localised with DAB-enhanced Perls' stainable iron compared to 81.09% in the Aβ model (p=0.0016, n=4 mice/group). Likewise, iron labelling around plaques was stronger in the Aβ+Iron model than the Aβ model, based on the ImageJ Transformed Mean Gray Value, a measure of staining intensity, of the iron halos surrounding the Congo red plaque

cores (fold change 1.4, p=0.0456, n=4 mice/group). However there was no difference in the mean area of the halos surrounding plaques between the two models (p=0.1007, n=4 mice/group).

Co-labelling was also performed for iron (DAB-enhanced Perls' stain) and Aβ peptide using antibody 4G8. This antibody, in addition to classical Aβ amyloid that is birefringent under polarised light, also detects other forms of insoluble Aβ peptide deposits. Antibody 4G8 and iron generally co-localised closely, with detectable iron usually though not always restricted to the 4G8 immunolabelled region.

In general, there were more amyloid plaques in brain areas with less iron staining compared to areas with high iron staining (correlation coefficient -0.97). For example, few if any amyloid plaques were detected in basal ganglia and thalamus with strong iron staining compared to regions such as the hippocampus and entorhinal cortex.

Overall, regional and cellular distributions of iron in the Aβ+Iron model were similar to those in the Iron model with the important exceptions that iron co-localised with amyloid plaques in the Aβ+Iron model and iron-laden cells were present in the immediate vicinity of plaques. Iron staining was most conspicuous in the choroid plexus by all methods used (DAB-enhanced Perls' stain and traditional or perfusion Turnbull stain for ferrous iron). Neurons contained very little stainable iron in any region examined, including hippocampus, cerebral cortex and midbrain. Co-labelling with DAB-enhanced Perls' stain and Luxol fast blue stain or a myelin-specific marker 2', 3'-cyclic-nucleotide 3'-phosphodiesterase (CNPase) revealed substantial amounts of iron in myelinated regions. Ferritin heavy and light chain immunolabelling co-localised with DAB-enhanced Perls' stain in a subset of myelin-associated cells with the morphology of oligodendroglial 'trains', consistent with previous literature demonstrating iron in a subset of oligodendroglia in rodents and humans.

Brain regions with numerous glial fibrillary acidic protein (GFAP) labelled astrocytes typically had few iron-laden cells, with few if any cells co-labelled for both GFAP and iron. Likewise regions with increased iron accumulation typically contained few astrocytes, suggesting there was little reactive astrogliosis in areas with increased iron accumulation, and little if any reactive astrogliosis was observed around amyloid plaques.

The proportion of plaques surrounded by iron-laden cells resembling activated amoeboid microglia or microglia transitioning into activation states was much greater in the Aβ+Iron model compared to the Aβ model (22% as opposed to 77%), suggesting iron may exacerbate microgliosis in response

to Aβ. This is potentially important since microglial activation appears to facilitate clearance of amyloid, although excessive accumulation of iron could eventually wind up damaging or killing microglia and weakening the brain's defensive responses.

Additional studies are required to investigate these possibilities since few if any cells co-labelled for both iron and the ionized calcium-binding adapter molecule 1 (Iba1), a marker for microglia and while Iba1 positive microglia were present in the immediate vicinity of iron-amyloid complexes, these did not co-label for iron, although reduced sensitivity of double and triple labelling procedures cannot be ruled out. There was no difference in the average count of Iba1-positive microglia in the vicinity of plaques between the Aβ+Iron and Aβ models (p=0.4073, n=4 mice/group).

There was limited preliminary evidence of oxidative damage in the Aβ+Iron model. While no labelling was detected in any model for 8-hydroxy-2'-deoxyguanosine (8-OHdG), which detects DNA oxidation damage, there was some putative positive but very weak immunolabelling in all models for lipid peroxidation damage as assessed by 4-hydroxynonenal (4-HNE) antibody that appeared slightly stronger in the Aβ+Iron and Aβ models but this also needs to be confirmed in further studies.

Increased levels of iron did not seem to increase neuronal loss in preliminary studies with neuronal nuclear (NeuN) antibody labelling. Specifically there was no significant decrease in relative neuronal counts per unit area at matched Bregma in the Aβ+Iron model compared to the Aβ model in the full cerebral hemisphere, excluding the cerebellum (p=0.3331, n=4 mice/group, one-tailed t test).

In summary, these results confirm that brain iron levels are increased in the Aβ+Iron model at 6 months of age and that iron co-localises with amyloid in this model but does not appear to affect measures of amyloid load. Although there was some preliminary evidence of lipid peroxidation damage and increased levels of ferrous iron in a few areas with high levels of iron by DAB-enhanced Perls' staining, amyloid formation was usually not observed in these regions and no neuronal death was observed across the cerebral hemisphere.

Several protective mechanisms may be involved. Most iron appears to remain sequestered within myelin, oligodendroglia or other unidentified glia, with neurons containing little if any Perls' stainable iron. Cells morphologically resembling transitional or activated amoeboid microglia appear to take up iron in the vicinity of amyloid plaques and may also have protective roles but these were not confirmed to be microglia by Iba1 labelling and remain unidentified.

This study has provided new insights into the nature of the relationship of iron and AD. The findings suggest that surplus iron may be safely sequestered by normal brain iron homeostatic and storage mechanisms and may not appreciably influence Alzheimer's disease pathogenesis at least in the earlier stages of the disease course corresponding to the period examined in the present study. In the light of these observations, the low levels of neuronal iron and the possibility that at least initially, iron may be important in increasing activation of microglia around plaques, facilitating amyloid clearance, iron chelation may be potentially deleterious, at least in the early stages of disease and extreme caution should be exercised before pursuing clinical trials or recommending iron chelation as a treatment for AD and other neurodegenerative conditions.

1. General Introduction

1.1 General introduction

Dementia is the term given to a group of conditions in which there is significant impairment in memory and one or more other cognitive domains that hamper an individual's capability to carry out daily activities. Alzheimer's disease (AD), a progressive neurodegenerative disease described in more detail below, is the most common cause of dementia, contributing to an estimated sixty to eighty percent of cases (Dementia Australia, 2017). In 2018, 436,366 Australians were estimated to have AD or a related dementia with this figure projected to reach 1,076,129 by 2058 (Dementia Australia, 2018). At least $9.1 billion annual direct cost was estimated for dementia care in Australia for the year 2017 and this figure is expected to continue to rise with the ageing population (Brown et al., 2017a; Dementia Australia, 2017). With 250 new cases each day, the annual societal and economic cost due to dementia in Australia is projected to be $15 billion in 2018 and it is expected to exceed $18.7 billion by 2025 (Brown et al., 2017b).

Alzheimer's disease is characterised initially by difficulty in remembering recent events or conversations, with one or more other cognitive problems which may include impaired communication, diminished decision making capability and difficulty in walking (LaFerla and Oddo, 2005; López and DeKosky, 2008; Youn et al., 2011). Impairment in swallowing reflexes can lead to dysphagia and aspiration pneumonia in the late stage, a frequent cause of death among AD patients (Beard et al., 1996; Burns et al., 1990; Easterling and Robbins, 2008).

1.2 Types of Alzheimer's disease

Based on the age of onset, Alzheimer's disease is broadly classified into two categories. They are described as follows.

1.2.1 Early Onset Alzheimer's disease (EOAD)

Age of onset of Early Onset Alzheimer's disease (EOAD) is usually before 65 years and accounts for ~10% of cases. These early forms of AD, which are typically more severe, usually exhibit a Mendelian pattern of inheritance and often run in families, hence termed Familial Alzheimer's disease (FAD) (Campion et al., 1999; Williamson et al., 2009). EOAD is caused by mutations in genes located on chromosomes 21, 14, or 1 resulting in abnormal formation of the proteins amyloid precursor protein (APP) (Goate et al., 1991; St George-Hyslop et al., 1987), presenilin 1 (PS1)

(Berezovska et al., 2005; Bruni, 1997) or presenilin 2 (PS2) (Cruts et al., 1998; Levy-Lahad et al., 1995), respectively and hence favouring the production of amyloidogenic Aβ42 peptides.

1.2.2 Late Onset Alzheimer's disease (LOAD)

Late Onset Alzheimer's disease (LOAD) accounts for ~90% of AD cases, with age of onset at 65 or older (Bertram and Tanzi, 2004; Pinkston, 1999). While LOAD often shows no clear familial inheritance pattern, the apolipoprotein E (APOE) gene, found on chromosome 19, is a significant genetic risk factor for developing LOAD and research is underway to gain more insight into the genetic basis of LOAD (Corder et al., 1993; Pericak-Vance et al., 1991). The APOE protein, which has three major forms, namely APOE epsilon 2(APOEε2), APOE ε3 and APOE ε4, carries cholesterol in bloodstream and supports transport of lipid and injury repair in the brain (Ghebranious et al., 2005; Hixson and Vernier, 1990; Liu et al., 2013).

APOE has also been reported to control transport, metabolism, deposition as well as clearance of a peptide called beta-amyloid, as described in Section 1.4.1 (Kanekiyo et al., 2014; Poirier, 2000; Verghese et al., 2013). Of these different isoforms, APOE ε4 is present in the majority of people with the LOAD; hence people with this allele are believed to have an increased risk of AD relative to people with any other allele (Corder et al., 1993; Farrer et al., 1997; Sadigh-Eteghad et al., 2012; Saunders et al., 1993).

1.3 Stages of AD

In the preclinical stage of AD, biomarker abnormalities in the brain, the cerebrospinal fluid (CSF) or blood have been described without clinical symptoms such as memory loss (Alzheimer's Association, 2013). In particular, amyloid plaques and neurofibrillary tangles (NFTs), two main pathological hallmarks of AD as will be described below, develop first in the entorhinal cortex & then start appearing in the hippocampus and the temporal lobe where neurons start degenerating (Braak and Braak, 1991; Braak et al., 2006).

Preclinical AD is followed by mild cognitive impairment (MCI). People with MCI have mild but measurable changes in thinking abilities and short term memory but this does not hamper the person's ability to carry out everyday activities (Albert et al., 2011; Alzheimer's Association, 2013).

Amyloid plaques and NFTs continue accumulating in temporal and limbic regions and start to aggregate in the neocortical regions (Braak and Braak, 1991).

In most of the cases, the clinical stage, also referred to as dementia due to AD, is characterized by memory, cognitive and behavioural symptoms that hamper an individual's ability to function in daily life (Alzheimer's Association, 2013). Plaques and tangles have occupied most of the limbic and neocortical regions, which is followed by synaptic loss & neurodegeneration (Braak and Braak, 1991; McKhann et al., 2011). However, few studies have also reported that aged individuals with plaques and tangles associated with AD fail to show significant cognitive impairment (Arnold et al., 2013; Davis et al., 1999; Zeineh et al., 2015).

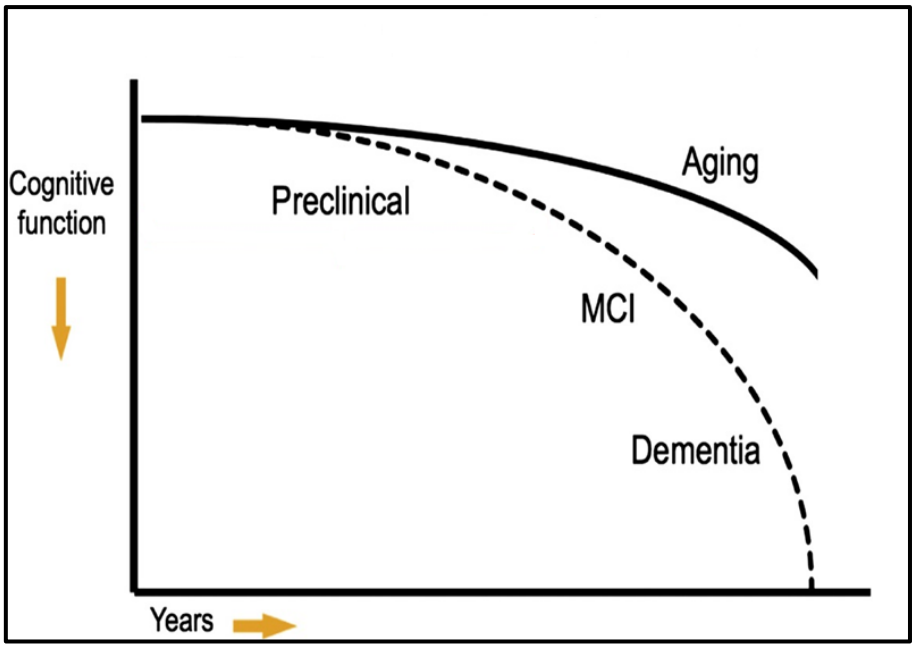

Fig. 1.1 Different stages of Alzheimer's disease (AD). AD progresses in three stages namely preclinical AD, Mild Cognitive Impairment (MCI) and dementia due to AD. Loss of cognitive function is sometimes associated with aging but is prominent as AD progresses through these three stages. Figure adapted and modified by R Aryal from (Sperling et al., 2011).

1.4 Alzheimer's disease neuropathology

Amyloid plaques and neurofibrillary tangles (NFTs) are two important hallmarks of AD. Besides these, synaptic loss (Hamos et al., 1989a; Terry et al., 1991a) and other neuronal damage or death (Good et al., 1996; Lassmann et al., 1995) are also observed in AD patients.

1.4.1 Amyloid plaques and the amyloid precursor protein (APP)

The amyloid plaques are extracellular aggregates chiefly comprised of beta amyloid (Aβ), a peptide formed by cleavage of a larger precursor molecule called the amyloid precursor protein (APP), described below in Section 1.4.1.1 (Glenner and Wong, 1984a; Glenner and Wong, 1984b; Masters et al., 1985; Soriano et al., 2001). These soluble peptides are released physiologically in healthy brains but accumulate to form less soluble species, including highly insoluble 'amyloid plaques' in AD (Masters et al., 1985; Puzzo and Arancio, 2013).

The APP molecule is a type 1 transmembrane protein consisting of 695–770 amino acids and is encoded by the *APP* gene, with three main protein isoforms generated by alternative splicing: APP695, APP751 and APP770 (Belyaev et al., 2010; Kitazume et al., 2012; LaFerla et al., 2007; Ponte et al., 1988; Tanzi et al., 1988). Amyloid-precursor-like protein-1 and -2 (APLP1 and APLP2), the mammalian type-1 integral transmembrane proteins found in many tissues, are also members of the APP gene family (Wasco et al., 1992; Wasco et al., 1993; Yang et al., 1996; Zhong et al., 1996).

APLP1 and APLP2 proteins have similar amino acid sequence and conserved possibly functional domains but lack the beta amyloid (Aβ) region. The homologs are present in human, mice, Drosophila and *C. elegans*. Along with APP, the homologs are highly expressed in brain (Zheng et al., 1995). Though the primary function of APP is still unclear, it is believed to regulate synapse formation, neural plasticity, neural protein trafficking and related functions (Chen and Yankner, 1991; Priller et al., 2006; Seabrook et al., 1999; Turner et al., 2003; Zheng and Koo, 2006). Recently, as discussed below, it was proposed to be a ferroxidase important in iron homeostasis (Duce et al., 2010), however this has now been refuted (Ebrahimi et al., 2013a; Ebrahimi et al., 2012).

1.4.1.1 Pathways of APP-processing

There are two pathways of APP processing which have been widely accepted in the past, the non-amyloidogenic pathway and the amyloidogenic pathway. These pathways will be described in more detail below together with some of the questions that still remain about APP processing.

1.4.1.1.1 Non-amyloidogenic pathway

As shown below (Fig. .2), one pathway by which most APP processing occurs is by cleavage within the Aβ peptide domain, thus precluding Aβ formation and aggregation. The first enzyme involved is the membrane-associated metalloprotease alpha (α)-secretase, producing the large soluble extracellular N-terminal portion of APP and an 83-residue long C-terminal fragment (C83) (Hooper and Turner, 2002; Roberts et al., 1994). Three enzymes belonging to the family of a disintegrin and metalloprotease (ADAM) are known to possess alpha secretase activity: ADAM9, ADAM10 and ADAM17 (Asai et al., 2003; LaFerla et al., 2007; Lammich et al., 1999). The C83 fragment undergoes further processing by a second enzyme called gamma (γ)-secretase, generating the APP intracellular domain (AICD) and the non-amyloidogenic P3 peptide (Kojro and Fahrenholz, 2005; Lannfelt et al., 1995; Roberts et al., 1994; Sisodia, 1992).

1.4.1.1.2 Amyloidogenic pathway

APP molecules which do not undergo non-amyloidogenic processing get cleaved by Beta (β)-secretase or BACE1 (β-site APP-cleaving enzyme 1) at the N-terminal region of the Aβ domain, releasing a soluble N-terminus and an amyloidogenic C-terminal peptide (C99) (Sinha et al., 1999; Vassar et al., 1999; Yan et al., 1999; Zhang et al., 2011). The presenilin 1 (PS1) transmembrane protein, which is genetically associated with AD, combines presenilin enhancer 2, nicastrin and anterior pharynx-defective 1 to form a catalytic gamma (γ)-secretase protease enzyme complex. This cleaves the C99 peptide to liberate the AICD and the Aβ peptide (Fraser et al., 2000; Selkoe et al., 1996; Selkoe, 2001). The Aβ peptide can have from 39 to 43 amino acid residues, with 40 or 42 residues most common in AD, the latter being most amyloidogenic (Citron et al., 1996; Klafki et al., 1996; Portelius et al., 2011; Zhao et al., 2007).

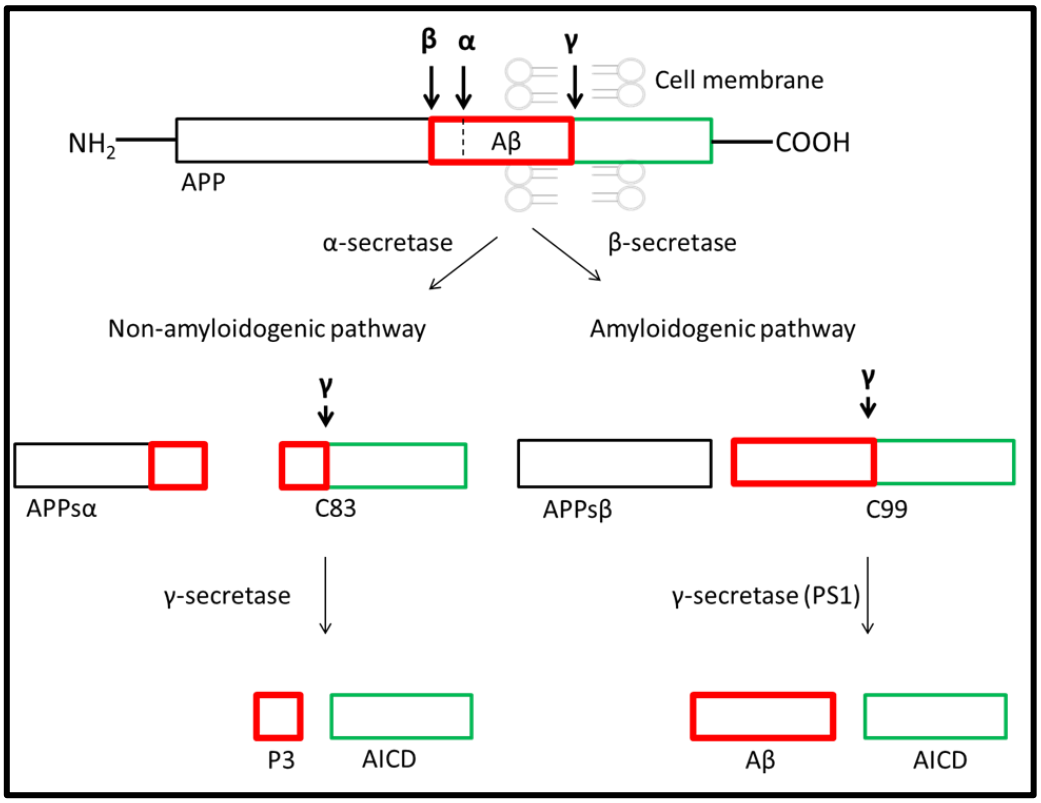

Fig. 1.2 Pathways of APP processing. In the non-amyloidogenic pathway, α-secretase cleaves inside the Aβ domain, producing N-terminal APPsα and C-terminal C83 fragments. The γ-secretase complex, containing Presinilin 1, generates the APP intracellular domain and P3 peptide from C83. In the amyloidogenic pathway, APP is processed by β-secretase at the N-terminus of Aβ, releasing N-terminal APPsβ and C-terminal C99 fragments. The γ-secretase complex cleaves C99, liberating the AICD and Aβ peptide. Figure reproduced and modified by R Aryal from (LaFerla et al., 2007; LaFerla and Oddo, 2005).

However it is now recognised that in fact these pathways have been oversimplified as more recent publications have reported that the processing of Aβ involves multiple different structures with complex biochemistry and cell biology (Cai et al., 2001; Castro et al., 2019; Roher et al., 2017).

The Aβ peptide, which initially exists as a random coil monomer, is reported to misfold into an intermediate state after which it may undergo either of these pathways: one that results into formation of insoluble fibrils and the other that doesn't (DaSilva et al., 2010; Wetzel, 2006). In the former pathway, also known as fibrillar pathway or 'on-pathway', the misfolded monomeric intermediate forms an unstable β-sheet intermediate (Granzotto and Zatta, 2012; Yang and Teplow, 2008). Further aggregation of monomer units generates Aβ oligomers and subsequently protofibrils. Until now, all of the transitional states are soluble but when the protofibrils aggregate further, they generate mature fibrils that are chief insoluble components of amyloid plaques (DaSilva et al., 2010; Granzotto and Zatta, 2012; Koh and Lee, 2006; Petkova et al., 2002; Tjernberg et al., 1999;

Wong et al., 1997). In the non-fibrillar pathway or 'off-pathway', the accumulation of monomeric misfolded intermediates forms soluble oligomers that cannot assemble further and hence do not form mature fibrils (DaSilva et al., 2010; Wetzel, 2006).

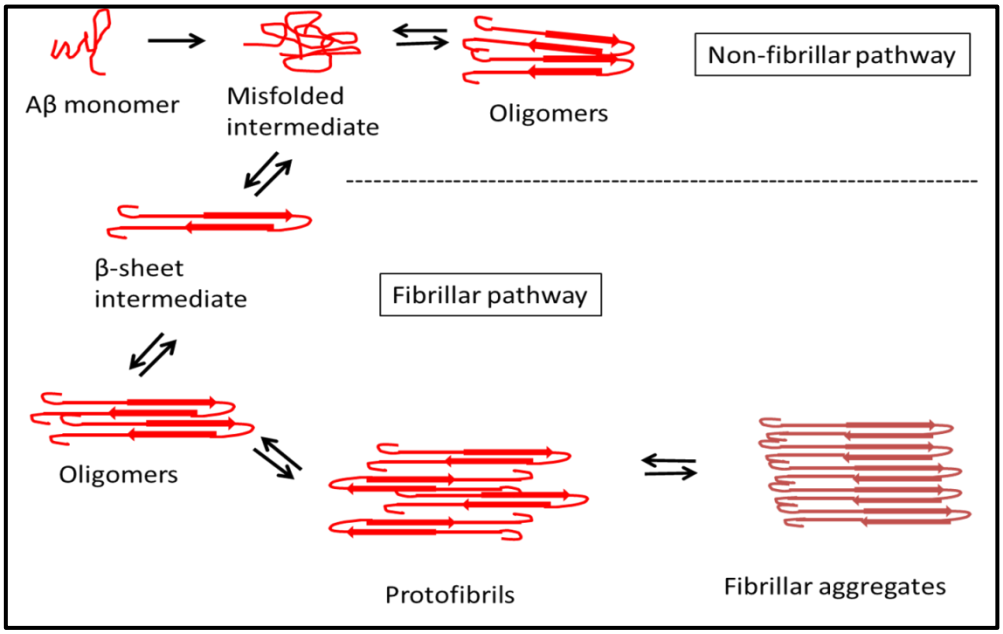

Fig. 1.3 Formation of amyloid fibrils from Aβ peptides. Misfolding of native monomeric Aβ peptides generates an intermediate state which undergoes conformational changes from β-pleated sheet to oligomers to protofibrils and finally to mature fibrils that deposit as amyloid plaques (fibrillar pathway). Alternatively, the misfolded intermediate may produce oligomers that do not have capacity to accumulate and hence cannot form fibrillar aggregates (non-fibrillar pathway). Red: soluble states; brown: insoluble state. Figure adapted and modified by R Aryal based on the mechanism discussed in (DaSilva et al., 2010; Wetzel, 2006).

As reviewed elsewhere, the brain has different mechanisms to clear Aβ: transvascular clearance across the blood-brain barrier, bulk flow via the interstitial fluid (ISF), traditional perivascular clearance, glymphatic paravascular clearance, cerebrospinal fluid (CSF) absorption and enzymatic degradation. Among these, most Aβ is cleared across the BBB (Kanekiyo and Bu, 2014; Ramanathan et al., 2015). Recent theories support the notion that the disturbance in the process of Aβ clearance rather than the overproduction of Aβ is a possible cause of the majority of LOAD (Kanekiyo and Bu, 2014; Mawuenyega et al., 2010).

1.4.2 Tau and Neurofibrillary Tangles (NFTs)

The microtubule-associated protein tau, from the *MAPT* gene (chromosome 17), has six human brain isoforms, generated by alternative splicing of exons 2, 3 or 10 (Goedert et al., 1989; Lee et al., 1988). In healthy individuals, soluble, phosphorylated tau protein binds tubulin (Correas et al., 1992; Goedert et al., 1997), promoting microtubule assembly and axon stabilization (Cleveland et al., 1977; Goedert and Jakes, 1990; Weingarten et al., 1975). In AD, tau has altered solubility, is abnormally phosphorylated (hyperphosphorylated), has reduced affinity for microtubules and accumulates as paired helical filaments (Bramblett et al., 1993; Grundke-Iqbal et al., 1986a; Grundke-Iqbal et al., 1986b; Liu et al., 2002; Morishima-Kawashima et al., 1995). These aggregate into masses called neurofibrillary tangles (NFTs) in the neuronal soma, leading to axonal dystrophy and impeding the trafficking of molecules such as neurotransmitters, and may eventually cause cell death (Goedert et al., 2006; Stokin et al., 2005).

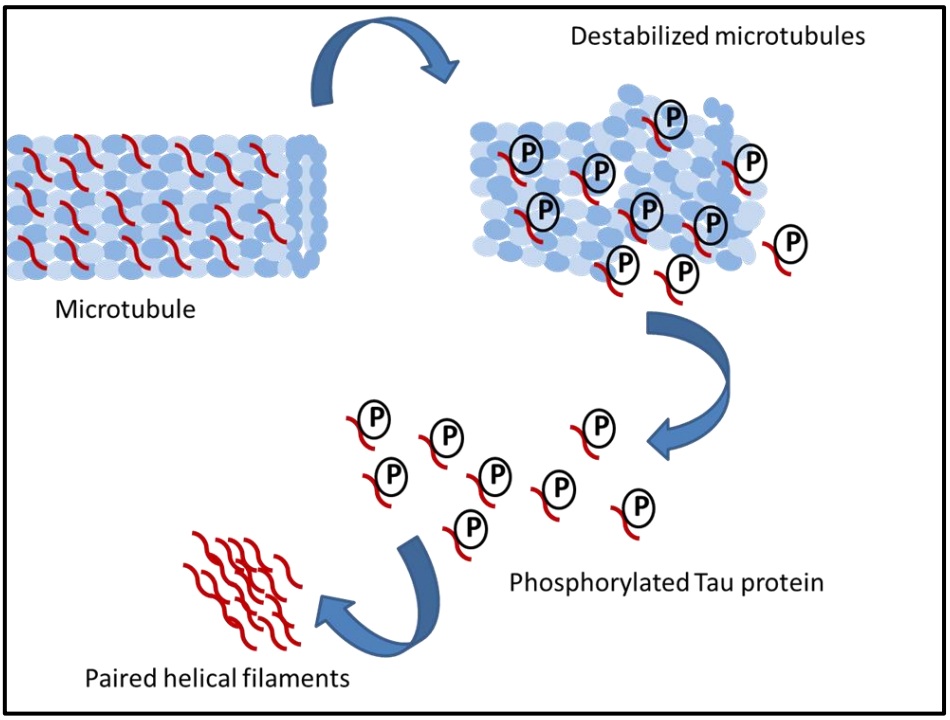

Fig. 1.4 Hyperphosphorylation of tau destabilizes microtubules. Tau normally stabilises microtubule but if hyperphosphorylated by different kinases, can give rise to paired helical filaments (PHFs) that accumulate in the neurofibrillary tangles. Figure reproduced and modified by R Aryal from (Paula et al., 2009).

Additionally, various studies have reported that cognitive impairment in AD is typically accompanied by damage or loss related to connectome which incorporates synapses and neuronal

processes (Hamos et al., 1989b; Rajendran and Paolicelli, 2018; Tampellini, 2015; Terry et al., 1991b). While some researchers have proposed the fibrillary form of Aβ to contribute to the synaptic abnormalities in AD (Grutzendler et al., 2007; Tsai et al., 2004), others have attributed this to the oligomeric Aβ deposits (Koffie et al., 2009; Pickett et al., 2016). This has led the field to incorporate synaptic dysfunction as well as neuronal loss in the study of AD therapeutics.

1.5 Iron homeostasis

Despite their importance in carrying out normal bodily functions, there has long been an assoication between abnormal levels of various metal ions like copper (Karr et al., 2004; Multhaup et al., 1996; Smith et al., 2006; White et al., 1999), zinc (Abelein et al., 2015; Bush et al., 1994; Dong et al., 2006; Huang et al., 1997; Miller et al., 2010; Religa et al., 2006), iron (Connor et al., 1992a; Connor et al., 1992b; Connor and Menzies, 1995; Everett et al., 2014a; Smith et al., 1997) and aluminium (Crapper et al., 1973; Perl and Brody, 1980; Trapp et al., 1978; Walton, 2006), with the pathogenesis and progression of AD and other neurodegenerative diseases (Adlard and Bush, 2006; Bush, 2003; Cherny et al., 2001; Lovell et al., 1998). This thesis focuses on investigating potential contributions of iron to AD. Iron homeostasis will be briefly reviewed before discussing the possible involvement of iron in AD.

1.5.1 Roles of iron in the body

Iron (symbol: Fe from Latin *Ferrum*) is a vital element present in human body. Not only is iron required for fetal development but it has equal importance after birth and throughout the life of an individual (Crichton et al., 2012; Rao et al., 2003). This is supported by the fact that iron is an essential component of a number of proteins and enzymes such as haemoglobin and myoglobin, which function as oxygen carriers in the erythroid tissue and muscles, respectively (Papanikolaou and Pantopoulos, 2005; Yu et al., 2015). Iron is present in cytochromes A, B and C, which are the haem proteins needed for ATP synthesis and mitochondrial respiration in the Electron Transport Chain (ETC).

Iron is also a part of ribonucleotide reductase, an enzyme that catalyzes formation of deoxyribonucleotides from ribonucleotides in DNA synthesis process (Reedy and Gibney, 2004; Sanvisens et al., 2011). Besides these, iron is a cofactor of 4Fe-4S cluster-containing proteins that are needed for protein synthesis by ribosomes as well as for DNA synthesis. Enzymes involved in inflammatory responses such as cyclooxygenase and lipoxygenase also contain iron (Ali-Rahmani

et al., 2014a; Papanikolaou and Pantopoulos, 2005). 3-hydroxy-3-methylglutaryl-coenzymeA reductase (HMGCoAR), squalene synthase and glucose-6-phosphate dehydrogenase, the key enzymes for biosynthesis of myelin, cholesterol and lipids are other iron-dependent enzymes (Ali-Rahmani et al., 2014b).

There is very little iron in certain brain regions at birth but it increases progressively with aging (Bartzokis et al., 1994; Drayer et al., 1986a; Schenker et al., 1993; Wayne Martin et al., 1998). Most of the iron contained in brain is known to be non-haem iron, with highest levels in regions such as basal ganglia (Hardy et al., 2005; Koeppen, 1995; Rouault, 2013). The brain has a high demand for oxygen, for which iron-containing neuroglobin is needed (Ali-Rahmani et al., 2014a; Drayer et al., 1986b). Examples of iron-dependent enzymes essential for proper brain functioning are tyrosine hydroxylase (synthesizes catecholamines including dopamine), tryptophan hydroxylase (synthesizes serotonin) and monoamine oxidase (involved in dopamine metabolism) (Colette Daubner et al., 1995; Goodwill et al., 1997; Youdim et al., 2004).

In rats, iron has been shown to have a crucial role in the development of dendritic spines in the hippocampus and in hippocampal metabolism as well as in the metabolism of γ-Aminobutyric acid (GABA) (Batra and Seth, 2002; Jorgenson et al., 2003). Furthermore, brain regions related to motor functions (extrapyramidal regions) are reported to have more iron than non-motor-related regions, which is believed to explain why iron imbalance in such regions may result into movement disorders (Allen et al., 2001; Rutledge et al., 1987).

1.5.2 Iron physiology

Most of the dietary iron (0.5 to 2 mg in a healthy adult) is absorbed by duodenal enterocytes. Most of the absorbed iron (around 70%) is used in haemoglobin synthesis while the remaining iron is carried in the bloodstream to various organs where it is either utilised for normal cellular functions or stored for future use. Liver is the main iron storage organ. Iron is also taken up by the bone marrow for production of erythrocytes and by cardiac muscles for production of myoglobin. Iron is transported across the placenta to developing fetus during pregnancy. Iron recycling occurs through phagocytosis of senescent erythrocytes which results into release of iron bound to haemoglobin (Andrews, 2000; Finch, 1994; Fleming and Bacon, 2005; McKie et al., 2001; McKie et al., 2000).

There is no known mechanism for the controlled excretion of iron from the body but it is believed that a significant amount of iron is lost during menstrual bleeding in females, desquamation of

epithelial surfaces and a small amount is lost through sweating, urination, faecal elimination and biliary excretion (Green et al., 1968; Hentze et al., 2010; Miller, 2016; Milstone et al., 2012; Stein et al., 2010).

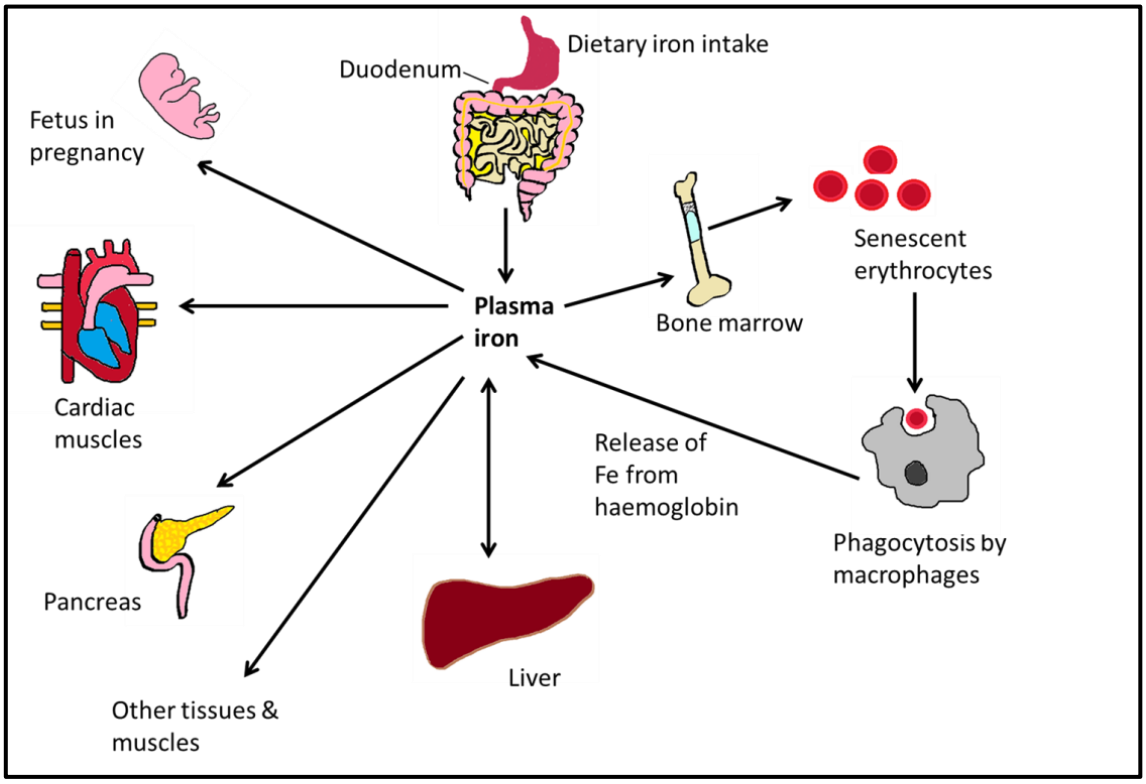

Fig. 1.5 Systemic iron homeostasis. Dietary iron is absorbed by duodenum and transported through bloodstream to liver, bone marrow, muscles, other tissues and to the developing fetus. Phagocytosis of senescent erythrocytes facilitates iron recycling. Figure modified by R Aryal from (Andrews, 2000).

1.5.3 Intestinal iron absorption, intracellular storage and release into circulation

Human diet contains two forms of iron: haem and non-haem iron. Haem iron is formed when iron combines with protoporphyrin IX. It forms about 10% to 15% of total iron of daily western diet (Hurrell and Egli, 2010). Myoglobin and haemoglobin contained in meat products of animals are the main sources of haem iron. It is transported by Haem Carrier Protein-1 (HCP1) from the apical surface of the gut lumen into the duodenal enterocytes. In endosome, haem oxygenase (HO) enzyme then converts haem iron into free iron along with bilirubin and carbon monoxide as by-products (Miret et al., 2003; Raffin et al., 1974).

Non-haem or inorganic iron is derived from plant-based food sources and dairy products. Ferric form of iron is reduced to ferrous form by brushborder ferrireductase duodenal cytochrome b

(Dcytb/ Cybrd1) (Hentze et al., 2010; McKie et al., 2000). This ferrous iron can be transported across apical membrane into enterocyte by Divalent Metal Transporter-1 (DMT1)/ Divalent Cation Transporter-1 (DCT1)/Nramp2. Free iron released from both haem and non-haem sources is stored in iron storage proteins like ferritin (described in more detail further below) and hemosiderin (Gruenheid et al., 1995; Gunshin et al., 1997).

Iron that is not stored in ferritin or hemosiderin in enterocytes is transported out into the circulation by a transporter protein called ferroportin (Donovan et al., 2000; McKie et al., 2000). The ferrous iron thus released is oxidised into ferric form by the enzymes hephaestin or ceruloplasmin and other unknown ferroxidases so that it can be taken up by an iron-binding glycoprotein called transferrin (Tf) for transport in the bloodstream (Aisen et al., 1978; Lee et al., 1968; McCarthy and Kosman, 2015; Osaki et al., 1966; Ranganathan et al., 2012; Vulpe et al., 1999).

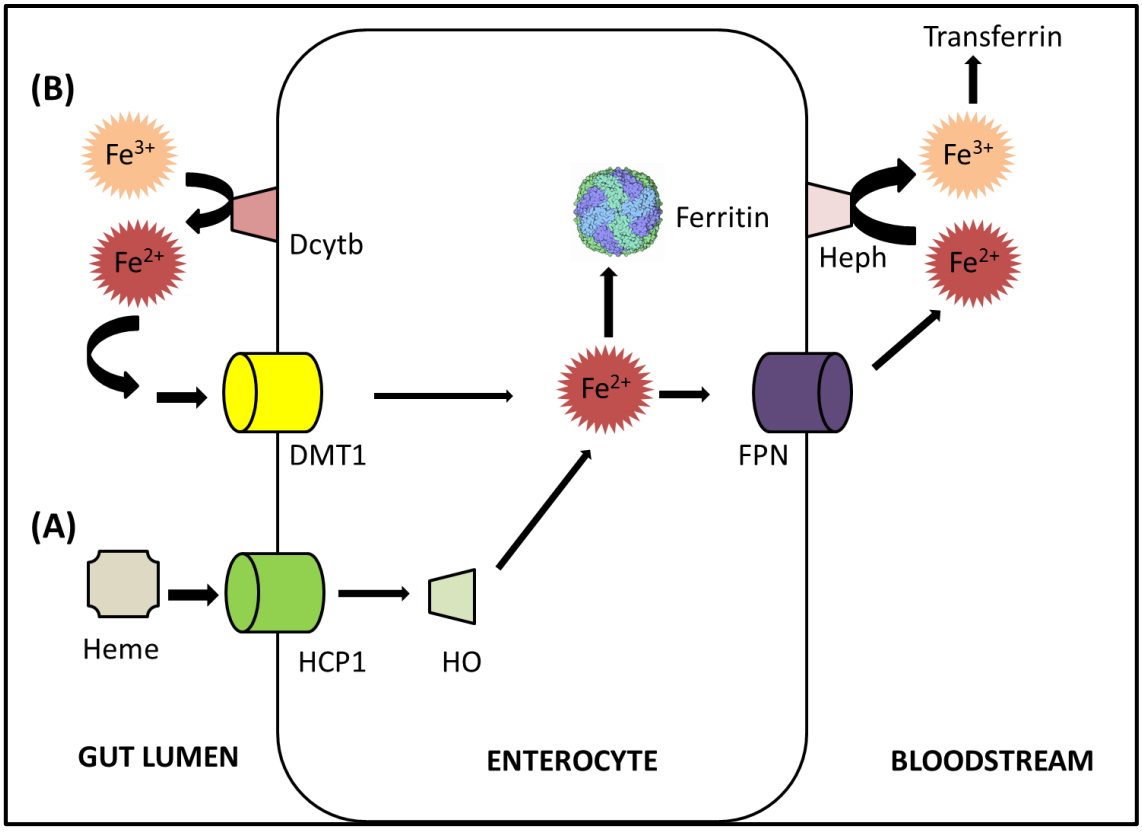

Fig. 1.6 Intestinal iron absorption. Haem and non-haem iron is taken up from gut lumen by the enterocyte. (A) Haem iron is transported by Haem Carrier Protein-1 (HCP1) from the gut lumen into the enterocyte. Haem oxygenase (HO) enzyme then converts haem iron into free iron. (B) Non-haem iron is reduced to ferrous form by duodenal cytochrome b (Dcytb) and transported into enterocyte by Divalent Metal Transporter-1 (DMT1). Intracellular iron is then either stored in ferritin or exported into bloodstream via ferroportin (FPN). Hephaestin (Heph) then oxidises ferrous

iron, which can be taken up by transferrin. Figure produced by R Aryal as reviewed in (Hentze et al., 2010).

1.5.4 Ferritin

The ferrous iron contained in the enterocyte and other cells is stored in soluble, non-toxic and bioavailable form in an iron-storage protein called ferritin, which is found in cytosol, nucleus, mitochondria and lysosomes. Each ferritin molecule contains 24 subunits and can store up to 4500 iron atoms. Iron is stored in the form of hydrous ferric oxide nanoparticle that has similar structure to ferrihydrite, a common mineral found at earth's surface (Chasteen and Harrison, 1999). Its structure consists of an outer shell and inner core. There are two types of subunits of ferritin: heavy chain (H) and light chain (L). H subunit has ferroxidase activity, oxidising ferrous iron to the ferric form, whereas the L subunit is responsible for iron-core nucleation (Boyd et al., 1985; Dörner et al., 1985; Harrison and Arosio, 1996). During conditions of iron overload, iron may also be stored as ferrihydrate structures in hemosiderin, which is a by-product of proteasomal or lysosomal degradation of ferritin (Fischbach et al., 1971; Richter, 1958; Vymazal et al., 2000).

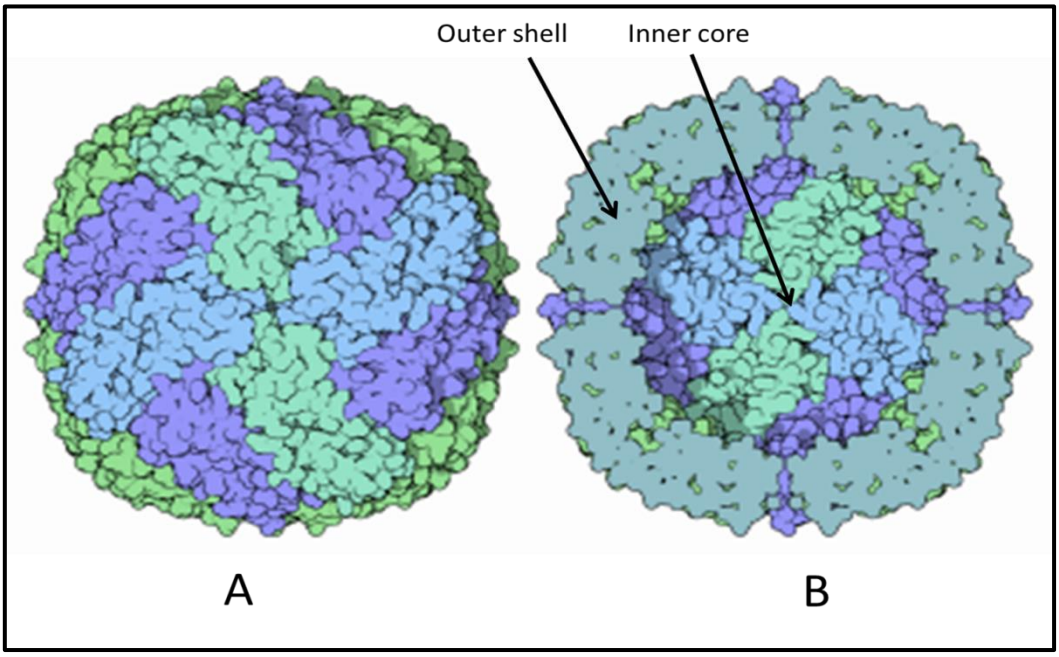

Fig. 1.7 Molecular structure of ferritin. (A) Hollow shell of ferritin contains 24 subunits represented by different colours. (B) Interior cross-section of ferritin shows outer shell and inner core. Figure adapted from Protein Data Bank (http://pdb101.rcsb.org/motm/35).

1.5.5 Cellular uptake, utilisation and release of iron

Iron is carried in the bloodstream by an 80-kDa bilobal glycoprotein transporter called transferrin, which has reversible, high affinity binding capacity for two ferric ions (Fe^{3+}) at neutral pH (~7.2)

(Aisen et al., 1978; Chasteen and Williams, 1981; Lestas, 1976). Two types of receptors on the membrane of cells that utilise iron, namely transferrin receptor 1 and 2 (TFR1, TFR2)[1], import diferric-transferrin (holotransferrin) into cells (Herbison et al., 2009; Kawabata et al., 1999; West et al., 2000). Under normal conditions, TFR1 has increased expression and imports most of the transferrin-bound iron into cells. A small fraction of this iron can also be taken up by TFR2, which is expressed at a lower level than TFR1, but has increased expression during conditions of iron overload (Chua et al., 2010; Fleming et al., 2000; Kawabata et al., 2000; Kawabata et al., 1999).

As shown in Fig. 1.8 below, the holotransferrin-TFR1 complex is imported into cells by a special clathrin-coated pit endocytosis mechanism, leading to formation of endosomes inside the cell (Booth and Wilson, 1981; Pearse, 1982). At lower pH, due to H^+ entry into the endosome, two ferric iron atoms dissociate from transferrin (Klausner et al., 1983; Paterson et al., 1984). These are thought to be reduced to the ferrous form by a metalloreductase such as 'six transmembrane epithelial antigen of the prostrate' (STEAP3) (Lambe et al., 2009; Ohgami et al., 2006) Ferrous iron is transported to the cytosol by divalent metal transporter 1 (DMT1) or another unknown transporter (Fleming et al., 1998) and used in cellular processes (eg. mitochondrial respiration), stored in ferritin or exported from the cell by the iron exporter ferroportin (Abboud and Haile, 2000; McKie and Barlow, 2004). Iron that is not used or stored or exported forms the labile iron pool (LIP), comprising redox-active free iron or other potentially reactive iron species, such as iron complexed with phospholipids or anions (Greenberg and Wintrobe, 1946; Jacobs, 1977; Kakhlon and Cabantchik, 2002). Excess redox-active iron can form reactive oxygen species, described further below, that can damage nucleic acids, lipids and proteins, proposed by some authors to be important in cellular degeneration observed in neurodegenerative disorders such as AD (Bartzokis et al., 1997; Meguro et al., 2008). The transferrin-TFR1 complex is transported back to the plasma membrane where transferrin detaches from its receptor and re-enters the circulation (Dautry-Varsat, 1986; Dautry-Varsat et al., 1983).

[1] [http://www.informatics.jax.org/mgihome/nomen/; as per the 'Guidelines for Human Gene Nomenclature of the HUGO Gene Nomenclature Committee and Guidelines for Nomenclature of Genes, Genetic Markers, Alleles, and Mutations in Mouse and Rat of the International Committee on Standardized Genetic Nomenclature for Mice': gene symbols in this thesis are italicised; protein symbols are non-italicised; human genes and human and mouse proteins are capitalised; mouse genes are in sentence case.

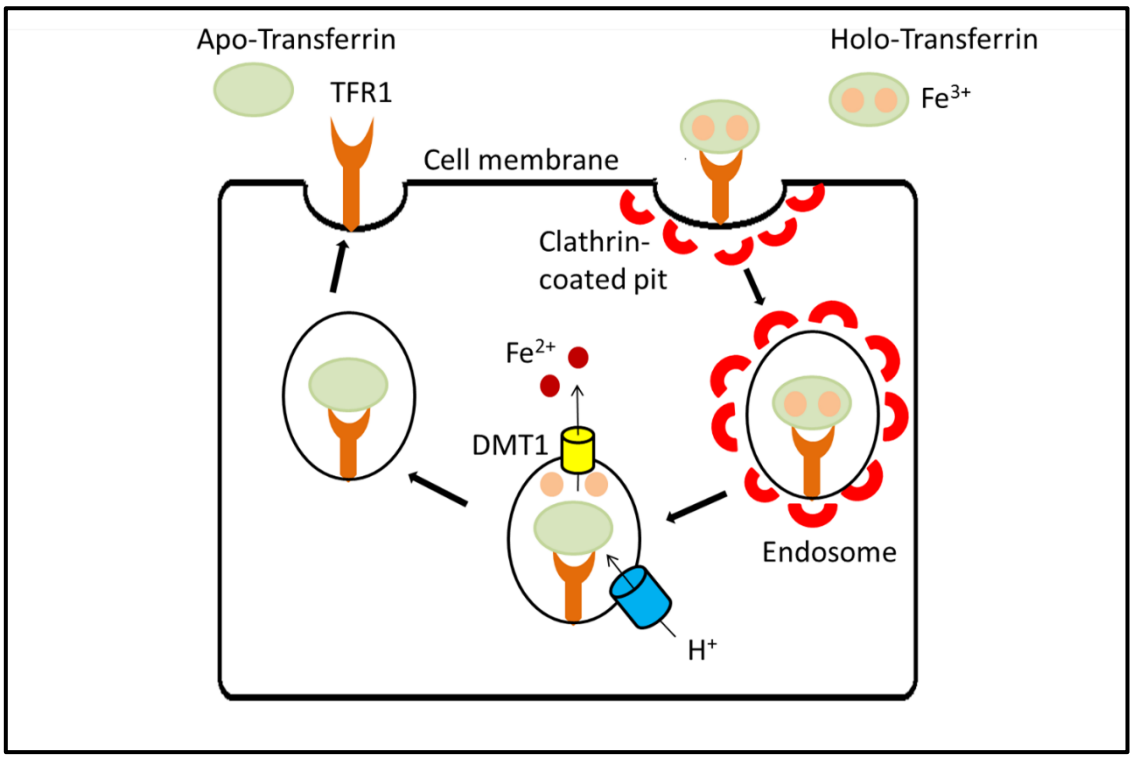

Fig. 1.8 Cellular uptake, utilisation and release of iron. At neutral pH, TFR1 binds diferric-transferrin and is internalised as clathrin-coated pits. At lower pH, ferric ions dissociate from transferrin, are reduced by a metalloreductase such as STEAP3 and transferred to the cytosol by DMT1. Transferrin-TFR1 recycles to the cell membrane. At slightly higher pH, transferrin detaches from TFR1 and returns to the blood. Figure modified by R Aryal from (Qian et al., 2002).

1.5.6 Regulation of iron homeostasis

Two different kinds of regulatory systems monitor bodily cellular iron levels. These systems are i) post-transcriptional regulation by iron responsive protein/ iron regulatory element (the IRE/IRP system) and ii) post-translational regulation of cellular iron release by the hormone hepcidin. Both of these systems are described below.

1.5.6.1 Post-transcriptional regulation by the IRE/IRP system

Intracellular iron levels are monitored and regulated through the Iron Responsive Element (IRE) / Iron Regulatory Protein (IRP) system. Transcripts of various genes such as ferritin and TfR1 are under the control of this regulatory system. The IRE is a conserved DNA motif in the untranslated regions (UTRs) of mRNA transcripts of various proteins, most having some known involvement in iron homeostasis (Casey et al., 1988; Kim et al., 1996). Two IRPs have been found, namely IRP1 and IRP2, that can bind to the IRE of particular gene transcripts to regulate iron metabolism (Addess et al., 1997; Crichton et al., 2012; Rouault, 2006; Samaniego et al., 1994).

When IRP binds to the 5' UTR of certain gene transcripts (e.g. transcripts encoding ferritin), there is translational repression whereas when IRPs bind to the 3' UTR of certain other gene transcripts (e.g. transcripts encoding TFR1), it protects the mRNA against degradation by nucleases, hence leading to transcriptional stabilization (Crichton et al., 2012; Koeller et al., 1989; Lymboussaki et al., 2003; Piccinelli and Samuelsson, 2007; Rouault et al., 1988). Human TFR2 mRNA transcript which is 45% identical with TFR1 does not contain any IREs. Hence the expression of TFR2 protein is not regulated by intracellular iron levels (Fleming et al., 2000; Trinder and Baker, 2003).

In case of high levels of cytosolic iron, IRP1 converts to an aconitase by integrating a 4Fe-4S cluster and no longer primarily exerts iron regulatory functions, while IRP2 is subjected to ubiquitination and proteasomal degradation. This prevents IRE/IRP binding and results in increased translation of ferritin mRNA whereas there is increased degradation of TFR1 transcripts and so decreased translation of TFR1 (Gehring et al., 1999; Iwai et al., 1998). When cytosolic iron is low, IRP-IRE binding increases, resulting in decreased ferritin translation and increased translation of TFR1 mRNA (Casey et al., 1988; Johnstone, 2010; Müllner and Kühn, 1988).

It should be noted that there are some transcripts which despite containing IREs in the 3' UTR, do not show any alterations in their expression in brain in response to changed iron conditions. One such example is a form of DMT1 transcript which seems to be unaffected by dietary iron supplementation in brain (Johnstone and Milward, 2010d; Ke et al., 2005). In the previous study from our group, there was no evidence of increased iron levels in the brain of dietary iron-supplemented mice (Johnstone and Milward, 2010d) .

1.5.6.2 Hepcidin regulation of iron homeostasis

Hepcidin is a 25 amino acid long peptide, encoded by *HAMP/ LEAP1* gene and located on human chromosome 19. It has a hairpin structure stabilized by 4 disulfide bonds. It is produced and secreted into the circulation primarily by hepatocytes (Nemeth et al., 2006; Nicolas et al., 2002). In the absence of hepcidin, iron is exported out of cells by ferroportin but if present, hepcidin attaches to the cell surface ferroportin and the resulting hepcidin-ferroportin complex is internalised by the cell and subjected to lysosomal degradation. Uptake of iron from the diet involves transport of iron from the gut into the blood by ferroportin located on the intestinal enterocyte surface. Increased hepcidin levels result in decreased iron efflux by ferroportin to the bloodstream, thus reducing the uptake of dietary iron from the intestine (De Domenico et al., 2009; De Domenico et al., 2007b;

Nemeth et al., 2006; Nemeth et al., 2004). Therefore hepcidin is a key regulator of uptake of iron into the body and reduction of uptake if body iron stores are high.

In different regions of human and mouse brain, hepcidin expression has been detected though in lower levels than that in liver (Hänninen et al., 2009; Johnstone and Milward, 2010d; Zechel et al., 2006). Ferroportin expression has also been identified in many cell types of rat and mouse brains. Hence hepcidin-ferroportin interaction is also proposed to regulate brain iron homeostasis (Johnstone and Milward, 2010d; Moos and Nielsen, 2006; Moos et al., 2007; Wu et al., 2004).

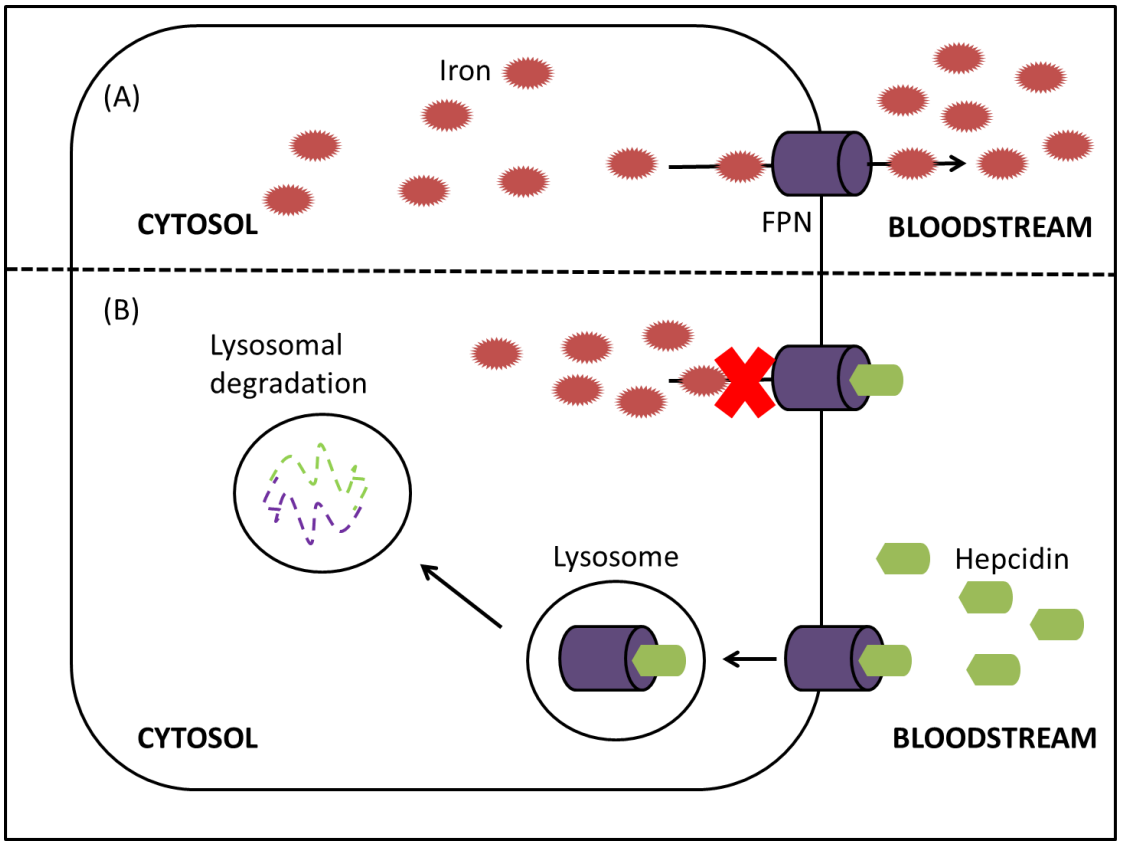

Fig. 1.9 Hepcidin regulation of cellular iron efflux. (A) In absence of hepcidin, ferroportin exports iron from cytosol to bloodstream. (B) In presence of hepcidin, ferroportin-hepcidin complex is internalised and then degraded in lysosome because of which ferroportin expression on cell surface is reduced resulting in decreased iron export into the bloodstream. Figure produced by R Aryal based on the mechanism described in (Nemeth et al., 2004).

Hepcidin synthesis is believed to be influenced by TFR2 (mentioned above) and the haemochromatosis protein (HFE; note that this is a standardized nomenclature and not an abbreviation). In the absence of holotransferrin, it is currently hypothesised that HFE binds to TFR1 whereas, when body iron is high, binding of iron-containing holotransferrin to TFR1 displaces HFE (Giannetti and Björkman, 2004; Lebrón et al., 1999). The displaced HFE may either remain free or

bind to TFR2, the latter acting as a trigger signalling for increased hepcidin expression, leading to reduced dietary iron uptake when body iron stores are high, as described above (Gao et al., 2009). Mutation in either HFE or TFR2 decreases hepcidin levels in blood, resulting in dysregulated uptake of dietary iron even when body iron is high, potentially leading to iron overload (Wallace et al., 2005; Zhou et al., 1998).

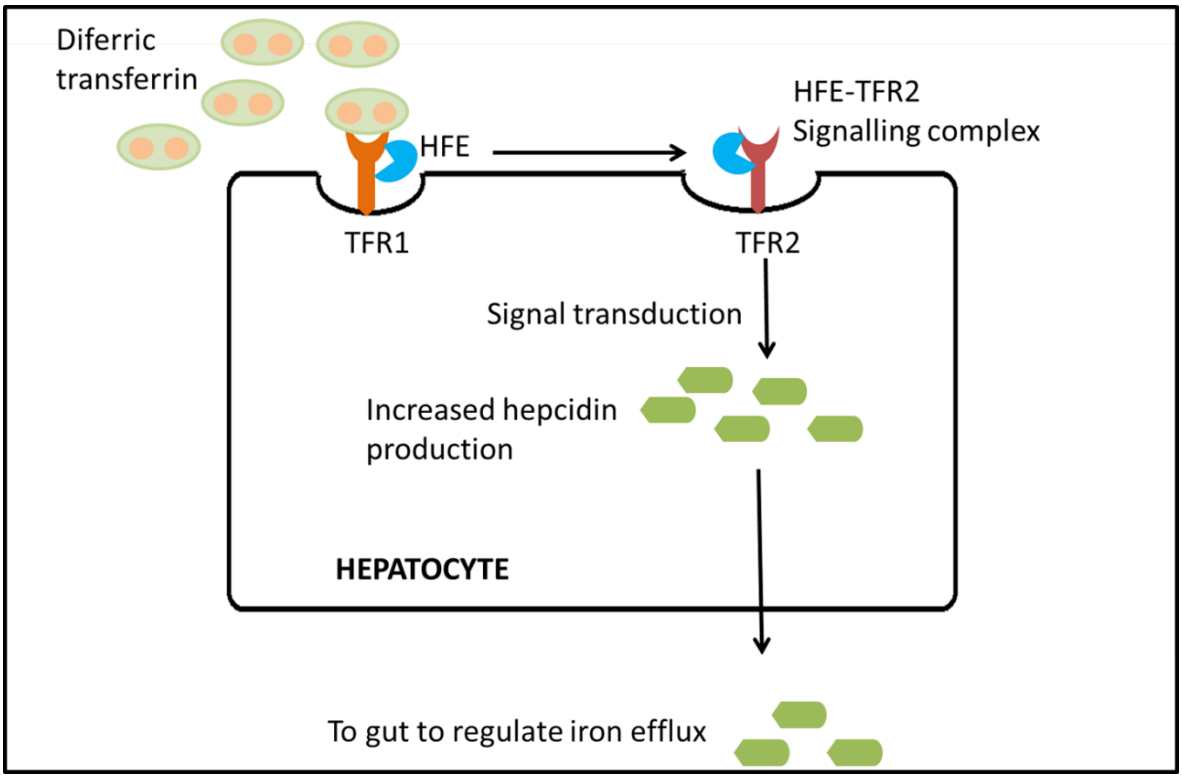

Fig. 1.10 Regulation of iron uptake. In the absence of diferric transferrin, HFE binds to TFR1. When iron levels are high, diferric transferrin displaces HFE to bind to TFR1. The displaced HFE binds to TFR2, signalling for up-regulation of hepcidin production. Hepcidin in turn regulates iron efflux through ferrroportin from gut enterocytes to the bloodstream, hence decreasing the body's uptake of iron from the intestine into the blood. Figure reproduced by R Aryal based on the mechanism described in (Muckenthaler, 2014).

1.5.7 Brain iron homeostasis

Brain has its own mechanism of regulating iron levels, in order to prevent iron deficiency or excess iron accumulation. Iron entry into the brain, its utilisation and exit from the brain is described briefly in this section.

1.5.7.1 The blood brain barrier

During early stages of life, brain is highly permeable to iron as iron is required for its growth and development. With the progression into adulthood, brain tightly regulates the entry and exit of iron just as it does for other useful elements and harmful toxins. The blood brain barrier (BBB) is a system that regulates trafficking of biomolecules and various compounds between blood and the brain.

As reviewed elsewhere (Banks, 2016; Sweeney et al., 2019), the BBB contains brain capillary endothelial cells (BCECs) joined by tight junctions; a basal lamina; pericytes partially surrounding the endothelium and astrocyte endfoot processes that form a complex network around the capillaries. The tight junctions seal the paracellular pathway and monitor passage of substances between brain and the circulation. Such an arrangement allows entry of important molecules like water and gases, glucose, amino acids, etc. through various forms of membrane transport and at the same time, prevents entry of potential neurotoxins and xenobiotics and protects the brain from fluctuations in plasma composition (Abbott, 2002; Abbott, 2005; Cardoso et al., 2010; Mathiisen et al., 2010; Persidsky et al., 2006). Disruption of the BBB has been known to result into cerebral dysfunction and is associated with various kinds of neurological disorders, including AD (Bell and Zlokovic, 2009; Biron et al., 2011; Garbuzova-Davis et al., 2007; Rosenberg, 2012).

1.5.7.2 Iron trafficking across the blood brain barrier

Iron trafficking across the BBB is regulated by the iron requirements of neurovascular unit, which comprises components of the BBB, neurons and other glia such as microglia and oligodendrocytes (Del Zoppo, 2010; McCarthy and Kosman, 2015; Scherrmann, 2010). Various theories of iron transport across the BBB have been proposed, of which the most common model supports a mechanism similar to most cell types: uptake and endocytosis of holotransferrin by TFR1 on luminal surface of the BCECs. The slightly acidic pH of endosome resulting from entry of hydrogen atoms causes ferrous iron to be released into cytosol by DMT1 and then into the brain interstitium through ferroportin. The apotransferrin and TFR1 are recycled to the luminal side of the endothelial cells (McCarthy and Kosman, 2015; Mills et al., 2010; Rouault and Cooperman, 2006; Taylor and Morgan, 1990). This model however is contentious because of the uncertainty of DMT1 expression in BCECs (Gunshin et al., 1997; Moos et al., 2007; Moos et al., 2006; Siddappa et al., 2002).

Studies have also suggested transferrin independent mechanisms for passage of iron across the BBB, eg. via transferrin homologues such as lactoferrin and melanotransferrin (Fillebeen et al., 1999; Rothenberger et al., 1996). Some studies have proposed roles of ferritin receptors namely

scavenger receptor, member 5 (Scara5) and T cell immunoglobulin mucin domain 2 (TIM-2) for transport of NTBI into the brain (Li et al., 2009; Mills et al., 2010; Todorich et al., 2008b). Recently, an *in vitro* model of the BBB has identified an endosomal cation/proton exchanger called Na^+/H^+ Exchanger 9 (NHE9) to regulate iron mobilization across the BBB, in response to iron deprivation (Beydoun et al., 2017).

1.5.7.3 Iron trafficking across the blood-cerebrospinal fluid barrier

Along with the BBB, there is another barrier for iron entry into brain: the blood-cerebrospinal fluid barrier. The choroid plexus present in the brain ventricles produce cerebrospinal fluid (CSF), a fluid that fills all ventricles and the brain interstitium. The expression of transferrin, TFR, Dcytb, FPN, ceruloplasmin, hephaestin and ferritin H on the choroid plexus suggests its importance in brain iron uptake (Marques et al., 2011; Rouault et al., 2009; Tu et al., 1991). Having said that, there are reports of transferrin being localised to the choroid plexus of many species but not humans (Aldred et al., 1987; Dickson et al., 1985; Tu et al., 1991). On the other hand, brain iron uptake via the blood-CSF barrier is contentious, as studies have shown that only a small proportion of total brain iron is acquired through the CSF (Crowe and Morgan, 1992; Ueda et al., 1993).

1.5.7.4 Iron transport within brain

The mechanisms of iron transport within the brain is still a subject of investigation. One hypothesis states that citrate and ATP secreted by astrocytes, release the iron from transferrin on the abluminal side of BCECs. Complexes of iron with citrate and ATP then flow in the brain extracellular fluid, which can be either taken up by various brain cells or they may be taken up by transferrin, the latter of which can be taken up by cells expressing transferrin receptors (Moos et al., 2007). Another postulation is that the astrocytic ceruloplasmin first oxidises the ferrous iron released from BCECs and then the ferric iron binds to transferrin (Jeong and David, 2003). It is also speculated that the cells such as astrocytes and oligodendrocytes, which do not express TFR1, may utilise the NTBI present extracellularly in the CSF and in the brain interstitium (Bradbury, 1997; Moos and Morgan, 1998).

1.5.7.5 Exit of iron from brain

The exact mechanism through which iron exits the brain is also unclear. It is suspected that iron exits the brain with bulk outflow of CSF through arachnoid villi and enters the venous drainage system (Bradbury, M., 1997; Rouault, T.A. and S. Cooperman. 2006). As described above, the expression of different iron transporters in the choroid plexus hints at their involvement in iron export out of the brain but this needs to be investigated further (Rouault et al., 2009).

1.5.7.6 Iron uptake, use and export by neurons

Iron is taken up by neurons from the brain interstitium via TFR1 or DMT1, as both of these receptors are expressed by neurons. This is believed to be followed by the receptor-mediated endocytosis and the release of iron from the endosomes for TFR1 uptake (Giometto et al., 1990; Moos and Morgan, 2004a; Moos et al., 2007). Neurons also take up and utilise the NTBI via various other iron transporters (Bishop et al., 2011; Codazzi et al., 2015; Ji and Kosman, 2015). Iron acquired by neurons is immediately used in relevant metabolic processes and is exported through ferroportin (Moos and Morgan, 2004b; Moos et al., 2007). Nevertheless, neurons in the brain regions with high iron content such as substantia nigra are assumed to store iron in the form of neuromelanin (Zecca et al., 2001; Zucca et al., 2006).

1.5.7.7 Iron uptake, use and export by astrocytes

Astrocytes do not have TFR1 but it is debated that they accept NTBI from endothelial cells through DMT1 (Moos and Morgan, 2004c; Wang et al., 2001). Zinc transporter Zip14 has also been proposed to be involved in the NTBI uptake by astrocytes (Bishop et al., 2010; Pelizzoni et al., 2013). Iron exits astrocytes through the combined action of ferroportin and glycophosphatidylinositide (GPI)-anchored ceruloplasmin (Cp) (Jeong and David, 2003; Jeong and David, 2006; Klomp et al., 1996). Little ferritin is present in astrocytes indicating that they store less iron and the presence of astrocytic endfeet suggests that astrocytes are involved in transport of iron to various cells in the brain (Connor et al., 1990; Dickinson and Connor, 1995; Dringen et al., 2007).

1.5.7.8 Iron uptake, use and export by oligodendrocytes

Oligodendrocytes are the predominant cells in the CNS that stain for iron (Baumann and Pham-Dinh, 2001; Connor et al., 1990; Connor and Menzies, 1996). As oligodendrocytes lack TFR1, they are believed to accept NTBI and use it mostly for myelin synthesis (Hulet et al., 1999a; Hulet et al., 1999b; Todorich et al., 2011). They export the iron through ferroportin (Boserup et al., 2011; Moos and Rosengren Nielsen, 2006; Wu et al., 2004). H-ferritin is reported to be the main source of NTBI for oligodendrocytes (Hulet et al., 2000; Todorich et al., 2011). An H-ferritin receptor called T cell immunoglobulin mucin domain 2 (Tim-2) has been discovered in different species (Chen et al., 2005; Todorich et al., 2008b) but no human ortholog has been described yet (Han et al., 2011; Santiago et al., 2007).

1.5.7.9 Iron uptake, use and export by microglia

Progenitor microglia have high iron and ferritin levels during early developmental stages. As they migrate into the central nervous system, they become quiescent and start losing their iron (Cheepsunthorn et al., 1998; Moos, 1995). Recent findings indicate that based on their polarization state, microglia uptake iron either from transferrin or from non-transferrin sources (McCarthy et al., 2018a). Microglial expression of a divalent cation transporter, natural resistance-associated macrophage protein 1 (Nramp1) hints at its role in iron recycling but the exact role of this transporter in microglia is not clear (Evans et al., 2001).

1.5.8 Harmful effects of excess brain iron

The regulation of different vital biological processes is facilitated by the ability of iron to accept as well as donate electrons hence making it suitable for undergoing redox reactions. However, abnormal or excessive body iron levels can cause detrimental effects in various ways. As brain has high oxygen turnover, one of the broadly accepted theories is that iron catalyses production of chemically reactive molecules known as reactive oxygen species (ROS), which in turn lead to oxidative stress and damage (Aisen et al., 2001; Emerit et al., 2001; Hentze et al., 2004; Lou et al., 2009). Oxidative damage is believed to contribute to neurodegeneration in various conditions including Alzheimer's disease (Butterfield, 1997; Good et al., 1996; Lin and Beal, 2006; Markesbery, 1997; Mecocci et al., 1994). The age risk factor of AD has widely been linked with increased oxidative damage resulting from age-dependent increase in brain iron levels (Maynard et al., 2002; Raven et al., 2013).

Free iron catalyses ROS production by Fenton and Haber-Weiss reactions. Briefly, iron reacts with superoxide ($\cdot O^{2-}$) and hydrogen peroxide (H_2O_2) to produce hydroxyl radicals ($\cdot OH$) (Aisen et al., 2001; Halliwell and Gutteridge, 2015; Kehrer, 2000). These hydroxyl radicals are highly toxic ROS and can oxidize DNA, RNA proteins and lipids, leading to oxidative stress and damage. The subsequent effect can be cell death by apoptosis or necrosis (Kohgo et al., 2008; Papanikolaou and Pantopoulos, 2005; Valko et al., 2005).

$$Fe^{3+} + \cdot O_2^- \rightarrow Fe^{2+} + O_2$$

$$Fe^{2+} + H_2O_2 \rightarrow Fe^{3+} + OH^- + \cdot OH \text{ (Fenton reaction)}$$

Net reaction:

$$\cdot O_2^- + H_2O_2 \rightarrow OH^- + \cdot OH + O_2 \text{ (Haber-Weiss reaction)}$$

Although brain is believed to have proper defence mechanisms against acute iron toxicity, chronic iron accumulation has been proposed to lead to various brain abnormalities. With ageing, it is believed that iron accumulation in lysosomes contributes to the formation of a toxic substance called lipofuscin (Brunk and Terman, 2002; Katz and Robison, 2002; Terman and Brunk, 2004). Lipofuscin cannot be degraded nor cleared away by lysosomes and its accumulation can damage the ubiquitin/proteasomal degradation pathway, thus causing serious impairments in brain functions (Katz et al., 1993; Kurz et al., 2008).

A previous study by our group reported expression changes in five of the seven lipofuscin-related genes, which were evaluated in the Hfe knock out mice (Johnstone et al., 2012a). Another assumption is that abnormal brain iron levels may change brain gene expression profile. Contradictory to this, there have also been reports of changes in brain gene expression profile resulting from Tfr2 dysfunction and systemic iron overload even if there is no visible change in total brain iron levels (Acikyol et al., 2013; Johnstone and Milward, 2010b). Local brain iron redistribution that doesn't contribute to alteration in overall brain iron levels in iron supplemented mice can cause lipid or protein modifications leading to changed brain gene expression (Johnstone and Milward, 2010a).

1.6 Relationship between iron and AD

Abnormal brain iron accumulation contributes to the development of different brain disorders resulting from mutations in various iron-related genes. Some examples are neurodegeneration with brain iron accumulation (NBIA), neuroferritinopathy and aceruloplasminemia. Likewise, unusual

iron loading has also been reported in human post-mortem brain tissue affected by AD and in various AD mouse models (Altamura and Muckenthaler, 2009; Connor et al., 1992b; Meyer et al., 2015).

The hypothesis that increased iron levels are associated with AD dates back to as early as 1950s (Everett et al., 2014a; Goodman, 1953). Since then, there has been ambiguity regarding whether brain iron accumulation causes AD or whether brain iron accumulation is a secondary consequence of AD. Possible association of iron with AD is implicated by the fact that as the brain ages, iron accumulates in regions of the brain that are mostly affected in conditions like AD and Parkinson's disease (Zecca et al., 2004). Some studies have described higher iron concentrations in particular cortical areas of Early Onset Alzheimer's disease (EOAD) patients than those of Late Onset Alzheimer's disease (LOAD) patients (Bartzokis et al., 2004b; Van Rooden et al., 2015).

Iron has been reported to accumulate in brain regions containing Aβ aggregates and NFTs suggesting a link between iron and AD (Altamura and Muckenthaler, 2008; Connor et al., 1992b; Good et al., 1992; Smith et al., 1997). Increased levels of Fe^{2+}-containing compounds like magnetite/ maghemite (Hautot et al., 2003; Pankhurst et al., 2008) and wustite have been reported to be present in AD tissue (Everett et al., 2014a; Pankhurst et al., 2008). Furthermore, excess iron is proposed to decrease activity of furin, a proconvertase that regulates non-amyloidogenic APP processing, leading to increased formation of Aβ (Bennett et al., 2000; Silvestri and Camaschella, 2008). Genome wide association studies have linked the locus of a protein involved in iron homeostasis named phosphatidylinositol binding clathrin assembly (PICALM) to AD (Harold et al., 2009; Parikh et al., 2014).

It was reported that APOE-ε4, a genetic risk factor of AD, raised CSF ferritin levels in the Alzheimer's Disease Neuroimaging Initiative (ADNI) cohort (Ayton et al., 2015; Wood, 2015). Another study noted increased neocortical iron levels in APOE-ε4 carriers with Mild cognitive impairment (Van Bergen et al., 2016). Both of these studies postulated elevated brain iron as a potential cause for APOE-ε4 being the chief risk allele for AD. Bergen et al. postulate that APOE-ε4 promotes colocalisation of iron and Aβ by accelerating Aβ accumulation by competing for the same clearance pathways as well as raising cerebral iron retention by damaging lipoprotein trafficking because of decreased affinity of APOE-ε4 to high-density lipoprotein. They also suggest examining whether various immunotherapies targeted against Aβ and tau have effects on the level of local iron accumulation (Van Bergen et al., 2016). Hare et al. attributed reduced plasma iron in AD to decreased loading of iron into transferrin (Hare et al., 2015). The Australian Imaging Biomarker and Lifestyle (AIBL) study found that AD patients had significantly lower haemoglobin

concentrations than healthy controls, which was believed to be a peripheral reflection of brain iron dyshomeostasis (Faux et al., 2014).

At least one study that directly examined the prevalence of AD in a community cohort of over 1000 people failed to demonstrate that high serum iron measures increase the risk of AD (Milward et al., 2010). The belief that iron is abnormally accumulated in AD brain is questioned by Schrag and colleagues, in a quantitative meta-analysis demonstrating publication bias in this area (Schrag et al., 2011b). They evaluated existing literature on comparison of brain iron levels of AD patients with age-matched controls and noted diverse results. They reported that an increase in neocortical iron levels in AD patients described by one laboratory was not observed by seven other laboratories. Their meta-analysis of the full set of studies found no significant difference between neocortical iron levels in AD and controls ($p = 0.76$). They also noted that a more than three-fold citation bias was found among narrative review articles, to favour outlier studies stating increases in iron (Schrag et al., 2011b).

However, brain iron quantification studies published since this meta-analysis have reported increased iron in various regions of the AD brain (Akatsu et al., 2012; Graham et al., 2014; Hare et al., 2016). Though not in brain, a separate systematic review and meta-analysis published in 2014, described that 2 studies reported decreased and 3 studies reported no significant alteration on plasma iron levels between human AD and control cases (Lopes da Silva et al., 2014). With all these uncertainties, the nature of the relationships between AD and iron still remain a mystery and it is important to investigate this further, given the potential problems with iron chelation therapy in the elderly (described below).

1.6.1 Iron chelation in AD therapeutics

Based on indirect evidence, a number of iron chelators are now being studied to check their efficacy against AD. A multi-target iron chelating-radical scavenging drug (5-[N-methyl-N-propargylaminomethyl] -8-hydroxyquinoline) or M30 reduces cerebral iron accumulation and levels of cerebral APP and plaques (Kupershmidt et al., 2012), has neuroprotective effects and regulates blood glucose levels, in the APP/PS1 mice (Amit et al., 2017; Mechlovich et al., 2014). With the discovery of the IRE in the 5' UTR of APP (Rogers et al., 2002), it is speculated that M30 and other iron chelators have potential to modulate translation of APP by chelating iron pool (Avramovich-Tirosh et al., 2007a; Avramovich-Tirosh et al., 2007b).

The trivalent iron chelator desferrioxamine (DFO) was reported to slow progression of dementia in a 2-year, single-blind study (Crapper McLachlan et al., 1991). *In vitro*, DFO was reported to prevent the fibrillisation of Aβ42, partly dissolve the preformed Aβ fibrils (House et al., 2004a) and also inhibit the amyloidogenic APP processing in an AD mouse model (Guo et al., 2013). Deferiprone is reported to readily cross the BBB whereas desferrioxamine doesn't. However in a study of iron chelation therapy for aceruloplasminemia it was reported that crossing of the BBB by DFO is not absolutely necessary for brain iron removal (Miyajima et al., 1997). This may imply that reducing systemic iron may have a flow-on effect on brain iron levels without DFO actually the brain although this question has still not been clearly resolved. Combined chelation therapy using both of these iron chelators has also been described to show promising results (Mourad et al., 2003).

Deferasirox, another iron chelator conjugated with lactoferrin mitigated Aβ induced learning deficits, when administered intraperitoneally in a rat model of AD (Kamalinia et al., 2013) and has shown potential to prevent age-related alterations in iron and Aβ peptide metabolism, in the aging rat brain (Banerjee et al., 2016). Administration of these drugs through intranasal route is believed to target the brain via olfactory and trigeminal nerves, hence evading the BBB (Frey et al., 1997; Guo et al., 2013).

However, some authors believe that iron chelation along with other forms of treatments such as venesection and dietary changes may not help in improving brain iron disorders in the same way as they do for systemic iron abnormalities (Burn and Chinnery, 2006; Johnstone and Milward, 2010d). This may be due to the fact that brain is possibly protected against damaging systemic iron changes by the blood-brain barrier and the blood-CSF barrier and has its own regulatory mechanisms for internal iron stores (Johnstone and Milward, 2010d).

It should be noted that the long-term usage of iron chelators may result in deficiency of systemic iron and potentially, subsequent anemia. Furthermore, iron chelation can have harmful consequences including agranulocytosis, vision or hearing impairment, particularly in older people, who have greater risk of renal and cardiovascular disease (Cuajungco et al., 2000; Guo et al., 2013). Chelators can also remove iron from ferritin and other compounds that are required for normal iron homeostasis. Keeping this in mind, it is essential to determine which iron specific compounds are involved in the disease progression and which are required for normal brain functioning, before treating individuals with iron chelators (Collingwood et al., 2008; Raven et al., 2013). Some researchers recommend that prospective clinical trials should consider providing iron chelation therapy to a targeted group of people, e.g. people with symptoms of both AD and cerebral

microbleeding (small chronic brain haemorrhage, described below), rather than giving it to all kinds of AD patients (Schrag et al., 2011a).

1.6.2 Evidence for a possible relationship between iron and APP

One way iron has been proposed to be involved in AD is through mechanisms involving APP (described above). A potential IRE-Type II sequence has been reported within the 146 nucleotide 5'-UTR of the APP mRNA (+51 to +94), located immediately upstream of an interleukin-1 (IL-1) responsive acute box domain. This sequence has 66% similarity to the H-ferritin IRE (+12 to +59) (Fig. 1.11) (Rogers et al., 2002). Two clusters of APP IRE-Type II display more than 70% similarity with H-ferritin IRE sequences. This suggests that iron may have roles in the post-transcriptional regulation of APP through the IRE/IRP system- possibly increased iron leading to increased APP production (Bandyopadhyay et al., 2006; Rogers et al., 2002), in addition to other roles (Connor et al., 2001; Mantyh et al., 1993). Rogers et al. reported in a subsequent paper that while the APP IRE interacts with the IRP1 (cytoplasmic cis-aconitase), the H-ferritin IRE RNA stem-loop interacts with the IRP2 in neural cell lines, the human brain cortical tissue and human blood lysates (Rogers et al., 2008).

Fig. 1.11 Similarity between the iron-responsive element (IRE) in the APP mRNA 5'-UTR and the ferritin IRE. The IRE in APP mRNA has 66% similarity (shown in red) to the IRE in H-ferritin mRNA; boxed regions highlight two similar clusters in IRE of APP mRNA with more than 70% similarity with ferritin IRE. Figure modified from (Rogers et al., 2002).

Following from this, Duce and colleagues proposed APP possesses ferroxidase activity (Duce et al., 2010). Some of their observations are highlighted below.

1) Duce and colleagues suggested that a REXXE ferroxidase consensus motif (Gutierrez et al., 1997; Lawson et al., 1991; Ninomiya et al., 1993; Toussaint et al., 2007; Wang and Ha, 2004) proposed to be present in the E2 domain of APP(Duce et al., 2010; Wang and Ha, 2004) is analogous to that previously reported in the ferroxidase active site of H-ferritin (Gutierrez et al., 1997; Lawson et al., 1991). They presented sequence alignments contending that the iron coordinating residues E62 and H65 of H-ferritin overlapped with the corresponding residues E412 and E415 which make up the proposed ferroxidase site of APP.

2) They also proposed that recombinant soluble APP695α, which represents the most abundant APP species in the brain and in neurons in particular (de Silva et al., 1997) possessed strong ferroxidase activity, as assessed by *in vitro* analysis of the rate of incorporation of ferric iron, the product of the ferroxidase reaction, into transferrin.

3) A 22-residue synthetic peptide (FD1) within the E2 domain, carrying the putative ferroxidase site of APP, as well as the purified E2 polypeptide, was reported to exhibit ferroxidase activity *in vitro* that was around 40% that of APP695α.

4) APP was proposed to promote iron release, lower the labile iron pool (LIP) and interact with ferroportin in Human Embryonic Kidney 293 cells (HEK293T cells) that lack the ferroxidase ceruloplasmin (De Domenico et al., 2007b). Suppression of APP expression in HEK293T cells by RNAi was reported to result in the cellular accumulation of significantly more radioactive ^{59}Fe than sham RNAi treated controls.

Addition of APP695α or the E2 domain of APP to the media was reported to significantly promote the efflux of ^{59}Fe into the media. Similarly, primary cultures of cortical neurons from an APP Knockout mouse model ($APP^{-/-}$) were reported to retain significantly more ^{59}Fe than neuronal cultures from wildtype (WT) mice. Addition of APP695α promoted ^{59}Fe export into the media after 12 hours from both the WT and $APP^{-/-}$ neurons and the iron levels in $APP^{-/-}$ neurons were reported to approach WT levels.

5) Aceruloplasminemic patients and ceruloplasmin knockout mice show iron accumulation with age in liver, pancreas and brain astrocytes but not cortical neurons (Harris et al., 1995; Patel et al., 2002). To assess effects of APP deficiency, 12-month-old $APP^{-/-}$ mice were compared to wild-type (WT) age-matched controls, both either on normal chow or a high iron diet (120 μg Fe/g body weight) for 8 days. Significant increases in iron levels were observed in brain (+26%), liver (+31%) and kidney (+15%) of $APP^{-/-}$ mice on normal chow than WT mice on the same diet.

Surprisingly, a high iron diet yielded no significant change in iron levels in liver or other tissues of WT mice, unlike other comparable studies in WT mice (Johnstone and Milward, 2010b). However Duce and colleagues observed that high iron diet led to increased iron in brain (+13%) and liver (+90%) of $APP^{-/-}$ mice on a high iron diet compared to $APP^{-/-}$ mice on a normal diet. $APP^{-/-}$ mice on the high iron diet had increased ferritin levels in brain and liver tissue. From this, Duce and colleagues proposed that APP protects against accumulation of iron and development of oxidative stress (Duce et al., 2010).

However Ebrahimi and colleagues subsequently put forward opposing findings requiring the re-evaluation of the Duce study, failing to find any evidence of APP ferroxidase activity by a range of

approaches including those used by Duce and colleagues (Ebrahimi et al., 2012). Besides measuring the ferroxidase activity of the FD1 synthetic peptide indirectly using transferrin as was done by Duce and colleagues, Ebrahimi and colleagues also measured it directly by observing the consumption of the substrate, molecular oxygen, and found no activity above background levels. This was subsequently further confirmed in a second paper by additional studies of the ferroxidase activity of the natural E2 domain of APP, tested by analysis of Fe^{2+} binding to this domain by isothermal titration calorimetry as well as both the transferrin assay and oxygen consumption measurements (Ebrahimi et al., 2013a). It was found that Fe^{2+} neither binds to the E2 domain nor does it get oxidised by this domain or another APP domain, E1, leading to the conclusion that the E2 and E1 domains of APP do not have ferroxidase activity.

In addition to this, questions were also raised regarding the putative ferroxidase site of APP. In the previous work of Duce et al., residues E412 and E415 of APP were arbitrarily aligned with E62 and H65, the two metal-coordinating residues of the ferroxidase centre of human H-chain ferritin. However Ebrahimi and colleagues noted that the two glutamates in the REXXE motif in ferritin are not ligands of the metals in the ferroxidase center and therefore that there was no significant overall similarity between the structure of the ferroxidase centre of ferritin and the REXXE putative ferroxidase activity carrying motif of APP (Ebrahimi et al., 2013a).

In 2014, Duce and colleagues re-examined their *in vitro* experiments testing soluble APPα (sAPPα) ferroxidase activity, within a buffer of physiological pH and anionic charge (Wong et al., 2014). They reported using a triplex Fe^{2+} oxidation assay that their previously-reported ferroxidase activity of APP originated from contaminant phosphate which co-eluted during protein purification (Wong et al., 2014). However, this does not appear to fully account for the discrepancy, since phosphate has only been reported to accelerate activity of other ferroxidases, rather than have ferroxidase activity itself (Ebrahimi et al., 2013b). The original paper from Duce and colleagues is therefore at least partly incorrect and other aspects of this paper also require re-evaluation, including the surprising lack of effects of their high iron diet in wildtype mice, mentioned above, as well as other data.

Duce and colleagues then claimed that endogenous APP is essential for stabilising ferroportin on the neuronal cell surface and to facilitate iron export from neurons, despite its lack of ferroxidase activity (Wong et al., 2014). Other independent researchers have also supported this hypothesis with relevance to the microvascular endothelial cells (McCarthy et al., 2014). This partly draws on a paper from Domenico and colleagues, who reported in 2007 that ceruloplasmin ferroxidase activity

is required for stability of cell surface ferroportin (De Domenico et al., 2007a). However many of this group's findings have been questioned and in some cases retracted so it is currently difficult to evaluate the conclusions from all these studies and more work is clearly required to clarify the role of APP.

1.6.3 Possible causes of brain iron dyshomeostasis in AD and other neurodegenerative disorders

Different causes of increased brain iron levels have been proposed in different neurodegenerative conditions. Many neurodegenerative disorders are associated with chronic inflammation, which in turn may lead to progressive iron accumulation in different brain regions (Andersen et al., 2014; Thomsen et al., 2015). It has been hypothesised that damaged or dead neurons are phagocytosed by iron rich inflammatory cells such as macrophages, though some authors propose the opposite mechanism, i.e., phagocytosis causes neuronal death (Neher et al., 2011).. Besides abnormal iron transport across the BBB, phagocytic cells rich in iron may enter the brain from bloodstream (Dusek et al., 2016; Schrag et al., 2010) and accompany neurodegeneration (Andersen et al., 2014; Thomsen et al., 2015). In a condition called superficial siderosis of the CNS, subarachnoid bleeding is thought to contribute to increased iron in the outer cerebral cortical surface (Koeppen et al., 2008).

Some authors have proposed microbleeding due to cerebral amyloid angiopathy (CAA)- a condition commonly observed in most but not all AD patients in which amyloid deposits are seen in the walls of the blood vessels (Greenberg and Vonsattel, 1997; Tian et al., 2004; Yamada, 2015) as a potential cause of increased brain iron levels (Dusek et al., 2016; Schrag et al., 2011a). Such deposition of amyloid is also reported to result in thickening of the wall of blood vessel with 'congophilic material'(Schrag et al., 2011a; Vinters, 1987) Iron and ferritin have been described to be present around blood vessels in AD brain (Connor et al., 1992a; Connor et al., 1992b; Goodman, 1953) which led some authors to postulate that uptake of iron into brain is not optimal in AD (Connor et al., 1992b).

In a study by Schrag and colleagues, AD patients with severe CAA had increased brain non-haem iron levels as compared to the AD patients that didn't show any indication of amyloidosis in vasculature (Schrag et al., 2011a). The same study reported association of high levels of iron in neocortex with intense CAA and a significant increase in haem degradation enzymes HO-1 and biliverdin reductase B in AD patients with CAA as compared to AD patients without CAA as well as normal controls (Schrag et al., 2011a). Peters et al. have also hypothesized in their recent review

that iron dysregulation and amyloidosis in AD correlate to a disrupted brain vasculature (Peters et al., 2015).

Raha and colleagues have described that loss of pericytes (cells important in maintenance of blood brain barrier integrity) and disruption of endothelium are associated with vascular damage and amyloidosis in human and mouse AD brains. They also noted that reduced levels of iron-related proteins ferroportin and hepcidin are linked to the deposition of haem-rich granules nearby small disrupted blood vessels of human AD brains (Raha et al., 2013). Such granules are described to be remnants of microhaemorrhage- a condition commonly observed in aging brain and they seem to colocalise with Aβ deposits (Cullen et al., 2005; Cullen et al., 2006). Alterations in Iron regulatory protein 2 (IRP-2) have been described to be associated with AD pathology and abnormal iron distribution in AD brain (Smith et al., 1998) but this has been questioned (Magaki et al., 2007; Schrag et al., 2011a).

1.6.4 Studying the iron-AD relationship using magnetic resonance imaging

Various experimental approaches have bolstered the theory of iron dyshomeostasis in AD. One such method is the use of magnetic resonance imaging (MRI) to measure iron levels in AD brains. However, MRI may have some drawbacks. For example, as cellular structure breaks down in AD, the amount of water increases in brain, which can conceal detection of iron (Kamman et al., 1988; Raven et al., 2013). Likewise, myelin has significant interference in magnetic susceptibility MRI, mainly in the white matter (Hare et al., 2016; Lodygensky et al., 2012). Hence it is also argued that the *in vivo* study of brain iron accumulation using MRI is more appropriate for diseases affecting brain areas with high iron and low myelin content (Hare et al., 2016; Rossi et al., 2013).

It is also described that MRI does not essentially reveal pathological iron or iron specific to just one pathological condition, as it can also detect iron in normal tissue (Bagnato et al., 2011). Differentiation of neocortical white matter and gray matter iron distribution using MRI is difficult as most MRI methods are not totally quantitative and their spatial resolution impedes distinction of fine details of brain iron at micrometer scales. Hence, brain MRI is mostly restricted to areas with high iron content such as basal ganglia (Hare et al., 2016).

1.6.5 Studying the iron-AD relationship using mouse models of the iron overload disease haemochromatosis

The relationship between iron, APP and AD can be studied by looking at changes relating to AD in animal models of iron loading. The most common iron overload disorder in humans is hereditary haemochromatosis (HH), which will be described briefly prior to the explanation of mouse models of haemochromatosis.

Hereditary haemochromatosis is a group of genetic disorders of iron overload, marked by increased iron levels in liver and other parts of the body (Ayonrinde et al., 2008; Camaschella, 2005; Cartwright et al., 1979; Pietrangelo, 2010). The most common polymorphism resulting in the HH is the cysteine to tyrosine substitution at the amino acid 282 (C282Y), positioned in the genomic region encoding the α3 domain of the HFE gene (Feder et al., 1996). This prevents interaction of HFE with β2-microglobulin, resulting in impaired HFE-TFR1 binding (Gao et al., 2009; Schmidt et al., 2008). The combination of the C282Y polymorphism and another HFE polymorphism: histidine to aspartic acid substitution at amino acid 63 (H63D), also results in HH. The H63D polymorphism affects the α1 domain of the HFE protein and may prevent HFE from stimulating the holotransferrin-TFR1 binding (Feder et al., 1998a; Gochee et al., 2002).

Besides these, there are other additional *HFE* mutations associated with HH (Barton et al., 1999; de Villiers et al., 1999; érald Le Gac et al., 2003). While 80% of the HH is resulted by the HFE mutations, the remaining 20% is caused by mutations in other iron-related genes, the latter of which constitute the non-HFE haemochromatosis. Four main genes involved in the non-HFE haemochromatosis are *Tfr2, haemojuvelin, hepcidin* and *ferroportin* (Aguilar-Martinez, 2007; Pietrangelo, 2005; Santos et al., 2012; Wallace and Subramaniam, 2007). Magnetic resonance imaging (MRI) suggests iron may accumulate in some haemochromatosis patient brains (Berg et al., 2000; Connor et al., 2001; Nielsen et al., 1995) but this is difficult to assess reliably without post-mortem studies and there is little evidence of effects on brain iron in most patients, as reviewed elsewhere (Johnstone and Milward, 2010d).

1.6.5.1 Mouse models of the iron overload disease haemochromatosis

Different mouse models of iron overload or haemochromatosis have been generated using different approaches. One method is to inject mice with high doses of iron.(Demougeot et al., 2003a; Lou et

al., 2009; Maaroufi et al., 2009) Although such models show higher iron accumulation in different parts of body including some brain regions, these doses are much higher than the normal human brain exposure levels, are given for short periods of time (Maaroufi et al., 2009) Hence, this kind of model doesn't demonstrate iron loading of the sort typically seen in humans in which iron accumulation takes place over long periods of time.(Barton and Edwards, 2000; Demougeot et al., 2003a; Lou et al., 2009; Maaroufi et al., 2009)

Another method is supplementing mice with short term high dietary iron (Fredriksson et al., 1999; Omara et al., 1992; Sobotka et al., 1996). One such model showed higher liver and serum iron loading but no obvious damage in liver and other tissues, so this is not a representative model for clinical haemochromatosis (Graham et al., 2010a; Johnstone and Milward, 2010a). This model also doesn't show increased iron loading in brain, probably because the blood brain barrier counteracts this, as suggested elsewhere (Deane et al., 2004; Johnstone and Milward, 2010a; Moos et al., 2000).

Having said that, our group has provided evidence of small gene expression changes in the absence of gross brain iron loading in dietary iron-supplemented mice (Johnstone and Milward, 2010b). However, dietary iron supplementation models are generally given inorganic forms of iron which do not replicate the iron deposition occurring in human body, thus questioning their appropriateness (Johnstone and Milward, 2010c). Some authors have reported that iron accumulates in brain at very high doses. Sobotka et al reported that brain non-haem iron in male weanling rats increases with increasing levels of dietary iron but this was significant only at the highest dose of iron overload (20,000 ppm in diet for 12 weeks; $p<0.05$) (Sobotka et al., 1996). Direct injection of iron into striatum to bypass the BBB shows acute damage to brain (Demougeot et al., 2003b; Hironishi et al., 1999), which does not correctly represent the chronic physiological human brain iron overload conditions.

To overcome the limitations of the models explained above, new mouse models of haemochromatosis containing intrinsic mutations in two key iron-related proteins have now been generated, as described below. These genes are *HFE* and *TFR2* as haemochromatosis is commonly caused by mutations in the *HFE* gene and occasionally by mutations in *TFR2* genes (Camaschella et al., 2000; Feder et al., 1996; Papanikolaou et al., 2004). As studies have shown abnormal iron loading in some brain regions such as basal ganglia of haemochromatosis patients, an ideal animal model of haemochromatosis should exhibit brain iron loading along with other obvious signs of the disease like increased serum and liver iron levels (Berg et al., 2000; Johnstone and Milward, 2010d; Nielsen et al., 1995; Rutgers et al., 2007).

1.6.5.1.1 Single HFE knockout mouse model of haemochromatosis

As described in Section 1.6.5, the HFE protein forms a heterodimeric complex with β2-microglobulin and gets processed, transported and expressed on the cell surface (Lebron et al., 1998; Lyon and Frank, 2001; Waheed et al., 1997). Mutations in HFE impair this association and fail to transport HFE out of the endoplasmic reticulum and Golgi compartments, where it is ultimately degraded (Waheed et al., 1997). This results in reduced hepatic expression of hepcidin, hence facilitating increased iron absorption from diet and depositing iron in various tissues (Ganz and Nemeth, 2016).

The HFE gene is the most commonly mutated gene in human haemochromatosis with two common mutations: C282Y and H63D (Feder et al., 1996; Feder et al., 1998b). About 80-90% of haemochromatosis patients have a homozygous C282Y mutation.(Bacon et al., 1999; Feder et al., 1996) Zhou and colleagues generated a mouse model on a C57BL/6J background with targeted deletion of the *HFE* gene. This model showed distinctive histopathological and biochemical abnormalities seen in human C282Y haemochromatosis patients, including increased serum and liver iron measures (Zhou et al., 1998).

Brain iron uptake could be affected by the HFE mutations as the HFE protein is present in the choroid plexus, blood vessels and the ependymal cells. Moreover, additional evidence in AD shows that the HFE protein is induced on neurons, on cells associated with neuritic plaques and on astrocytes linked with blood vessels (Connor et al., 2001). Polymorphisms in HFE have also been proposed to increase AD risk as the chromosomal region 6p21 containing the HFE gene shows genetic association to AD in some studies {Kehoe, 1999 #416;Blacker, 2003 #418;Combarros, 2003 #1074}.

Another study found that onset of AD was 5 years earlier in patients with H63D mutations than in those with the wild-type allele, independent of gender (Sampietro et al., 2001). However, there are other studies which failed to find such association (Ellervik et al., 2007; Johnstone and Milward, 2010d). Johnstone and colleagues examined changes in the brain transcriptome of an $Hfe^{-/-}$ deletion mutant mouse model using microarrays and real-time reverse transcription-PCR (Johnstone et al., 2012c). The mouse strain used was AKR as it maximizes the iron loading phenotype.(Fleming et al., 2001; Johnstone et al., 2012a) Evidence was seen for changes in the brain gene expression profile but not in total brain iron levels as compared to wildtype controls (Golub et al., 2005;

Johnstone and Milward, 2010d; Knutson et al., 2001). Also, while some changes were observed for AD-related transcripts, these were not in directions consistent with increased risk of AD.(Johnstone et al., 2012c)

1.6.5.1.2 *Tfr2Y245X* mutation mouse model of haemochromatosis

The *Tfr2Y245X* mutant mouse model of haemochromatosis (analogous to the *Tfr2*Y250X mutation in human) has a mutated *Tfr2* gene that prevents TFR2 protein expression and the interaction of TFR2 with holotransferrin.(Camaschella et al., 2000; Nemeth et al., 2004) As the hepcidin response is partly blunted in these mice, ferroportin expression is only partially downregulated in response to iron loading, so iron transport into the circulation from the gut is only partially regulated when body iron stores are high, leading eventually to iron loading in the liver and various other organs of the body (Camaschella et al., 2000; Kawabata et al., 2005; Wallace and Subramaniam, 2007; Wallace et al., 2008). Acikyol and colleagues found that this model has significantly higher liver iron levels but again no change in levels of brain iron and no brain transcript changes of strong relevance to AD(Acikyol et al., 2013).

1.6.5.1.3 *Hfe*$^{-/-}$x*Tfr2Y245X* mouse model of haemochromatosis

In the studies reported above, both models showed increased serum iron measures but no tissue damage, corresponding to pre-clinical human iron overload. Also neither of these models shows brain iron loading. Hence, their use in studying the effect of brain iron loading in haemochromatosis is limited.(Acikyol et al., 2013; Graham et al., 2010b; Johnstone et al., 2012a; Johnstone and Milward, 2010c) A double mutation model has now been generated that has both of the above mutations, resulting in higher levels of iron loading (*Hfe*$^{-/-}$x*Tfr2Y245X* on the AKR background strain). To produce this model, mice with deletion of *Hfe* and mice with the Y245X mutation of the *Tfr2* gene were each backcrossed for 10 generations onto an AKR genetic background (Animal Resource Center, Murdoch, Western Australia, Australia). The two genotypes were then cross-bred to generate *Hfe*$^{-/-}$ x*Tfr2*^{mut} mice (Delima et al., 2012).

The double mutation mice had many features consistent with mild clinical human iron overload or haemochromatosis, including two-fold or more increased hepatic and plasma iron levels, elevated markers of hepatic oxidative stress and early liver injury in the form of fibrosis as compared to both single mutation models (Delima et al., 2012). Higher iron measures were found in many brain regions of *Hfe*$^{-/-}$*xTfr2*^{mut} mice compared to age- and gender-matched controls, using inductively coupled plasma-atomic emission spectroscopy, non-haeme iron measurement and ferritin

immunoblotting (>1.4-fold increase, $p<0.002$, $n\geq4$/group) (Heidari et al., 2016b). This mouse model is thus the most useful haemochromatosis model for studying iron loading in the brain as it has concurrent liver damage and brain iron loading.

Furthermore, molecular profiling exhibited alterations in the expression of different iron-related genes, genes associated with the Neurodegeneration with Brain Iron Accumulation (NBIA) disease family and the over-representation of expression changes in myelin-related genes (Heidari et al., 2016b). Such observations corroborate that increase in brain iron levels can affect brain systems. Brain transcript levels of ferritin was increased in this model but transcripts of transferrin (*Tf*), TFR1 (*Tfrc*), ceruloplasmin (*Cp*) and hepcidin (*Hamp1*) were decreased (Johnstone, Heidari et al., unpublished). Increased ferritin and decreased TFR1 expression in this model bolsters the hypothesis that when there is surplus intracellular iron, cells are protected against labile iron by limiting iron uptake and increasing cellular iron storage capacity. Decreased brain hepcidin transcripts suggests that ferroportin on neuronal cell surface is conserved and may contribute to iron export and protection of neurons and other cells against excess iron accumulation. Furthermore, decreased ceruloplasmin and transferrin levels may reduce iron delivery to neurons and protect them against iron overload.

While it is possible that the altered levels of some iron-related transcripts potentially contribute to elevated brain iron levels, some other transcriptomic alterations may not be directly associated with net changes in iron levels but may reflect unknown effects of disruption of *Hfe* and *Tfr2* genes. All three models- the $Hfe^{-/-}$x$Tfr2^{mut}$, the *Hfe*-knockout and the *Tfr2Y245X* mutant mice exhibit increased brain transcripts of the typical immediate-early gene FBJ osteosarcoma oncogene (*Fos)* and the early growth response (*Egr)* gene at three months of age, although no changes in total brain iron concentrations were detected in the single mutation models (Acikyol et al., 2013; Johnstone et al., 2012b). Only the $Hfe^{-/-}$x$Tfr2^{mut}$ mice show increased transcripts of Jun B proto-oncogene (*JunB)*, another important immediate-early transcription regulator, indicating this may explicitly reflect the increased brain iron levels in this model (Johnstone, Heidari et al., unpublished).

Considering these facts, the $Hfe^{-/-}$x$Tfr2^{mut}$ model is suitable for studying effects of excess brain iron accumulation. Nevertheless, as these mice do not exhibit natural AD neuropathology such as plaques and tangles, they are not suitable to be used for deriving any conclusion regarding the effects of iron loading in AD. Considering this limitation, our team has genetically engineered a novel mouse model incorporating mutations in both *Hfe* and *Tfr2* genes along with human

transgenes containing familial AD mutations (described below). To our knowledge, this model is the first of its kind in the world.

1.6.6 Studying the iron-AD relationship using mouse models of AD

The question of whether brain iron dyshomeostasis/ brain iron accumulation causes AD or whether brain iron accumulation/ brain iron dyshomeostasis is just a secondary consequence of neuropathology/ degenerative process of AD is difficult to answer using post-mortem human brain tissues in which AD will already have reached advanced stages, most of the time. Unlike the post-mortem human brain, use of animal models of AD provides an option for studying different phases of disease progression.

1.6.6.1 APPswe/PS1ΔE9 mouse model

The APPswe/PS1ΔE9 mouse model of AD contains modified APP and presenilin1 (PS1) genes under the mouse prion promoter (Xiong et al., 2011). Human Aβ sequence replaces the mouse Aβ sequence (within the mouse APP) and this APP transgene also contains a mutation called the Swedish mutation. The PS1 transgene has exon 9 of the PS1 gene deleted (Haass et al., 1995; Xiong et al., 2011). Both these mutations promote amyloidogenic processing of APP and increase the Aβ1-42/Aβ1-40 ratio (Borchelt et al., 1996; Haass et al., 1995). Deposition of insoluble Aβ aggregates is reported to be observed in the cortex and the hippocampus of these mice by 4 months and plaque numbers increase gradually up to 12 months and beyond (Garcia-Alloza et al., 2006; Jankowsky et al., 2004) with plaque deposition reported to continue till at least 20 months of age in one study (van Groen et al., 2006). Impaired spatial learning and synaptic plasticity are observable by 12 months (Lalonde et al., 2005; Volianskis et al., 2010; Yan et al., 2009).

1.6.6.2 APPswe/PS1ΔE9 *x* $Hfe^{-/-}xTfr2^{mut}$ mouse model

The models of AD have a limitation that they cannot reproduce features of both chronic iron accumulation and AD. To solve this problem, our team has developed a novel mouse model by cross-breeding $Hfe^{-/-}xTfr2^{mut}$ mice with APPswe/PS1ΔE9 (Jackson Labs stock # 004462) mouse model of AD. Mice were backcrossed onto an AKR genetic background to maximize the iron loading phenotype (Fleming et al., 2001; McLachlan et al., 2010). These APPswe/PS1ΔE9 *x* $Hfe^{-/-}xTfr2^{mut}$ mice are referred to as the Aβ+Iron mice. These mice have iron loading as the primary, initial disease phenotype and display chronic brain iron loading and AD-related amyloidosis, simultaneously.

Based on these observations, the Aβ+Iron model was therefore considered as an appropriate model to investigate the effects of increased brain iron loading in the aggravation of cerebral amyloidosis. A broad hypothesis and three specific hypotheses were designed for this purpose which are explained in the following section.

1.7 Hypotheses

This thesis examined the broad hypothesis that high brain iron levels may exacerbate Alzheimer's amyloid pathology. To address this question, the project tested three specific hypotheses in three different chapters.

Hypothesis 1

a) Brain iron level is increased in the Aβ+Iron model as compared to the Aβ model.

b) Excess brain iron may augment cerebral amyloidosis in the Aβ+Iron model as compared to the Aβ model.

c) Excess brain iron may co-localise with insoluble Aβ pathology in the Aβ+Iron model.

Hypothesis 2

Brain iron distribution in different cell types and structures is generally similar in the Aβ+Iron model and the *Hfe*$^{-/-}$*xTfr2*^{mut} model (the 'Iron model') with the main exception of iron associated with amyloid plaques and iron-associated cells in the vicinity of amyloid plaques in the Aβ+Iron model (plaques are not present in the 'Iron model').

Hypothesis 3

Microglia surround amyloid plaques in the mouse models and may have increased intracellular iron content, as has been observed in humans and that increased levels of brain iron may augment oxidative damage or neuronal loss in the mouse model of amyloidosis.

1.8 Aims

Aim 1

To examine brain iron levels and cerebral amyloidosis and to characterise the relationship of iron with insoluble Aβ pathology in the Aβ+Iron model compared to the age-, gender- and strain-matched Aβ model. This will be examined by non-haem iron assay and histochemistry and immunohistochemistry techniques such as single labelling or co-labelling iron and amyloid, using iron and amyloid-specific stains/antibodies.

Aim 2

To examine the relationship between regional iron loading and amyloid plaque location and to characterise the distribution of iron in different brain regions, structures and cell types in the Aβ+Iron model. This will be studied by using histochemistry and immunohistochemistry techniques such as single labelling or co-labelling of iron and amyloid, myelin or different cell types using histochemical stains for iron, amyloid and myelin and immunolabelling of particular cell markers.

Aim 3

To investigate cell damage and neuronal loss and to examine glial co-localisation with amyloid plaques and uptake of iron by microglia or other glia in the Aβ+Iron model compared to the age-, gender- and strain-matched Aβ model. This will involve immunohistochemistry and histochemistry techniques such as labelling with markers for lipid damage or neurons and co-labelling iron, amyloid and glia using iron and amyloid-specific stains and specific markers for microglia or other glia.

2. Materials and methods

2.1 Animals

The APPswe/PS1ΔE9*xHfe*$^{-/-}$*xTfr2*^{mut} mouse model (the 'Aβ+Iron model') was generated by cross-breeding the APPswe/PS1ΔE9 model (the 'Aβ model') of amyloidosis (Jackson Labs stock #004462) with the *Hfe*$^{-/-}$x*Tfr2*^{mut} model (the 'Iron model') of haemochromatosis (Delima et al., 2012; Heidari et al., 2016b). Mice were backcrossed onto an AKR genetic background to maximize the iron loading phenotype (Fleming et al., 2001; McLachlan et al., 2010).

Four groups of mice namely the AKR model, the Iron model, the Aβ model and the Aβ+Iron model, were maintained on a standard AIN-93G diet comprising 0.02% iron (Reeves et al., 1993). These mice were sacrificed at 6 months of age (unless specified otherwise). All protocols were approved by the Animal Ethics Committee of University of Sydney, where the mice were bred and accommodated.

2.2 Iron measures

2.2.1 Tissue collection

Mice were sacrificed under anaesthesia by using 60 mg/kg sodium pentobarbital or Lethabarb (Virbac Pty Limited). An incision was made below the diaphragm, the ribs were cut open and the diaphragm was pricked to expose the heart. A small incision was then made in the right atrium allowing the blood to flow out of it. For histological purposes, mice were perfused through the left ventricle using 20 mL of the freshly made fixative containing 4% paraformaldehyde (PFA) in 0.1M PBS (w/v), pH 7.4. For non-haem iron assay, mice were perfused with isotonic saline.

Following the dissection, mouse brains that were to be used for the non-haem iron assay were snap frozen in liquid nitrogen and immediately stored at -80 ˚C. Brains that were to be used for histology and immunohistochemistry were placed in a tube containing 4% PFA in 0.1 M PBS fixative and stored at 4 ˚C overnight. Next day, the fixative was removed, the brains were washed with PBS and then stored in PBS containing a small amount of (0.01%) sodium azide (Sigma), at 4˚C.

2.2.2 Non-haem iron assay

Non-haem iron levels in brain tissue homogenates (n ≥11/group, with ≥4 per sex in each group) were measured as explained by Kaldor (Kaldor, 1954). All glassware were thoroughly cleaned and

soaked in 2M HCl (MERCK Pty Ltd) overnight and washed with deionised, distilled water (ddH_2O) on the next day. Brain weights were recorded before homogenising on ice in 0.9% cold NaCl (1 ml NaCl per 50 mg tissue; Baxter Healthcare Pty Ltd) in a chilled glass hand-held homogenizer. A standard solution was prepared by diluting ferrous sulphate in 0.1M HCl (MERCK Pty Ltd) to a get a final iron concentration of 5 mM. This standard solution was then diluted in ddH_2O in separate Eppendorf tubes to obtain various concentrations of standard iron solutions in the range of 0 to 8 µg/ml iron.

Next, 150 µl of 12% HCl (50 µl per reaction mix) was added to a triplicate reaction mix of tissue homogenate (100 µl) and standard iron solution (100 µl), vortexed and then incubated at 85°C for 30 min. This was followed by addition of 75 µl of 50% trichloroacetic acid (25 µl per reaction mix; MERCK Pty Ltd) into the triplicate reaction mix, chilling on ice for 10 min and then centrifugation for 15 min at 16,000 rpm to allow protein precipitation. The supernatant containing iron (100 µl) was then combined with the colour reagent (100 µl; 816 µM bathophenanthroline disulfonic acid, 1.9 M sodium acetate, 0.2% (v/v) thioglycolic acid; all from Sigma-Aldrich) and incubated at RT for 60 min. The optical density (OD) of individual standard iron solutions was measured at 540 nm, based on which a standard curve was created. This curve enabled the determination of iron concentrations in various tissue samples, which were assayed.

2.3 Histology

2.3.1 Preparation of tissue sections for histology

2.3.1.1 Preparation of brain slices

Mouse brains were taken out of the PBS azide solution using a sterile spatula. Brains were placed (with the ventral side up and the dorsal side down) into a mouse brain slicer matrix (Zivic Instruments), containing a few drops of PBS (to avoid tissue drying). Five razor blades were inserted into 5 slice channels in the coronal orientation to obtain 6 brain blocks, each with a thickness of 2 mm. Brain slices were then stored in separate wells of a 24-well plate containing PBS and 0.01% sodium azide at 4˚C.

2.3.1.2 Selection of brain blocks

A mouse brain atlas (Paxinos, 2013) was used to select brain blocks 4 and 5 for this thesis. These blocks contained structures strongly affected in AD, namely hippocampus, entorhinal cortex and the cerebral cortex. Names of all brain structures in this thesis are accordant with the nomenclature of the mouse brain atlas (Paxinos, 2013).

2.3.1.3 Slide coating

Microscope slides need to be treated with some adhesive compounds so that the tissue sections are retained on the slides during the histological procedures. Slides (Livingstone) were immersed in clean water containing (3g/litre) Pyroneg detergent powder (Diversey) and then incubated at 50^0C overnight. Next day, the slides were washed in running tap water for 1 hour, and then in running de-ionised water for 30 minutes.

A solution containing 2% Gelatin (Sigma) and 0.1% Chromium potassium Sulfate (Sigma) was prepared while stirring at 50^0C on a hotplate, until the solution was clear. After the solution was cooled to 20-30^0C, the slides were placed in this solution for 20 minutes. This was followed by drying in an oven at 50^0C overnight. The slides were then kept in 0.004% poly L-lysine (Sigma) in 1% Tris HCl (UNIVAR) (1 M, pH 8) for 15 minutes and dried at 50^0C overnight. Dried slides were stored safely in paper boxes, at RT.

2.3.1.4 Cryoprotection and tissue sectioning

Sucrose is commonly used as a cryoprotectant to prevent formation of ice crystal artefact in frozen tissue specimens. Mouse brains (blocks 4 and 5) were kept in 15% sucrose (MERCK) in 1X PBS (pH 7.4) at 4^0C for 24 hours and then in 30% sucrose in 1X PBS at 4^0C for another 24 hours. In both of these steps, it was ensured that the brain blocks sank completely in the sucrose and PBS solution. Brain blocks were then embedded in cryomolds containing TissueTek Optimal Cutting Temperature Compound (OCT) (SAKURA) and snap-frozen indirectly in 2-methylbutane (Sigma) and liquid nitrogen. The cryomolds were stored at -20^0C until they were used for sectioning.

Brain blocks were sectioned coronally at 20 µm using Leica CM1900 cryostat (Leica Microsystems, Wetzlar, Germany) at -20^0C, mounted on slides (coated as above in Section 2.3.1.3) and then stored at -20^0C.

2.3.1.5 Selection of brain sections for histology

Four brain sections per mouse from all groups (n=4/group, 2 males and 2 females in each group, 6 months old) were selected at a sampling rate of 1 in 10, starting from -2.46 mm Bregma to -3.16 mm Bregma (Fig. 2.1). These sections incorporated structures strongly affected in AD, namely hippocampus, entorhinal cortex and the cerebral cortex. As each section is of thickness 20 µm, selection of sections as described above allowed us to sample approximately 600 µm of mouse brain.

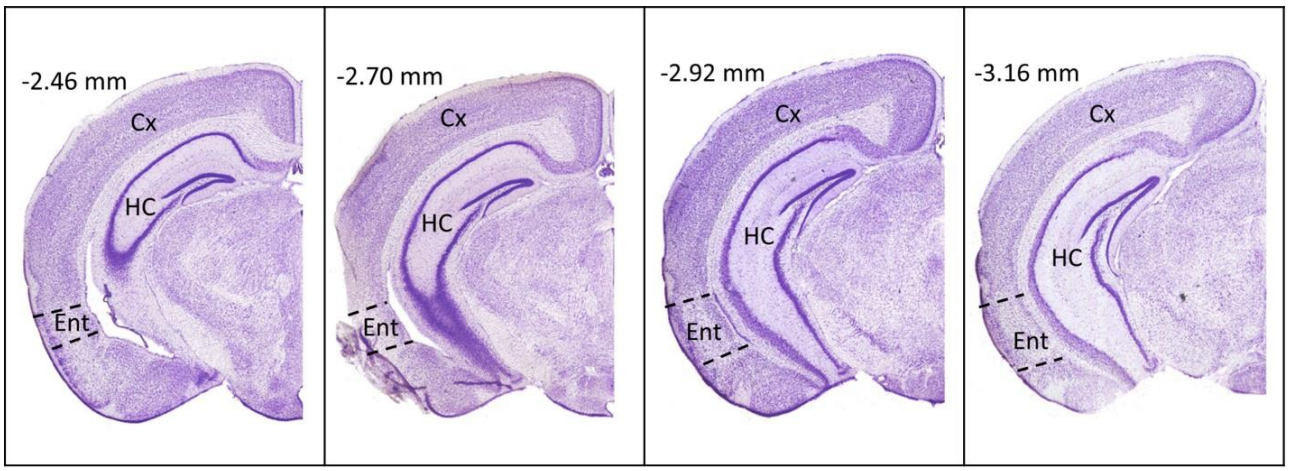

Fig. 2.1 Selection of mouse brain sections. Brain blocks containing the regions that enclosed -2.46 Bregma to -3.16 Bregma were selected as they comprised huge extents of hippocampus (HC) and cerebral cortex (Cx), particularly entorhinal cortex (Ent). These structures are reported to be strongly affected in AD. Images copied from the mouse brain atlas (Paxinos, 2013).

2.3.2 Iron staining by DAB-enhanced Perls' stain and DAB-enhanced Turnbull stain

3'3'-diaminobenzidine-tetrahydrochloride (DAB)-enhanced Perls' staining protocol was followed to detect iron in brain sections of the Aβ+Iron model and the Aβ model (Nguyen-Legros et al., 1979). This method is routinely used to visualise ferric iron in various tissues but it is also known to detect some ferrous iron (Meguro et al., 2007). Additionally, DAB-enhanced Turnbull staining was done separately to detect ferrous iron specifically.

Slides were incubated at 37^0C for 1 hour to allow the sections to dry. They were kept in 70% ethanol (UNIVAR) for 10 minutes to remove the Optimal Cutting Temperature Compound and rehydrated using ddH_2O for 10 minutes. These steps were adopted as three standard processes at the beginning of all histological or immunohistochemical staining procedures which will not be explained hereafter, unless there's a mention of any change in protocol.

Tissue sections were incubated either in the Perls' solution or in the Turnbull solution, based on the purpose of the experiment (i.e., to detect ferrous or ferric iron as described above). For Perls' staining procedure, sections were incubated in freshly prepared Perls' solution (1% potassium ferrocyanide (AnalaR), pH <1) for 30 minutes. For Turnbull staining, sections were kept in freshly prepared Turnbull solution (1% potassium ferricyanide (AnalaR), pH <1). All of the other steps were same for both stains.

After washing with ddH_2O (3x2 mins), sections were incubated in methanol (Fronine) containing 0.01M NaN_3 (MERCK) and 0.3% H_2O_2 (Sigma) for 1 hour. This was followed by washing with

0.1M PBS (3x2 mins) and then incubation in 0.025% 3'3'- Diaminobenzidine-4HCl (DAB) (MP Biomedical) and 0.005% H_2O_2 in 0.1M PBS (pH 7.4) for 30 minutes. After washing the sections with ddH_2O (3x2 mins), they were dehydrated by ethanol washes – 50%, 70%, 90%, 100% (twice) for 2 minutes each, cleared with xylene (VWR) and coverslipped using DEPEX mounting medium (BDH Chemical).

2.3.3 Iron staining by perfusion Turnbull method

Due to the possible loss of loosely bound iron or the oxidation of non-haem ferrous iron during tissue treatment, it is difficult to visualise ferrous iron using the traditional Turnbull staining method. On the other hand, transcardial perfusion of Turnbull solution allows the formation of insoluble and stable compounds of non-haem ferrous iron before the tissue treatment, hence facilitating the visualisation of ferrous iron (Meguro et al., 2003).

The perfusion Turnbull method uses cardiac perfusion of anaesthetised mice with a Turnbull stain solution of 1% potassium ferricyanide in 10% formalin, followed by post-fixation in 10% formalin after the brain is removed (Meguro et al., 2003).

Brain sections perfused with the Turnbull solution were then subjected to the same procedure as the traditional Turnbull staining method (Section 2.3.2) except with the modification that brain sections were pre-incubated and dried at 37 degrees overnight.

2.3.4 Myelin staining

Brain sections were delipidated overnight in 70% ethanol at RT. Sections were washed with ddH_2O for 10 min and then incubated in the Luxol Fast Blue solution (IHC World LFB Kit) at 56˚C overnight (ensuring no longer than 16 hours for frozen sections). Excess stain was removed with 95% ethyl alcohol for 30 sec, followed by washing in ddH_2O for 1 min.

Sections were differentiated in lithium carbonate solution (IHC World LFB Kit) for 1 min. Differentiation was continued in 70% ethyl alcohol for 1 min and then sections were briefly washed with ddH_2O. Sections were checked under a microscope to make sure that the gray matter was clear and white matter was sharply defined. Sections were then dehydrated in 100% ethanol 2x5 min and then cleared with 2x5 min xylene washes. Slides were mounted with DEPEX and then coverslipped.

2.3.5 Bright field imaging

Sections stained with DAB-enhanced Perls' stain, Turnbull stain and Luxol Fast Blue stain were scanned using Qlympus DP72 and ZEISS Axio Scan.Z1 Slide Scanner (Bosch Institute, University of Sydney).

2.3.6 Immunohistochemistry

2.3.6.1 Immunofluorescence method

At least four brain tissue sections from the Aβ+Iron model and the Aβ model were included in each immunolabelling experiment. The cryostat sections were soaked in PBST (0.01 M sodium phosphate buffer, pH 7.4, containing 0.1% Triton X 100 (Sigma) for 30 min on a shaker. Where antigen retrieval was needed, slides were treated with 10mM sodium citrate (Merck) and 0.1% Triton (pH 6) and kept in hot water bath (95 degrees) for 20 min. Sections were allowed to cool at RT for 20 min and washed in PBS 2x5 min.

A water repellent circle was drawn around brain sections using PAP-PEN liquid blocker. Sections were covered with a blocking solution prepared by diluting normal goat serum/NGS (Sigma) to 10% in PBS and kept horizontally within a humidified chamber on a shaker for 1 hour (at RT). This was followed by incubation in primary antibody (Table 2-1) diluted in 1% NGS, at 4^0C overnight. In each run, a negative control was included, which did not contain primary antibody.

After an overnight incubation, sections were washed in 0.1M PBS for 15 min (thrice) on shaker. Note that separate containers were used for the negative control and test slides for this step and any other washing step following through in the protocol. Secondary antibody diluted in 1% NGS was used to cover all sections, including the negative control in a humidified chamber. The chamber was covered with aluminium foil and kept on shaker at RT for 1 hour. Note that the concentrations of various primary and secondary antibodies are mentioned in Table 2-1.

From this stage onwards, care was taken to prevent light from coming in contact with slides as it could quench the fluorescence of secondary antibody. Slides were rinsed in 0.1M PBS for 15 min (thrice) and then coverslipped with antifade aqueous mounting medium (Sigma). They were stored at 4^0C until visualised using a fluorescent microscope.

2.3.6.2 Horse radish peroxidase (brightfield) method of immunohistochemistry

The Horse Radish Peroxidase (HRP) method is a widely accepted avidin/biotin-based immunoperoxidase detection system. Vectastain ABC-HRP kit (Vector Laboratories, Catalog no PK-6200) was used for brightfield immunolabelling. Sections were incubated in 0.3% H_2O_2 in PBS for 30 mins (for quenching endogenous peroxidase). All solutions were prepared as per the instructions of the kit. Sections were then blocked with 10% normal horse serum for 20 mins. This was followed by primary antibody incubation for 30 mins and then washing in PBS (2x2 min).

Sections were then incubated in biotinylated universal secondary antibody for 30 mins. Sections were washed twice in PBS for 2 mins and incubated in Vectastain ABC-HRP reagent for 30 mins and washed for 5 mins in PBS. Following this, the sections were incubated in SG substrate solution (made immediately before use) for 5 minutes. Slides were rinsed with ddH_2O, dehydrated using 3 exchanges of 100% ethanol, cleared using 2 changes of xylene (2 min each) and mounted using DEPEX mounting medium (BDH Chemical).

Table 2-1 Antibodies used for immunohistochemistry

Primary antibody	**Host species**	**Catalogue number**	**Company**	**Dilution factor of primary antibody**	**Dilution factor of secondary antibody**
Neuronal nuclear (NeuN)	Mouse	MAB377	Merck Millipore	1:100	1:100
Ferritin Heavy (H)	Mouse	sc-376594	Santa Cruz	1:50	1:500
Ferritin Light (L)	Mouse	sc-74513	Santa Cruz	1:50	1:500
Anti-β-Amyloid (4G8)	Mouse	SIG-39220	Jomar Bioscience	1:500	N/A*
Ionized calcium-binding adapter molecule 1 (Iba1)	Rabbit	WDJ3047	WAKO	1:500	1:200
Glial fibrillary acidic protein (GFAP)	Rabbit	Z0334	DAKO	1:200	1:300
2',3'-cyclic nucleotide 3' phosphodiesterase (CNPase)	Rabbit	sc-30158	Santa Cruz	1:100	1:100
4-Hydroxynonenal (4-HNE)	Rabbit	HNE-11S	Alpha Diagnostic	1:100	1:200

Note: Goat anti-mouse Alexa Fluor® 488 secondary antibody (A-11029; Thermo Fisher Scientific) was used for NeuN, Ferritin H and Ferritin L antibodies; goat anti-rabbit Alexa Fluor® 488 secondary antibody (A-11034; Thermo Fisher Scientific) was used for Iba1, GFAP, CNPase and 4-HNE antibodies. *Biotinylated universal secondary antibody (Vectastain ABC-HRP kit) was prepared according to instructions in the kit and used for 4G8 labelling. Vectastain protocol was also followed for Iba1 labelling, for the purpose of microglial quantification (Chapter 5).

2.3.6.3 Co-labelling of DAB-enhanced Perls' stain with various antibodies

DAB-enhanced Perls' staining followed by immunofluorescence labelling (and not the other way round) is a routine procedure followed in our lab so that fluorescence of secondary antibody gets preserved and fading is minimised. Even with the ABC-HRP method, same order was followed for consistency.

2.3.6.4 Imaging

Imaging was done by three different methods, which are mentioned in the respective contexts of different chapters of this thesis.

1) Using the CellSens 1.12 digital imaging software platform and Olympus DP72 microscope (Medical Sciences Building, The University of Newcastle).
2) Using the ZEISS Axio Scan.Z1 Slide Scanner system (Bosch Institute, University of Sydney).
3) Using the Leica DM2700P polarised light microscope (Earth Sciences Building, The University of Newcastle).

2.4 Iron and amyloid co-localisation studies

2.4.1 Visualisation of amyloid with Congo red stain (Modified Puchtler's method)

Modified Puchtler's method was used for Congo red labelling of amyloid (Puchtler et al., 1962). 100 ml Congo red stain (52 mg/ml) was prepared in advance as the stock solution. Slides were kept in 80% ethanol saturated with NaCl in a humidified chamber for 20 min. Working solution was prepared by adding 1 ml of 1% NaOH per 100 ml Congo red stock solution, which was then used to stain slides for another 20 min. Slides were dehydrated quickly in 3 changes of 100% ethanol, cleared in xylene and mounted in DEPEX. Slides were air dried overnight and then refrigerated.

Amyloid was visualised using two standard methods. In both methods, the same parameters (exposure time, magnification, light intensity, brightness, etc.) were maintained for all images to be analysed. The first approach was the visualisation of structures which appear pinkish red under the bright field of ZEISS Axio Scan.Z1 Slide Scanner; then subsequent visualisation of the same structures under the Texas Red filter set (excitation wavelength 542-582 nm, emission wavelength 604-644 nm). This approach is stated to be highly sensitive but less specific (Linke, 2006)as false positive results may be obtained by detection of aberrant particles (eg. dirt), or some other proteins with β-pleated sheet secondary structure (Khurana et al., 2001; Linke, 2006). This method will be mentioned as Congo red fluorescence method in this thesis.

The second approach was use of Leica Petrog software for Leica DM2700P polarised light microscope to view amyloid under 90° crossed polarisers. This method is known to be less sensitive but highly specific as only the structures that emit yellow-green birefringence when bound to Congo red are detected (Linke, 2006; Puchtler et al., 1962). This method will be called the Congo red polarisation method hereafter. The overlapping images spanning one brain hemisphere were captured and then stitched together using the Stitching plugin of Fiji distribution of ImageJ (Preibisch et al., 2009a).

2.4.1.1 Amyloid detection by Congo red fluorescence technique

Sections stained with Congo red solution were scanned at 10x objective using the ZEISS Axio Scan.Z1 Slide Scanner system (Bosch Institute, USyd) and analysed using a semi-automated approach in Fiji distribution of ImageJ. A user-defined algorithm was developed which allows conversion of the images into black and white (8 bit), background subtraction and applying threshold to remove background without losing the required signal (Fig. 2.2).

A user-defined algorithm allowed the measurement of number, area and density of Congo red positive structures and the percentage of the image containing Congo red positive pixels above the threshold. After finishing the algorithm, a ‘mask’ was generated which displayed the objects counted as Congo red positive structures with numbered labels. This mask was overlayed with the original image to see if any aberrant particles were counted and also to manually count any objects that were missed by the algorithm.

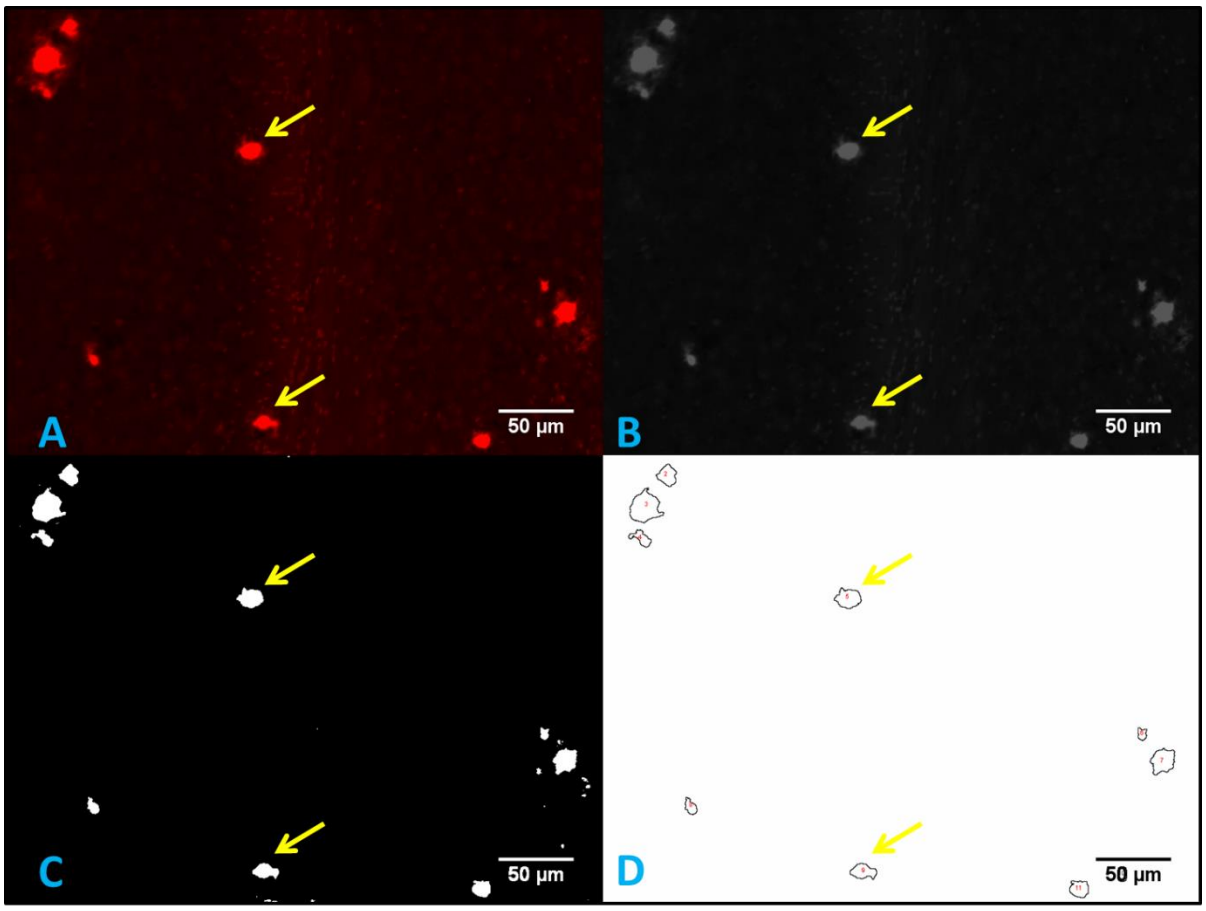

Fig. 2.2 Detection and quantification of amyloid deposits using Congo red fluorescence technique. Amyloid deposits were detected by red Texas filter set of fluorescence microscope (A) A user-defined algorithm in Fiji distribution of ImageJ allowed conversion of the image into 8-bit and background subtraction (B), applying threshold (C) and quantification (D).

2.4.1.2 Amyloid detection by Congo red polarisation technique

Sections stained with Congo red solution were visualised at 10x objective using Leica DM2700P polarised light microscope. Overlapping images were captured as tiles and stitched together using the Stitching plugin in ImageJ (Preibisch et al., 2009b). Application of colour threshold function in a user-defined algorithm detected percentage of the image containing Congo red positive pixels above the threshold (in this case 'yellow-green' birefringence). Then, manual counting of yellow-green birefringent structures was done using ImageJ to get the total number of amyloid plaques (Schindelin et al., 2012).

2.4.2 Co-labelling of DAB-enhanced Perls' stain with Congo red stain

Optimisation of protocol for co-labelling of Congo red stain and DAB-enhanced Perls' stain is shown in Fig. 2.3. When stock concentration (52 mg/ml) of Congo red stain was applied before DAB-enhanced Perls' staining procedure, a very blunt staining was observed for the Congo red

positive objects, under both brightfield and red Texas filter of the fluorescence microscope (panel A). Use of stock concentration of Congo red after the DAB-enhanced Perls' staining protocol gave good fluorescence signal but Congo red staining was very strong under brightfield, which appeared to dominate the brown staining of DAB-enhanced Perls' stain (panel B). When the concentration of the Congo red solution was reduced to 13 mg/ml, and the Congo red stain was applied after the DAB-enhanced Perls' staining protocol, optimum staining was obtained as details of both stains were preserved (Panel C).

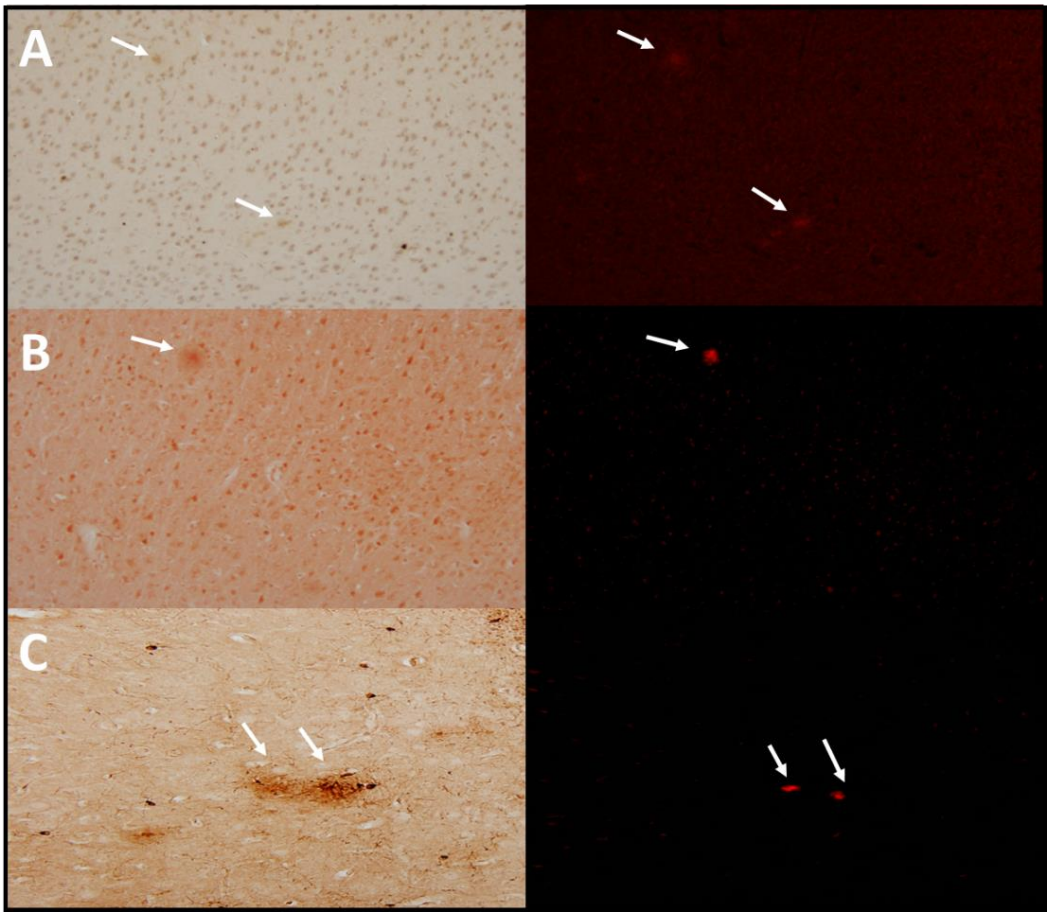

Fig. 2.3 Optimisation of combined Congo red staining and DAB-enhanced Perls' staining procedure. (A) Application of Congo red stock solution (52 mg/ml) before DAB-enhanced Perls' staining procedure resulted faint staining of Congo red positive objects under brightfield and fluorescence microscopy. (B) Application of Congo red stock solution (52 mg/ml) after the DAB-enhanced Perls' staining protocol gave good fluorescence signal but affected the brown coloration of DAB-enhanced Perls' stain. (C) When 13 mg/ml Congo red solution was applied after DAB-enhanced Perls' staining protocol, fine staining was obtained. Left panels illustrate brightfield imaging and right panels illustrate fluorescence imaging.

2.5 Quantification of Iba1-labelled microglia surrounding amyloid plaques

Brain sections were selected at a sampling rate of 1 in 10, starting from -2.46 mm Bregma to -3.16 mm Bregma (n=4 mice/group). For simultaneous detection of amyloid plaques and microglia, brain sections were co-labelled with the Congo red stain for amyloid plaques (13 mg/ml) and the ionized calcium binding adaptor molecule 1 (Iba1) antibody using the Vectastain Elite ABC horseradish peroxidase universal kit (Vector Laboratories, Catalog no. PK-6200). Z-stacked images were taken using the 20X magnification of the ZEISS Axio Scan.Z1 Slide Scanner.

Fiji distribution of ImageJ was used for manual quantification of Iba1-labelled microglia surrounding amyloid plaques. Specifically, Iba1-labelled microglia concentrated around plaques were selected and quantified using the built-in 'multi-point tool' in ImageJ (Fig. 2.4).

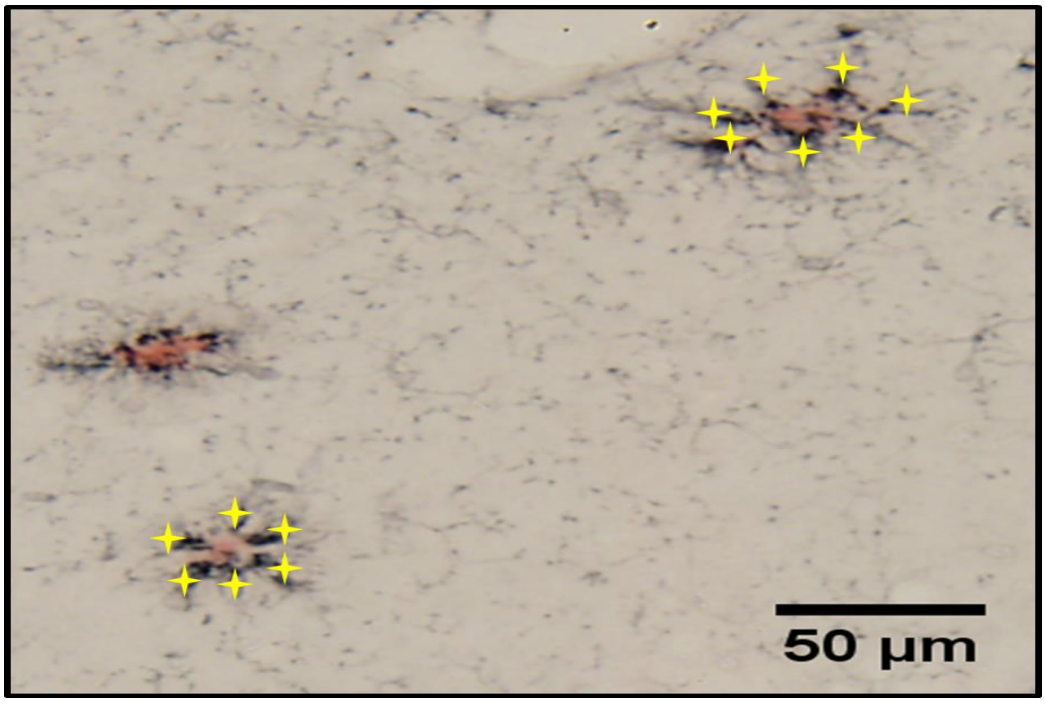

Fig. 2.4 Manual counting of Iba1-labelled microglia around amyloid plaques. Microglia labelled with the ionized calcium binding adaptor molecule 1 (Iba1) antibody were quantified around amyloid plaques by using the multi-point tool of ImageJ (illustrated by yellow stars).

2.6 Estimation of neuron count

Immunofluorescence labelling for neurons in brain tissue sections was done using neuronal nuclear (NeuN) antibody (1:100 dilution) and Alexa Fluor 488 secondary antibody (1:100 dilution). Imaging was done at 20X magnification with FITC filter set (excitation 493nm, emission 520nm) of the ZEISS Axio Scan.Z1 Slide Scanner (Bosch Institute, USyd). Automated counting method was

employed for quantification of NeuN immunoreactive structures in Fiji distribution of ImageJ, as described below.

Images of brain sections stained with NeuN antibody were first converted to 8-bit grayscale images. This was followed by background subtraction and adjusting the threshold, in order to enable background removal without losing the required signal. NeuN immunoreactive structures were then quantified using the 'analyse particles' function of ImageJ (Fig. 2.5).

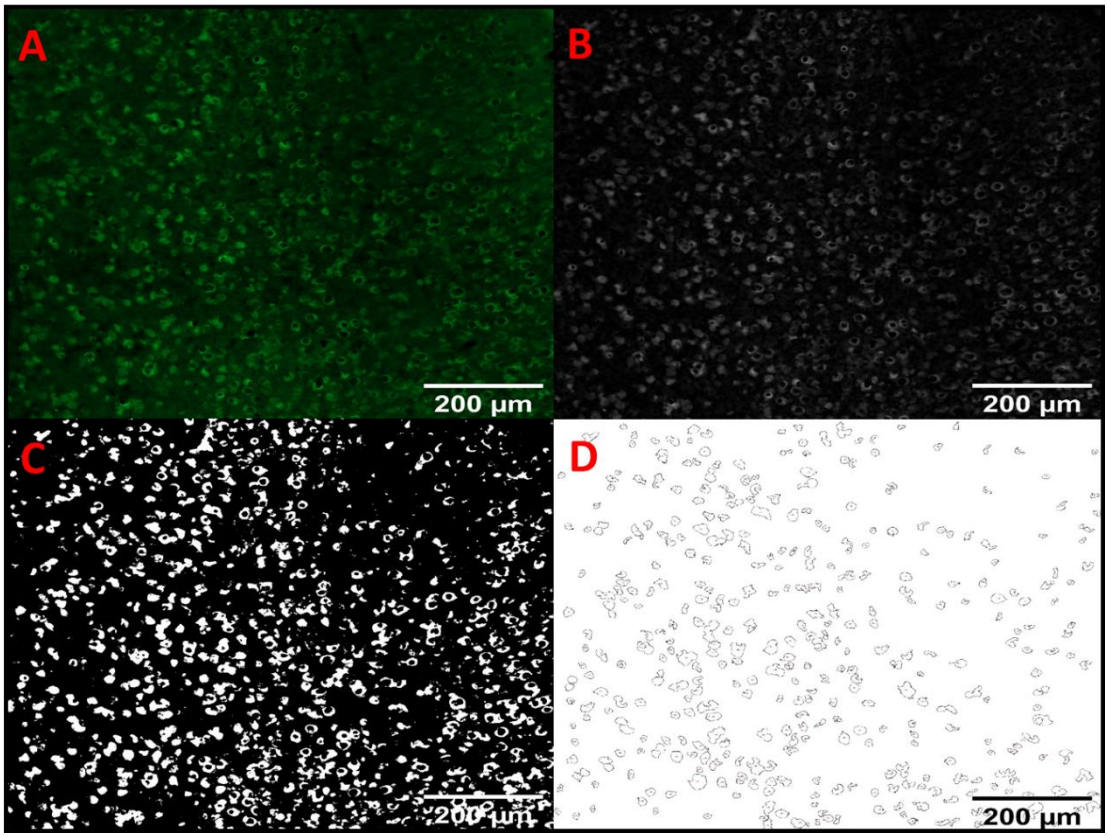

Fig. 2.5 Automated quantification of neurons using ImageJ. Brain section labelled for neurons using NeuN antibody (A); conversion of the image into 8-bit and background subtraction (B); adjusting threshold to highlight NeuN immunoreactive objects (C) and automated quantification (D).

3. Investigation of amyloid deposition in the brain of the Aβ+Iron mouse model

3.1 Introduction

As described in Section 1.6, a question that has been in debate for some time is whether brain iron dyshomeostasis contributes to the exacerbation of Alzheimer's disease (AD) related pathology. To investigate this, a mouse model has been developed which displays chronic brain iron accumulation and characteristics of AD, simultaneously. The *Hfe*$^{-/-}$*xTfr2*^{mut} mouse model of haemochromatosis (the 'Iron model') has now been established as a suitable model for studying chronic brain iron accumulation (Heidari et al., 2016b). However, as previously described in the General Introduction (Section 1.6.5.1.3), the Iron model does not display natural AD neuropathology (e.g. cerebral amyloidosis), making this an unsuitable model to study the effects of brain iron accumulation in AD, unless some AD mutations are added into it.

This limitation led our team to crossbreed the Iron mice with the APPswe/PS1ΔE9 mouse model of amyloidogenesis (the Aβ model) to develop the APPswe/PSEN1dE9x*Hfe*$^{-/-}$*xTfr2Y*^{245X} mouse model, also referred to here as the 'Aβ+Iron' model (Section 2.1). Earlier studies have reported clear visualisation of amyloid plaques and AD-related symptoms in the APPswe/PS1ΔE9 mice by six months of age (Garcia-Alloza et al., 2006; Jankowsky et al., 2004). Similarly, a substantial amount of iron accumulation in various brain regions has been previously described in the 6 month old Iron model (Heidari et al., 2016b), making this a suitable age for studying effects of increased brain iron on Alzheimer's amyloid-related pathology.

This chapter tests the first hypothesis of this thesis which is divided into three parts: a) brain iron level is increased in the Aβ+Iron model as compared to the Aβ model; b) excess brain iron may augment cerebral amyloidosis in the Aβ+Iron model as compared to the Aβ model; c) excess brain iron may co-localise with insoluble Aβ pathology in the Aβ+Iron model.

To address these hypotheses, brain iron was detected using 3,3'-diaminobenzidine tetrahydrochloride (DAB)-enhanced Perls' histochemical staining and brain non-haem iron levels were measured by non-haem iron assay in the Aβ+Iron model and compared with the age-, gender- and strain-matched Aβ model. Brain distribution and localisation of Alzheimer's amyloid-related pathology in the brains of the Aβ+Iron model as compared to the age-, gender- and strain-matched Aβ model was examined using an amyloid-specific stain called Congo red. Co-localisation of iron and amyloid was assessed using double-labelling of DAB-enhanced Perls' stain with either Congo red stain or the monoclonal antibody 4G8, recognising Aβ peptide.

3.2 Materials and methods

3.2.1 Mice and tissue collection

The generation of the Aβ+Iron model and the Aβ mouse model is described in (Section 2.1). Mice were fed a standard AIN-93G diet containing approximately 0.02% iron (Reeves et al., 1993). All protocols were approved by the Animal Ethics Committee of the University of Sydney where the mice colonies were bred and maintained.

3.2.2 Non-haem iron assay

Mice (n ≥11/group, with ≥4 per sex in each group) were anaesthesized and perfused with PBS. Brains were dissected, snap frozen in liquid nitrogen and stored at -80°C (Section 2.2.1). Brain non-haem iron levels were quantified for the Aβ mice and the Aβ+Iron mice, using the protocol described by Kaldor (Kaldor, 1954) which is detailed in General methods (Section 2.2.2).

3.2.3 Histological studies

Brains were dissected and fixed in 4% PFA (Section 2.2.1). Brain blocks were cryosectioned into 20 micron thick sections and transferred onto gelatin-coated slides (Section 2.3.1.3). Four brain sections from each mouse for both groups of mice (n=4 mice/group) were selected at the rate of 1 in 10 starting from -2.46 mm Bregma to -3.16 mm Bregma as described in (Section 2.3.1.5). Based on Paxinos and Franklin's mouse brain atlas (Paxinos, 2013), these regions contained structures strongly affected in AD, namely hippocampus, entorhinal cortex and the cerebral cortex.

3.2.4 DAB-enhanced Perls' staining for iron

As described in General Methods chapter (Section 2.3.2), 3'3'-diaminobenzidine tetrahydrochloride (DAB) enhanced Perls' staining was used to detect iron in brain sections of the AKR model, the Iron model, the Aβ model and the Aβ+Iron model (n=4/group).

3.2.5 Labelling of amyloid plaques

As described in General Methods chapter (Section 2.4.1), the modified Puchtler's method of Congo red staining was used to detect amyloid plaques (Puchtler et al., 1962). Images were taken under the Texas red filter of fluorescence microscope as well as under the polarised light microscope.

3.2.6 Double labelling of iron and amyloid plaques

As detailed in General Methods Chapter (Section 2.4), DAB-enhanced Perls' staining was performed on brain sections of Aβ+Iron mice and Aβ mice. This was followed by Congo red staining on the same brain tissue sections for simultaneous detection of iron and amyloid plaques.

Additionally, on other sections, the monoclonal antibody 4G8 recognising Aβ peptide was used subsequent to DAB-enhanced Perls' stain, in order to visualise deposits of Aβ peptide in addition to deposits that correspond to classical Aβ amyloid and are detected by Congo Red. The use of immunolabelling with antibodies against Aβ peptide such as antibody 4G8 or antibody 6E10 is able to reveal the presence of the peripheral zone, which might be missed by Congo red-based methods, as well as the central core of classical plaques (Rajamohamedsait and Sigurdsson, 2012; Wisniewski et al., 1989).

3.2.7 Characterisation of iron-amyloid plaques co-localisation

Double labelling of DAB-enhanced Perls' stain and Congo red stain under bright field microscopy revealed amyloid plaques (pink) surrounded by 'iron halos' (brown) in the brains of both of the Aβ mice and the Aβ+Iron mice (Fig. 3.14). These plaques were referred to as Perls'-positive plaques and any plaque that appeared free of iron halo was termed Perls'-negative plaque. Two circles were manually drawn around each Perls'-positive plaque using Fiji distribution of ImageJ - the inner circle enclosed the amyloid plaque and the outer circle enclosed both the amyloid plaque and iron halo. Hence, the region of interest was a doughnut ring-shaped structure which covered the area of the iron halo only. Though this analysis was done using brightfield images, the pink coloured Congo red stained objects were also checked for Congo red-positivity by fluorescence microscopy.

3.2.8 Statistical analyses

GraphPad Prism 7 software was used for statistical analysis and data plotting. Brain non- haem iron measures in the Aβ+Iron mice and the Aβ mice were compared by unpaired *t*-tests. Different parameters of Congo red staining and DAB-enhanced Perls' staining in the Aβ+Iron mice and the Aβ mice were compared by unpaired *t*-tests and two-way ANOVA, with Sidak's multiple comparisons test. Sidak's method was used as it has more power than other tests of multiple comparisons (GraphPad Prism version 7).

3.3 Results

3.3.1 DAB-enhanced Perls' staining for iron in four mouse models

DAB-enhanced Perls' staining demonstrated iron distribution across different anatomical regions in the AKR model, the Iron model, the Aβ model and the Aβ+Iron model (Fig. 3.1). As expected, more iron staining was observed in the Iron model compared to the age-matched AKR model, which has been previously published by our group (Heidari et al., 2016b). Furthermore, more iron staining was observed in the Aβ+Iron model compared to the age-matched Aβ model. The heterogeneous distribution of iron and more detailed analyses of how this is related to plaques are further considered in Chapter 4 (Section 4.3.1).

To demonstrate the iron staining difference between the Aβ+Iron model and the Aβ model in more detail, a digitalised version of coronal hemisphere sections from these models has also been included in the figure below (Fig. 3.1).

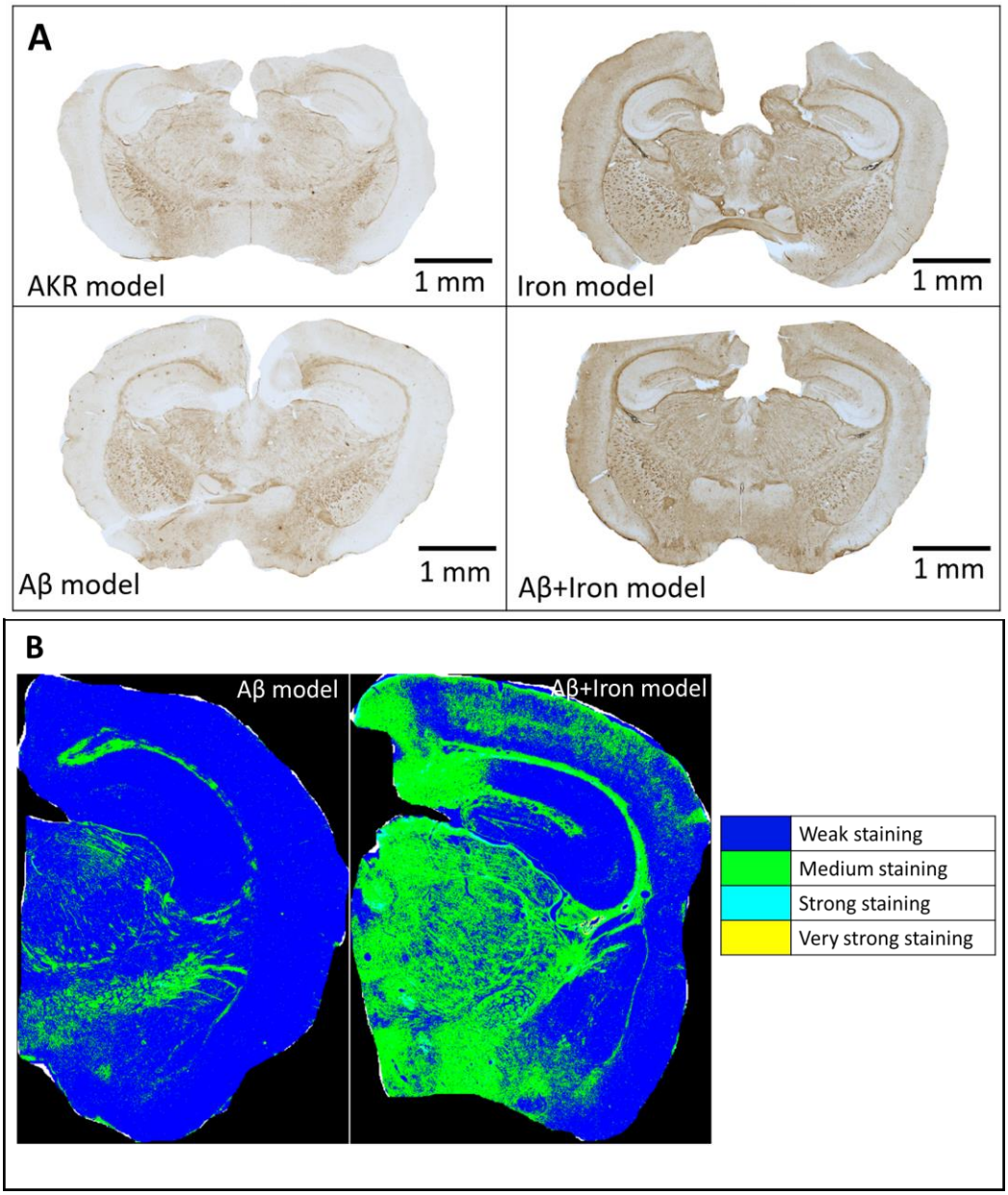

Fig. 3.1 Iron labelling by DAB-enhanced Perls' staining in different mouse groups. (A) Iron labelling by DAB-enhanced Perls' stain was relatively stronger in the Iron model compared to the AKR model and the Aβ+Iron model compared to the Aβ model. (B) The figure below is an example of digitally coloured images illustrating percentage positive pixels for different levels of DAB-enhanced Perls' staining in (A) Aβ model and (B) Aβ+Iron model. Based on pixel intensity values, a user-defined algorithm classified each brain image into areas of weak (0 to 63, dark blue), medium (64 to 127, green), strong (128 to 191, cyan) and very strong (192 to 255, yellow) Perls' staining. Such classification permits binning of intensities of Perls' staining for image analysis.

When traditional Perls' Prussian blue stain was used alone without enhancement by DAB, the choroid plexus was the only region that had discernible staining in the Aβ+Iron model whereas there was little if any apparent staining in the absence of DAB enhancement in the Aβ model.

Consistent with this, there was Prussian blue staining in the choroid plexus in the brains of the Iron model but not in the wildtype model (Fig. 3.2).

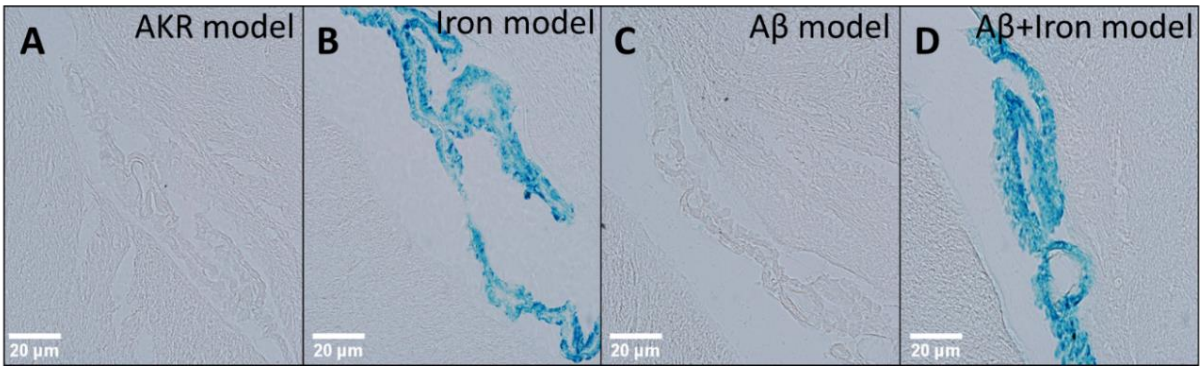

Fig 3.2 Prussian blue staining for detection of iron. Some staining was seen with Prussian blue solution without DAB enhancement in the choroid plexus region of the Iron model and the Aβ+Iron model but not in the Aβ model and the AKR model, while most of the other brain regions remained unstained. A) AKR model B) Iron model C) Aβ model D) Aβ+Iron model. All mice were examined at 6 months of age.

3.3.2 Brain non-haem iron is increased in the Aβ+Iron mice

At 6 months of age, whole brain homogenates of Aβ+Iron mice contained higher levels of non-haem iron than age-matched Aβ mice, for both sexes (Fig. 3.3, (fold change ≥ 1.8, n ≥11/group, with n ≥4 per sex in each group, unpaired *t*-test, $p<0.0001$). It was observed that female mice had significantly lower non-haem iron levels than male mice in both groups (approximately 26% lower in Aβ mice and 35% lower in Aβ+Iron mice; both $p<0.05$).

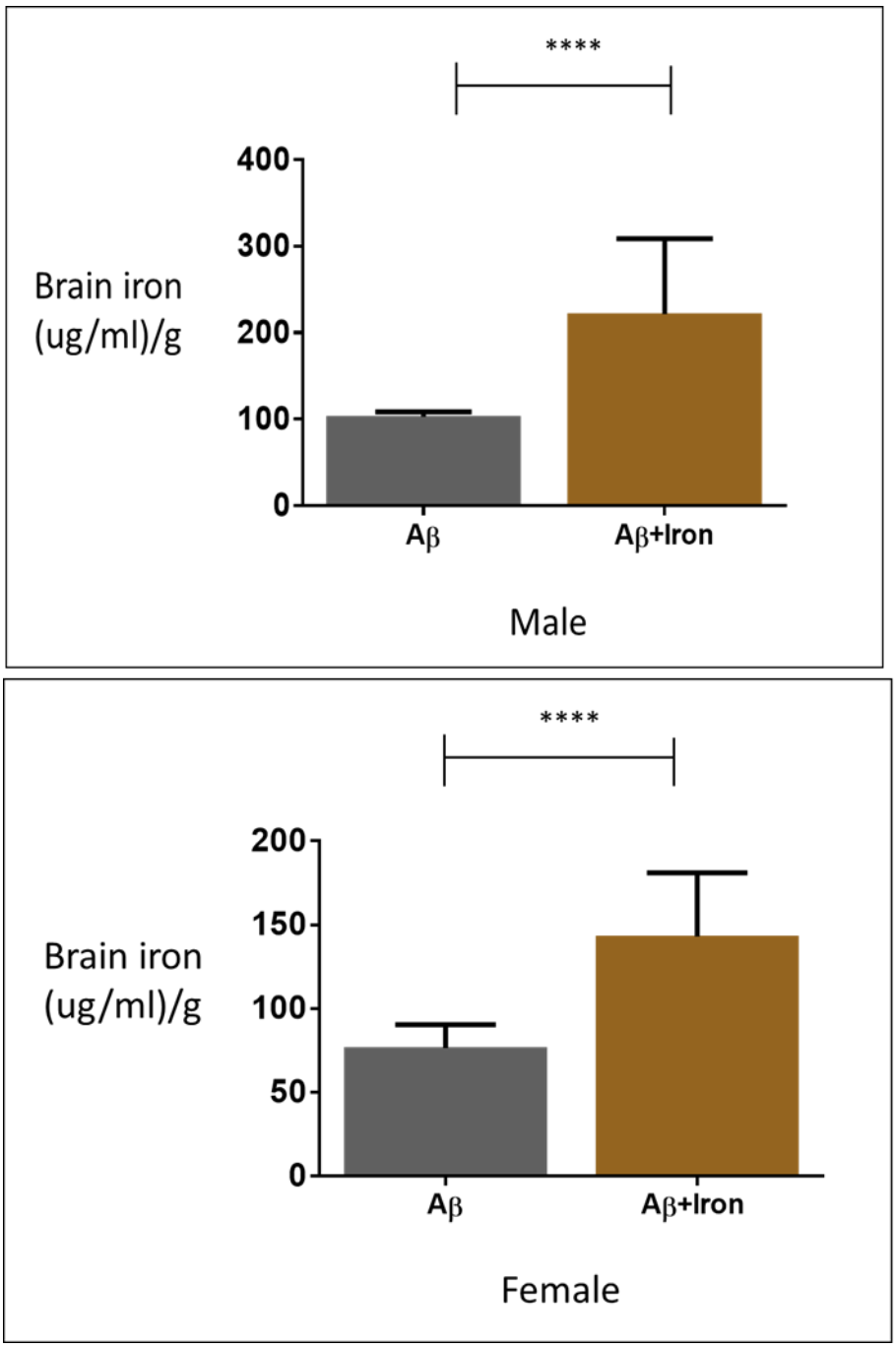

Fig. 3.3 Non-haem iron assay of brain homogenates from Aβ mice and Aβ+Iron mice. Data are presented as mean ± SD (****p<0.0001; n ≥11/group, with n ≥4 per sex in each group).

3.3.3 Amyloid detection by Congo red labelling

As described in Section 2.4.1, Congo red labelled amyloid deposits were visualised using two methods: 1) under the Texas Red filter set of the fluorescence microscope and 2) under 90^0 crossed polarisers of the polarised light microscope. The Congo red fluorescence technique (Fig. 3.4) is known to be highly sensitive but less specific, as false positive results may be obtained by detection

of aberrant particles (e.g. dirt), or some other proteins with β-pleated sheet secondary structure (Khurana et al., 2001; Linke, 2006).

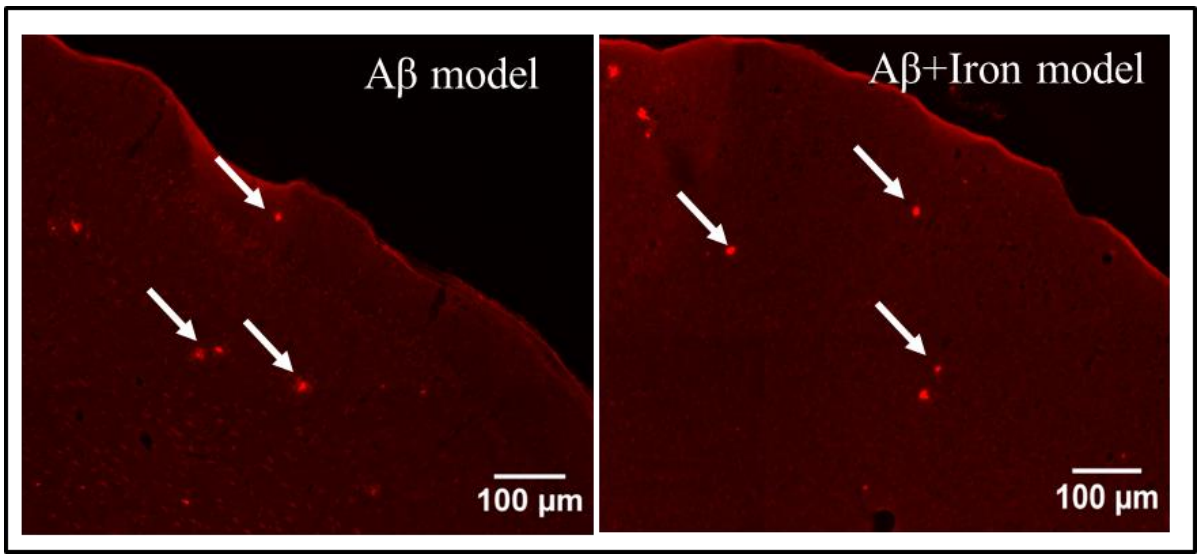

Fig. 3.4 Amyloid deposition in the brains of the Aβ model and the Aβ+Iron model as detected by fluorescence microscopy. White arrows indicate examples of structures positive for Congo red (Texas Red filter), which detects possible amyloid plaques.

On the other hand, the visualisation of Congo red stained amyloid fibrils under 90° crossed polarisers is known to be less sensitive but highly specific, as only the structures that emit yellow-green birefringence when bound to Congo red are detected (Linke, 2006; Puchtler et al., 1962). Hence, only the structures displaying yellow-green birefringence characteristic of amyloid were detected and quantified using this technique (Fig. 3.5).

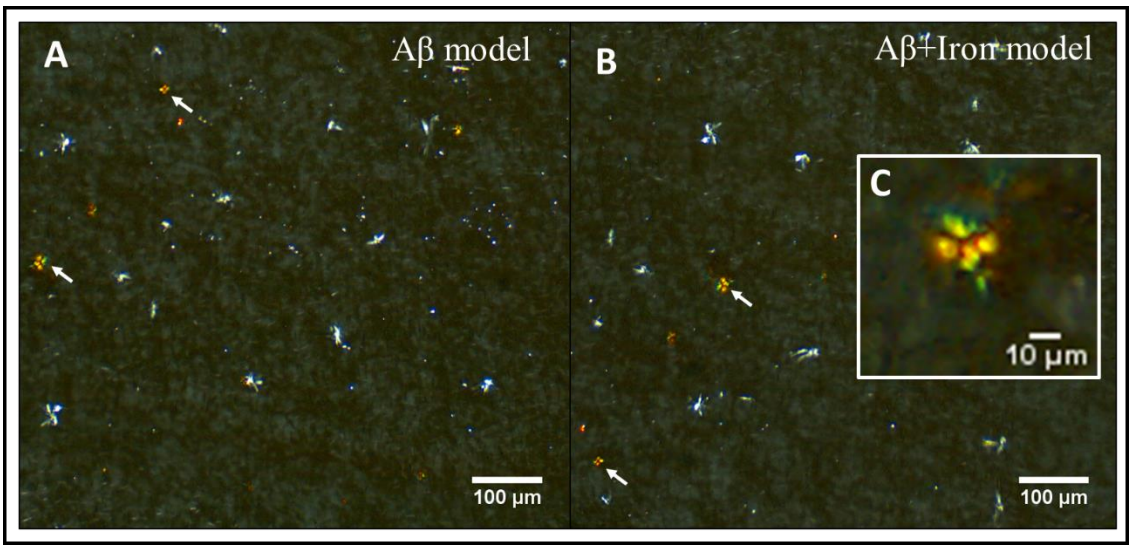

Fig. 3.5 Amyloid deposition in the brains of the Aβ model and the Aβ+Iron model as detected by the polarised light microscopy. White arrows indicate amyloid fibrils in (A) Aβ model; (B) Aβ+Iron model; (C) inset shows the enlarged image of a yellow-green birefringent amyloid fibril.

Detailed analysis was done to evaluate if there were more amyloid plaques in total or in particular brain regions in the Aβ+Iron model compared to the Aβ model, if plaques per unit area were different and if plaques were bigger on average or if size distribution of plaques had altered in some way. Data obtained using Congo red-based methods as described above for all of these different parameters of amyloid deposition are presented below. Data for complete brain hemispheres are presented first, followed by specific data for each of the cerebral cortex and hippocampus, both of which are known to be strongly affected in AD.

3.3.3.1 Amyloid detection by fluorescence microscopy

3.3.3.1.1 Amyloid detection in the left brain hemisphere by fluorescence microscopy

As illustrated in Fig. 3.6, no difference was observed between the left brain hemispheres of the Aβ mice and the Aβ+Iron mice by one-tailed unpaired *t*-test, for either the mean count of Congo red-positive structures (p=0.4523) or the amyloid burden, assessed by the percentage of the image containing Congo red-positive pixels (p =0.2005). There was also no significant difference for amyloid density, calculated as mean count of Congo red-positive structures divided by mean area of the hemisphere (p =0.0829), as revealed by one-tailed unpaired *t*-test. There was also no difference in the frequency distributions of area of the Congo red-positive structures in both groups of mice (p =0.9693, two-way ANOVA with Sidak's multiple comparisons test). As detailed in Methods (Section 3.2.3), all comparisons were done on sections matched for Bregma with two male and two female mice were compared for each group. While statistical comparisons could not be performed there were no apparent differences noted across the regions examined or between sexes.

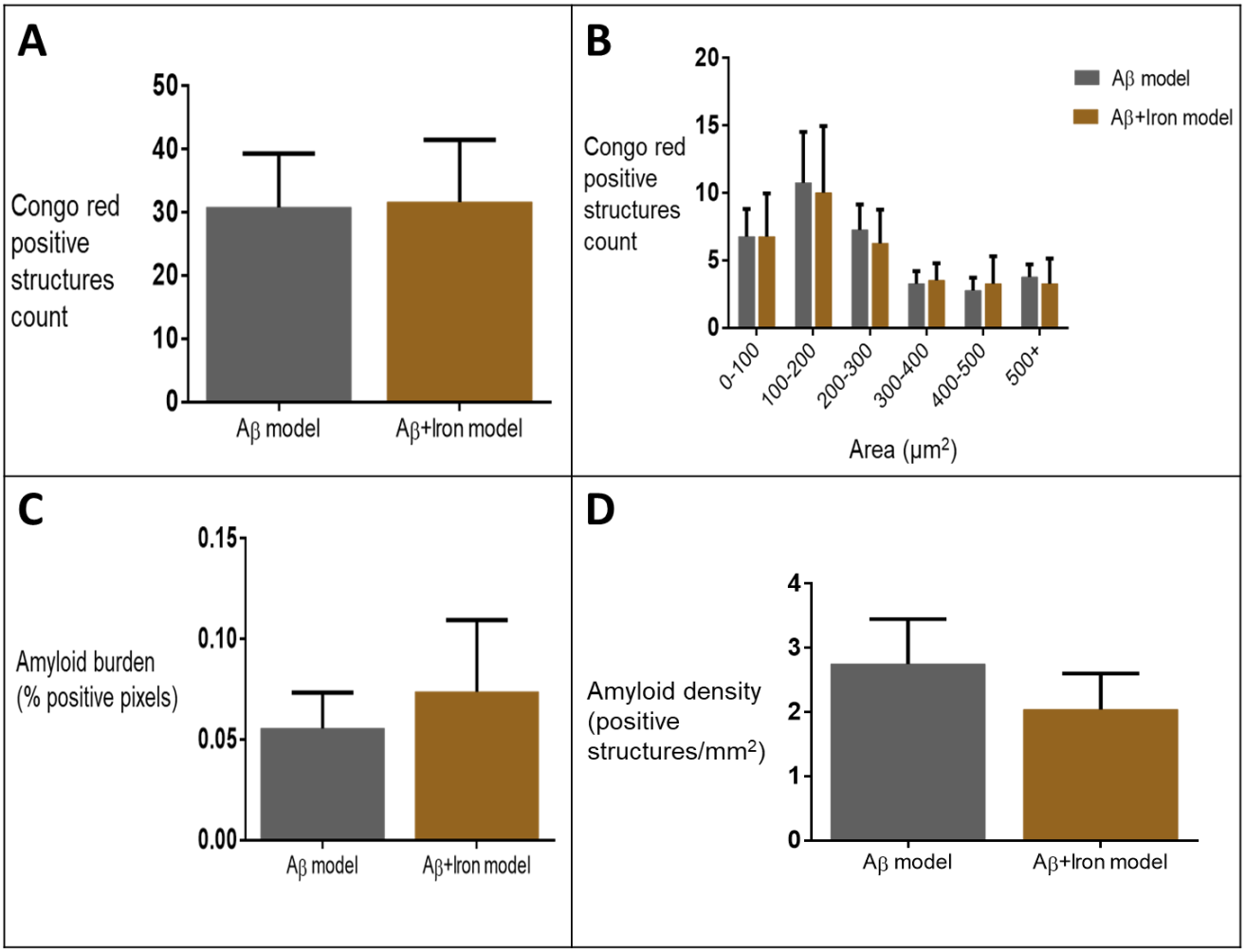

Fig. 3.6 Key characteristics of amyloid deposition do not differ in the left brain hemispheres of Aβ+Iron mice as compared to Aβ mice, using Congo red fluorescence technique. No difference was observed in A) mean count of Congo red-positive structures, B) frequency distributions of area of the Congo red-positive structures, C) the percentage of the image containing Congo red-positive pixels and D) density of Congo red-positive structures, in the left brain hemispheres of Aβ+Iron mice as compared to Aβ mice. Data are presented as means ± SD (p >0.05, n=4 mice/group).

3.3.3.1.2 Amyloid detection in the left cerebral cortex by fluorescence microscopy

The findings from left brain hemisphere failed to reveal remarkable difference in any of the parameters related to amyloid deposition, in Aβ+Iron mice as compared to Aβ mice. Cerebral cortex, which includes the entorhinal cortex, is a region that is affected badly in AD. It was chosen as a subset of the cerebral hemisphere and was further analysed to see if any of the parameters for amyloid deposition reaches statistical significance. Consistent with the findings from left brain hemisphere, as shown in Fig. 3.7, by one-tailed unpaired t-test, no difference was observed for the mean count of Congo red-positive structures (p=0.3649) and the percentage of image containing Congo red-positive pixels (p=0.2318), in the left cerebral cortex of the Aβ mice versus the Aβ+Iron

mice. However the amyloid density, assessed by mean count of Congo red-positive structures divided by mean area of cerebral cortex, was trending towards significance (p=0.0948, one-tailed unpaired t-test). There was also no difference in the frequency distributions of area of the Congo red-positive structures (p=0.9046, two-way ANOVA with Sidak's multiple comparisons test).

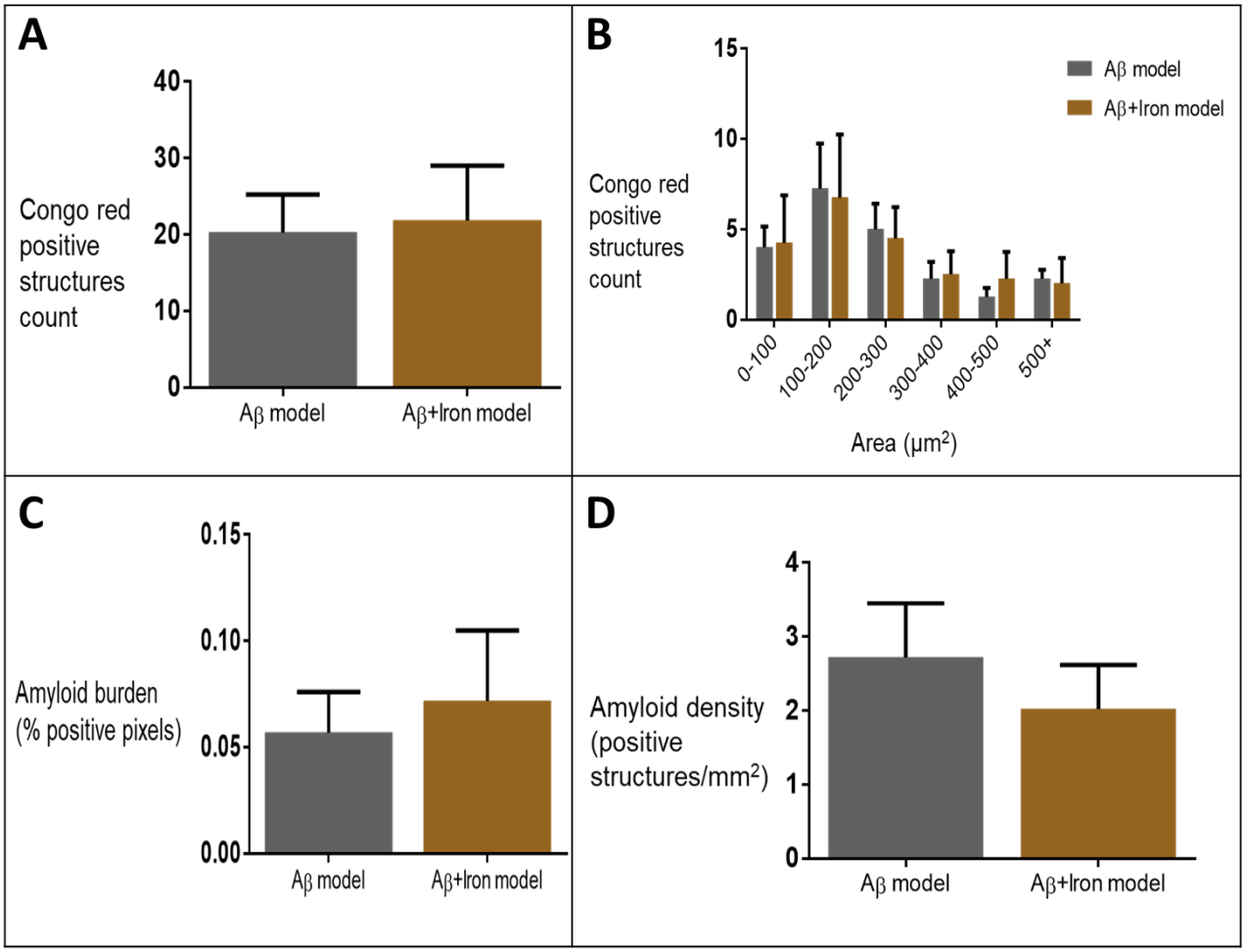

Fig. 3.7 Key characteristics of amyloid deposition do not differ in the left cerebral cortex of Aβ+Iron mice as compared to Aβ mice, using Congo red fluorescence technique. No difference was observed in A) mean count of Congo red-positive structures, B) frequency distributions of area of the Congo red-positive structures, C) the percentage of the image containing Congo red-positive pixels and D) density of Congo red-positive structures, in the left cerebral cortex of Aβ+Iron mice, compared to Aβ mice. Data are presented as means ± SD (p >0.05, n=4 mice/group).

3.3.3.1.3 Amyloid detection in the left hippocampus by fluorescence microscopy

Hippocampus was chosen as another subset of brain hemisphere as this region is also crucial in AD pathogenesis. In the left hippocampus of Aβ+Iron mice and Aβ mice, no difference was observed in mean count of Congo red-positive structures (p=0.3723), the percentage of the image containing Congo red-positive pixels (p =0.4735) and the density of Congo red-positive structures, measured by mean count of Congo red-positive structures divided by mean area of hippocampus (p =0.1212), all revealed by one-tailed unpaired t-test (Fig. 3.8). Likewise, frequency distributions of area of the Congo red-positive structures were similar between two groups of mice (p=0.9876, two-way ANOVA with Sidak's multiple comparisons test).

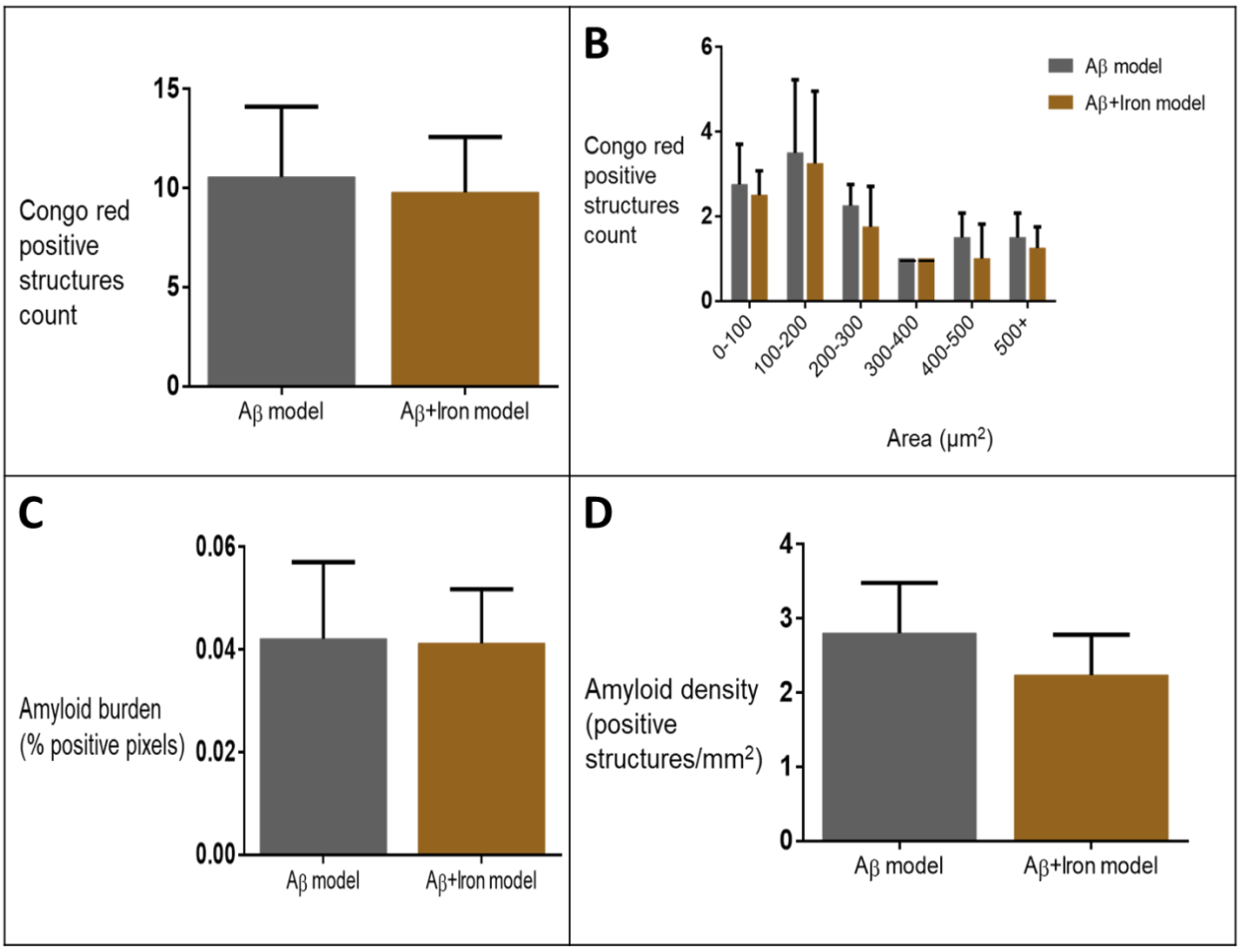

Fig. 3.8 Key characteristics of amyloid deposition do not differ in the left hippocampus of Aβ+Iron mice as compared to Aβ mice, using Congo red fluorescence technique. No difference was observed in A) mean count of Congo red-positive structures, B) frequency distributions of area of the Congo red-positive structures, C) the percentage of the image containing Congo red-positive pixels and D) density of Congo red-positive structures, in the left hippocampal region of Aβ+Iron mice, compared to Aβ mice. Data are presented as means ± SD (p >0.05, n=4 mice/group).

3.3.3.2 Amyloid detection by polarised light microscopy

3.3.3.2.1 Amyloid detection in the left brain hemisphere by polarised light microscopy

Data obtained for various parameters of amyloid deposition using polarised light microscopy were in agreement with the findings from Congo red fluorescence technique. No difference was seen in the mean count of Congo red-positive structures (p=0.2333), amyloid burden, evaluated by the percentage of image containing Congo red-positive pixels (p=0.2684) and the density of the Congo red-positive structures (p=0.4345), between the Aβ+Iron mice and Aβ mice, as revealed by one-tailed unpaired t-test (Fig. 3.9). Similarly, there was no difference in the frequency distributions of area of the Congo red-positive structures between two groups of mice (p=0.9915, two-way ANOVA with Sidak's multiple comparisons test).

Though none of the parameters showed remarkable difference in the overall brain hemisphere using either Congo red fluorescence or polarisation techniques, there were some notable features. Firstly, lower counts of structures positive for Congo red staining were obtained using the polarisation technique (mean ± SEM: 22.46 ± 5.425 for Aβ+Iron mice; 17.56 ± 3.199 for Aβ mice; n=4), compared to the fluorescence method (mean ± SEM: 31.63 ± 4.921 for Aβ+Iron mice; 30.81 ± 4.253 for Aβ mice; n=4). This difference may be attributable to false positive results from Congo red fluorescence technique, as described above. Secondly, the highest count of Congo red-positive structures was in the area range of 100-200 μm^2 using either techniques, in both groups of mice.

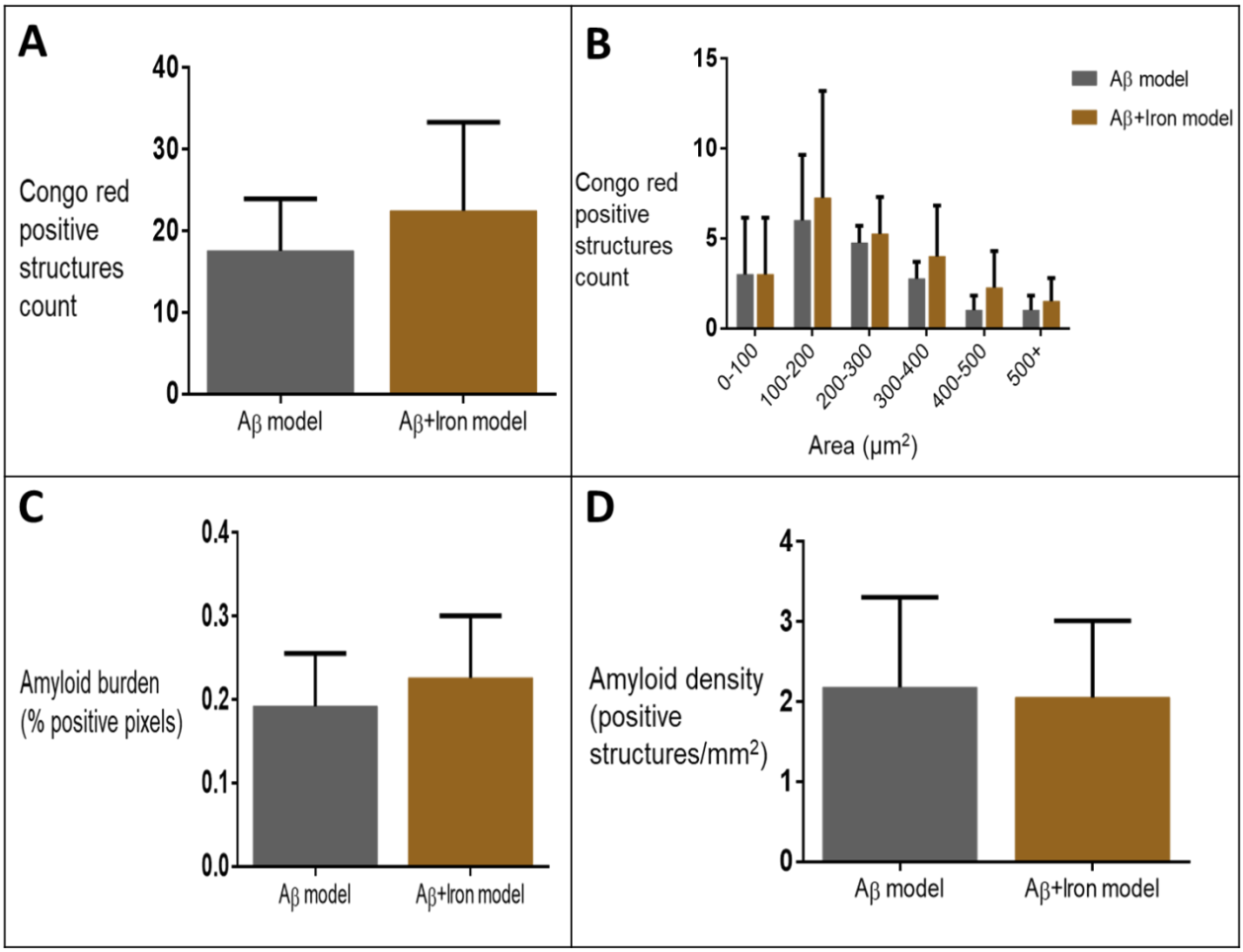

Fig. 3.9 Key characteristics of amyloid deposition do not differ in the left brain hemisphere of Aβ+Iron mice as compared to Aβ mice, using Congo red polarisation technique. No difference was observed in A) mean count of Congo red-positive structures, B) frequency distributions of area of the Congo red-positive structures, C) the percentage of the image containing Congo red-positive pixels and D) density of Congo red-positive structures, in the left brain hemisphere of Aβ+Iron mice, compared to Aβ mice. Data are presented as means ± SD (p >0.05, n=4 mice/group).

3.3.3.2.2 Amyloid detection in the left cerebral cortex by polarised light microscopy

Consistent with the observations from left brain hemisphere, no difference was observed for mean count of Congo red-positive structures (p=0.2566), the percentage of image containing Congo red-positive pixels (p =0.4011) and the density of Congo red-positive structures (p=0.4203) between the Aβ mice and the Aβ+Iron mice (one-tailed unpaired t-test). Besides these, there was no difference in the frequency distributions of area of the Congo red-positive structures (p=0.9458, two-way ANOVA with Sidak's multiple comparisons test).

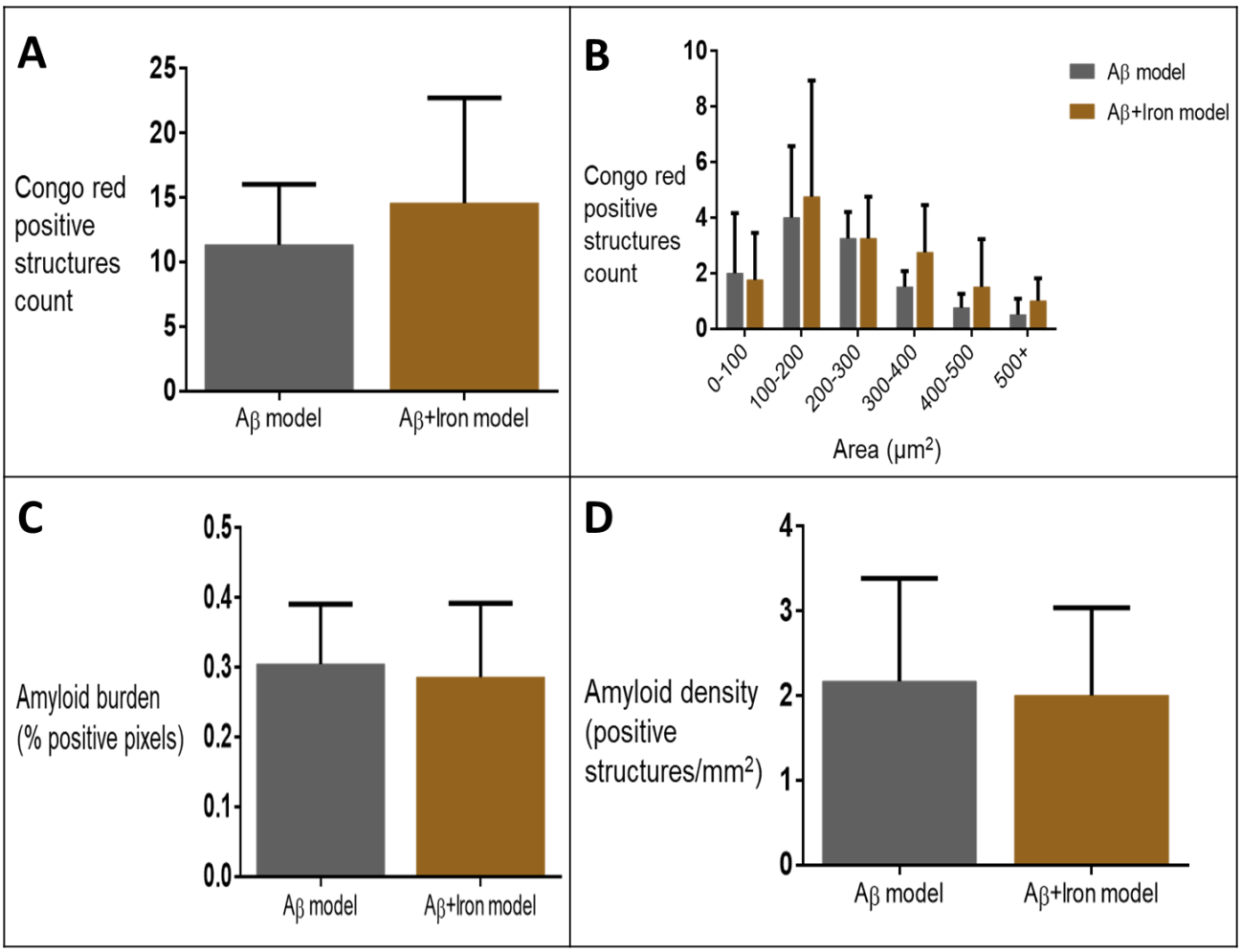

Fig. 3.10 Key characteristics of amyloid deposition do not differ in the left cerebral cortex of Aβ+Iron mice as compared to Aβ mice, using Congo red polarisation technique. No difference was observed in A) mean count of Congo red-positive structures, B) frequency distributions of area of the Congo red-positive structures, C) the percentage of the image containing Congo red-positive pixels and D) density of Congo red-positive structures, in the left cerebral cortex of Aβ+Iron mice, compared to Aβ mice. Data are presented as means ± SD (p >0.05, n=4 mice/group).

3.3.3.2.3 Amyloid detection in the left hippocampus by polarised light microscopy

In accordance with data from left brain hemisphere and cerebral cortex, mean count of Congo red-positive structures (p=0.2023), the percentage of image containing Congo red-positive pixels (p=0.0580) and the density of the Congo red-positive structures (p=0.3847) in the left hippocampus of the Aβ+Iron mice were not different from the Aβ mice (one-tailed unpaired t-test). Similarly, no difference was observed for the frequency distributions of area of the Congo red-positive structures (p=0.9838, two-way ANOVA with Sidak's multiple comparisons test).

While no obvious differences were observed in amyloid loading and related measures in the above analyses, it remains possible that iron may be interacting with plaques in other ways. This is considered in the following sections.

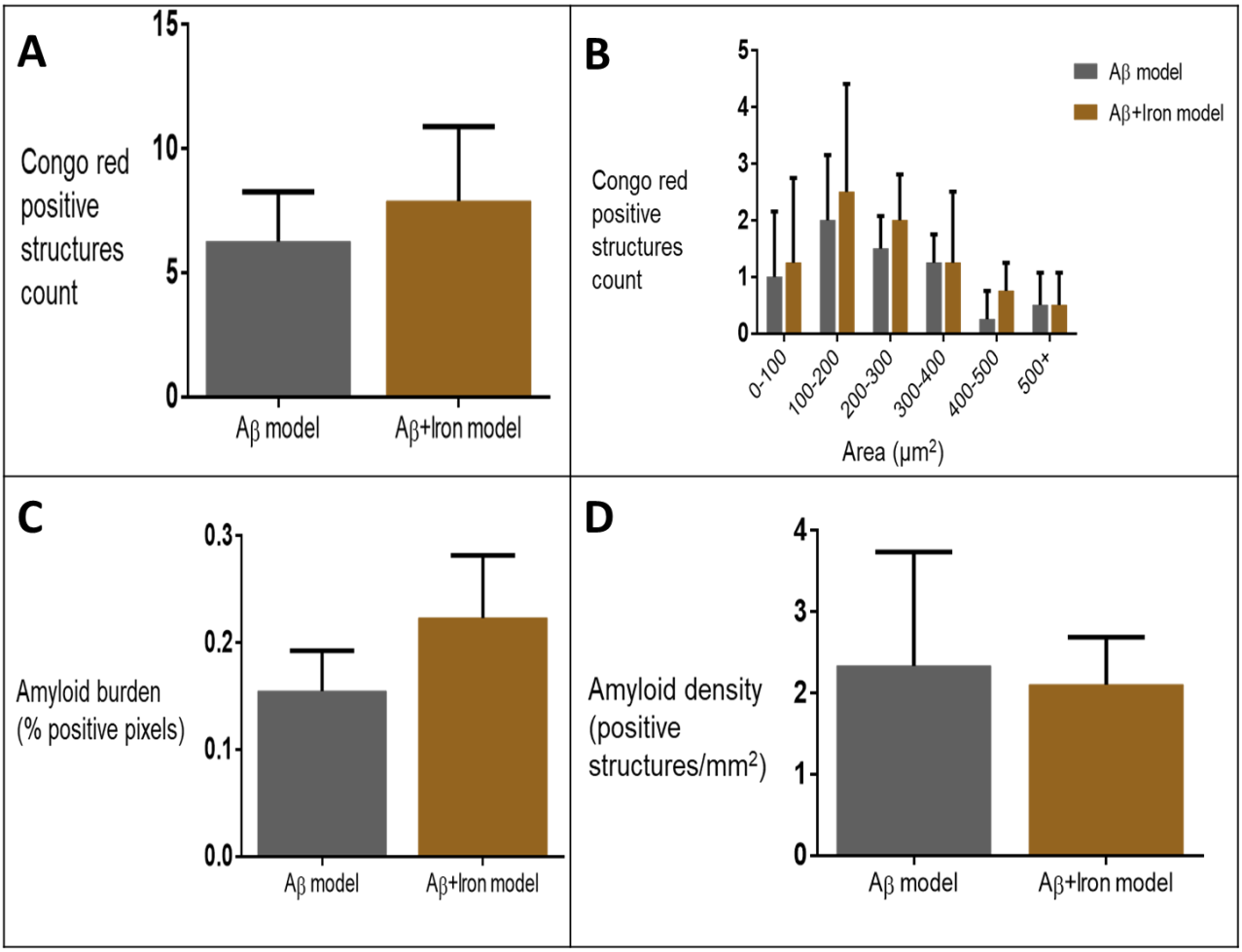

Fig. 3.11 Key characteristics of amyloid deposition do not differ in the left hippocampus of Aβ+Iron mice as compared to Aβ mice, using Congo red polarisation technique. No difference was observed in A) mean count of Congo red-positive structures, B) frequency distributions of area of the Congo red-positive structures, C) the percentage of the image containing Congo red-positive pixels and D) density of Congo red-positive structures, in the left hippocampus of Aβ+Iron mice, compared to Aβ mice. Data are presented as means ± SD (p >0.05, n=4 mice/group).

3.3.3.3 Iron-amyloid co-localisation studies

Co-localisation of DAB-enhanced Perls' iron staining and Congo red-labelling was observed in the Aβ+Iron model and the Aβ model, using polarised light microscopy, brightfield, microscopy and fluorescence microscopy (Texas red filter).

3.3.3.3.1 Visualisation of iron-amyloid co-localisation by polarised light microscopy

The next part of the project investigated the relationship of iron and amyloid plaques at the level of individual structures. Yellow-green birefringent amyloid plaques surrounded by iron halos were observed in brain sections stained with DAB-enhanced Perls' stain and Congo red stain, from both the Aβ+Iron model and the Aβ model, when viewed by polarised light microscopy (Fig. 3.12 A, B). Birefringent Congo red labelled plaques were not observed in AKR wildtype mice or the Iron model. Iron deposits were observed even in plaques that showed barely detectable birefringence (Fig. 3.12 A, C), which may correspond to less mature plaques. [As addressed in more detail in Chapter 4 (Section 4.3.3), small 'white' circles of very low iron staining typically correspond to neurons or sometimes small blood vessels.]

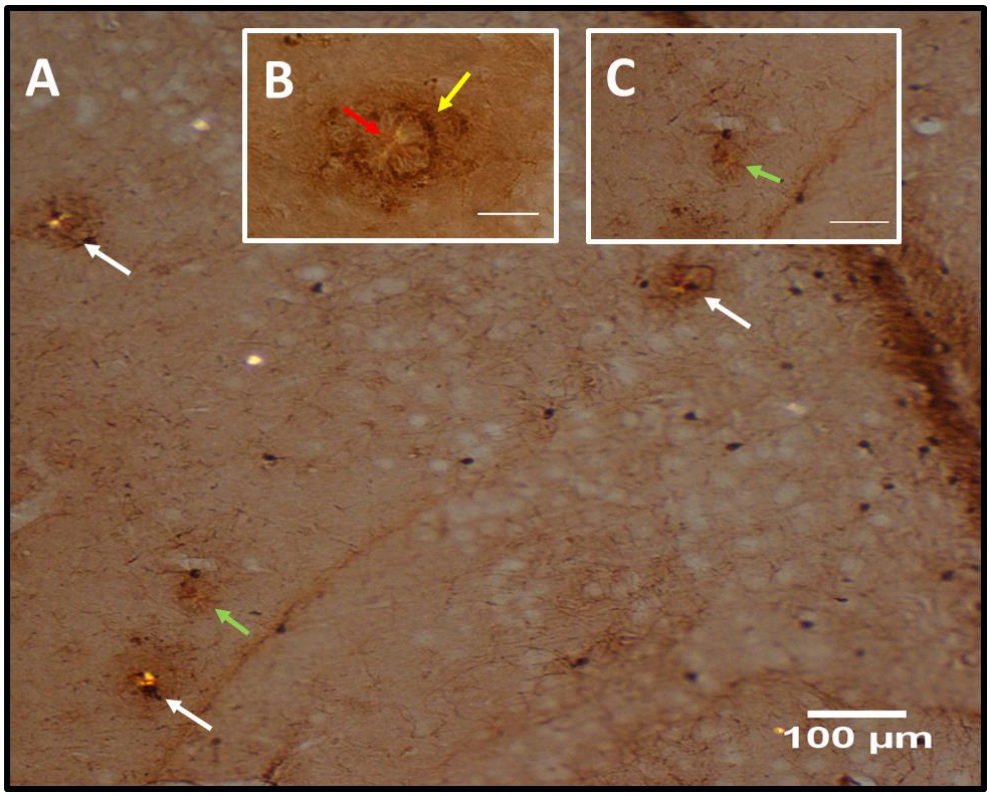

Fig. 3.12 Iron-amyloid co-localisation visualised with polarised light microscopy. (A) Many amyloid plaques labelling with iron were detected under polarised light microscopy (white arrows); figure inset (B) shows iron halo (yellow arrow) around a yellow-green birefringent amyloid plaque

in centre (red arrow); figure inset (C) shows co-localisation of iron with a potential less mature plaque, which exhibits weak yellow-green birefringence (green arrow), in the Aβ+Iron model.

As the polarised light microscopy did not give sufficiently high quality brightfield images for quantitative analysis, the ZEISS Axio Scan.Z1 Slide Scanner was used to obtain brightfield images for this purpose. This is described in the section below.

3.3.3.3.2 Visualisation of iron-amyloid co-localisation by brightfield microscopy and fluorescence microscopy

Co-localisation of DAB-enhanced Perls' iron staining and Congo red-labelling was observed in the Aβ+Iron model and the Aβ model by brightfield microscopy and fluorescence microscopy (Fig. 3.13). However, there were a few iron-amyloid complexes which were clearly identifiable under brightfield microscopy but hardly visible under fluorescence microscopy in the Aβ+Iron model (Fig. 3.13). This presumably reflects at least in part the presence of deposits that stain strongly enough for iron to be readily detectable in brightfield but contain relatively little Congo red labelled amyloid, which could be due to differences in the relative amounts of the two substances but could also arise from sensitivity differences between the two methods.

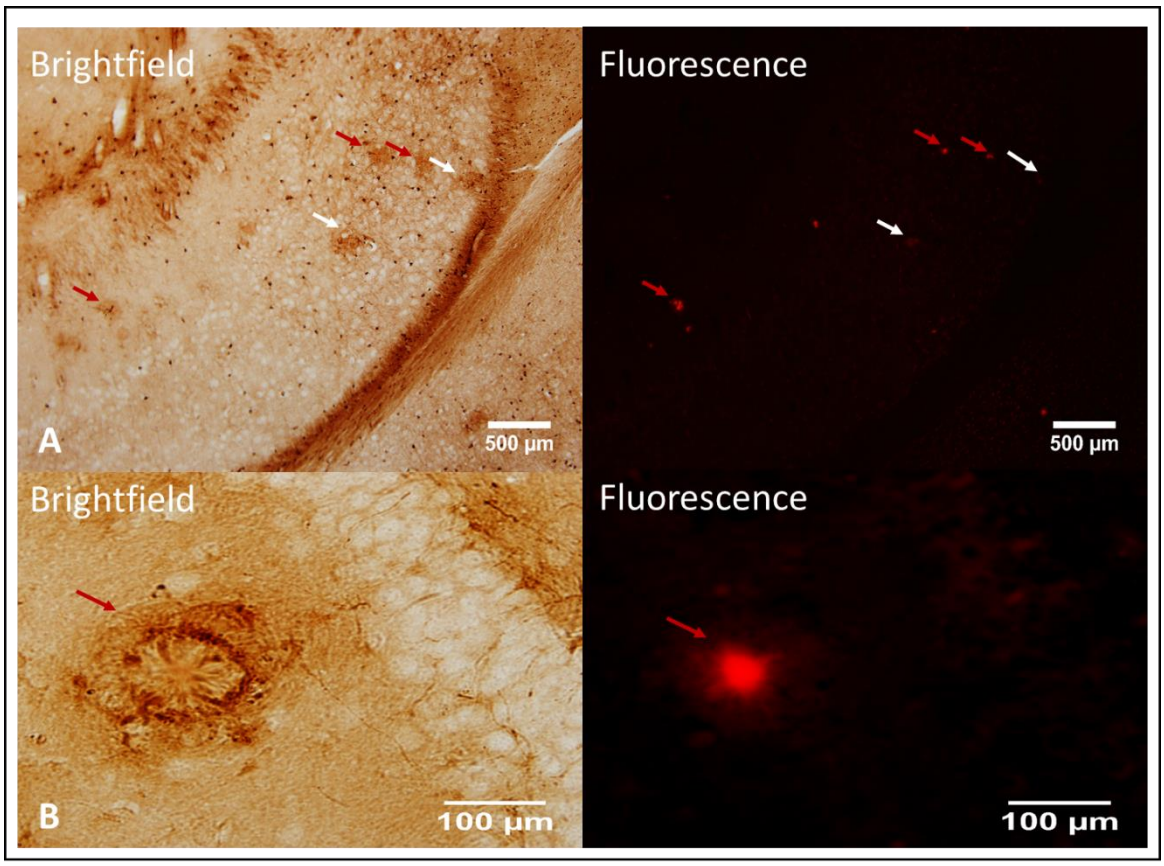

Fig. 3.13 Co-localisation of iron with cerebral amyloid pathology in the Aβ+Iron model. (A) Combined DAB-enhanced Perls' stain for iron and Congo red stain for amyloid in the Aβ+Iron model showed clear co-localisation of iron and amyloid plaques under brightfield and the corresponding fluorescence image (red arrows). Some iron deposits which appeared distinct under brightfield however labelled faintly with Congo red, under fluorescence microscopy (white arrows). (B) Magnified images of an iron-amyloid complex under brightfield and fluorescence microscopy. Small 'white' circles typically correspond to neurons (Section 4.3.3).

The iron-amyloid complexes were quantified in both groups of mice as detailed in Section 3.2.7 and illustrated in Fig. 3.14. Data obtained for different parameters of the iron-amyloid co-localisation are detailed in this section.

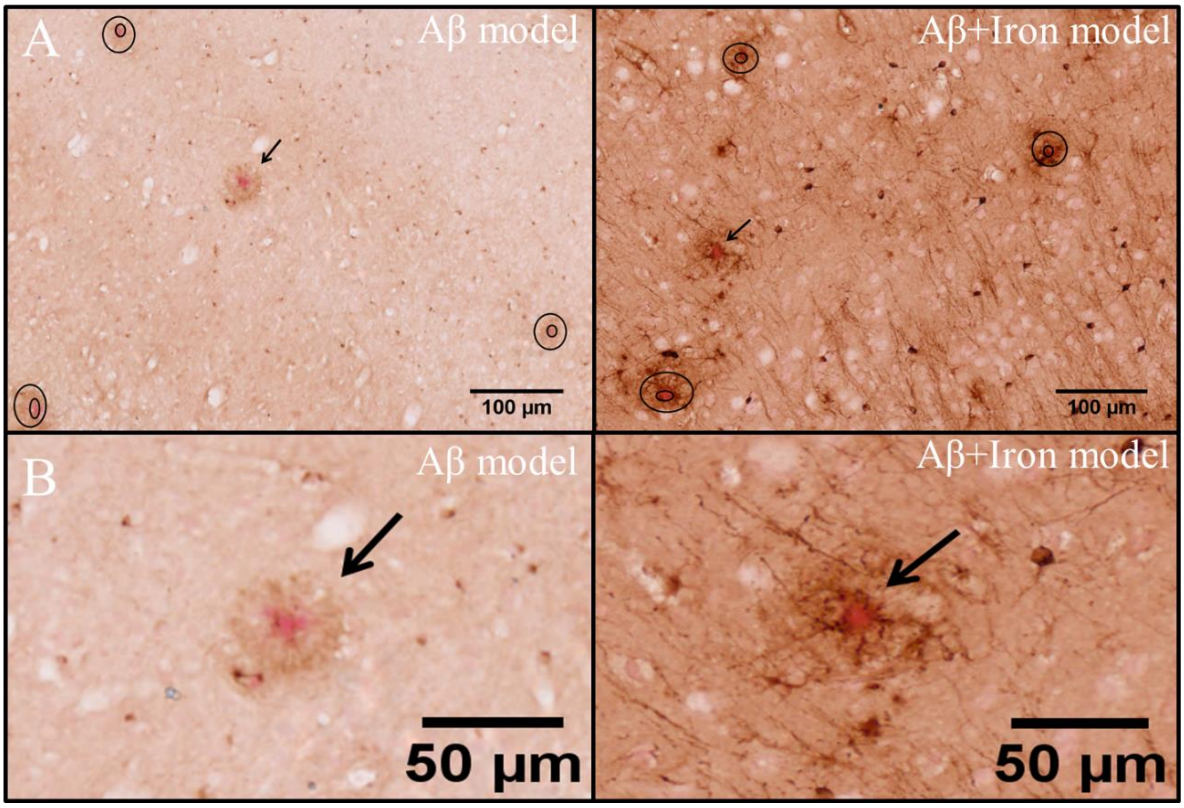

Fig. 3.14 Co-localisation of iron with amyloid plaques. (A) Double labelling of DAB-enhanced Perls' stain and Congo red stain showing iron halos (brown) surrounding the amyloid plaques in centre (pink), in the brain sections of the Aβ mice and the Aβ+Iron mice. The outer circle enclosed both iron-amyloid complex and the inner circle enclosed amyloid only; the band shaped structure covered most of the iron halo. (B) Magnified images displaying iron-amyloid co-localisation in both groups of mice.

3.3.3.3.2.1 Increase in proportion of plaques labelling for iron

There was no statistically significant difference in mean count of the plaques labelling for iron, also known as the Perls'-positive plaques, in the left brain hemispheres of the Aβ+Iron mice as compared to the Aβ mice (p=0.2303, one-tailed unpaired t-test, Fig. 3.15A). However, mean proportion of Perls'-positive plaques (i.e., total number of Perls'-positive plaques divided by total number of plaques, multiplied by 100) was higher in the Aβ+Iron mice than the Aβ mice (p=0.0016, one-tailed unpaired t-test, Fig. 3.15B). Specifically, 99.25% of detected amyloid plaques were co-localised with Perls' stainable iron in the brain sections examined in the Aβ+Iron mice, compared to 81.09% in the Aβ mice.

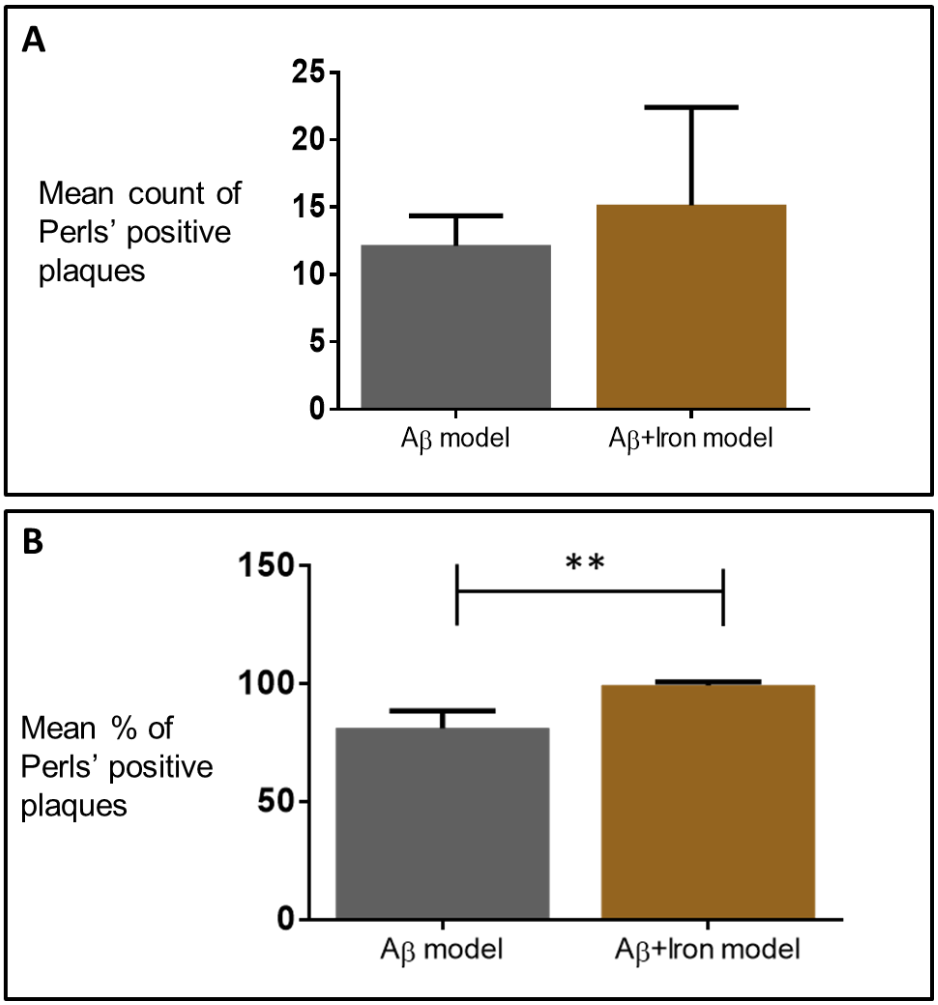

Fig. 3.15 Quantification of amyloid plaques labelling with iron. (A) Count of plaques labelling for iron (Perls' positive plaques) in the left brain hemispheres of the Aβ+Iron mice as compared to the Aβ mice, using combined DAB-enhanced Perls' and Congo red staining (p >0.05, n=4 mice/group); (B) The proportion of plaques which were Perls' positive was higher in the Aβ+Iron mice than the Aβ mice (p <0.05, n=4 mice/group). Data are presented as means ± SD.

3.3.3.3.2.2 Stronger iron labelling around plaques

Next, the level of DAB-enhanced Perls' staining of the iron halos surrounding the amyloid plaques was compared between two groups of mice. The parameter that was used to measure the level of DAB-enhanced Perls' staining was Mean Gray Value (MGV), which is the average gray value within a selection. Lower values correspond to darker staining due to increased iron content, as assessed indirectly from the oxidisation of greater amounts of DAB. This can be counterintuitive since it leads to an inverse relationship between MGV and iron content i.e. the pixel intensity values correspond to gray scale values where 0 means pure black and 255 means pure white. For ease of interpretation, data were therefore transformed using the formula MGV(T)=K-MGV in which K=255, such that pixels corresponding to white on the 'gray scale' were allocated a value of 0 and

pixels corresponding to black a value of 255. Accordingly, it was hypothesised that iron associated with plaques and likewise the transformed MGV would be higher in the Aβ+Iron mice as compared to the Aβ mice. Consistent with this hypothesis there was a statistically significant increase in the transformed MGV for DAB-enhanced Perls' staining in the brain of the Aβ+Iron mice as compared to the Aβ mice (fold change 1.4, p=0.0456, one-tailed unpaired t-test, Fig. 3.16).

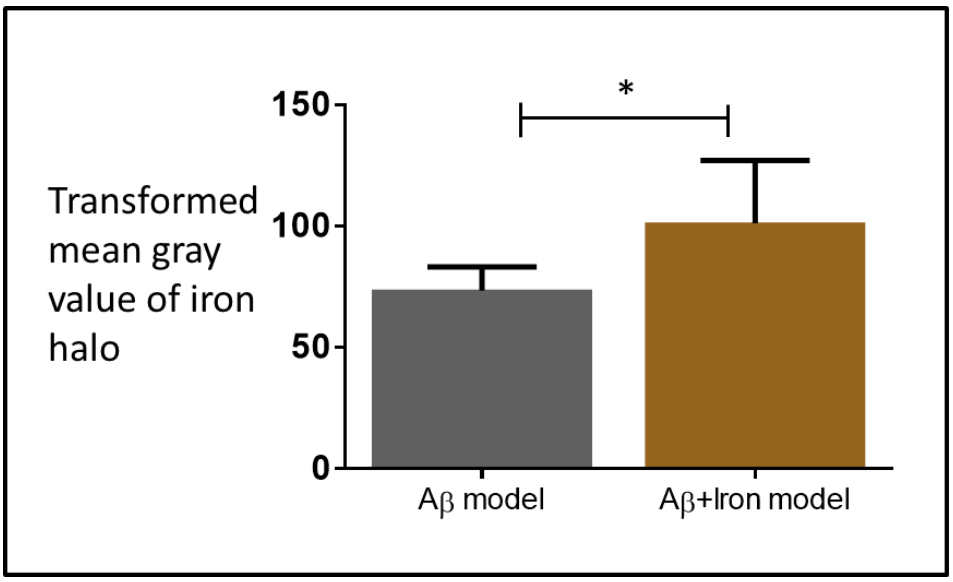

Fig. 3.16 Strong staining for iron around amyloid plaques in the Aβ+Iron mice. The amount of DAB-enhanced Perls' staining in the iron halos surrounding amyloid plaques was assessed through transformed mean gray value. DAB-enhanced Perls' staining was stronger in iron halo of the Aβ+Iron mice compared to the Aβ mice (p<0.05, n=4 mice/group). Data are presented as means ± SD.

3.3.3.3.2.3 No difference in mean area of iron halos surrounding plaques

The stronger iron staining around plaques in the Aβ+Iron model may mean that more iron may be co-localised with plaques in this model as compared to the Aβ model. The next question that was addressed was whether there was any difference in the area covered by the iron halos in the Aβ+Iron mice as compared to the Aβ mice. This was performed on brain tissue sections matched for Bregma as described in Methods (Section 3.2.3) and there was no apparent correlation between Bregma and plaque iron halo areas. No significant difference was seen in the mean area of iron halos surrounding plaques when both groups were compared (p=0.1007). As more iron was observed to be associated with amyloid plaques in the Aβ+Iron model, this might mean that there are higher amounts of iron concentrated within regions of similar size around plaques in this model

compared to the Aβ model. As considered in more detail in the Discussion (Section 3.4), this could reflect binding of iron to existing deposits of Aβ even though these may not be within the detection limits of Congo red staining. More iron may therefore bind to deposits of similar size in the Aβ+Iron model as opposed to iron deposition independent of Aβ, which might be predicted to show increases in the area of iron deposition at higher iron levels.

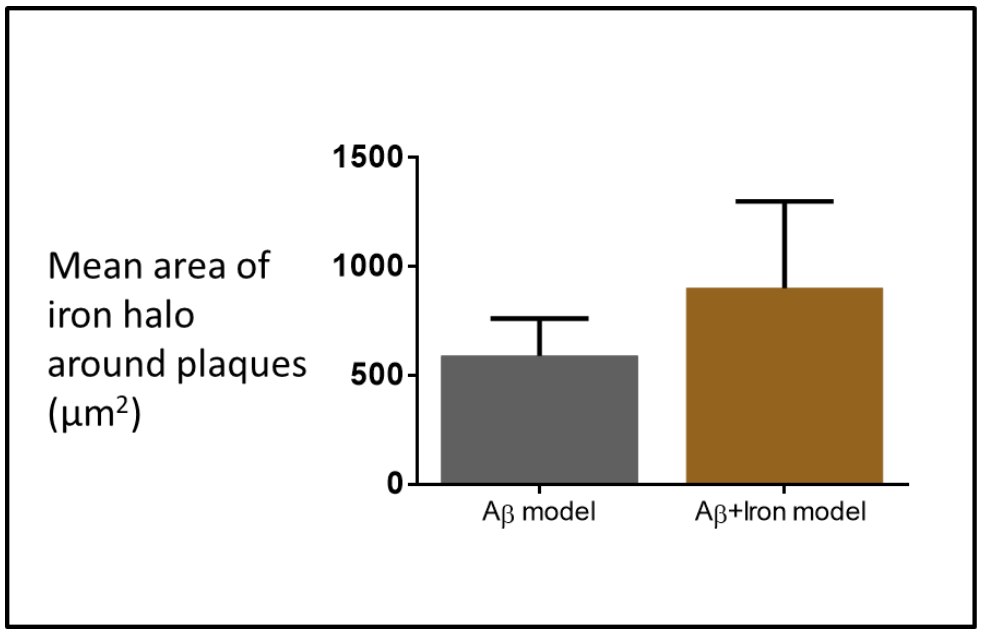

Fig. 3.17 Mean area of iron halo surrounding amyloid plaques. No difference was observed in the mean area of iron halos around all visible amyloid plaques in Bregma-matched regions of the left brain hemispheres of the Aβ+Iron model versus the Aβ model (p>0.05, n=4 mice/group; minimum of 200 plaques counted per group). Data are presented as means ± SD.

In order to check whether there is any difference in the distributions of the iron halo sizes between the Aβ+Iron mice and the Aβ mice, the area values of the iron halos co-localised with Perls' positive plaques, determined as illustrated in Fig. 3.17 above, were distributed into 9 bins, each with an area range of 500 µm^2. No statistically significant difference was observed overall for the distributions of iron halo areas of the Aβ+Iron mice compared to the Aβ mice (p=0.6515, two-way ANOVA, Sidak's multiple comparisons test). However, as illustrated in Fig. 3.18, there appeared to be a few plaques that had much larger iron halos in the Aβ+Iron mice (over 3,500 µm^2).

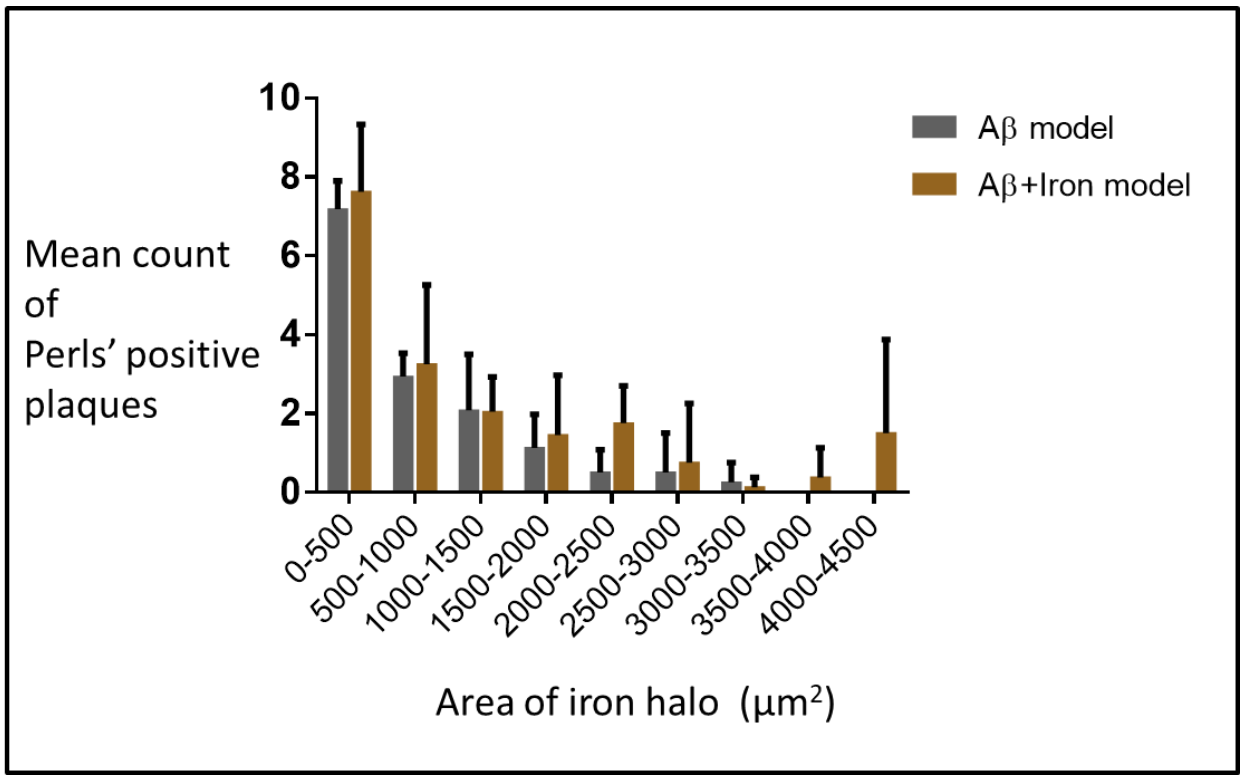

Fig. 3.18 Frequency distributions of area of iron halos surrounding amyloid plaques. For area values of iron halos associated with plaques in the left brain hemispheres of the Aβ+Iron model and the Aβ model, the interaction of bin width and mean count of Perls' positive plaques was not significant (p>0.05, n=4 mice/group). Data are presented as means ± SD.

3.3.3.3.3 Visualisation of iron-amyloid co-localisation by immunolabelling with Aβ antibody and DAB-enhanced Perls' staining

The halos were defined originally as the Perls' positive zone outside the region labelled with Congo red. Therefore the presence of a few large iron-containing halos not labelled with Congo red may reflect iron deposition in the absence of any Aβ peptide but could also potentially reflect iron co-localised with deposits of Aβ peptide that have not formed classical plaques and are not detected by Congo red. This was investigated by co-labelling with DAB-enhanced Perls's stain and antibody 4G8 which recognises all forms of Aβ peptide, including amorphous deposits as well as classical plaques. This antibody also labels the peripheral zone as well as the central core of classical amyloid plaques (Rajamohamedsait and Sigurdsson, 2012; Wisniewski et al., 1989).

In preliminary experiments, iron was observed to co-localise with 4G8 positive structures in the Aβ+Iron model and the Aβ model (Fig. 3.19). Most 4G8 positive structures did not appear to have clear large iron halos extending beyond the region labelled with 4G8 (Fig. 3.19 panels B, C), suggesting iron was co-localising with Aβ peptide deposits outside the central amyloid core.

However occasional structures appeared to have large iron halos extending beyond the 4G8 positive region (Fig. 3.19 panel D), suggesting that both possibilities can occur.

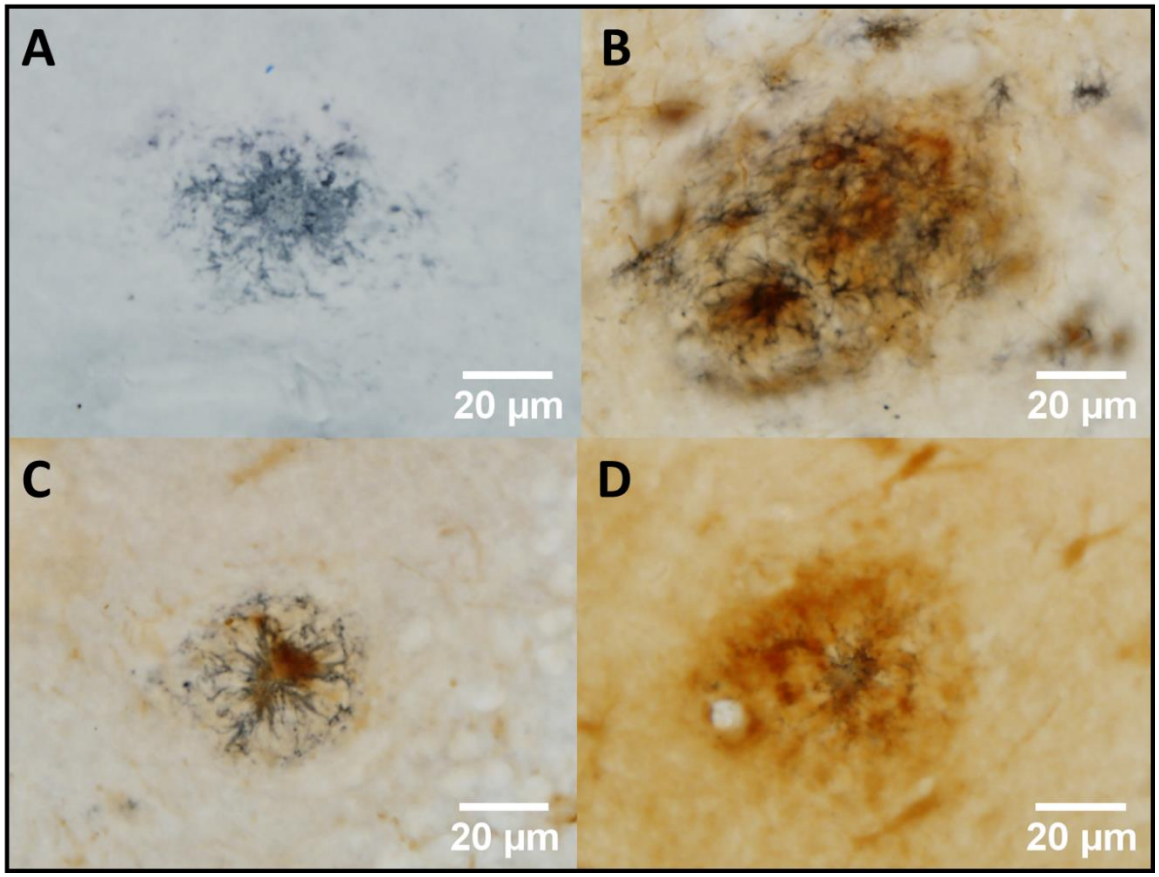

Fig. 3.19 Co-localisation of antibody 4G8 immunolabelling of Aβ peptide with iron. (A) Example of a deposit labelled with antibody 4G8 in the Aβ+Iron model. (B-D) Co-localisation of iron with deposits of Aβ peptide, detected by both DAB-enhanced Perls' stain and antibody 4G8, in the Aβ+Iron model (blue-gray: antibody 4G8 staining, brown: DAB-enhanced Perls' staining). (B, C) Examples of 4G8 positive structures with no clear large iron halos spreading beyond the region labelled with antibody 4G8 suggest that iron co-localised with Aβ peptide deposits outside the central amyloid core. (D) Example of a 4G8 positive structure with large iron halo extending beyond the 4G8 positive region.

3.4 Discussion

Overview

As described in the chapter General Introduction (Section 1.7), this chapter tested the first hypothesis of this thesis which was divided into three parts: a) brain iron level is increased in the Aβ+Iron model as compared to the Aβ model; b) excess brain iron may augment cerebral amyloidosis in the Aβ+Iron model as compared to the Aβ model; c) excess brain iron may co-localise with insoluble Aβ pathology in the Aβ+Iron model.

Data obtained in this chapter support the first part of the hypothesis as brain iron levels measured by non-haem iron assay and detected by DAB-enhanced Perls' histochemical staining in the Aβ+Iron model were increased compared to the brain iron levels of the Aβ model. However the second part of the hypothesis was not supported by the experimental data as there was no evidence of an increase in the amount of amyloid deposition in the Aβ+Iron model compared to the Aβ model. The third part of the hypothesis was supported as iron and amyloid were found to co-deposit in both Aβ+Iron mice and Aβ mice.

Increased brain iron levels in the Aβ+Iron model are not accompanied by changes in amyloid measures at 6 months of age

As expected, there was a significant increase ($p<0.0001$) in brain non-haem iron levels of the Aβ+Iron model as compared to the Aβ model at 6 months of age (Fig. 3.3). However there was no significant difference in the amyloid count and other key features of amyloid deposits in the Aβ+Iron model compared to the Aβ model at this age. This may suggest that although iron co-localises with amyloid, increased iron does not contribute to the exacerbation of cerebral amyloidosis at least at the earlier stages of the disease. Nevertheless, this needs to be investigated in older mice to see if the effects are similar at later stages of the disease.

However, within each of these groups of mice, the brain non-haem iron levels were found to be 25-35% lower in females compared to males. It is generally known that iron loading is often greater in human males than in pre-menopausal females, at least in part because of menstruation (Harrison-Findik, 2010; Miller, 2016). However female mice do not menstruate (Brasted et al., 2003; Emera et

al., 2012) and the reasons for the difference in non-haem iron content between two sexes are not clear, although factors such as hormonal differences may be involved. Conversely, females may have greater risk of AD as reported in some human studies and female transgenic APP/PS1 mice may have increased plaque numbers compared to age-matched males (Gallagher et al., 2013; Vina and Lloret, 2010; Wang et al., 2004a). While lower levels of iron in female mice did not appear to be affecting the amount of iron associated with plaques, this needs to be validated statistically in larger studies and it remains possible that low iron levels in combination with increased amyloid measures in female mice may be masking some effects of iron on plaques.

Comparisons with other studies of iron and amyloid co-localisation in transgenic mouse models and AD patients

The observation of iron-amyloid co-localisation in the Aβ+Iron model and also in the Aβ model supports the final component of the overarching hypothesis of the chapter and is consistent with several studies which have reported iron-amyloid co-localisation in the APP/PS1 model and various other transgenic mouse models of AD (Bourassa et al., 2013; Chamberlain et al., 2011; El Tannir El Tayara et al., 2006; El Tayara et al., 2006; Falangola et al., 2005; Jack et al., 2004; Jack et al., 2005; Lovell et al., 1998; Meadowcroft et al., 2009; Meadowcroft et al., 2015a; Smith et al., 1997; Wadghiri et al., 2012). Similarly, many groups have reported iron and amyloid co-localisation in post-mortem human AD brains (Collingwood et al., 2008; Connor et al., 1992b; Lovell et al., 1998; Meadowcroft et al., 2009). Some of these studies have used different techniques to those used here, such as electron microscopy or x-ray spectroscopy whereas others used similar methods i.e. combinations of DAB-enhanced Perls' stain and Aβ -specific labelling (Falangola et al., 2005; Meadowcroft et al., 2015a). This provides evidence that the findings here are unlikely to be solely an artefact of the methods used.

Notably the results confirm and extend observations in three 18 month old PS/APP transgenic mice and one age-matched non-transgenic control mouse by Falangola and colleagues using single staining of adjacent sections for antibody 6E10 and DAB-enhanced Perls' stain (Falangola et al., 2005). These authors reported strong iron staining in white matter tracts in the caudate-putamen and observed that the majority of amyloid plaques in the PS/APP transgenic mice contained iron (consistent with observations in this model in the present study as discussed in Chapter 4). The authors claim their paper to be the first study which used DAB-enhanced Perls' staining and Aβ immunolabelling to show that iron co-localises with amyloid plaques in the PS/APP mouse model.

However the authors did not report simultaneous co-labelling for iron and amyloid on single sections such as was done in this study. Meadowcroft and colleagues (Meadowcroft et al., 2015a) used brain tissues from 24-month old APP/PS1 mice (n=5) and age-matched non-carrier mice (n=4). The authors also used entorhinal cortex from AD patients (n=5) and age-matched controls (n=3). In this study, to help visualise iron within plaques, sections were first treated with proteinase K followed by sodium borohydride treatment, both widely used in antigen retrieval (Chen et al., 2010; Ramos-Vara, 2005). This was followed by DAB-enhanced Perls' staining then thoflavin-S staining. Similar approaches are often necessary for post-mortem human tissue whereas visualisation of iron in plaques was achieved without antigen retrieval steps in the present mouse study, which used cryostat sections of brains perfusion-fixed in 4% paraformaldehyde, methods usually considered to be favourable for immunohistochemistry and immunofluorescence.

Meadowcroft and colleagues (ibid.) observed that the traditional method of DAB-enhanced Perls' staining followed by thioflavin-S staining could detect iron associated with plaques in human AD brains but were unable to detect iron in 24-month old APP/PS1 mouse brains using this method. The authors commented that a modified DAB-enhanced Perls' staining procedure which involved proteinase K treatment enabled visualisation of tiny amount of iron associated with plaques in the APP/PS1 mice. However this modified method now failed to stain plaques in human with thioflavin-S because of Aβ degradation and absence of intercalation of Aβ with thioflavin-S.

Compared to the methods used by Meadowcroft and colleagues, the combination of the traditional DAB-enhanced Perls' staining and the modified Puchtler's method of Congo red staining (Section 3.2.6) in this thesis facilitated visualisation of iron-amyloid complexes at 6 months of age in both Aβ+Iron mice and Aβ mice. Other methodological differences may have contributed to the failure of these authors to detect iron in plaques in the APP/PS1 mice. For example, the DAB-enhanced Perls' staining protocol used by Meadowcroft and colleagues had a 5 minute incubation in DAB (0.067%) compared to the 30 minute incubation in DAB (0.025%) used in this thesis so the shorter incubation may have contributed to the failure to detect iron in plaques despite the higher concentration used. In addition, in the experience of our laboratory it can be considerably harder to visualise Perls' staining in combination with a fluorescent label than in combination with Congo red in brightfield.

However, future investigations could incorporate proteinase K treatment prior to DAB-enhanced Perls' staining to examine if the modification in the protocol makes any difference in the

visualisation of iron-amyloid complexes. In addition, as the methodology used in this study has not been expanded to human studies, this is another possible area of future investigation.

Is the 'sticky' nature of amyloid responsible for iron attachment to plaques?

Another possibility is that the 'sticky' nature of Aβ may facilitate binding of iron to the existing Aβ peptides in both Aβ+Iron mice and Aβ mice. Many substances have been reported to be found in amyloid *in vitro* and within amyloid plaques *in situ* – just a few examples include collagen type XXV, tyrosine phosphatase, mitochondrial fumarate hydratase and somatostatin, along with many others (Armstrong et al., 1989; Lutz and Peng, 2018; Xiong et al., 2019). It may also be plausible that Aβ peptides may attach to iron already present in the brain environment of these mice. Both have been considered in the literature. Many *in vitro* studies have supported the hypothesis that iron promotes the aggregation of Aβ peptide (Bolognin et al., 2011; Boopathi and Kolandaivel, 2016; Collingwood et al., 2008; House et al., 2004b; Mantyh et al., 1993; Tahmasebinia and Emadi, 2017). Other studies have reported that Aβ peptide is involved in the accumulation and reduction of iron (III) within amyloid aggregates (Everett et al., 2014a; Everett et al., 2014b). The observations from this thesis suggest that both of these possibilities may occur. This will be considered further below in the context of co-labelling of DAB-enhanced Perls' stain and antibody 4G8. For instance, Aβ may stick to iron in people with brain iron abnormalities hence resulting in aggregation of more Aβ peptides. Conversely, iron may stick to Aβ aggregates that are already existing in the brains afflicted by AD.

It is not possible to make firm conclusions based on our findings at this point due to the sensitivity issue of different stains. As described in Section 3.3.3.3.2 and Fig. 3.13, occasional iron clusters that had strong brown coloration under brightfield microscopy (in the sections co-labelled with DAB-enhanced Perls' stain and Congo red stain) stained faintly for Congo red under the Texas red filter. This may possibly mean that iron is appearing even before the appearance of visible plaques. On the other hand, it is also likely that the combination of two stains might have affected this observation (i.e., one stain may be more sensitive than the other or DAB-enhanced Perls' stain may affect the fluorescence intensity of Congo red stain).

In spite of the fact that there was no significant difference in the mean sizes and overall size distributions of iron halos of the Aβ+Iron model compared to the Aβ model, co-labelling with DAB-enhanced Perls' stain and Congo red stain showed that there were a few amyloid plaques with

very large iron halos in the Aβ+Iron model that were not observed in the Aβ model (Section 3.3.3.3.2.3 and Fig.3.18). Since iron is laid down around the plaque but outside the area detectably stained with Congo red, this suggests strongly that Aβ doesn't need to be in the form of classical amyloid in order to bind iron *in vivo* and that iron can bind to other Aβ species in the extracellular matrix, consistent with findings *in vitro* previously reported for example by Everett and colleagues, in the absence of other potentially competing or masking molecules such as extracellular matrix proteins (Everett et al., 2014a).

The large halos observed around a few amyloid plaque cores could consist of deposits of iron alone without Aβ peptide or iron co-deposited with Aβ peptide species other than classical Congo red birefringent amyloid. While this needs to be checked in the future in more brain regions and more mice, the question of whether iron co-localises with deposits of non-amyloid Aβ peptide in addition to deposits that correspond to classical Aβ amyloid was considered in preliminary observations from co-labelling of brain sections with DAB-enhanced Perls' stain and antibody 4G8 (Section 3.2.6 and Fig. 3.19). These observations were consistent with two different scenarios, as follows.
In most cases, antibody 4G8 and iron co-localised closely and iron did not spread detectably beyond the 4G8 immunolabelled region. In the Iron model (*Hfe*$^{-/-}$*xTfr2Y*^{245X} mice), which does not contain human mutant Aβ sequence, round iron aggregates resembling those often observed around plaques in the other human Aβ-containing models are rarely if ever seen (unpublished findings, Milward lab). This suggests that increased iron does not normally form round structures of this kind. Therefore in this first scenario, it is considered likely that Aβ deposition occurs first and iron then sticks to it.

However in some cases, a large iron halo appeared to surround antibody 4G8. In this second scenario, it is possible that iron is laying down first and Aβ sticks to it afterwards since, if iron and Aβ peptide bind each other with high affinity, it is feasible that irrespective of which accumulates first, the other then sticks to it. However, this scenario may be less likely since as noted above it is not clear that iron does deposit extracellularly in round structures in the absence of Aβ peptide. The large iron halos may indicate the presence of Aβ peptide deposits below the detection limits of the 4G8 protocol.

Further studies are needed with more sensitive techniques such as scanning transmission X-ray microscopy and transmission electron microscopy (Everett et al., 2014a) since just like any other co-labelling procedures, the likelihood of one stain being more sensitive than the other cannot be ruled out in the co-labelling of DAB-enhanced Perls' stain and antibody 4G8. For example, if

sensitivity of iron detection is comparatively higher than the sensitivity of the protocol used for Aβ detection by antibody 4G8, iron may appear to extend beyond the limits of detectable 4G8 staining. Conversely, if antibody detection is more sensitive it is possible that iron is at levels below the threshold of detection before Aβ peptide deposits. Additional studies are also required to investigate co-labelling brain sections with DAB-enhanced Perls' stain, antibody 4G8 and Congo red or thioflavin-S.

Is iron that co-localises with amyloid plaques deleterious?

The hypothesis of the association of redox-active iron with amyloid plaques and neurofibrillary tangles was initially put forward by Smith and colleagues (Smith et al., 1997). The authors speculated that iron accumulation could contribute to oxidative damage in AD. Telling and colleagues detected ferrous iron in nanoscale Aβ aggregates of APP/PS1 brain tissue (Telling et al., 2017). The authors hypothesize that fibrillary and amorphous forms of Aβ coat ferrous iron and hence prevent its oxidation into ferric form. They compare this phenomenon to that of the membranes of special organelles called magnetosomes which are present in magnetotactic bacteria. These membranes are known to protect magnetite nanocrystals found within the magnetosomes from oxidation (Zhu et al., 2015). However it is important to note that ferric and ferroxide (magnetite) forms of iron were also reported in the nanoscale Aβ aggregates analysed by these authors, with iron apparently present throughout the aggregates. This is consistent with co-aggregation of Aβ and iron from extremely early stages in plaque formation since the aggregates reported by the authors were ~1-5um and often considerably smaller (<100nm), well below the size range of ~20+ um of the birefringent aggregates analysed in the present study and other light microscopy studies (Dudeffant et al., 2017; Meadowcroft et al., 2009).

House and colleagues (House et al., 2004a) examined fibrillisation of $A\beta_{42}$ in the presence or absence of Fe^{3+} *in vitro* for a period of 32 weeks. The authors observed that both the $A\beta_{42}$ alone and $A\beta_{42}$ combined with Fe^{3+} treatments formed amyloid fibrils with beta-pleated sheet conformation. However the process of fibrillisation was prevented by the iron chelator desferrioxamine (DFO) when incubated for up to 8 weeks. Furthermore, the already formed Aβ fibrils were also partly dissolved when they were incubated with DFO. Therefore the authors proposed that iron was involved in either the formation or stabilisation of amyloid plaques.

Although the presence of redox-active ferrous form of iron in the vicinity of amyloid plaques was not checked within the timeframe of this thesis, preliminary inspection of perfusion Turnbull staining of Aβ+Iron brain did not show any evidence for labelling of structures morphologically resembling plaques. However this could be checked in the future by co-labelling brains with Congo red stain and Turnbull stain (which detects ferrous iron only), possibly also including investigation of nickel-cupric enhancement of DAB (Gallyas and Merchenthaler, 1988; Moos and Mollgard, 1993).

What if iron attached to plaques is actually beneficial in some ways? Is it likely that preventive venesection/chelation will clear this iron attached to plaques?

Based on indirect evidence, iron chelators are now being studied by various researchers to check their effectiveness in AD (Banerjee et al., 2016; Guo et al., 2013; Kupershmidt et al., 2012). However, data obtained in this chapter may instead provide indirect evidence that iron chelation may not be useful in slowing amyloidogenesis, at least at the earlier stages of the disease corresponding to those investigated in the present study. It will also be important to study this in older mice which are at later stages of the disease.

Although clinical trials are now focusing on early chelation of iron to prevent AD (Adlard and Bush, 2018), there is as yet still a lack of convincing evidence showing effectiveness of early iron chelation in the treatment of AD. It is also to be noted that excess iron to near double normal levels is present throughout adult life in the Aβ+Iron model, on a par with (Ayton et al., 2019) or considerably beyond the extent of reported increases in human brain iron for most individuals with Alzheimer's disease as based on current evidence (Schrag et al., 2011b), and yet this doesn't seem to exacerbate cerebral amyloidosis in this model.

The question also arises as to whether approaches like preventive venesection or iron chelation will be effective in getting rid of iron that is attached to amyloid. Furthermore chelation may also perturb iron-dependent intrinsic physiology of the brain and the rest of the body since chelators may inappropriately remove iron compounds that are required for normal iron homeostasis (Collingwood et al., 2008; Raven et al., 2013). This highlights the importance of thoughtful administration of chelation therapy on an evidence-based, case-by-case basis, if at all. Considerations relating to iron chelation are addressed in more detail in subsequent chapters and in the General Discussion.

Limitations and future directions

Six month old mice were chosen for this study as pathological changes are clearly visible at this age, for the APP/PS1 model. However, plaque deposition is reported to continue till at least 20 months of age in the APP/PS1 model (van Groen et al., 2006). Future studies could incorporate older aged mice to see if iron affects amyloid burden at later ages. As described earlier (Section 2.1), the AKR background was chosen for this study to maximize iron-loading phenotype (Fleming et al., 2001; McLachlan et al., 2010). However, mice on the AKR background seem to have reduced life expectancy as compared to the other background strains and this has so far restricted procurement of older aged mice (e.g. beyond 9 months). To overcome this, other strains of mice are being studied by other members of our group for generating mice with the same mutations as those of the Aβ+Iron model but this may come with the limitation of reduced tissue iron accumulation..

In addition, younger mice could be studied in the future to investigate whether iron deposition precedes or is secondary to amyloid plaque formation and, if the former, whether amyloidosis can be modified by iron chelation. Studying younger mice may also help in examining if there is any significant difference in the amount of amyloid deposition right at the time when plaques first start to form. This is currently underway in another ongoing PhD project (Freeman-Acquah in progress).

Recent findings have postulated that soluble forms of Aβ are more toxic and correlate more strongly with cognitive impairment in AD than the insoluble aggregated plaques (Haass and Selkoe, 2007; Sengupta et al., 2016; Tomic et al., 2009). This project focused on characterising the relationship of iron with insoluble Aβ pathology in the Aβ+Iron model since the co-localisation of amyloid pathology and iron are central to past proposals that iron has causal roles in Alzheimer's disease (Connor et al., 1992b; Peters et al., 2015; Smith et al., 1997). The methods used here do not allow analysis of soluble forms of Aβ and this could not be investigated within the timeframe of this thesis. However experiments involving the enzyme-linked immunosorbent assay (ELISA) method to measure the levels of soluble amyloid deposits/oligomers will be undertaken in follow-up projects.

Stereological methods of counting amyloid plaques have been used by some researchers to estimate amyloid load in post-mortem brain tissue from AD patients (Iacono et al., 2014; Madsen et al., 2018). This could be performed in future studies as an additional method of amyloid quantification in the Aβ+Iron model to determine possible differences more accurately, although based on results

to date any such differences appear likely to be small. Structural changes, amyloidosis and other features of AD have also been investigated by different groups in the cerebellum and brainstem regions of the APP/PS1 model and human AD brains (Cole et al., 1993; Lee et al., 2015; Thal et al., 2002; Uematsu et al., 2018). As these regions were not examined in our study, they could be potential regions to consider for amyloid detection and analysis in the future.

The DAB-enhanced Perls' stain is widely known to detect ferric as well as ferrous forms of iron (Meguro et al., 2007). This suggests that both ferric and ferrous iron co-localised with amyloid plaques in the Aβ+Iron model and the Aβ model, consistent with previous reports (Everett et al., 2014a; Everett et al., 2014b; Telling et al., 2017). While this was beyond the scope of this thesis, some studies have used techniques like transmission electron microscopy and x-ray spectroscopy and reported the dominance of iron oxide compounds such as magnetite and maghemite in the amyloid plaque cores in human AD brain (Collingwood et al., 2008; Collingwood et al., 2005; Kirschvink et al., 1992). Similar observations have been described *in vitro* (Everett et al., 2014a; Everett et al., 2014b) and in the APP/PS1 brain (Gallagher et al., 2012). This could be another potential area of future study in the Aβ+Iron model.

Conclusion

In summary, increases of almost 2-fold in brain iron levels were observed in Aβ+Iron mice compared to Aβ mice, yet this did not appear to exacerbate various measures of cerebral amyloidosis even though iron appeared to be present in all amyloid plaques and usually coincided closely with deposition of insoluble Aβ peptide. Firm conclusions cannot be made about whether iron is necessary for initial seeding of Aβ aggregates, as proposed by some authors, as described above (Bolognin et al., 2011; Collingwood et al., 2008; House et al., 2004b; Mantyh et al., 1993). However the findings are consistent with recent studies of human brain suggesting iron may co-deposit from the very earliest stages of Aβ aggregation (Telling et al., 2017). However amyloid deposition was not evident in the Iron model which suggests that iron does not appear to be sufficient for amyloid deposition in the mouse in the absence of abnormalities in APP such as the Swedish mutation present in our Aβ-producing mouse models.

The following chapter will compare the overall distribution of Aβ aggregation and brain iron labelling and examine what brain regions, cells and structures besides amyloid plaques contain iron in the Aβ+Iron model and how, if at all, iron distribution differs in this model compared to the other mouse models examined in the thesis.

4. Iron distribution and localization in the brain of the Aβ+Iron model

4.1 Introduction

In the previous chapter, it was demonstrated that brain non-haem iron levels were increased in the Aβ+Iron model compared to the Aβ model. Likewise, an increased proportion of plaques were found to contain iron in the Aβ+Iron model. However, excess brain iron did not appear to exacerbate cerebral amyloidosis in the Aβ+Iron model as compared to the Aβ model.

One important question which needs to be investigated is whether amyloid plaques are more commonly found in brain regions with high levels of overall iron. Next question is what other brain regions and cell types contain iron besides amyloid plaques in the Aβ+Iron model. Previous studies by our group on the *Hfe*$^{-/-}$*xTfr2*^{mut} model showed increased iron loading in the choroid plexus, myelinated structures, a subset of oligodendrocytes and some unidentified cells as compared to the wildtype AKR model whereas most neurons, microglia and astrocytes stored very little iron (Heidari et al., 2016b). Similar pattern of iron loading is expected in the Aβ+Iron model as it was developed by crossbreeding the *Hfe*$^{-/-}$*xTfr2*^{mut} model with the Aβ model, which is described in General Methods chapter (Section 2.1).

This chapter tests the second hypothesis of this project that brain iron distribution in different cell types and structures is generally similar in the Aβ+Iron model and the *Hfe*$^{-/-}$*xTfr2*^{mut} model (the 'Iron model') with the main exception of iron associated with amyloid plaques and iron-associated cells in the vicinity of amyloid plaques in the Aβ+Iron model (plaques are not present in the 'Iron model').

The brain iron distribution and localisation in the Iron model has been published by our group (Heidari et al., 2016b) and will not be presented here. However, observations from both the Aβ+Iron model and the Aβ model will be described. Iron distribution in the brains of the Aβ+Iron model and the Aβ model was examined by 3'3'-diaminobenzidine-tetrahydrochloride (DAB)-enhanced Perls' staining. To detect presence of ferrous iron in these mice, both traditional Turnbull staining and perfusion Turnbull staining methods were employed. Furthermore, immunohistochemistry for different brain cell markers was used to study localization of iron in different cells and structures in the Aβ+Iron model and the Aβ model.

4.2 Materials and methods

4.2.1 Mice age and tissue collection

The generation of the Aβ+Iron mice and the Aβ mice has been detailed in Section 2.1. For histological studies, mice (n=4/group, 2 males and 2 females in each group) were used at six months of age, unless stated otherwise. Mice were fed with a standard AIN-93G diet containing approximately 0.02% iron (Reeves et al., 1993). All protocols were approved by the Animal Ethics Committee of the University of Sydney, where the mice colonies were bred and maintained.

4.2.2 Histological studies

Brains were dissected and fixed in 4% PFA (Section 2.2.1). Brain blocks were further cryosectioned into 20 micron thick sections and transferred onto gelatin-coated slides (Section 2.3.1.3). Four brain sections each from both groups of mice (n=4/group, 2 males and 2 females in each group) were selected at a sampling rate of 1 in 10 starting from -2.46 mm Bregma to -3.16 mm Bregma as described in Section 2.3.1.5. Based on Paxinos and Franklin's mouse brain atlas (Paxinos, 2013), these regions contain the hippocampus and the cerebral cortex, both of which are strongly affected in AD. Furthermore, these regions also include various structures of the midbrain which were investigated earlier in the Iron model (Heidari et al., 2016b).

4.2.3 DAB-enhanced Perls' and Turnbull staining

As described in General Methods chapter (Section 2.3.2), 3'3'-diaminobenzidine tetrahydrochloride (DAB) enhanced Perls' staining and Turnbull staining (Meguro et al., 2007; Nguyen-Legros et al., 1979) were used to detect iron in brain sections of the Aβ+Iron mice and the Aβ mice (n=4/group). DAB-enhanced perfusion Turnbull staining was also performed on these mice as described in Section 2.3.3.

DAB-enhanced Perls' stained sections were scanned under 10X objective using the ZEISS Axio Scan.Z1 Slide Scanner (Bosch Institute, University of Sydney). Using Fiji distribution of ImageJ, the percentage of left brain hemisphere containing DAB-enhanced Perls'-positive pixels (%Area or Area fraction) was determined. Generally, the pixel intensity values correspond to gray scale values where 0 means pure black and 255 means pure white. This can be counterintuitive since it leads to an inverse relationship between %Area and iron content. For ease of interpretation, the pixels corresponding to white on the 'gray scale' were allocated a value of 0 and pixels corresponding to black a value of 255. An algorithm was designed using the 'Auto Threshold' function to classify the analysed images into four categories based on their pixel intensities: weak staining (0 to 63), medium staining (64 to 127), strong staining (128 to 191) and very strong staining (192 to 255).

Likewise, the intensity of DAB-enhanced Perls' staining across the brain hemisphere of Aβ+Iron mice was compared with that of Aβ mice, by measuring the mean gray value, which is the average gray value within the tissue section (Schindelin et al., 2012).

4.2.4 Distribution of iron-amyloid plaques

The distribution of hundred randomly selected amyloid plaques labelled with Congo red stain was examined across left brain hemispheres from four different Aβ+Iron mice. This was done to check if plaques were more common in regions with high iron. The mean gray value (MGV), which is the average gray value within the tissue section, was used to indirectly assess the level of iron staining. Lower values correspond to darker staining due to increased iron content, as assessed indirectly from the oxidisation of greater amounts of DAB. This can be counterintuitive since it leads to an inverse relationship between MGV and iron content i.e. the pixel intensity values correspond to gray scale values where 0 means pure black and 255 means pure white. As described in Section 4.2.3, pixels corresponding to white on the 'gray scale' were therefore instead allocated a value of 0 and pixels corresponding to black a value of 255. The distribution of amyloid plaques was examined across four levels of DAB-enhanced Perls' staining for iron as described in Section 4.2.3.

4.2.5 Combined DAB-enhanced Perls' staining and immunolabelling

As described in Section 2.3.6.3, fluorescent immunolabelling was performed on four tissue sections per animal from -2.46 mm Bregma to -3.16 mm Bregma (n=4 mice/group, 2 males and 2 females in each group). Adjacent tissue sections were immunolabelled for the same antigen after first staining with DAB-enhanced Perls' stain, for simultaneous detection of iron accumulation and identification of cells/structures containing iron. Imaging was done using the CellSens 1.12 digital imaging software provided with the Olympus DP72 microscope. Brightfield and fluorescent images were overlayed using the Image Calculator function of Fiji distribution of ImageJ.

4.2.6 Myelin staining

As described in General methods (Section 2.3.4), Luxol fast blue solution (IHC World Luxol fast blue Kit) was used for myelin staining on three tissue sections per animal (n=4 mice/group) of the Aβ+Iron model and the Aβ model. Luxol fast blue staining was also performed on the adjacent brain sections which were first stained with DAB-enhanced Perls' staining.

4.2.7 Statistical analysis

GraphPad Prism 7 software was used for statistical analysis and data plotting. Quantification of different parameters for DAB-enhanced Perls' staining in the Aβ+Iron model and Aβ model was done by unpaired *t*-tests. Significance was set at $p<0.05$.

4.3 Results

4.3.1 Relationship between regional iron loading and amyloid plaque formation

Within any region, different amounts of iron may be present in the extracellular matrix as well as in myelin or cell processes and cell bodies. As expected, and as previously reported in Chapter 3 (Section 3.3.1, Fig. 3.1), increased levels of iron as assessed by DAB-enhanced Perls' stain were observed in the brain of Aβ+Iron mice as compared to the age- and gender-matched Aβ mice. A user-defined algorithm was used to classify levels of DAB-enhanced Perls' staining across brain regions based on pixel intensity values, as described in Section 4.2.3. Most staining in the Aβ model fell under the pixel intensity range 0 to 63, corresponding to weak Perls' staining whereas most staining in the Aβ+Iron model fell under the pixel intensity range 64 to 127, corresponding to medium Perls' staining, followed by the range 128 to 191, corresponding to strong Perls' staining. There was virtually no staining in the intensity range of 192 to 255, corresponding to very strong Perls' staining. This was represented by the digitally coloured images shown in Fig. 3.1, in which weak iron labelling was represented by dark blue, medium by green, strong by cyan and very strong by yellow.

In order to see if amyloid plaques were more commonly found in regions with high levels of overall iron, 100 randomly selected amyloid plaques examined across left brain hemispheres of four Aβ+Iron mice, as described in Methods (Section 4.2.4). As amyloid plaques were so concentrated in areas with lower iron staining, most of the plaques fell into lower quartiles of levels of Perls' staining as described above. Hence, iron staining was further stratified into 4 different levels corresponding to the quartiles of the range from minimum to maximum iron staining as described in Methods (Section 4.2.4).

In general, there were more amyloid plaques in brain areas with less iron staining compared to areas with high iron staining (correlation coefficient -0.97, SD 7.135). Specifically, there were 48 plaques located in regions with weak (40-65) iron staining, 36 plaques in regions with medium (65-90) iron staining, 10 plaques in regions with strong (90-115) iron staining and 6 plaques in regions with very strong (115-140) iron staining such as the thalamus (Fig. 4.1). With regard to areas recognised to have higher numbers of plaques, iron staining within the hippocampus and nearby structures ranges from strong (e.g. in the stratum lacunosum-moleculare layer of the hippocampus and regions of nearby corpus callosum) through medium (e.g. molecular layer of hippocampus) to weak (e.g. neuronal layers of hippocampus), with plaques generally restricted to the areas of weak to medium

iron labelling and the cerebral cortex is typically also only weakly stained for iron, as shown in more detail in the subsequent sections of this chapter.

A. Colorised images illustrating different levels of Perls' staining

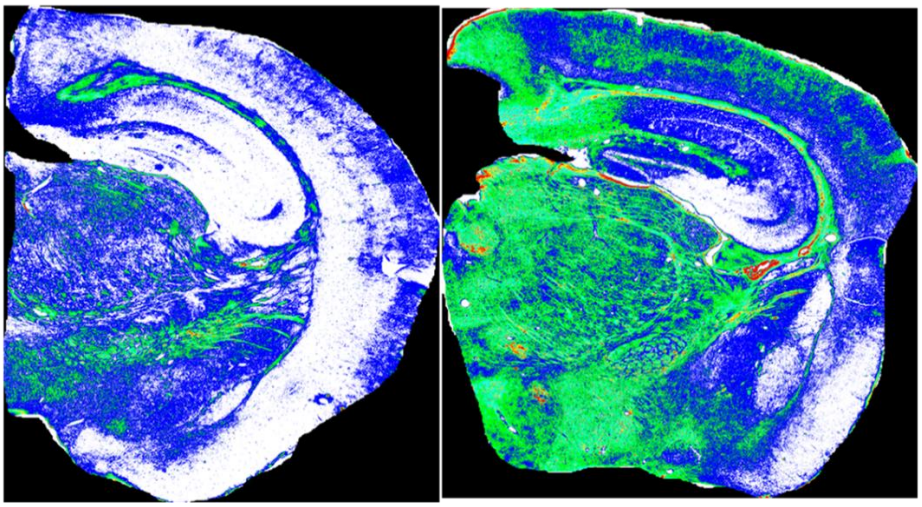

Pixel intensity values
0-40
40-65
65-90
90-115
115-140
140-255

B. Plaque numbers in brain regions with different levels of Perls' staining

Levels of DAB-enhanced Perls' staining (Transformed mean gray value)			
Weak staining (40-65)	Medium staining (65-90)	Strong staining (90-115)	Very strong staining (115-140)
48	36	10	6

Fig. 4.1 Most amyloid plaques were located in regions with less iron staining. The distribution of 100 amyloid plaques from four different Aβ+Iron mice across four different levels of DAB-enhanced Perls' staining is shown. Most of the amyloid plaques were detected in the regions with weak iron staining (dark blue), followed by medium iron staining (green). Lesser number of plaques were detected in the regions with strong iron staining and very few were detected in the regions with very strong iron staining.

One-tailed unpaired *t*-test showed decreased percentages of positive pixels for weak Perls' staining (pixel values 0-63; $p<0.0001$) in the Aβ+Iron model as compared to the Aβ model. One-tailed unpaired *t*-test showed increased percentages of positive pixels for medium Perls' staining (pixel values 64-127; $p<0.0001$), strong Perls' staining (pixel values 128-191; $p<0.0001$) and very strong Perls' staining (pixel values 192-255; $p=0.0003$) in the Aβ+Iron model as compared to the Aβ model (Fig. 4.2).

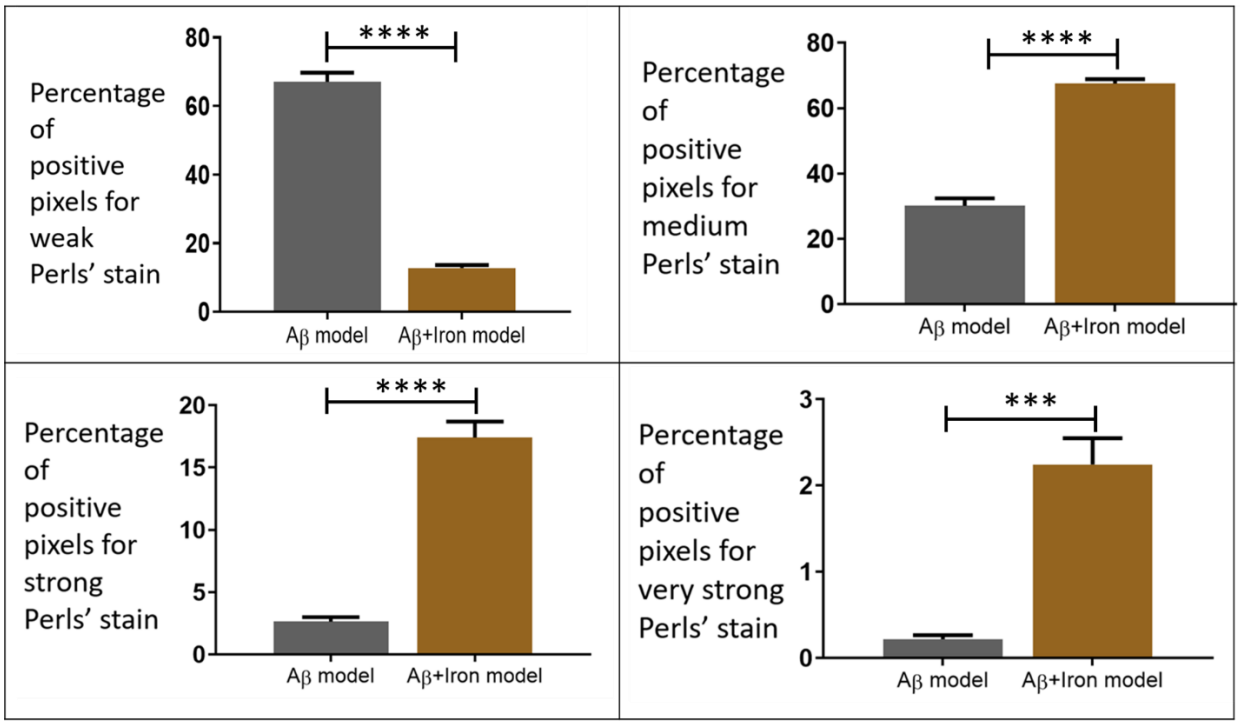

Fig. 4.2 Brain iron assessed by a user-defined algorithm which determines percentage positive pixels for DAB-enhanced Perls' staining in Aβ mice and Aβ+Iron mice (6 months of age). Data are presented as mean ± SD (****p<0.0001, ***p=0.0003; n=4 sex-matched mice/group, region of interest= left brain hemisphere).

As explained in Section 4.2.3, another parameter that was used to measure the level of DAB-enhanced Perls' staining was Mean Gray Value (MGV), which is the average gray value within a selection. Lower values correspond to darker staining due to increased iron content, as assessed indirectly from the oxidisation of greater amounts of DAB. This can be counterintuitive since it leads to an inverse relationship between MGV and iron content i.e. the pixel intensity values correspond to gray scale values where 0 means pure black and 255 means pure white. For ease of interpretation, data were therefore transformed using the formula MGV(T)=K-MGV in which K=255, such that pixels corresponding to white on the 'gray scale' were allocated a value of 0 and pixels corresponding to black a value of 255. There was a statistically significant increase in transformed mean gray value for Perls' staining in the Aβ+Iron mice as compared to the Aβ mice, as depicted by one-tailed unpaired t-test (fold change 1.7, p<0.0001) (Fig. 4.3).

The localisation of ferric and ferrous iron at the level of individual cell types and cellular structures such as the choroid plexus is described below.

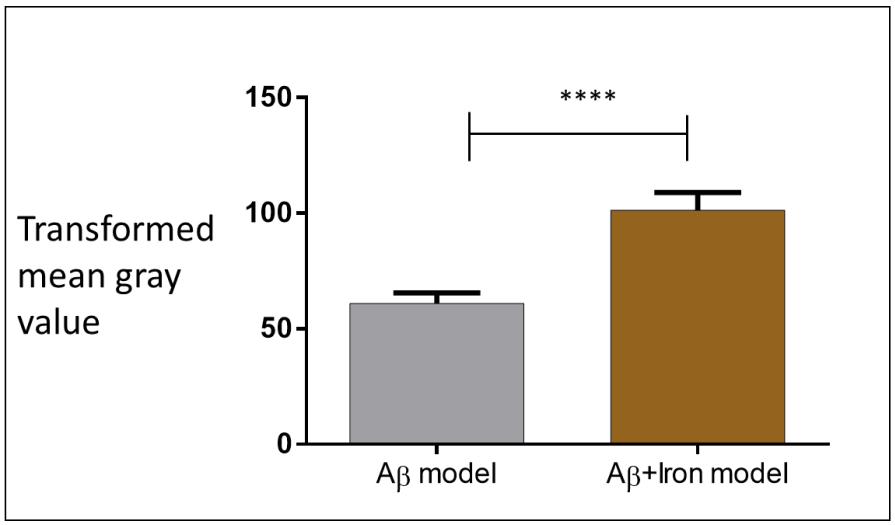

Fig. 4.3 Brain iron assessed by transformed mean gray value of DAB-enhanced Perls' staining in Aβ mice and Aβ+Iron mice at 6 months of age. Data are presented as mean ± SD (****p<0.0001, n=4 mice/group; region of interest= left brain hemisphere).

4.3.2 Stronger iron labelling in the choroid plexus of the Aβ+Iron mouse

Strong iron labelling by DAB-enhanced Perls' stain was most conspicuous in the choroid plexus of the Aβ+Iron mice. Staining in this region was also noticeable in the Aβ mice but with less intensity as compared to the Aβ+Iron mice (Fig. 4.4).

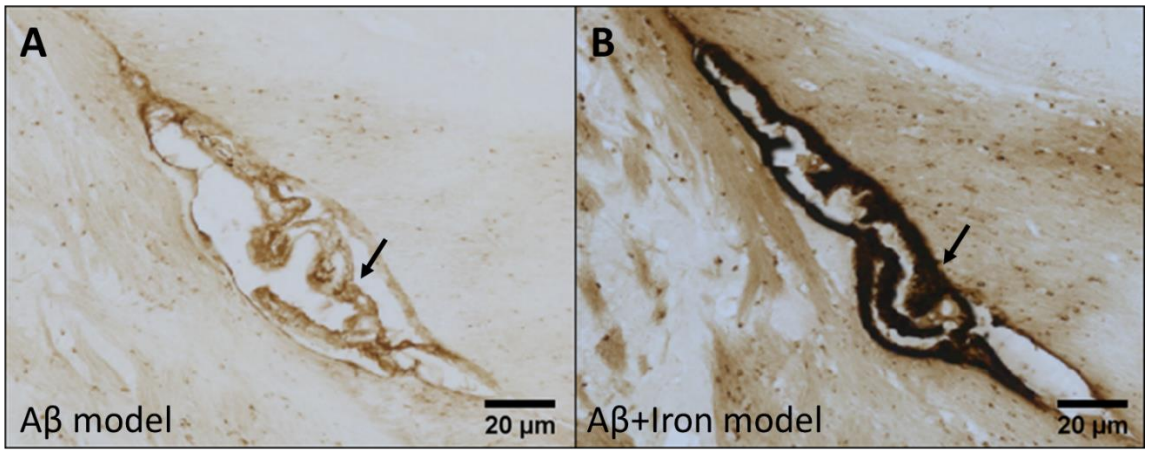

Fig. 4.4 Iron labelling by DAB-enhanced Perls' staining in the choroid plexus. The choroid plexus region in the Aβ+Iron mice was strongly stained for iron with DAB-enhanced Perls' stain, as compared to the Aβ mice. A) Aβ mice B) Aβ+Iron mice.

Choroid plexus was also the only region that showed some labelling with the traditional Turnbull stain for the detection of ferrous iron (Fe^{2+}) in the Aβ+Iron mice and the Iron mice. There was little if any labelling in the Aβ mice or the AKR mice (Fig. 4.5).

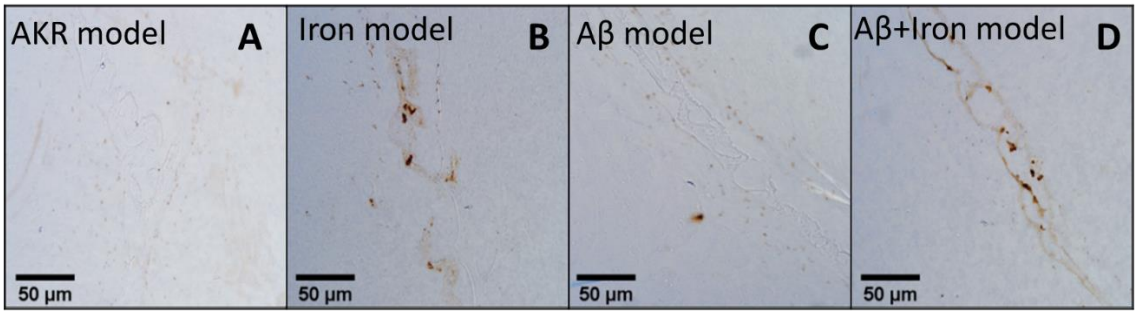

Fig. 4.5 Turnbull staining for detection of ferrous iron. Some staining was seen with the traditional Turnbull stain in the choroid plexus of Aβ+Iron mice and Iron mice, with very little staining apparent in other regions. A) AKR model B) Iron model C) Aβ model D) Aβ+Iron model.

At the end of this study, a preliminary trial of a 'perfusion Turnbull' method was undertaken after learning about this method when older literature was checked for insights into how to improve labelling with this stain. This method uses cardiac perfusion of anaesthetised mice with a Turnbull stain solution of 1% potassium ferricyanide in 10% formalin, followed by post-fixation in 10% formalin after the brain is removed and subsequent DAB enhancement (Meguro et al., 2003). This was tested on 9 month old mice (n=1 mouse/group) which were the oldest age available since iron abnormalities often accumulate with age. It has not been possible to extend this to additional mice for statistical comparisons or at other ages in the timeframe of the thesis.

Preliminary observations using the perfusion Turnbull staining method also detected labelling in the choroid plexus of the Iron model and the Aβ+Iron model, as described above. In addition to the labelling observed with the traditional post-fixation Turnbull staining method, the perfusion technique also enabled detection of iron-loading cells in a few other brain regions, notably midbrain. This was more noticeable in the Aβ+Iron model and the Iron model compared to the Aβ model and the AKR model (Fig. 4.6 A-D). However it needs to be noted that these differences may be at least partly attributable to the fact that the mice used for the perfusion trial were older (9 months vs 6 months of age). In addition the distribution of Turnbull staining in the Aβ+Iron model suggested that while fixation and penetration had occurred in some periventricular regions the solutions had failed to reach other regions due to inadequacy of cardiac perfusion in this animal (Fig. 4.6 G, H), further limiting the conclusions that can be drawn. Additional experiments to refine these methods on larger numbers of mice are underway in other student projects in our group.

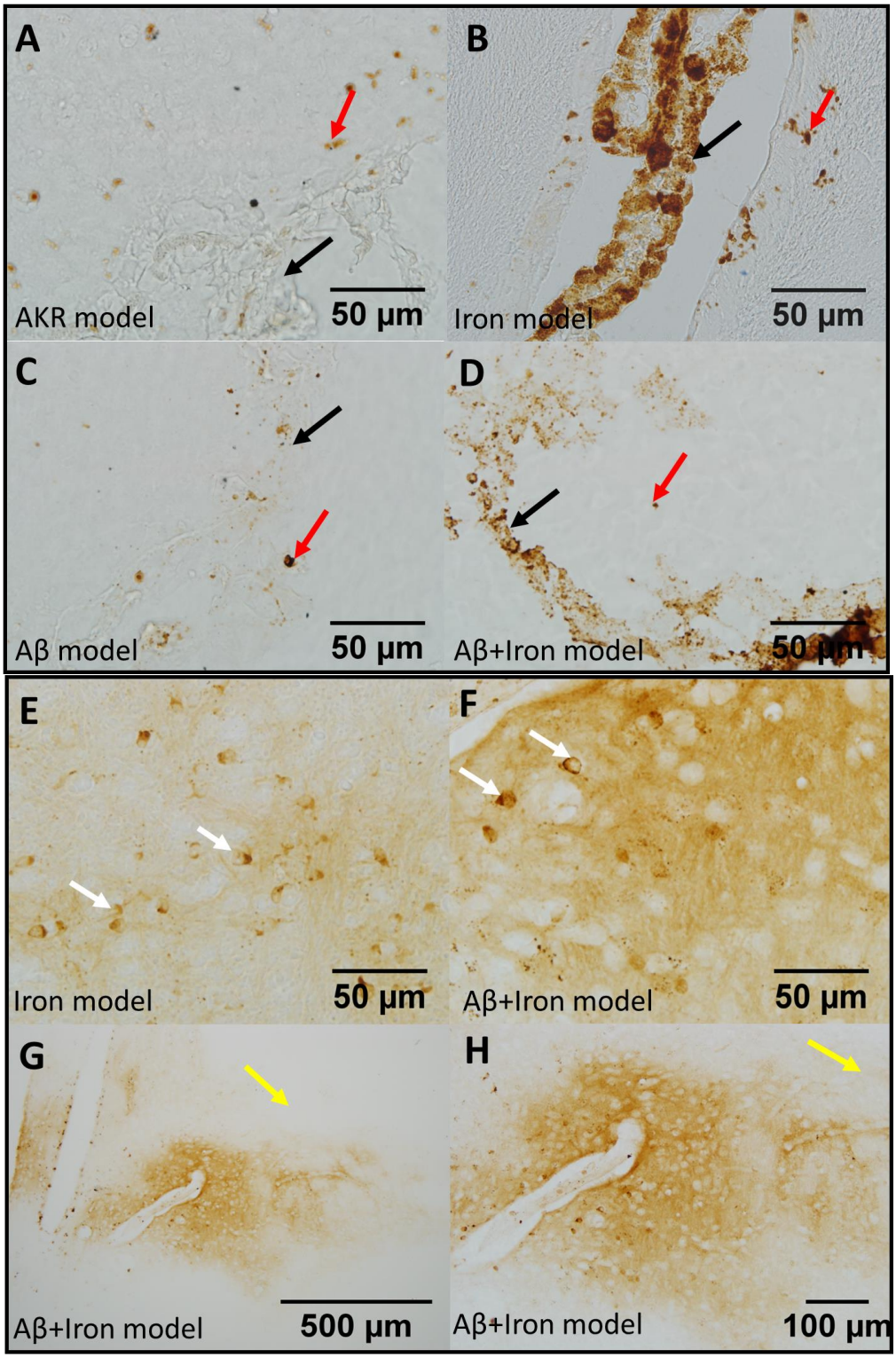

Fig. 4.6 Detection of iron by DAB-enhanced 'perfusion Turnbull staining'. Staining of choroid plexus by perfusion Turnbull staining was conspicuous in the Iron model and the Aβ+Iron model and less obvious in the AKR model and the Aβ model (panels A-D, black arrows). Staining was also observed in occasional cells within the neuropil in all mice (panels A-D, red arrows). Notably there was staining in the midbrain of a few cells with morphologies similar to some cells observed with DAB-enhanced Perls' staining of the Iron model and the Aβ+Iron model (panels E, F, white arrows) but not the other models. However it was noted that there were areas of brain in the Aβ+Iron model where the fixative/Turnbull solution may not have reached due to inadequate perfusion (panels G, H, yellow arrows).

4.3.3 Neurons contain very little Perls' stainable iron in the hippocampus and the cerebral cortex

The neuronal layers of hippocampus were almost clear from any DAB-enhanced Perls' staining for iron in both Aβ+Iron mice and Aβ mice. Specifically, the granular cell layer of the dentate gyrus showed extremely weak staining for iron in both groups of mice. However, the outer molecular and inner polymorphic layers of the dentate gyrus and the stratum lacunosum-moleculare layer of CA1 showed some level of staining for iron in the Aβ+Iron mice and this was faintly apparent in the Aβ mice (Fig. 4.7). Consistent with our previous observations in the *Hfe*$^{-/-}$x*Tfr2*^{Y245X} model, cells staining for iron in these regions were more of perivascular or oligodendroglial appearance (Heidari et al., 2016b).

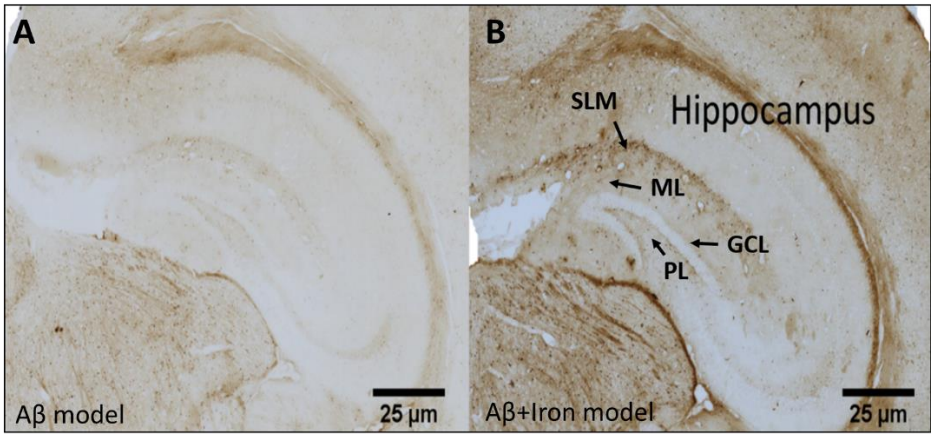

Fig. 4.7 Neurons contain very little Perls' stainable iron in the hippocampus. The magnified images show DAB-enhanced Perls' staining in different regions of the hippocampus of Aβ mice (A) and Aβ+Iron mice (B). While the granule cell layer (GCL) shows little evidence of staining for iron, other layers show some staining, namely the polymorphic layer (PL), molecular layer (ML) and the stratum lacunosum-moleculare layer (SLM) in the Aβ+Iron mice, whereas these layers had little observable staining in the Aβ mice.

Double labelling of sections by DAB-enhanced Perls' stain and the neuronal marker NeuN also failed to show co-localisation of DAB-enhanced Perls' stainable iron and neurons in the hippocampus of either Aβ+Iron mice or Aβ mice (Fig. 4.8).

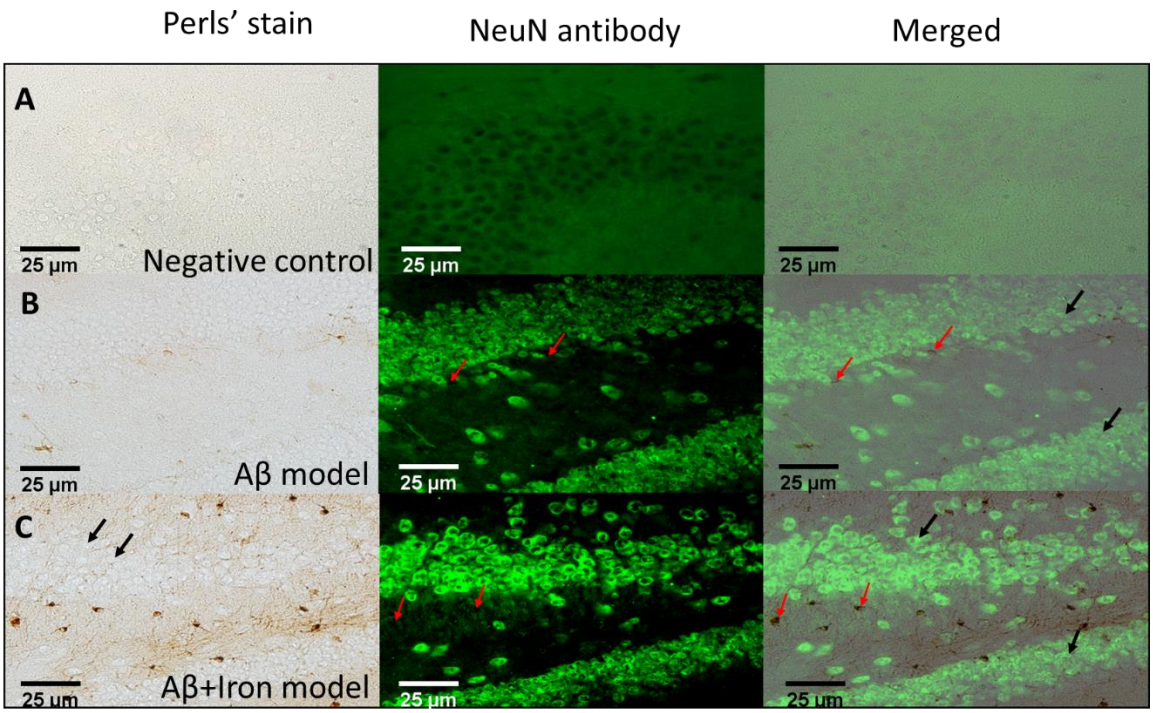

Fig. 4.8 Neuronal layers contain very little Perls' stainable iron in the hippocampus. Double labelling of DAB-enhanced Perls' stain with the neuronal marker NeuN failed to show clear co-localisation of iron with hippocampal neurons, which often appeared virtually unstained (black arrows). Occasional nearby cells conspicuously loaded with iron were typically NeuN negative (red arrows). A) Negative control without DAB-enhanced Perls' stain and NeuN antibody, B) Aβ model C) Aβ+Iron model.

These results were also confirmed with cresyl violet stain, which is another widely used neuronal stain, although it may also detect some non-neuronal glial cells (Fig. 4.9). While virtually most neurons do not appear to be staining positive for DAB-enhanced Perls' stain, we cannot rule out the possibility that a small number of neurons maybe loading iron.

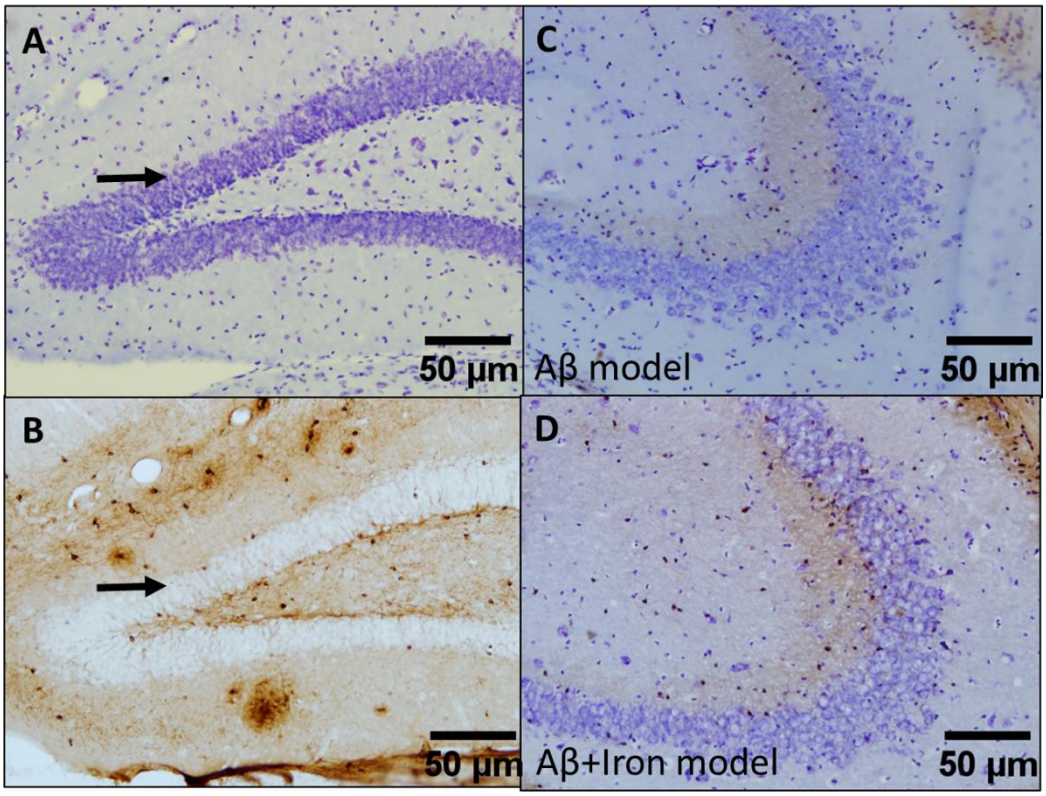

Fig. 4.9 Neurons contain very little Perls' stainable iron in the hippocampus. (A) Cresyl violet staining, (B) DAB-enhanced Perls' staining in hippocampus. Co-labelling of DAB-enhanced Perls' stain with Cresyl violet stain shows little evidence of iron coinciding with the hippocampal neuronal layers which typically seem to contain very little iron, appearing almost white (black arrows) in Aβ mice (C) and Aβ+Iron mice (D).

Labelling of cerebral cortex with DAB-enhanced Perls' stain was slightly darker in Aβ+Iron mice compared to Aβ mice. As in the hippocampus, neurons in this region again showed little if any co-localisation with Perls' stainable iron in either Aβ mice or Aβ+Iron mice.

As illustrated in Fig. 4.10, at least two distinctive kinds of cells were detected by the combined Perls'/NeuN labelling in the cortex as well as the hippocampus and other regions. The first type of cell was larger in size and labelled for NeuN. The second type of cell had relatively smaller size and an eccentric nucleus, characteristics which are distinctive of the iron-loading cells.

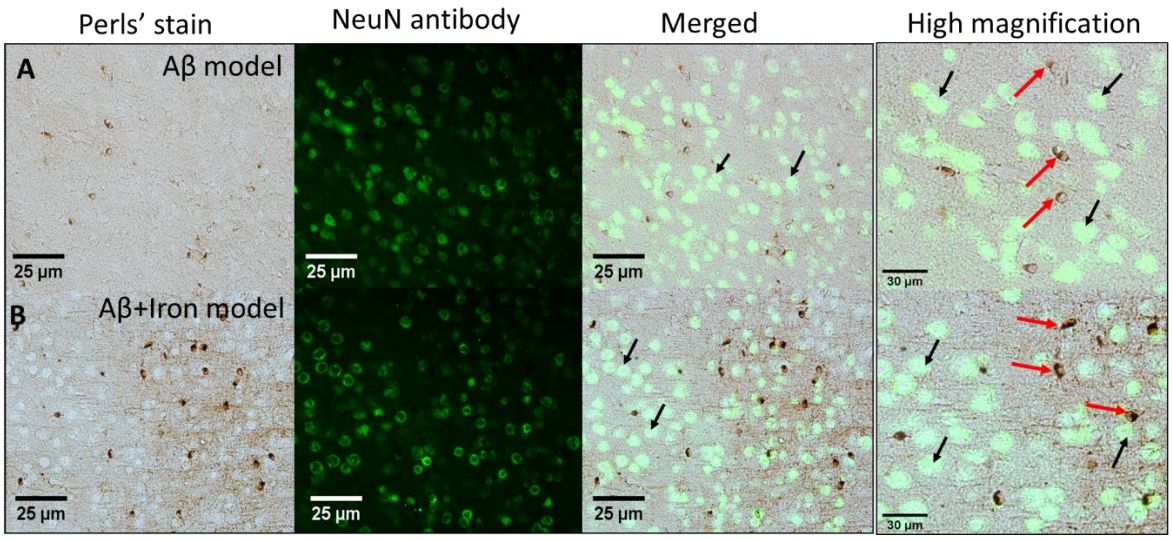

Fig. 4.10 Neurons contain very little Perls' stainable iron in the cerebral cortex. Although the cerebral cortex showed slightly darker staining for iron in Aβ+Iron mice (B) as compared to Aβ mice (A), double labelling of DAB-enhanced Perls' stain with NeuN failed to show clear co-localisation of iron and neurons in both groups (black arrows). Even when the cells were very closely adjacent, there still appeared to be two types of distinct cell bodies: NeuN positive cells with larger morphology (black arrows) and cells of smaller size with an eccentric nucleus, a feature characteristic of many of the iron-loading cells (red arrows).

4.3.4 Neurons contain very little if any Perls' stainable iron in the midbrain and associated regions

As in the hippocampus and the cerebral cortex, DAB-enhanced Perls' staining combined with NeuN immunolabelling also failed to show co-localisation of iron with neurons in the midbrain and associated regions. Iron was noticed in the fibre tracts in these regions, which have the typical appearance of myelin. Iron was also observed in myelin-associated cells with oligodendroglial appearance (Fig. 4.11).

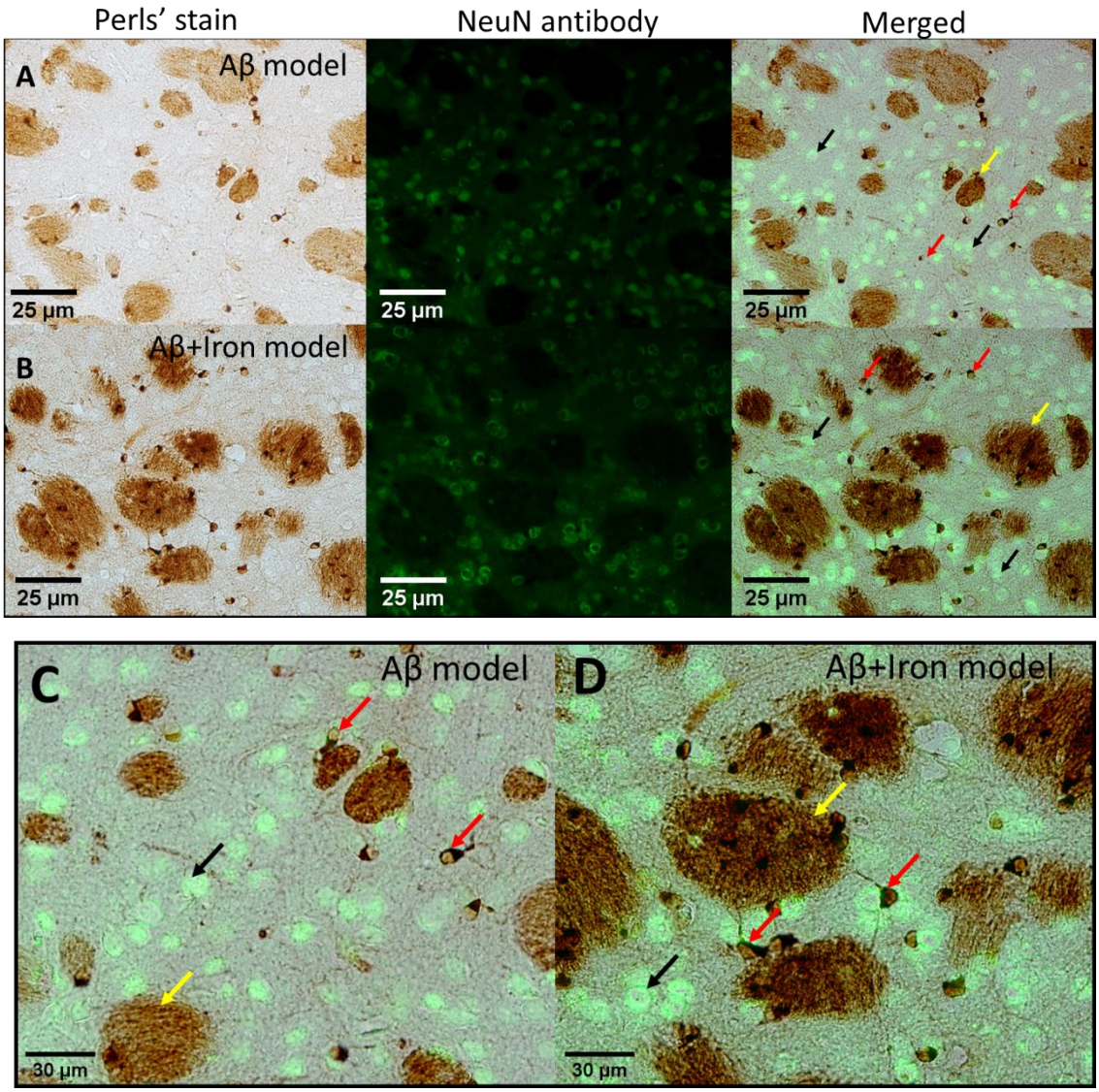

Fig. 4.11 Neurons contain very little Perls' stainable iron in the midbrain even in regions with considerable iron staining. Combination of DAB-enhanced Perls' stain with NeuN antibody in the midbrain regions of Aβ mice (A) and Aβ+Iron mice (B), indicated by black arrows and shown at higher magnifications for (C) Aβ mice and (D) Aβ+Iron mice. In all of these images, iron was concentrated in patches that looked like myelinated tracts (yellow arrows) and cells with oligodendrocyte-like morphologies associated with these tracts (red arrows).

To see the distribution of iron and to confirm the identity of these iron-containing fibre tracts, the highly myelinated regions were studied in more detail using the combination of DAB-enhanced Perls' stain and either of two myelin stains (CNPase, Luxol fast blue), as discussed below.

4.3.5 Iron co-localises with myelin and myelin-associated cells

As illustrated in Fig. 4.12, region with long myelin fibre tracts, such as the corpus callosum were shown to have strong labelling for iron in Aβ+Iron mice, which was also present although less

prominent in Aβ mice. The DAB-enhanced Perls' stain revealed strong iron labelling in 'patches' in regions such as the midbrain, caudate putamen and thalamus of both Aβ+Iron mice and Aβ mice.

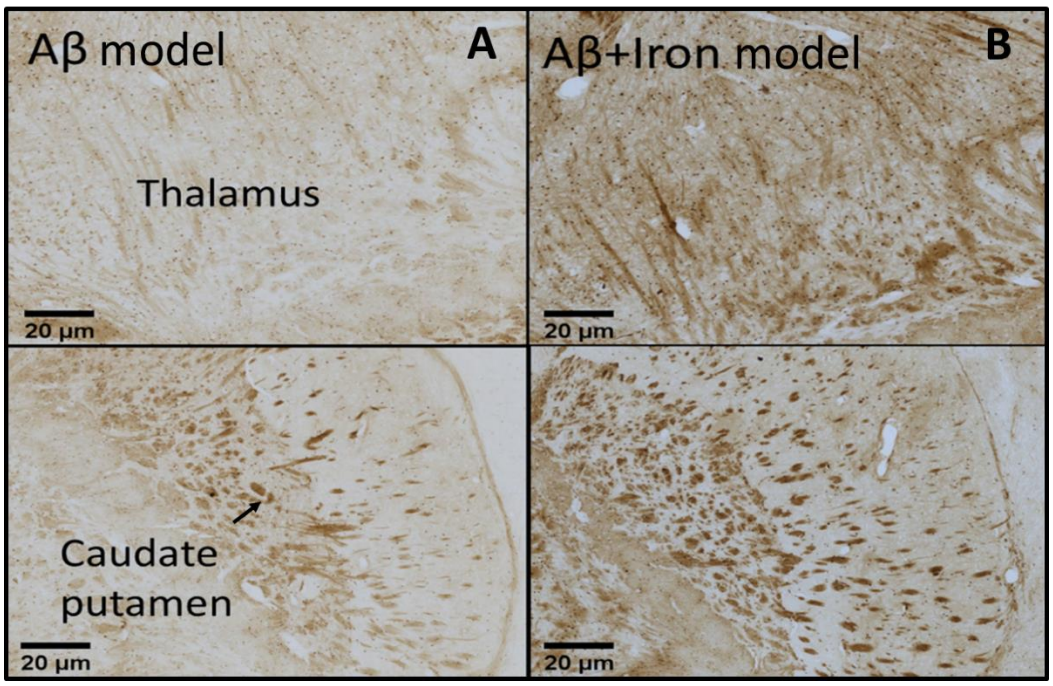

Fig. 4.12 Iron staining in the midbrain and nearby regions. Strong iron labelling was seen in patches in the thalamus, caudate putamen and the associated regions. Staining was darker in the Aβ+Iron mice (B), as compared to Aβ mice (A).

Staining of consecutive sections with DAB-enhanced Perls' stain for iron, Luxol fast blue stain for myelin and co-labelling with both stains showed that the iron-loading tracts present in both Aβ+Iron mice and Aβ mice contained myelin (Fig. 4.13). Iron localisation in these structures has been previously reported by our group for the *Hfe*$^{-/-}$x*Tfr2*^{Y245X} model (Heidari et al., 2016b).

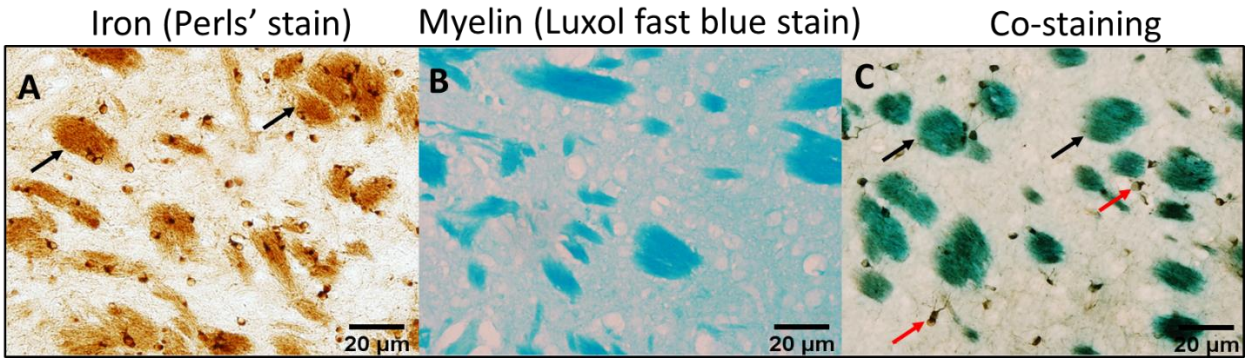

Fig. 4.13 Co-localisation of iron with myelin and myelin associated cells. A) DAB-enhanced Perls' stain B) Luxol fast blue stain C) Co-staining demonstrating co-localisation of myelin with iron (black arrows). Red arrows show myelin-associated cells with processes labelled for iron.

Iron-myelin co-localisation was further confirmed by co-labelling of the sections with DAB-enhanced Perls' stain and a myelin-specific marker 2',3'-cyclic-nucleotide 3'-phosphodiesterase (CNPase). Consistent with observations from our group reported previously for the *Hfe*$^{-/-}$x*Tfr2*^{Y245X} model (Heidari et al., 2016b), there was variability in the amount of iron loading in the myelin tracts, with some myelin patches containing relatively high amounts of iron labelling whereas others appeared to have considerably less labelling (Fig. 4.14).

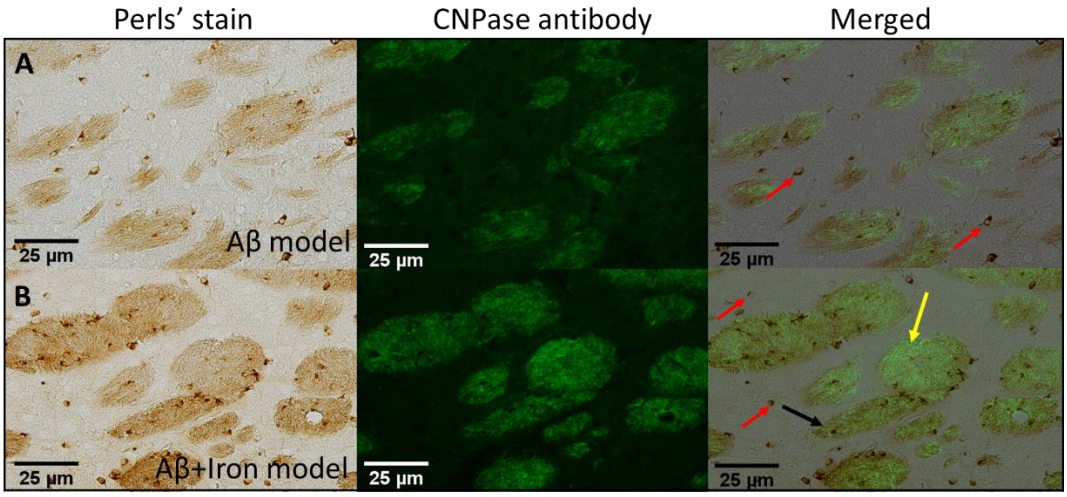

Fig. 4.14 Iron co-localises with myelin and myelin-associated cells. Combined DAB-enhanced Perls' stain and 2',3'-cyclic nucleotide 3'-phosphodiesterase (CNPase), a myelin-specific marker, showed that iron was present to variable degrees in myelin patches. The figure shows an example of a myelin patch containing relatively high amounts of iron labelling (black arrow), as compared to an immediately adjacent myelin patch with notably less iron labelling (yellow arrow). Red arrows indicate myelin-associated cells loaded with iron. (A) Aβ model, (B) Aβ+Iron model.

The myelin-associated cells were occasionally observed either in duos or in groups and linear rows resembling a train or a chain. This was clearly visible along the myelin rich layers of the corpus callosum. Such an arrangement of cells has been described as the typical characteristics of oligodendrocytes (Heidari et al., 2016b; Peters and Sethares, 2004; Todorich et al., 2009b). Labelling of sections with ferritin heavy and ferritin light antibodies also showed similar linear arrangement of cells, mostly visible in the corpus callosum (Fig. 4.15, personal communication J.Woods).

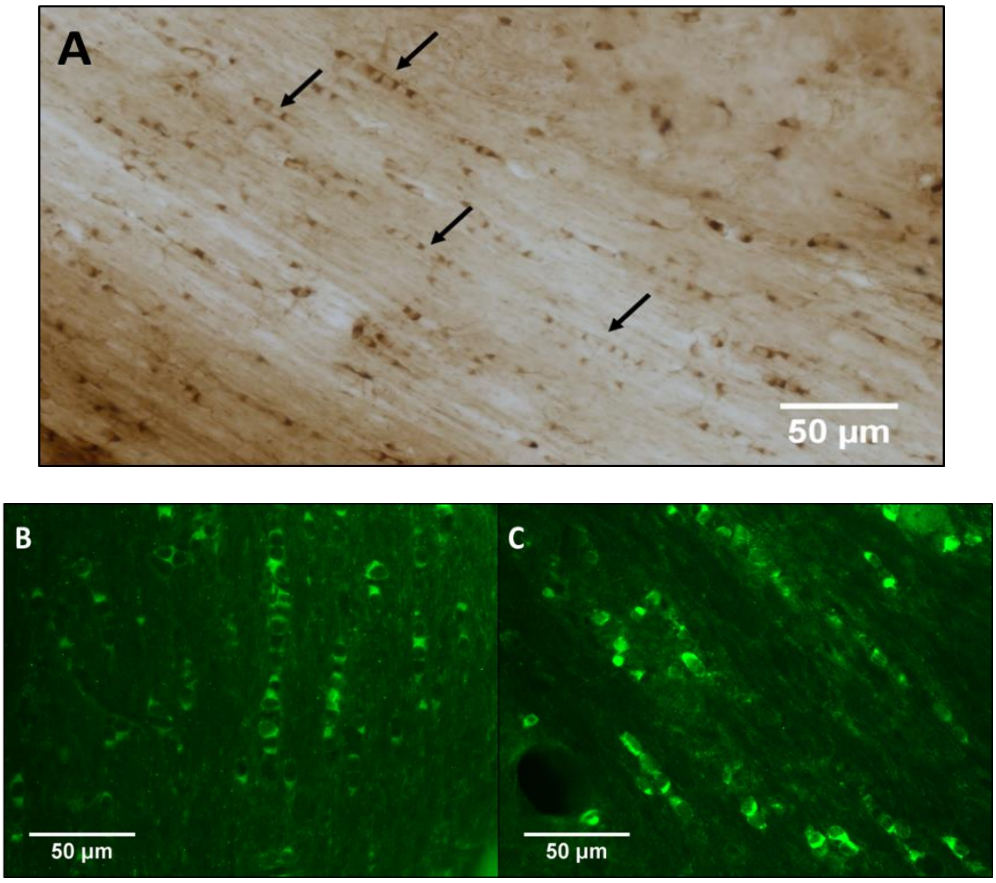

Fig. 4.15 Iron-labelling cells in linear rows. A) Cells were occasionally arranged in pairs or linear rows in Aβ+Iron mice as well as Aβ mice. Similar linear arrangement of cells was seen on labelling the sections with B) ferritin heavy antibody, and C) ferritin light antibody (Images 4.15 B and 4.15 C: Courtesy of J Woods)

4.3.6 Astrocytes contain very little Perls' stainable iron

In general, the combination of immunolabelling for glial fibrillary acidic protein (GFAP) and DAB-enhanced Perls' stain for iron showed that GFAP positive astrocytes contain very little Perls' stainable iron (Fig. 4.16). This was clearly observable in regions such as the hippocampus where GFAP expression in some areas was high for both the Aβ+Iron model and the Aβ model, as

compared to other brain regions i.e., regions with many astrocytes typically had relatively few iron loading cells. Conversely, regions with very high iron loading usually contained relatively few GFAP-positive cells, consistent with an absence of reactive gliosis even in areas of high iron loading. Likewise, preliminary observations (data not shown) suggest that the iron-laden cells in the vicinity of amyloid plaques (which will be described in more detail in Section 4.3.7) are not astrocytes, although this remains to be confirmed in ongoing studies in the lab.

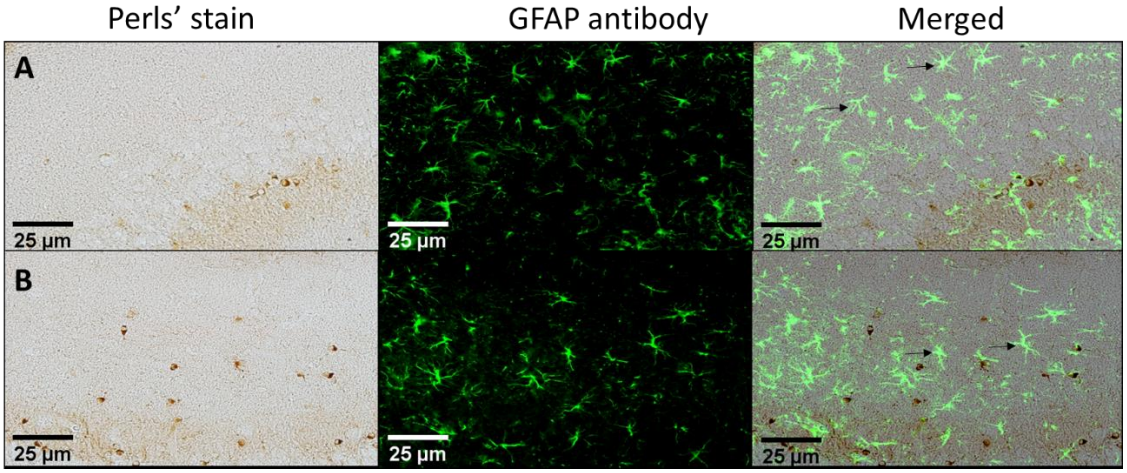

Fig. 4.16 Astrocytes contain very little Perls' stainable iron. DAB-enhanced Perls' stain combined with glial fibrillary acidic protein (GFAP) antibody showed minimum co-localisation of iron with astrocytes in Aβ+Iron mice (B) and Aβ mice (A), indicated by black arrows. Brain regions with many astrocytes appeared to have few iron-loading cells.

4.3.7 Iron loading in unidentified cells

As described above, DAB-enhanced Perls' staining of Aβ+Iron mice and Aβ mice labelled cells with distinctive morphologies, which could not be identified using the above-mentioned immunological markers. There appeared to be four main types of such unidentified cells with high iron loading, as detailed below and illustrated in Fig. 4.17.

I. One type of iron-laden cells, which sometimes but not always contain multiple processes, are closely associated with myelin patches (e.g. Fig. 4.17 B, D) and have been described previously (Heidari et al., 2016b)

II. A second type of iron-laden cells consists of 'solitary' or 'independent' cells which are not clearly associated with any obvious structures such as myelin, blood vessels or amyloid plaques. These cells often look like a teardrop, with no processes or a single process and with an eccentric nucleus at one end (e.g. Fig. 4.17 A, C, I).

III. A third type of iron-laden cells are closely associated with blood vessels and sometimes but not always have a small number of processes (e.g. Fig. 4.17 E, F).

IV. A fourth type of iron-laden cells are associated with amyloid plaques. These cells typically have several processes and exhibit possible transitional or activated ‘amoeboid’ microglia microglial morphology (e.g. Fig. 4.17 G, H). These cells were observed around approximately 22% plaques in the Aβ model and 77% plaques in the Aβ+Iron model, out of a total of 100 plaques examined in each mouse group (n=4 mice/group). This is explored in more depth in the next chapter.

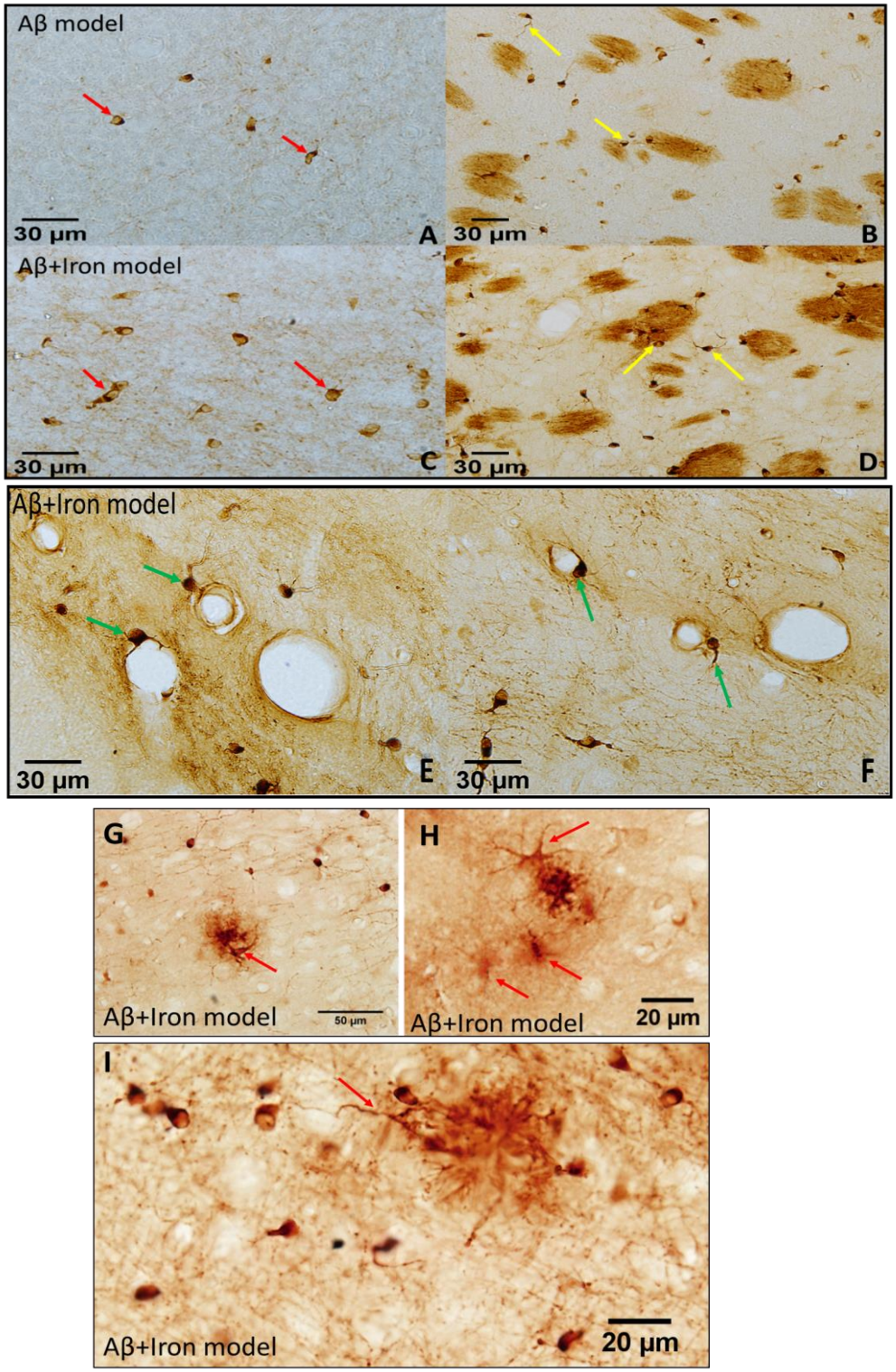

Fig. 4.17 Examples of four main types of unidentified cells with high iron loading. One type of cells are 'solitary' or 'independent' cells which have an appearance of teardrops, have an eccentric nucleus and contain no processes or a single process (A,C). A second type of cells are associated with myelin patches and may sometimes contain multiple processes (B, D). A third type of cells are associated with blood vessels and may sometimes contain a small number of processes (E, F). A fourth type of cells are associated with plaques, usually have multiple processes and tend to have a possible microglial appearance (G, H, I).

Careful examination of some of the iron-stained amyloid plaques by polarised light microscopy also showed unidentified iron-loading cells with microglial morphology in the immediate vicinity of iron-amyloid complexes (Fig. 4.18).

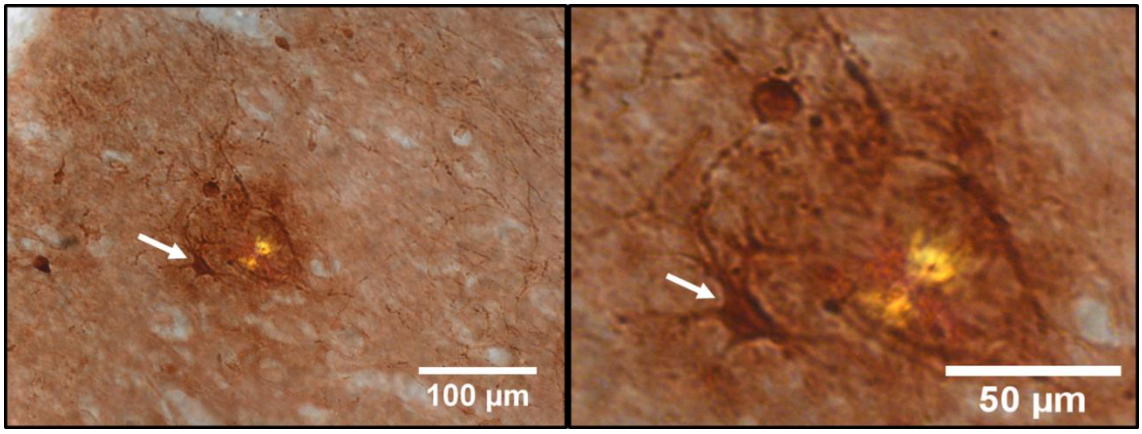

Fig. 4.18 High iron loading in unidentified cells with microglial morphology nearby amyloid plaques. Unidentified cells loaded with iron (white arrows) were seen to be co-localised with yellow-green birefringent plaques in the centre, in the Aβ+Iron model.

Likewise, in the preliminary experiments of co-labelling with DAB-enhanced Perls' stain and 4G8 antibody (Chapter 3, Section 3.3.3.3.3), unidentified iron-loading cells with the morphology of microglia were seen in the Aβ+Iron model and the Aβ model (Fig. 4.19). These cells were located predominantly immediately adjoining the iron and 4G8 positive structures.

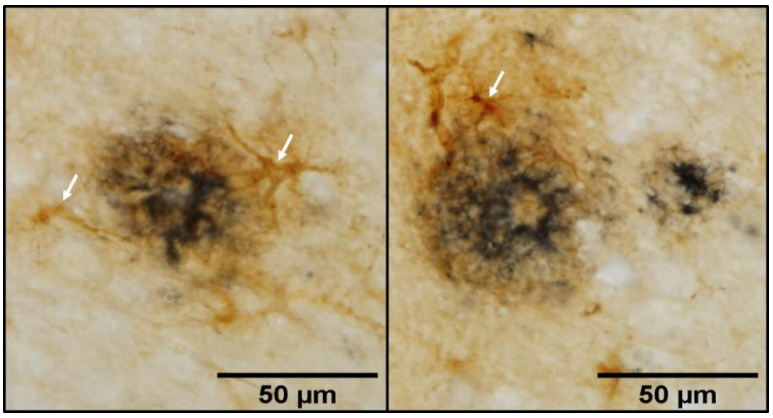

Fig. 4.19 Iron loading in unidentified cells nearby structures immunolabelled with antibody 4G8. Unidentified cells loaded with iron (white arrows) were observed adjoining 4G8 positive structures (blue-gray) in the Aβ+Iron model.

4.4 Discussion

Overview

In general, the findings of this chapter supported the second hypothesis of this thesis that brain iron distribution in different cell types and structures is generally similar in the Aβ+Iron model and the *Hfe*$^{-/-}$*xTfr2*^{mut} model (the 'Iron model'), as discussed in more detail below. Iron was primarily localised in the choroid plexus and myelin-associated structures in all models examined, with little if any detectable iron in neurons. The main difference between the models was that iron associated with amyloid plaques and cells often morphologically resembling transitional or activated amoeboid microglia in the vicinity of amyloid plaques in the Aβ and the Aβ+Iron models (amyloid plaques are not present in the Iron model).

Perfusion Turnbull staining suggested ferrous iron was generally restricted to regions with high levels of DAB-enhanced Perls' staining (such as the choroid plexus and midbrain). Importantly, such regions contained few if any amyloid plaques, which were instead generally restricted to areas with low Perls' iron staining and no detected ferrous iron such as cortex and hippocampus.

Most of the amyloid plaques were detected in areas with less iron staining

Although most amyloid plaques in both the Aβ+Iron model and the Aβ model contained iron (Chapter 3, Section 3.3.3.3), there were more plaques in areas with weak iron staining such as the cerebral cortex, hippocampus and entorhinal cortex, the regions typically affected the most in AD. This occurred both under the conditions of increased iron loading in the Aβ+Iron model as well as under normal iron conditions in the Aβ model. Consistent with this, few if any plaques were detected by brightfield, fluorescence or polarised light microscopy techniques for Congo red staining (described in Chapter 3, Section 3.3.3.3) in brain regions such as thalamus and basal ganglia which stained strongly for iron. As these regions of the midbrain appear to be least affected by amyloid deposition, it is likely that movement control and executive functioning may be not be much affected in the Aβ+Iron model, at least at 6 months of age. This needs to be confirmed by cognitive and behavioural studies, which are underway in another PhD project (Freeman-Acquah, in progress).

Some studies have reported amyloid deposits in the thalamus of other transgenic mouse models, with thalamic plaques appearing at 12 months in Tg2576-mutant PS1M46L mice (Wengenack et al., 2011) and at 8 months of age in double transgenic APPK670N,M671L–PS1M146L mice (Kurt

et al., 2001). Consistent with this, Braak and colleagues reported thalamus was affected later than hippocampus in AD (Braak et al., 1996). As the present research focused on six-month old Aβ+Iron model, investigation of older mice could answer whether plaques spread to other brain regions with age, as described by the above studies, and whether this affects behaviour or other functional outcomes.

Studies of brain iron levels in human and transgenic mouse models of AD

As discussed in General Introduction chapter (Section 1.6), Schrag and colleagues suggested in their quantitative meta-analysis that claims of increased levels of iron accumulation in AD brain reflect publication bias (Schrag et al., 2011b). The authors reported that increased iron levels in the neocortex of AD patients observed by one laboratory were not confirmed by seven other laboratories and found no significant difference between neocortical iron levels in AD and controls in the full set of studies ($p = 0.76$). Subsequent brain iron quantification studies, although sometimes reporting small and often highly variable increases in iron levels in restricted samples or disease stages (e.g. severe but not moderate AD) or restricted regions such as amygdala, have so far still failed to provide clear evidence for relationships between pathology and increased iron levels (Akatsu et al., 2012; Graham et al., 2014; Hare et al., 2016). However this will need to be re-assessed on an ongoing basis as more studies are performed.

As described in Section 4.3, the observations from the present study using DAB-enhanced Perls' staining showed similar patterns of iron distribution in the Aβ model and the Aβ+Iron model, although iron staining was more prominent in the Aβ+Iron model. The distribution in both these models was similar to that already reported in the Iron model (Heidari et al., 2016b), with substantial iron accumulation in the choroid plexus, corpus callosum and in myelinated patches in regions such as the midbrain, the basal ganglia (e.g., caudate) and the thalamus.

Brain regions with high levels of ferric or ferrous iron not clearly associated with myelin

The choroid plexus is a network of cells present in the four ventricles of the brain that produces cerebrospinal fluid (CSF) and influences the distribution of various substances between the brain and the CSF (Richardson et al., 2015). By all methods used (Perls', regular Turnbull and perfusion Turnbull stains, all with DAB enhancement), more iron was observed in the choroid plexus of the Iron model compared to the AKR model. Similarly more iron was observed in the choroid plexus of the Aβ+Iron model compared to the Aβ model (there were no clear differences apparent between the Iron model and the Aβ+Iron model). Though abnormal levels of iron have been reported in the choroid plexus of some patients with the iron overload disease haemochromatosis (Cammermyer,

1947; Russo et al., 2004), the consequences, if any, of iron loading in the choroid plexus are unclear.

No obvious staining was seen in brain regions other than the choroid plexus of the Aβ+Iron model and the Iron model by the traditional Turnbull staining for the detection of ferrous iron. This may mean that most iron in these models is mainly in the ferric form. However, preliminary observations showed that a few cells in the midbrain of the Iron model and the Aβ+Iron model labelled for ferrous iron by the perfusion Turnbull method (Fig. 4.6). The perfusion Turnbull staining in the midbrain represents labile ferrous iron which could potentially react with cellular components such as lipid, protein or DNA to cause damage. This will be investigated further in Chapter 5. It should also be noted that cells positive for perfusion Turnbull staining were not seen in regions with many amyloid plaques such as the cortex and the hippocampus. However, as mentioned earlier (Section 4.3.2), this approach needs to be refined in additional animals to minimise possible methodological artefacts and this is under investigation in other student projects in our group.

Use of paraffin-embedded sections can result in considerable leaching of iron from myelin and other brain tissue during histological processing, hence different tissue processing methods (in particular fixed-frozen as opposed to paraffin-embedded sections) can cause variation in the patterns of DAB-enhanced Perls' and Turnbull staining and fixed-frozen tissue sections can also be preferrable for immunolabelling (unpublished studies, Milward lab). Different patterns of iron labelling with different tissue processing methods are being explored further in ongoing studies. Other staining modifications such as post-DAB intensification methods are also being tested to see if this affects iron staining patterns (LeVine, 1997; Meadowcroft et al., 2015a; Moos and Mollgard, 1993).

Rouault and colleagues reported higher expression of transcripts for several iron-related proteins by in situ hybridisation (e.g. DMT1, ferroportin, hephaestin, ceruloplasmin and ferritin H) in the choroid plexus, compared to other brain regions (Rouault et al., 2009). Follow-up studies at the RNA as well as the protein level could also examine expression levels of different iron-related genes in the choroid plexus and other regions of both models. Further studies in larger numbers of mice and at older ages are required to investigate all the above questions.

Iron storage in myelin and potential consequences for AD

Findings from this chapter provided evidence that there was no clearly apparent large-scale redistribution of iron from myelin and myelin-associated cells to other cell types in the Aβ+Iron

model and the Aβ model. This suggests that myelin may act as a reservoir for excess iron in these models, as proposed for the Iron model (Heidari et al., 2016b). However, although iron accumulation was observed in myelinated structures, light microscopy could not distinguish if iron is in myelin itself or in the periaxonal space. Use of DAB-enhanced Perls' staining combined with electron microscopy could answer where exactly iron is residing in the myelinated structures i.e. whether iron is in myelin, in the fluid between myelin and the axon or within the axon itself.

White matter abnormalities have been suggested by different authors to be involved in AD pathogenesis although it is unclear whether such abnormalities are primary casual contributors to AD or secondary consequences of the disease (Radanovic et al., 2013; Scheltens et al., 1995; Xie et al., 2006). Age-dependent myelin breakdown may release iron, which is turn is suggested to stimulate Aβ oligomerisation and plaque deposition (Bartzokis et al., 2007; Bartzokis et al., 2004a). Considering this hypothesis, it may be speculated that some of the iron associated with amyloid plaques in the Aβ+Iron model and the Aβ model (observed in Chapter 3) may be iron released from myelin or myelin-associated cells with oligodendroglial morphology.

Myelin abnormalities in the Aβ+Iron model could also be investigated, for example by assessing corpus callosum changes as described elsewhere (Donovan et al., 2014; Heidari et al., 2016b; Saadoun et al., 2009). Inducing demyelination by placing Aβ+Iron mice on a cuprizone diet (Ludwin, 1978; Matsushima and Morell, 2001) or using lysophosphatidylcholine (Ghasemlou et al., 2007; Plemel et al., 2018; Schulz et al., 2012) or cross-breeding with a myelin deficient model (Duncan et al., 2011) could help understand where iron loads if there is less myelin available for iron storage.

While it was beyond the scope of the thesis to examine whether iron accumulation was accompanied by signs of myelin damage and deterioration, this could be a potential area of future investigation. However it is important to recognise that amyloid burden estimated by Congo Red imaging is less than 0.1% of brain cross-sectional area in the Aβ+Iron model (Fig. 3.6) whereas well over 50% of matched brain cross-sections shows medium to very strong iron staining (Fig. 3.1). Therefore release of only a minute proportion of the total iron stored in myelin or in cells with high iron content may be sufficient account for all amyloid-associated iron in this model. As discussed in Chapter 6 General Discussion, this may have consequences for the success of chelation therapies.

Iron in myelin-associated cells with oligodendroglial morphology

Histological studies suggest oligodendrocytes are rich in iron compared to other brain cell types examined (Connor and Menzies, 1996; Erb et al., 1996; Todorich et al., 2009a). As discussed in Section 4.3.4, myelin-associated cells with oligodendroglial morphology showed evidence of iron loading by DAB-enhanced Perls' staining in the Aβ+Iron model and the Aβ model. Immunolabelling for ferritin heavy and ferritin light antibodies (Section 4.3.5) also revealed a linear arrangement of cells resembling oligodendroglial trains in the Aβ+Iron model. Cells with similar morphology which co-localised with DAB-enhanced Perls' staining in the Iron model have been identified to be a subset of oligodendrocytes, as reported previously by our group (Heidari et al., 2016b). It will be important in the future to conduct detailed studies of cell lineage subtypes and various precursor progenitor cell species using batteries of antibodies to specific cell markers and iron-related proteins, for example platelet-derived growth factor receptor alpha PDGFRα for oligodendrocyte progenitor cells and T cell immunoglobulin and mucin domain-containing protein-2 (Tim2) for H-ferritin receptor on oligodendrocytes (Todorich et al., 2008a). Other approaches such as single cell transcriptomics will also be valuable. Detailed analyses of marker expression profiles of these cells are now commencing in our laboratory.

Neurons contain very little if any Perls' stainable iron

Co-labelling of brain sections with DAB-enhanced Perls' staining and neuronal marker NeuN in both Aβ mice and Aβ+Iron mice showed little if any evidence of neuronal iron staining, similar to what our group has previously reported for Iron mice (Heidari et al., 2016b). This suggests there may be specific mechanisms that are not yet well understood which prevent neuronal iron overload even in circumstances of high external iron concentrations and even when neurons are potentially more vulnerable due to the presence of mutations associated with AD-related neurodegenerative disease processes.

These protective mechanisms may in part involve maximisation of iron export out of neurons by ferroportin because the *Hfe*$^{-/-}$ and *Tfr2*^{mut} mutations in our models may prevent the normal upregulation of hepcidin levels within the brain in response to increased iron loading, as our group has also previously reported for Iron mice (Heidari et al., 2016b). This would be predicted to reduce hepcidin binding to ferroportin and subsequent internalisation and degradation, leading to preservation of ferroportin expression on the neuronal surface. However low neuronal iron loading has also been observed in another mouse model with raised brain iron levels without the *Hfe*$^{-/-}$ and

Tfr2^{mut} mutations (Aryal, Milward and others, unpublished data). This needs to be investigated in depth in future studies.

While neurons may be protected against internal iron overload in these mice, other mechanisms of neuronal damage such as oxidative damage of cell surface membranes by extracellular reactive species generated by labile iron cannot be ruled out. Neuronal oxidative damage and loss of neurons will be investigated further in Chapter 5. Another possibility is that if internal neuronal iron levels become inappropriately low, neuronal intracellular iron insufficiency may compromise normal neuronal functions. This has been reported previously in mice deficient for the iron regulatory protein Irp2 (Jeong et al., 2011; Zumbrennen-Bullough et al., 2014), and may also occur in the models with iron dyshomeostasis used in the present study although the mechanism involved will differ. Again this may make iron chelation therapy inappropriate, as further considered in the Chapter General Discussion.

Lack of evidence for increased uptake of iron by astrocytes or for astrogliosis in areas of elevated iron

Some authors propose myelin damage can lead to assembly and activation of astrocytes at the site of damage and subsequent engulfment of iron along with cell debris (Izawa et al., 2010; Raven et al., 2013; Schulz et al., 2012). Other authors suggest uptake of excess iron by astrocytes may contribute to neuroprotection (Pelizzoni et al., 2013; Peters et al., 2015). However, as astrocytes showed little if any evidence of iron loading by DAB-enhanced Perls' and GFAP co-labelling in Aβ+Iron mice or Aβ mice, it can be speculated that astrocytes do not play large roles in taking up excess iron in these models. Also brain regions with numerous GFAP-labelled astrocytes typically had few iron-laden cells and regions with increased iron loading typically contained few astrocytes, suggesting there was little reactive astrogliosis in brain areas with increased iron accumulation.

Iron loading in other unidentified cells

As described in Section 4.3.7, Fig. 4.17, various iron-laden cells could not be identified with the markers used for this chapter, including solitary or independent cells which appear like teardrops with only one or a few processes and are not clearly associated with myelin and amyloid-plaque associated cells. The latter often had morphologies resembling those of transitional or activated 'amoeboid' microglia and were present in the vicinity of approximately triple the number of plaques in Aβ+Iron mice compared to Aβ mice (77% as opposed to 22%). These observations raise the

important possibility that these cells may be involved in taking up excess iron along with amyloid. This will be investigated in more detail in the following chapter.

Other limitations and future directions

Some other mouse genetic models that have shown brain iron loading, and in particular models with mutations involving the IRE-IRP regulatory system, have been discussed previously (Heidari et al., 2016b). As detailed in Chapter 1 General Introduction Section 1.5.6.1, the IRE-IRP regulatory system plays a crucial role in maintaining body iron homeostasis when there are changes in tissue iron levels. A putative IRE in human APP has been speculated to lead to increased APP expression in response to increased brain iron levels (Rogers et al., 2002).

However one potential limitation of the present study is that the human Aβ sequence in the APP/PS1 mouse model (Jankowsky et al., 2004) doesn't have an IRE (confirmed by personal communication, David R. Borchelt). Since this is the same model as the 'Aβ model' used in the present project, this also applies to the Aβ+Iron model. Inspection of the mouse APP sequence identified a region (+52 to +92 of the mouse APP sequence) with ~82% similarity to the putative human APP IRE (+51 to+94 of the human APP sequence). However this had little if any similarity with IRE sequences from either the human or the mouse genes for transferrin, ferritin light or heavy chains and divalent metal transporter 1 (Sanchez et al., 2011). Therefore while it is possible (although not yet confirmed) that in the human brain, APP expression is up-regulated in response to increases in brain iron levels, this may not be the case for the mouse models used in our study.

However it is important to recognise that in mouse models in general, increasing APP alone does not result in amyloid formation unless there are mutations related to Aβ present such as those already present in our models (Xu et al., 2015). Therefore the absence of an IRE is considered unlikely to affect the general features of iron and amyloid relationships reported here. Furthermore, as noted above, neuronal iron levels do not appear to increase in our models even though total brain iron loading is increased. This suggests that even if the human IRE sequence were to be introduced, intraneuronal APP would not be up-regulated, although APP expression may be up-regulated in other cell species with higher intracellular iron levels, making consequences for amyloidogenesis difficult to predict.

It would therefore be of interest to examine potential IRE-IRP regulation in these mouse models and determine for example which if any cells up-regulate APP expression in response to introduction of the human IRE and whether this accelerates the rate of amyloidogenesis in the Aβ+Iron model. Follow-up investigations could incorporate the use of appropriate gene editing

technology (e.g. clustered regular interspaced short palindromic repeats 'CRISPR') to investigate the potential effects of the IRE/IRP regulatory system on APP transgene expression in the Aβ+Iron model.

Conclusion

In summary, the findings of this chapter showed that brain regions with increased DAB-enhanced Perls' staining for iron (such as the midbrain) also contained ferrous iron detectable by perfusion Turnbull staining. These regions contained few if any amyloid plaques whereas plaques were more commonly observed in regions with reduced DAB-enhanced Perls' iron staining and no detected ferrous iron, such as the hippocampus and the cortex. Following on from these observations, the next chapter will investigate whether brain iron loading above normal in the Aβ+Iron model and labile forms of iron may be accompanied by increased oxidative damage or neuronal loss in these mice. Additionally, some unidentified cells with high levels of iron staining in the immediate vicinity of amyloid plaques displayed microglial morphology in this model. Further characterisation of these cells will be carried out using double and triple labelling of brain sections with stains and markers specific for iron, amyloid and microglia.

5. Investigating possible effects of increases in iron levels on microglia, oxidative damage and neuronal loss

5.1 Introduction

Several lines of evidence have shown that Alzheimer's disease (AD) is typically accompanied by an activation and upregulation of microglial cells, in conjunction with various inflammatory responses (Barger and Harmon, 1997; Mattson, 2004; Wood, 2017; Wyss-Coray, 2006b). Moreover amyloid plaques have been observed in various studies to be surrounded and infiltrated by clusters of activated microglia (Bolmont et al., 2008; Rozemuller et al., 1986; Stalder et al., 1999). These observations have led some authors to speculate that microglia are involved in either the deposition of amyloid plaques (Baik et al., 2016; Frackowiak et al., 1992; Perlmutter et al., 1990; Venegas et al., 2017) or the clearance of amyloid plaques (Koenigsknecht and Landreth, 2004; Mandrekar et al., 2009; Ries and Sastre, 2016) or both (Hickman, 2008; Liu et al., 2010).

Some immunohistochemical studies on post-mortem human brains affected with AD have reported iron accumulation in microglia (Connor et al., 1992a; Grundke-Iqbal et al., 1990; Jellinger et al., 1990; Zeineh et al., 2015). Despite their clinical significance, these studies may be limited by variable post-mortem intervals and methodological concerns like leaching of iron out of the tissue specimen. It is therefore important to investigate whether microglia are associated with amyloid plaques in the Aβ+Iron model and if so, whether these cells contain iron.

Furthermore, various researchers have debated about the relationships between AD and increased oxidative stress and cellular damage. It is still unclear whether oxidative damage contributes to the disease pathogenesis or if it is a secondary consequence of disease progression. Some studies have suggested that the reduction of ferric iron to ferrous form can occur within amyloid deposits (Everett et al., 2014a; Everett et al., 2014b; Khan et al., 2006). Nevertheless, most of these studies are *in vitro* and do not consider factors such as glial cells surrounding amyloid plaques or proteins in the extracellular environment which may have the ability to alter the valence states and hence the redox capacity of iron bound to amyloid. On the other hand, previous studies from our group on various mouse models of iron loading have shown little evidence for increases in the expression of genes relating to oxidative damage (Heidari et al., 2016b; Johnstone et al., 2012a; Johnstone and Milward, 2010a). Hence it is important to investigate whether the Aβ+Iron model displays signs of oxidative damage and potential neuronal damage or death.

This chapter tests the third hypothesis of this project that microglia surround amyloid plaques in the mouse models and may have increased intracellular iron content, as has been observed in humans and that increased levels of brain iron may augment oxidative damage or neuronal loss in the mouse model of amyloidosis.

5.2 Methods

5.2.1 Mice and tissue collection

The generation of the AKR model, the Iron model, Aβ model and the Aβ+Iron model is described in (Section 2.1). Mice were fed a standard AIN-93G diet containing approximately 0.02% iron (Reeves et al., 1993). All protocols were approved by the Animal Ethics Committee of the University of Sydney where the mice colonies were bred and maintained.

5.2.2 Histological studies

Brains were dissected, fixed in 4% PFA, cryosectioned (20 μm) and transferred to gelatin-coated slides (Section 2.3.1.3). Four brain sections from each mouse (n=4 mice/group) were selected starting from -2.46 mm Bregma to -3.16 mm Bregma (Section 2.3.1.5).

5.2.3 Quantification of microglia surrounding amyloid plaques

The modified Puchtler method of Congo red staining (Puchtler et al., 1962) was used to detect amyloid plaques (Section 2.4.1, 13 mg/ml). As described in (Section 2.3.6.2), microglia were detected by ionized calcium binding adaptor molecule 1 (Iba1) antibody labelling, using the Vectastain Elite ABC horseradish peroxidase universal kit (Vector Laboratories, Catalog no. PK-6200). Z-stacked images were taken using 20X magnification of the ZEISS Axio Scan.Z1 Slide Scanner. The Iba1-labelled microglia surrounding amyloid plaques were quantified manually using the multi-point tool of ImageJ,as previously described in the General methods chapter (Section 2.5)

5.2.4 Triple labelling of iron, amyloid plaques and microglia

The DAB-enhanced Perls' staining protocol (Section 2.3.2), followed first by Congo red staining (Section 2.4.1, 13 mg/ml) and then by ionized calcium binding adaptor molecule 1 (Iba1) antibody labelling (1:500 dilution) on the same brain tissue section was done for simultaneous detection of iron, amyloid plaques and microglia. Performance of Iba1 labelling after Perls' staining was necessary when using the immunofluorescence protocol for Iba1 labelling, to prevent loss of fluorescent activity that otherwise occurred if Perls' staining was done second. For consistency, the same order was chosen while using the Vectastain Elite ABC horseradish peroxidase universal kit (Vector Laboratories, Catalog no. PK-6200) for Iba1 labelling. Single labelling of adjacent tissue sections with DAB-enhanced Perls' stain only, Congo red stain only and Iba1 antibody only was done for comparison to check for potential artefacts in the triple labelling procedure.

5.2.5 Double labelling of iron and microglia

To check if iron coincides with microglia, the 3,3'-diaminobenzidine tetrahydrochloride (DAB)-enhanced Perls' staining protocol was followed by ionized calcium binding adaptor molecule 1 (Iba1) antibody labelling (immunofluorescence method, 1:500 dilution), on the same brain tissue section. Single labelling of adjacent tissue sections with DAB-enhanced Perls' stain only and Iba1 antibody only, was done for comparison to check for potential artefacts in the double labelling procedure. One brain tissue section without the Perls' solution and without primary antibody was used as the negative control.

5.2.6 Labelling with the oxidative damage marker 4-Hydroxynonenal

As described in (Section 2.3.6), brain tissue sections were immunolabelled for the oxidative damage marker 4-hydroxynonenal (4-HNE, 1:100 dilution), which specifically detects an aldehydic product of lipid peroxidation. A brain section without primary antibody was used as the negative control. A testis section with high amount of oxidative damage from a mouse model of oxidative damage (provided by Prof John Aitken and Dr Geoffry De Iuliis, the University of Newcastle) was used as the positive control.

5.2.7 Estimation of neuronal loss

Immunofluorescent labelling of neurons in matched brain tissue sections of four mouse groups (n=4mice/group) was done with neuronal nuclear (NeuN) antibody (1:100 dilution) and Alexa Fluor 488 secondary antibody (1:100 dilution). Imaging was performed at 20X magnification with FITC filter set (excitation 493nm, emission 520nm) of the ZEISS Axio Scan.Z1 Slide Scanner. Automated quantification of neurons was done using the 'analyse particles' function in the Fiji distribution of ImageJ, as described in General Methods (Section 2.6). Total number of neurons labelled with NeuN antibody was counted in left cerebral hemisphere (excluding cerebellum).

5.2.8 Statistical analysis

The mean count of microglia around amyloid plaques in the Aβ+Iron model was compared with that of the Aβ model by unpaired *t*-test. Two-way ANOVA was used to compare the mean differences in neuronal counts between 4 groups of mice (AKR mice, Iron mice, Aβ mice and Aβ+Iron mice) that were stratified on two independent variables ('iron' status and 'amyloid' status). Specifically, the question that was investigated was whether increased iron has an effect on neuron count irrespective of amyloid status (presence/absence) and vice versa i.e., whether amyloid status has an effect on neuronal count irrespective of iron status (normal/increased).

5.3 Results

5.3.1 No difference in mean count of Iba1-labelled microglia surrounding amyloid plaques

As hypothesised, most of the amyloid plaques in the Aβ+Iron model and the Aβ model had one or more cells clearly labelled with antibody to the microglial marker Iba1 in the immediate vicinity (Fig. 5.1).

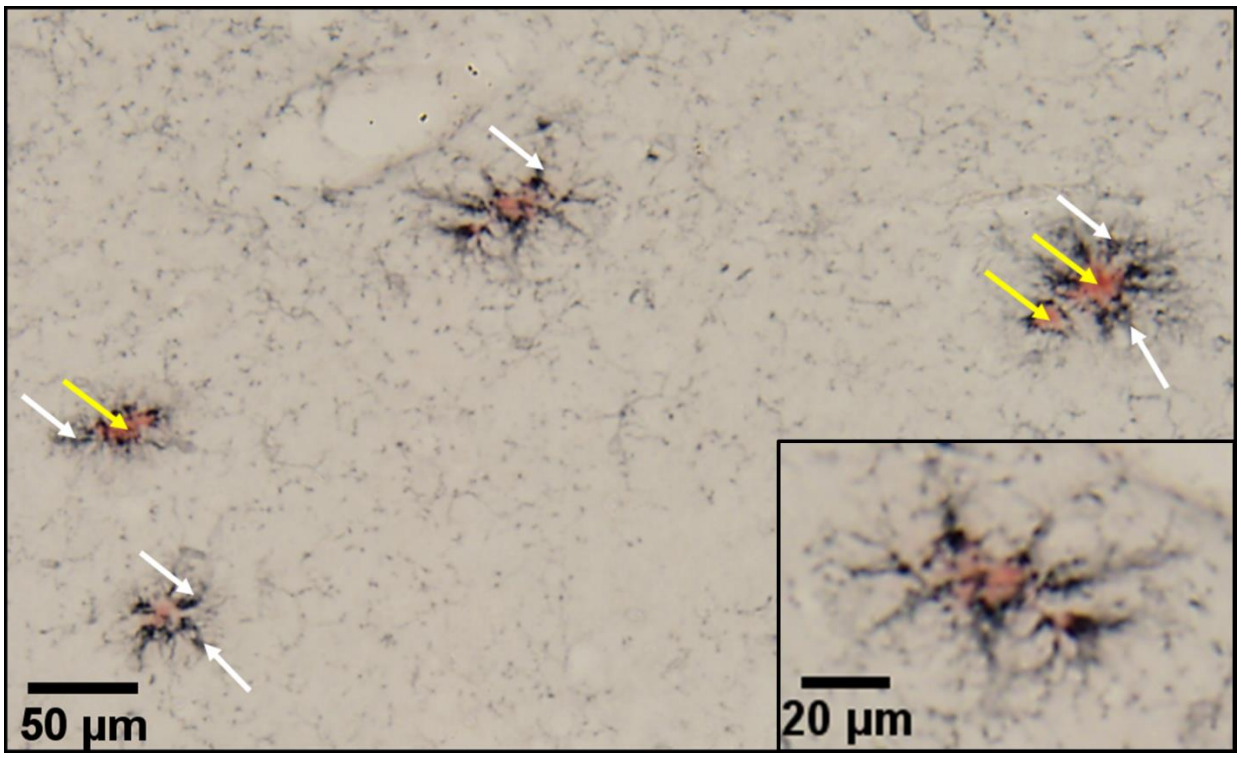

Fig. 5.1 Co-labelling of amyloid plaques and microglia. The figure illustrates amyloid plaques detected by Congo red staining (yellow arrows) and microglia labelled with the Iba1 antibody (white arrows) in Aβ+Iron mice.

As illustrated in Fig. 5.2, there was no significant difference in the mean count of Iba1-labelled microglia surrounding amyloid plaques in the Aβ+Iron model (mean ± SEM: 3.654 ± 0.2488, n=4), as compared to the Aβ model (mean ± SEM: 3.784 ± 0.4646, n=4), by unpaired *t*-test (p=0.4073). Additionally, out of 102 amyloid plaques examined across four mice per group, 98% of plaques in the Aβ+Iron model and 93% of plaques in the Aβ model were surrounded by Iba1-labelled microglia (unpaired *t*-test, p>0.9999). These proportions are considerably larger than the proportions of approximately 77% and 22% of amyloid plaques in the Aβ+Iron and the Aβ models respectively that were estimated in the preceding chapter (Section 4.3.7) as having adjacent Perls' positive cells identified morphologically as putative transitional or amoeboid microglia. This may be because antibody Iba1 is detecting ramified microglia not easily identified based on morphology

alone. Taken together, these results suggest the proportions of microglia clustered around plaques that are potentially activated or transitioning into activation are much smaller in the Aβ model compared to the Aβ+Iron model. This will be discussed further in the Chapter 5 Discussion (Section 5.4).

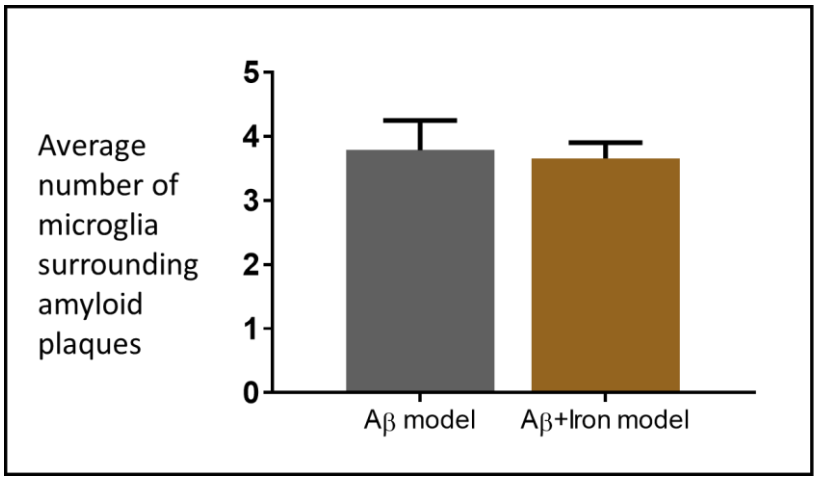

Fig. 5.2 Mean count of Iba1-labelled microglia surrounding amyloid plaques. Mean number of Iba1-labelled microglia around amyloid plaques in the Aβ model and the Aβ+Iron model. Data are presented as mean ± SEM (p>0.05, n=4 mice/group).

5.3.2 Morphology of Iba1-labelled microglia in general brain regions and around amyloid plaques

Cells detected with Iba1 antibody in the Aβ+Iron model and the Aβ model usually exhibited distinctive morphologies corresponding to descriptions of microglia in the literature (Crews and Vetreno, 2016; Davis et al., 2017; Nimmerjahn et al., 2005a), including ramified cell processes typically displayed by resting microglia (Fig. 5.3) through cells surrounding plaques with transitional morphologies or amoeboid morphologies corresponding to those displayed by activated microglia (Fig. 5.4).

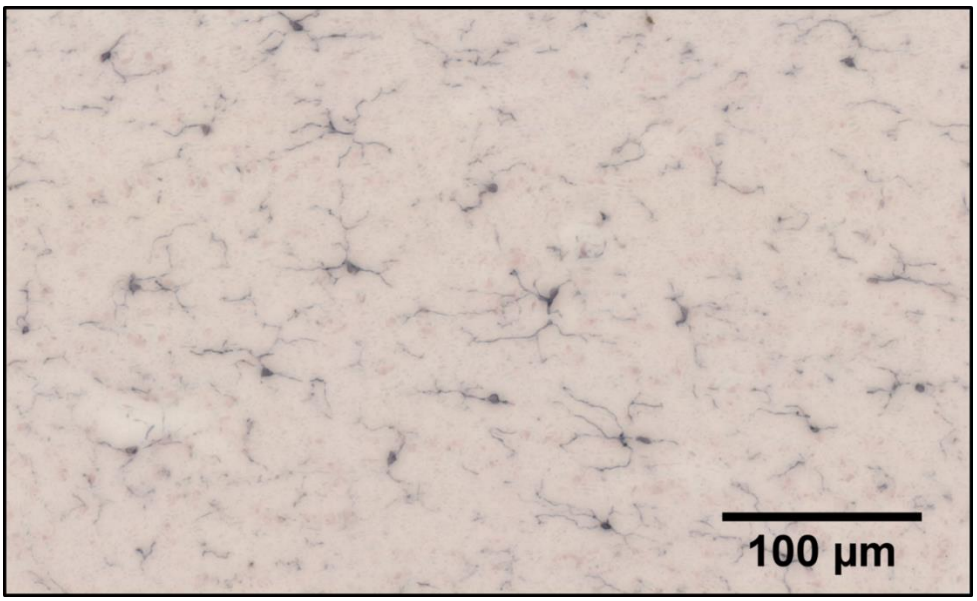

Fig. 5.3 General morphology of microglia labelled with Iba1 antibody. Cells labelled with Iba1 antibody Aβ+Iron mice with morphologies corresponding to those of ramified microglia.

In contrast, some Iba1-labelled microglia around amyloid plaques appeared to have shorter and fewer processes (Fig. 5.4) than microglia in other brain areas (Fig. 5.3). Also some Iba1-labelled microglia around plaques in Fig. 5.4 appeared to have the 'amoeboid' morphology suggestive of the activated stage whereas others seemed to display the intermediate or transitional stages of activation with fewer processes than resting or ramified microglia (Davis et al., 2017; Gomes-Leal, 2012; Kreutzberg, 1996; Ling and Wong, 1993; Ziebell et al., 2015).

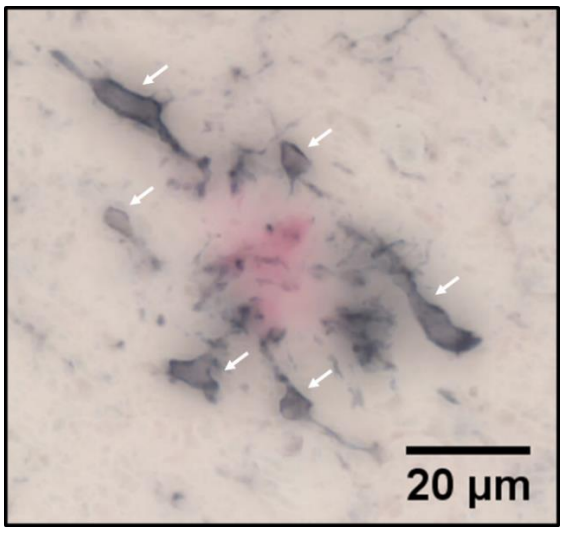

Fig. 5.4 Microglial labelling around an amyloid plaque in the Aβ+Iron model. Magnified image of a Congo red-stained amyloid plaque in the centre, surrounded by Iba1-labelled microglia (white arrows) in the Aβ+Iron model.

5.3.3 Visualisation of Iba1-labelled microglia and yellow-green birefringent amyloid plaques

Complexes of Iba1-immunoreactive microglia and amyloid plaques were also visualised by 90^0 crossed polarisers of the polarised light microscope. As illustrated by Fig. 5.5, Iba1-immunoreactive microglia were observed in the immediate vicinity of yellow-green birefringent amyloid plaques (as already described in previous chapters, these are the classical amyloid plaques detected by polarised light microscopy).

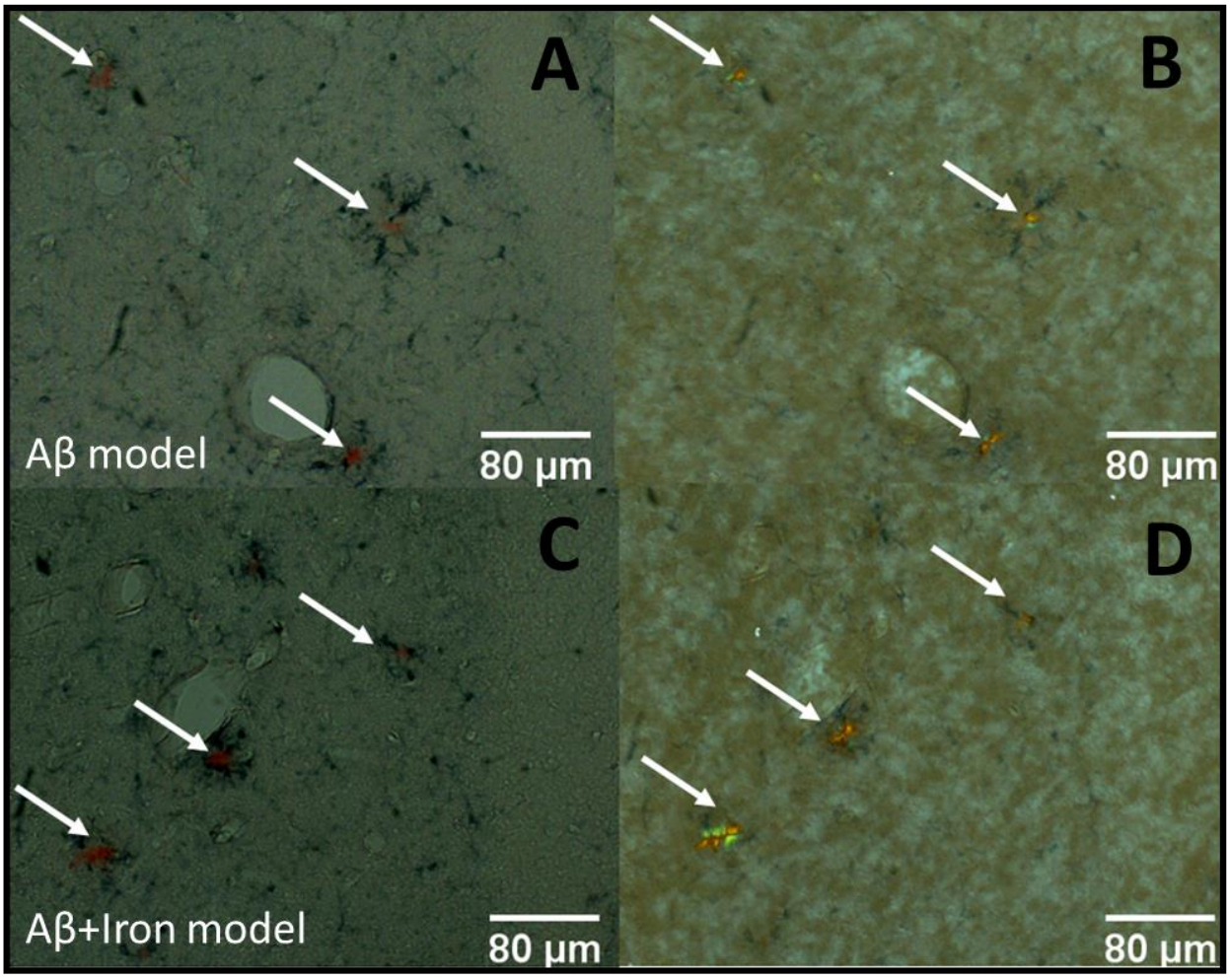

Fig. 5.5 Labelling of microglia with Iba1 antibody in the vicinity of yellow-green birefringent amyloid plaques. Light microscopy with 90^0 crossed polarisers was used to visualise Iba1-labelled microglia around amyloid plaques confirmed by yellow-green birefringence (B, D); same sections visualised without the polarisers (A, C). Note that the images taken by polarised light microscope have a different brightfield appearance than other images in this thesis which were taken using other microscopes.

As described in detail in Chapter 3 (Section 3.3.3.3.2.1), 99.25% of detected amyloid plaques were co-localised with DAB-enhanced Perls' stainable iron in the brain sections examined in the

Aβ+Iron model as compared to 81.09% in the Aβ model. In order to examine if microglia surrounding the amyloid plaques phagocytose iron, triple labelling was done for amyloid, microglia and iron which is described in the following section.

5.3.4 Most iron-loaded cells do not show Iba1 labelling but Iba1-immunoreactive cells are found in the vicinity of iron-amyloid complexes

To investigate whether microglia surround aggregates of iron and amyloid, brain sections were triple-labelled with DAB-enhanced Perls' stain, Congo red stain and Iba1 antibody (n=4 mice/group). Fig. 5.6 shows clustering of Iba1-immunoreactive cells in the vicinity of iron-amyloid complexes. Microglia were noted around some but not all aggregates of iron and amyloid including some with very little clear amyloid labelling. However the combination of three different labels in this procedure made each label appear considerably weaker including DAB-enhanced Perls' staining, making findings inconclusive.

With that caveat, the iron-loaded cells residing in the vicinity of iron-amyloid complexes failed to show clear co-localisation with Iba1 antibody (Fig. 5.6, panel G, red arrow). Conversely, in the Aβ+Iron model, a few faintly labelled Iba1-immunoreactive cells surrounded iron-amyloid clusters which were clearly labelled with DAB-enhanced Perls' stain but showed faint Congo red staining under red Texas filter set (Fig. 5.6, white arrows). However these also did not appear to be co-labelled with Perls' stain, similar to Iba1 positive cells in other brain areas.

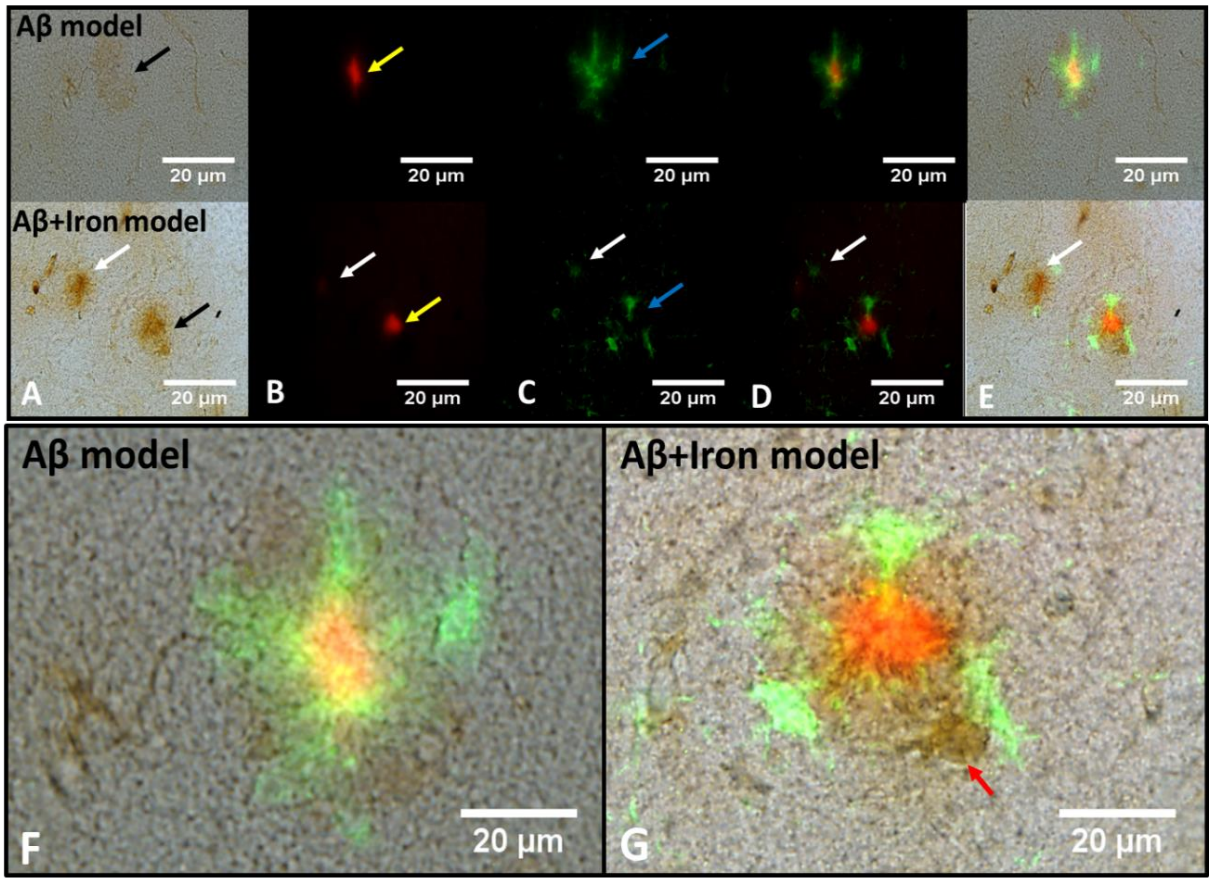

Fig. 5.6 Iba1-immunoreactive cells are found in the vicinity of iron-amyloid complexes. Clusters of Iba1-immunoreactive cells (blue arrows) which did not show clear co-localisation with DAB-enhanced Perls' stain were seen in the vicinity of iron (black arrows) and amyloid plaques (yellow arrows). A few weakly labelled Iba1 positive cells which did not appear to co-localise with DAB-enhanced Perls' stain were found in the vicinity of iron-amyloid complexes. These iron-amyloid complexes showed clear labelling for iron with DAB-enhanced Perls' stain but weak staining for amyloid with Congo red stain under red Texas filter set (white arrows). (A) DAB-enhanced Perls' staining, (B) Congo red staining, (C) Iba1 labelling, (D) Merge of Congo red staining and Iba1 labelling, (E) Merge of DAB-enhanced Perls' staining, Congo red staining and Iba1 labelling, (F) and (G) Magnified images of triple labelled iron-amyloid-Iba1 complex; red arrow in (G) indicates an iron-loaded cell which did not label with Iba1 antibody.

The above observations raise the possibility that the triple labelling procedure might have been affected by spectral bleed-through or signal interference, hence affecting the visualisation of either of the three labels. These limitations suggest that the staining procedure needs further optimisation.

Because of the limitations of the triple labelling procedure described above, an alternative approach was used where the immunofluorescence labelling for Iba1 antibody was replaced by the Vectastain

horseradish peroxidase protocol with SG substrate (Section 2.3.6.2). This procedure was expected to help in visualising iron, amyloid and microglia using brightfield microscopy. Although all three labels were still somewhat weaker when combined than when used separately, faintly labelled Iba1-immunoreactive cells were observed to be assembling in the vicinity of iron-amyloid complexes in the Aβ+Iron model and the Aβ model (this is illustrated in the Aβ+Iron model by Fig. 5.7). Iron-containing cells near the iron-amyloid complexes again failed to show co-localisation with Iba1 antibody (Fig 5.7, red arrows), although as before this is subject to the caveat that both labels were weaker with the combined method.

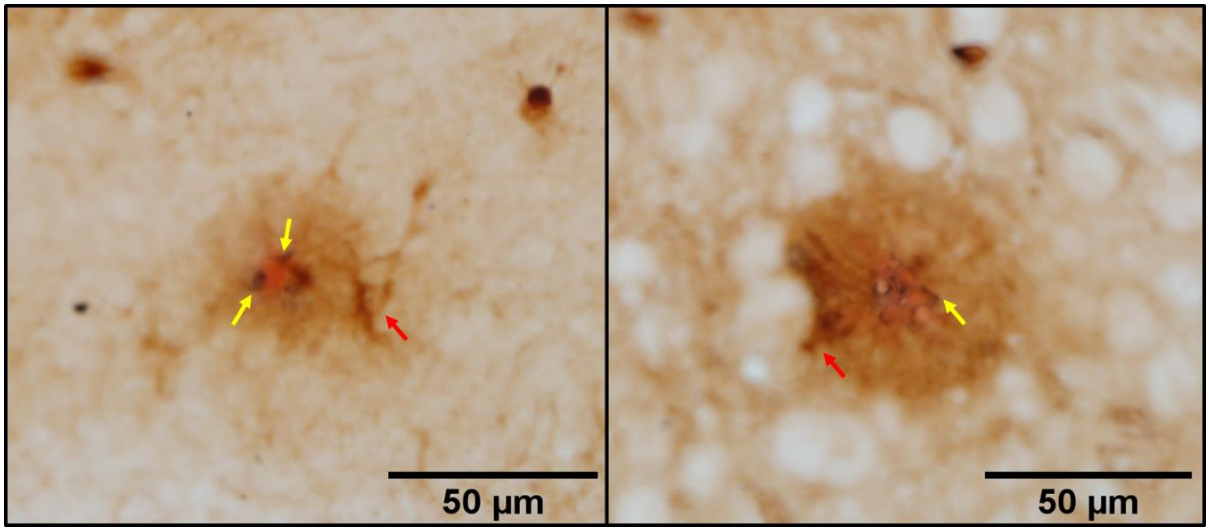

Fig. 5.7 Visualisation of Iba1-immunoreactive cells in the vicinity of iron-amyloid complexes. Iba1-immunoreactive cells (dark bluish-grey staining, yellow arrows) were seen in the vicinity of iron-amyloid complexes but the iron-loaded cells (red arrows) did not appear to label with Iba1 antibody in the Aβ+Iron model.

In addition to the triple labelling procedure discussed above, double labelling for iron and microglial marker Iba1 (immunofluorescence labelling) was also performed. However in general, co-labelling of the DAB-enhanced Perls' stain with the microglial marker Iba1 also did not provide clear evidence that all iron-loaded cells are microglia (Fig. 5.8, n=4 mice/group). Very few iron-loading cells in Aβ+Iron mice and Aβ mice appeared to coincide with Iba1 labelling. Likewise, few if any Iba1-immunoreactive cells showed clear DAB-enhanced Perls' staining. It is possible that combining the two labelling protocols also reduces the sensitivity of either or both stains, as considered more in the Chapter discussion below.

With this caveat, co-labelling with DAB-enhanced Perls' stain and Iba1 antibody also detected many Iba1-immunoreactive cells which did not appear to contain iron (by DAB-enhanced Perls' staining) within or in the vicinity of large round deposits of iron. These deposits had the distinctive

morphology of iron-amyloid co-aggregates and although the presence of amyloid could not be confirmed without triple labelling for Congo red, it is noted that such deposits were not observed in the absence of amyloid in the Iron model or wildtype mice.

A small number of Iba1-immunoreactive cells possibly containing iron were also detected within or in the vicinity of some of these iron aggregates, although it was difficult to assess if the iron was actually within the Iba1 immunoreactive cell in each case due to the very high iron staining levels in the aggregates in question (Fig. 5.8 D, E).

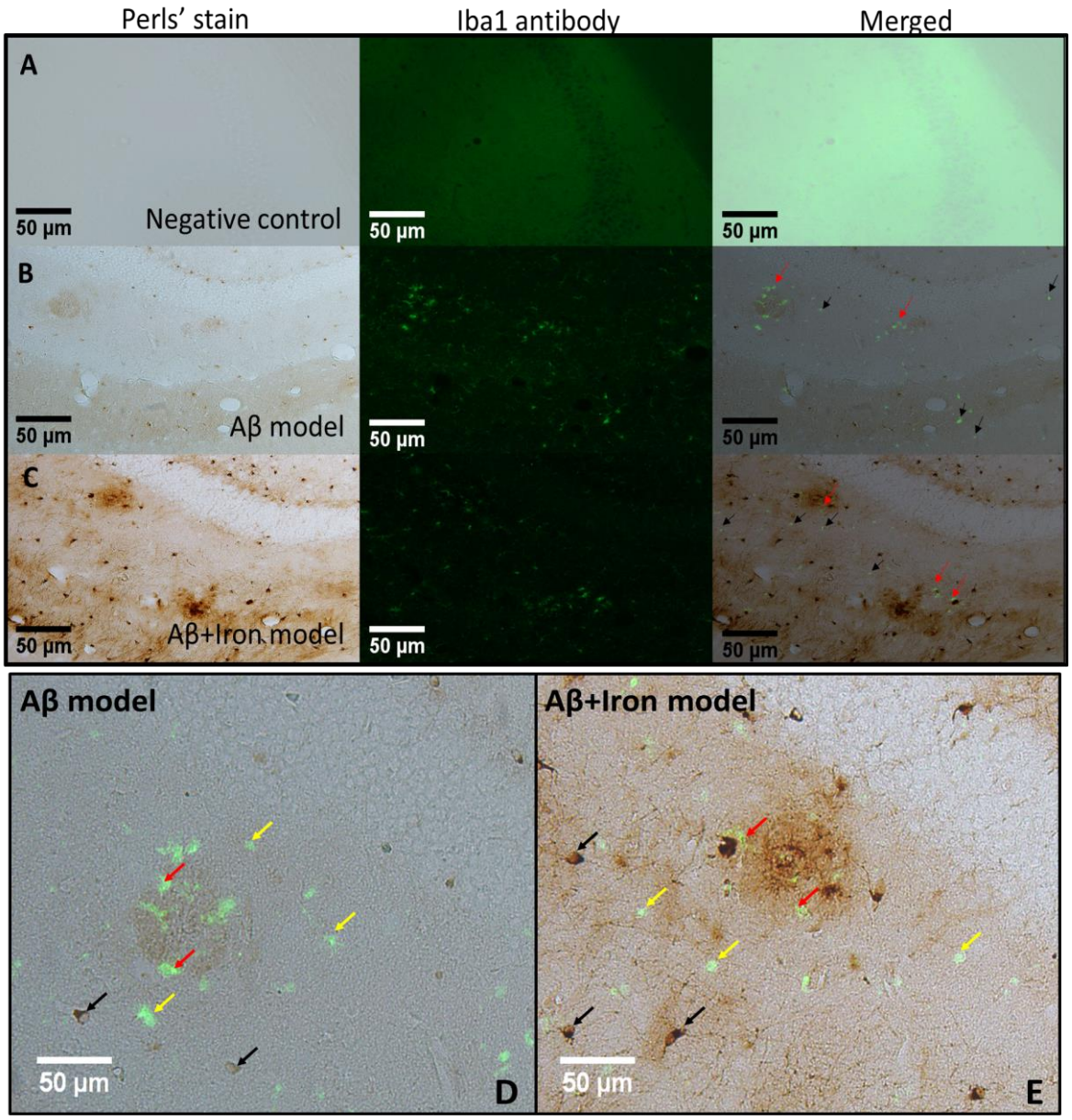

Fig. 5.8 Few if any Iba1-immunoreactive cells show clear DAB-enhanced Perls' staining in general brain regions but Iba1-immunoreactive cells are found in the immediate vicinity of iron aggregates. In general, very few iron-loading cells detected by DAB-enhanced Perls' stain coincided with the microglial marker ionized calcium-binding adapter molecule 1 (Iba1) (black arrows). Similarly, few if any Iba1-labelled cells coincided with DAB-enhanced Perls' staining (yellow arrows). However, many Iba1-immunoreactive cells were detected in the vicinity of ion aggregates (red arrows). (A) Negative control (no Perls' stain, no primary antibody), (B) Aβ model, (C) Aβ+Iron model, (D) and (E) magnified images show DAB-enhanced Perls' stain and Iba1 antibody co-labelling.

From the above observations using the triple and double labelling procedures, the fourth type of unidentified iron-loading cells in the vicinity of amyloid plaques described in Chapter 4 (Section 4.4) cannot be reliably identified as microglia and these cells remain to be characterised in future follow-up studies as further discussed below.

5.3.5 Oxidative damage studies

In order to examine whether increased brain iron augmented oxidative damage in the mouse model of amyloidosis, brain sections from AKR mice, Iron mice, Aβ mice and Aβ+Iron mice were labelled with the marker for oxidative damage 4-hydroxynonenal (4-HNE).

There was putative faint positive labelling in areas near dark regions postulated to be myelinated patches in the midbrain region of the Iron model, the Aβ model and the Aβ+Iron model, as compared to the AKR model, which in turn was slightly higher than the negative control without primary antibody (Fig. 5.9 A-F). However, it is to be noted that immunolabelling with 4-HNE antibody on all mouse groups was hard to assess easily due to the relative faintness of fluorescence and also it was unclear if the labelling was real or just background. Furthermore, the AKR model showed putative positive labelling with the 4-HNE antibody in some other regions like corpus callosum and cortex, which was also observed in the other three groups of mice, hence complicating the interpretation (Fig. 5.9 G, H).

The other marker of oxidative damage 8-hydroxydeoxyguanosine (8-OHdG) was also tried in collaboration with the members from Aitken laboratory who are experienced in this area but the staining was even weaker including in the testis positive controls, suggesting possible methodological issues. Hence the results were inconclusive in the time available.

Additional experiments are required with an optimised protocol for 4-HNE and 8-OHdG immunofluorescence labelling. Moreover co-labelling or labelling of adjacent sections with DAB-enhanced Perls' stain or Luxol fast blue stain could facilitate simultaneous detection of myelinated patches as well as possible iron-laden cells and structures. Having said that, co-labelling procedures may be affected by the sensitivity of individual stain/antibody (described earlier in Section 5.3.4), so this needs to be optimised too. It hasn't been possible to complete these experiments in the timeframe of this thesis.

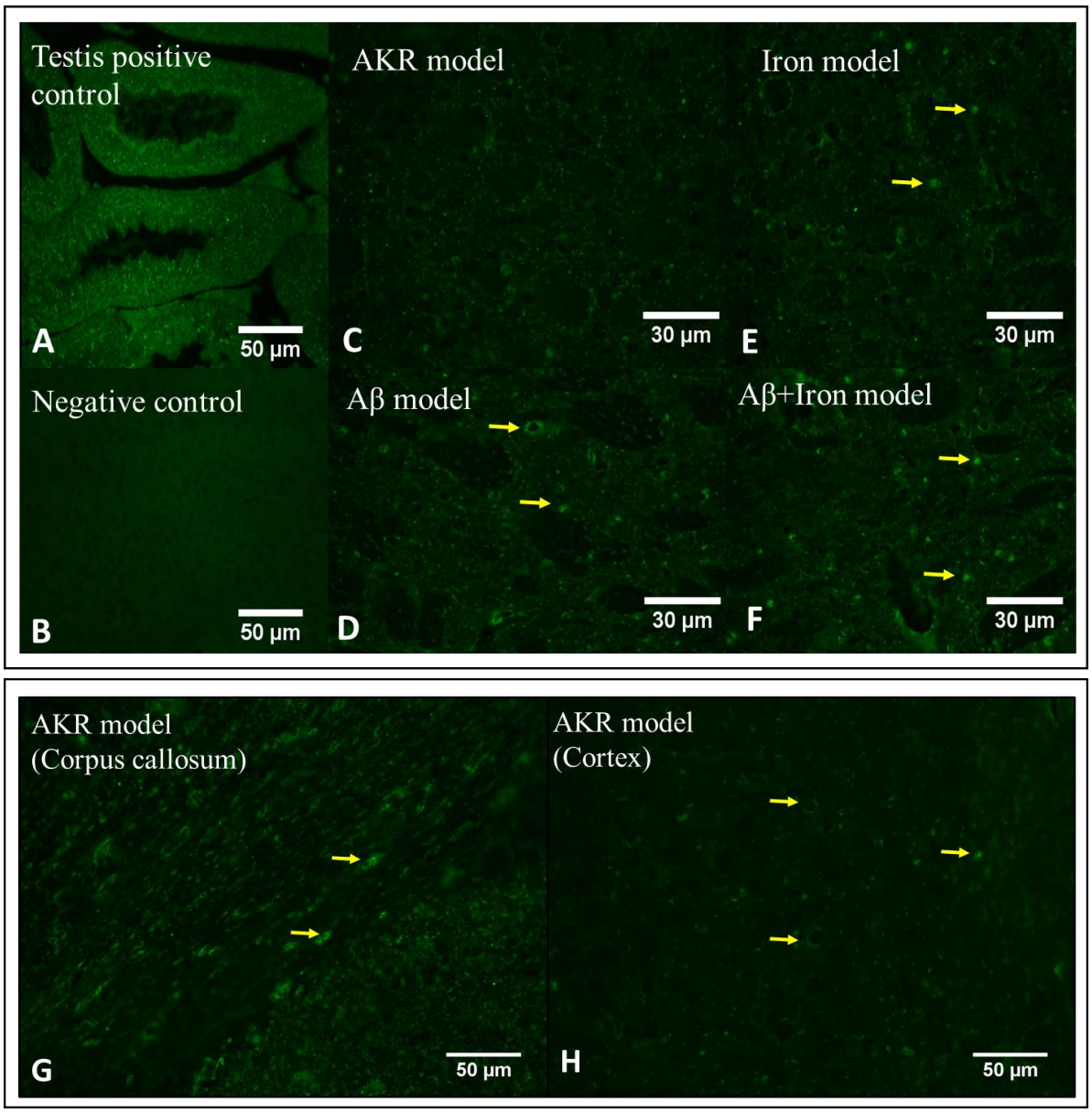

Fig. 5.9 Immunolabelling of mouse brain sections with the 4-HNE antibody. Brain sections immunolabelled for the oxidative damage marker 4-hydroxynonenal (4-HNE) showed putative faint positive labelling in possible myelinated patches in the Iron model, the Aβ model and the Aβ+Iron model (yellow arrows), as compared to the wildtype AKR model (C-F). However, 4-HNE labelling was seen in the corpus callosum (G) and the cortex (H) of the AKR model, which was also detected in the Iron model, the Aβ model and the Aβ+Iron model, hence making the assessment difficult.

5.3.6 Preliminary data on the estimation of neuronal loss

In order to examine whether increased brain iron augmented neuronal loss in the mouse model of amyloidosis, Bregma matched brain sections from the Aβ+Iron model and the Aβ model were labelled with the neuronal marker NeuN (n=4 mice/group). Quantification of neurons in left cerebral hemisphere (excluding cerebellum) was done using 'analyse particles' function of ImageJ.

This has been described briefly in Section 5.2.7 of this chapter and in detail in Section 2.6 of the General Methods chapter.

As illustrated by Fig. 5.10, there was no significant decrease in relative neuronal counts per unit area in the full cerebral hemisphere (excluding cerebellum) (p=0.3331, n=4 mice/group, one-tailed t test) of the Aβ+Iron model compared to the Aβ model. These preliminary observations suggest that there is no clear evidence of neuronal loss resulting from increased brain iron levels in the Aβ+Iron model however more detailed sampling from more mice needs to be done in the follow-up analyses.

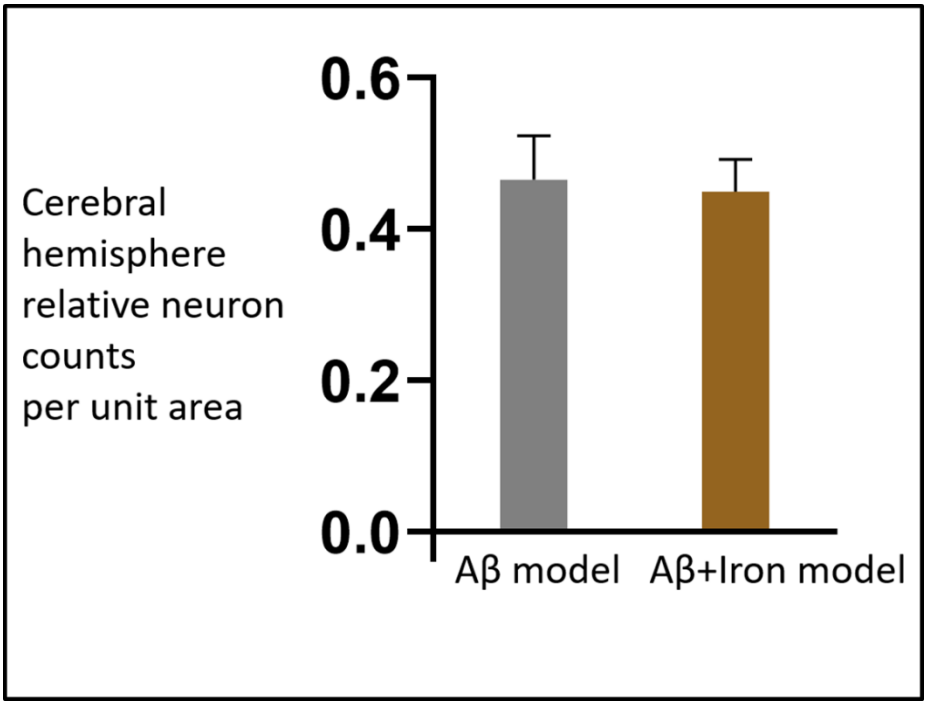

Fig. 5.10 Relative neuronal counts per unit area of left cerebral hemispheres in the Aβ+Iron model and the Aβ model. Data are presented as mean ± SEM, p=0.3331, n=4 mice/group.

5.4 Discussion

Overview

This chapter tested the third hypothesis of this project. It investigated whether microglia surround amyloid plaques in the mouse models and may have increased intracellular iron content, as has been observed in humans. It also examined whether increased levels of brain iron may augment oxidative damage or neuronal loss in the mouse model of amyloidosis.

Observations from this chapter provided evidence that microglia were found in the immediate vicinity of amyloid plaques in both the Aβ+Iron model and the Aβ model. In general, most iron-loading cells in these mouse models did not appear to coincide with microglia labelled with Iba1 antibody, as previously observed by our group in the 'Iron' model i.e. the *Hfe*$^{-/-}$*xTfr2*^{mut} mice (Heidari et al., 2016b). However Iba1-labelled microglia were found to congregate in the vicinity of iron-amyloid complexes and it is possible that issues with simultaneous labelling with Iba1 interfered with iron detection. The Iba1-labelled microglia surrounded amyloid plaques in both Aβ+Iron mice and Aβ mice in similar numbers. However, as discussed previously in Chapter 4 (Section 4.4), iron-laden cells with microglial morphology in the transitional or activated stages were detected in the vicinity of approximately 77% of plaques in Aβ+Iron mice as compared to 22% in Aβ mice.

Although methodological limitations cannot be ruled out, putative positive labelling with 4-HNE antibody was observed in all mouse groups examined, suggesting oxidative damage and specifically lipid peroxidation, although the level was low compared to the positive control (testis). There appeared to perhaps be more 4-HNE labelling near myelinated patches of midbrain in the Aβ+Iron model compared to other models. However labelling was also seen in other regions such as the corpus callosum and cortex of all animals, including the wildtype AKR model, and it was not feasible to perform robust quantitative comparisons across the brain or its subregions within the timeframe of the project.

Consistent with the lack of evidence for substantial oxidative damage, preliminary data obtained in this chapter showed that increased brain iron levels did not result in significant decrease in relative neuronal counts per unit area in full cerebral hemispheres of the Aβ+Iron model compared to the Aβ model.

Investigation of microglia surrounding amyloid plaques

Clustering of microglia around amyloid plaques has been described in various mouse models of amyloidosis as well as brains of AD patients (Bolmont et al., 2008; Haga et al., 1989; Itagaki et al., 1989; Liebmann et al., 2016; Stalder et al., 1999; Wegiel and Wisniewski, 1990). Consistent with these studies, microglia labelled with Iba1 antibody were detected in the vicinity of amyloid plaques in both Aβ+Iron mice and Aβ mice.

In this thesis, similar number of microglia (approximately 4 on average) were observed surrounding amyloid plaques in the Aβ+Iron model and the Aβ model. There are some other studies which have reported microglial count around amyloid plaques. Stalder and colleagues studied two age groups of APP23 mice: 6 month old and 14 to 18 month old. Amyloid plaques were surrounded by 2 to 3 microglia in 6 month old mice, similar to the mean number of microglia (approximately 4) present around plaques in the 6 month old Aβ+Iron mice and Aβ mice as assessed by Iba1 labelling. Depending on the sizes of plaques in the 14 to 18 month old mice, the authors noted between 3 and 20 microglial cell bodies in the vicinity of amyloid plaques (Stalder et al., 1999). It is difficult to directly compare the latter values with the data here which are in younger mice. Also the diameter of the smallest plaque these authors studied was less than 5 μm (no information is given on diameters of larger plaques) whereas on average, plaques in both the Aβ+Iron mice and Aβ mice had a diameter of around 20 μm.

However the mice values are reasonably similar to those reported for human AD by Wegiel and colleagues, who observed 5-6 microglial cells associated with amyloid plaques (average diameter of 35 μm) in the cortex of a patient with AD (Wegiel and Wisniewski, 1990). Although most studies of AD have not reported plaque dimensions in detail, ranges of 30-100 μm diameter have been reported previously for human amyloid plaques (Mann et al., 1988).

Morphology and activation states of microglia

The microglial immune response involves activation of microglia from a quiescent or resting state which is typically accompanied by various morphological changes, as widely reported in the literature, with just a few examples listed here. Overall, the consensus is that ‘ramified’ morphology correlates with resting or quiescent states and ‘amoeboid’ morphology with phagocytic or activated states, with one or more transitional states in between (Crews and Vetreno, 2016; Davis et al., 2017; Gomes-Leal, 2012; Hristovska and Pascual, 2015; Nimmerjahn et al., 2005b; Tam et al., 2016; Ziebell et al., 2015).

As described in Section 5.3.1 and 5.3.2, common morphologies exhibited by the Iba1-immunoreactive microglia in the Aβ model and the Aβ+Iron model were consistent with either resting ramified or activated amoeboid states, with some Iba1-labelled microglia showing morphologies consistent with intermediate or transitional stages of activation with fewer processes than ramified microglia (Section 5.3.2, Fig. 5.4). Similar microglial morphologies have been described in the human brain and animal models of AD (Karperien et al., 2008; Meadowcroft et al., 2015a).

Possible relationships of microglia and amyloid

Uncontrolled microglial reaction has often been speculated to have detrimental effects on neurons. For instance, some studies report that uncontrolled microglial activation may cause neuronal injury by releasing cytokines and neurotoxins (Heneka et al., 2015; Liddelow et al., 2017; Stalder et al., 1999). The concept that there may be dichotomous beneficial and detrimental effects of microglia in AD has been put forward by many authors – for example with an early neuroprotective microglial reaction in AD clearing β-amyloid but subsequent release proinflammatory cytokines in response to ongoing amyloid accumulation eventually having deleterious affects on brain function (Gomes-Leal, 2012; Hickman, 2008; Jin, 2012; Wyss-Coray, 2006a).

However this is not fully born out by many studies relevant to AD, with a wide range of microglial activation states in various mouse models of AD rarely having direct 'neuricidal' effects and instead often primarily enhancing amyloid clearance, as reviewed elsewhere (Lee et al., 2013). Nonetheless, the nature of the microglia-amyloid interaction in Aβ+Iron mice and Aβ mice is still not fully clear, and some lines of evidence have suggested that microglia may instigate amyloid plaque formation. For example, some early studies reported that microglia contribute to APP expression and initiation of amyloidogenesis (Banati et al., 1993a; Bitting et al., 1996; Haass et al., 1991). Stalder and others speculated that microglia may produce amyloid based on their observation using electron microscopy of potential intracellular amyloid fibrils in direct contact with the microglial endoplasmic reticulum (Stalder et al., 1999). This followed from an earlier study demonstrating nucleoside diphosphatase (NDPase) enzyme, which is generally found in the smooth endoplasmic reticulum and cell membrane of microglia, within newly formed amyloid fibers. This paper also concluded that microglia are involved in the formation of amyloid deposits (Wisniewski et al., 1990).

However it remains to be conclusively established if microglia cause amyloid formation and if so, what mechanisms are involved, or whether microglia are activated in response to amyloid formation

arising from other causes. If so, this activation could still lead to additional neuronal damage and possibly further amyloid formation over extended time periods in human patients even if not in shorter-lived mouse models.

Alternatively, it has been suggested that microglia may form a protective barricade around amyloid, compressing amyloid fibrils into a firmly packed and less lethal form. This is believed to prevent axonal dystrophy in the neighbouring neurons (Condello et al., 2015; Wang et al., 2016; Yuan et al., 2016; Zhao et al., 2017). Other researchers have hypothesised that microglia may induce a 'glial scar', which is believed to protect the brain from toxicity of β-amyloid. According to Chakrabarty and colleagues, this occurs when astrocytes move closer to plaques which are already sequestered by microglia (Chakrabarty et al., 2010).

As reviewed elsewhere, a primary role of microglia is to release inflammatory and cytotoxic modulators and induce phagocytosis against potential threats to the central nervous system (Banati et al., 1993b; Giulian, 1987; Kim and de Vellis, 2005; Nelson et al., 2002). Likewise, activated microglia surrounding amyloid plaques are postulated to be involved in the phagocytosis and clearance of β-amyloid (Gyoneva et al., 2016; Sheng et al., 1997; Stalder et al., 1999).

Some i*n vitro* studies have shown that microglia can take up amyloid via the receptor for advanced glycation end products (RAGE) and scavenger receptors (Lue et al., 2001; Paresce et al., 1996; Yan et al., 1996). However, amyloid was not detected within the cell bodies of Iba1-labelled microglia in the Aβ+Iron model and the Aβ model, although as mentioned before, it cannot be ruled out that this observation may have been affected by the methodological issues of double and triple labelling procedures (Section 5.3.4) and as further discussed below.

Iron staining in microglia

Abnormal iron homeostasis (e.g. levels, forms, locations /distribution) may add to the detrimental effects on neurons. Some authors have proposed that microglia may be involved in the uptake and clearance of excess iron (Gillen et al., 2018; McCarthy et al., 2018b; Nnah and Wessling-Resnick, 2018).

As described earlier (Section 5.3.1), Iba1-labelled microglia were found in the vicinity of iron-amyloid complexes but otherwise rarely coincided with areas of high iron in either Aβ+Iron mice and Aβ mice. There was no clear evidence of Iba1-labelled microglia taking up iron in these mice by double labelling with DAB-enhanced Perls' stain and Iba1 antibody. However this is not consistent with the observations made with Perls' staining alone of strongly iron-laden cells

morphologically resembling activated microglia around plaques, as discussed in Section 4.4 it has already been noted above (Section 5.3.4) that the double and triple labelling procedures for detecting iron, amyloid and microglia may deplete DAB-enhanced Perls' staining from brain sections. Furthermore, the triple labelling procedure may also be affected by spectral bleed-through or signal interference, hence affecting the visualisation of either Congo red staining or Iba1 labelling. These issues are being followed up by other members of our group in order to optimise the staining protocols. As microglia in brains affected with AD are known to contain ferritin, co-labelling of ferritin and Iba1 or other microglial markers may avoid some of these issues and provide more insight into iron-microglia colocalisation (Connor et al., 1992a; Hopperton et al., 2017; Lopes et al., 2008).

For example, Connor and colleagues performed immunohistochemistry of ferritin antibody and Ricinus Communis Agglutinin 1 (RCA 1) antibody for microglia and noted that most ferritin-containing cells associated with plaques were microglia (Connor et al., 1992a). Grundke-Iqbal and colleagues detected ferritin-microglia co-localisation by using immunohistochemistry for ferritin and microglial markers anti-CD45, anti-HLADR and MRP 14 (Grundke-Iqbal et al., 1990). Jellinger and colleagues observed ferritin-positive microglia detected by anti-CD 45 and MRP 14 markers for microglia (Jellinger et al., 1990). Zeineh and colleagues performed DAB-enhanced Perls' stain with microglia labelled with CD163 (Zeineh et al., 2015).

One other factor that may be important to take into account in future studies is the activation state of the microglia. Although the staining protocols used in this thesis did not confirm that the iron-laden cells around amyloid plaques were microglia, some studies have reported the presence of iron in activated microglia around amyloid plaques (Grundke-Iqbal et al., 1990; Meadowcroft et al., 2015a; van Duijn et al., 2017; Zeineh et al., 2015). Other authors have described that microglia accumulate iron when these cells are activated by stimuli such as hypoxic/ischemic insult or inflammation (Cheepsunthorn et al., 2001; Leitner et al., 2015; Urrutia et al., 2013).

Based on the type of inflammatory cytokines released by microglia, the activation of microglia is also correlated with the M1 and M2 states of macrophage activation. Broadly, the M1 state is characterised by the release of pro-inflammatory cytokines and the M2 state is characterised by the release of anti-inflammatory cytokines (Orihuela et al., 2016; Satoh, 2018; Tang and Le, 2016; Zhou et al., 2017). The relationships of resting and active microglia to M1, M2 and transitional M1/M2 states is still being clarified (Cherry et al., 2014; Franco and Fernandez-Suarez, 2015; Sarlus and Heneka, 2017). This will be a potential area of future study in the Aβ+Iron model.

Considering the above hypothesis that activated microglia accumulate iron, it may be speculated that microglia which did not label with Iba1 antibody in general brain regions of Aβ+Iron mice and Aβ mice may not be in an activated state. However, the iron-laden cells around plaques may be activated microglia which could not be labelled with Iba1 antibody due to the methodological limitations of the double/triple labelling procedure. This was beyond the scope of the present study but needs to be investigated in future research by using various markers of microglial activation states (described further below).

Preliminary investigations of oxidative damage and neuronal loss in the Aβ+Iron mice

As described above, some researchers speculate that excess iron catalyses the production of reactive oxygen species (ROS), which leads to oxidative damage (Aisen et al., 2001; Emerit et al., 2001; Hentze et al., 2004; Lou et al., 2009). Also some authors believe that β-amyloid induces activation of microglia and astrocytes, followed by production of nitric oxide and superoxide, resulting in oxidative damage (Gallagher et al., 2012; Wang et al., 2004b).

To see if increased iron and amyloid deposition resulted in damage due to oxidative stress in Aβ+Iron mice compared to other mouse models, brain sections were labelled with the oxidative damage marker 4-HNE. As mentioned earlier (Section 5.3.5), putative positive labelling was observed although this could not be confirmed by additional studies in the timeframe of this thesis.

To investigate the possibility of neuronal loss directly, neuronal nuclear (NeuN) antibody was used for immunolabelling of neurons in all groups of mice. NeuN is a transcription factor that is expressed in the nucleus and cytoplasm of mature neurons (Mullen et al., 1992; Wolf et al., 1996).

Healthy neurons are generally known to exhibit strong NeuN staining whereas NeuN immunoreactivity has been stated to decline under numerous pathological conditions such as cerebral ischemia, hypoxia and trauma. Under these conditions, several studies have presented a diminution in NeuN immunoreactivity as evidence of neuronal loss (Davoli et al., 2002; Igarashi et al., 2001; Unal-Cevik et al., 2004; Xu et al., 2002).

There have been diverse findings on progressive death or damage of neurons, in various neurodegenerative conditions, including AD (Baron et al., 2017; Fu et al., 2018; Oakley et al., 2006; West et al., 1994; Whitehouse et al., 1982; Zhang et al., 2017). However, the preliminary data obtained from NeuN labelling and quantification in this chapter (Section 5.3.6) suggest there is no significant decrease in neuronal counts in the Aβ+Iron model. One possible explanation for this maybe that microglia are protecting neurons by isolating and shielding off toxic β-amyloid species

as suggested by other researchers and discussed above (Keren-Shaul et al., 2017; Yuan et al., 2016; Zhao et al., 2017).

Follow-up studies are needed to reduce variability and gain more insights into these questions, including using more mice per group and by sampling more sections which span the full brain hemispheres of the animals rather than just focusing on strongly affected regions such as the hippocampus. Also, although not directly relevant in the current context, since no neuronal loss was observed, it is important to recognise immunolabelling with NeuN alone is not enough for determining neuronal loss as it may reflect reduction of NeuN protein or loss of its antigenicity rather than neuronal death (Gusel'nikova and Korzhevskiy, 2015; Unal-Cevik et al., 2004; Wu et al., 2010). An injured but still viable neuron may lose NeuN immunoreactivity due to metabolic perturbations (Unal-Cevik et al., 2004) or due to temporary suspension of NeuN protein synthesis (Gusel'nikova and Korzhevskiy, 2015). Bearing in mind these speculations, additional methods of studying neuronal loss need to be considered in the future, which will be described in more detail further below.

In the future, confocal microscope can be used to enhance the image quality of NeuN-labelled brain tissues. This microscope may enable the selection and imaging of regions of interest at higher magnification. Likewise, neuronal damage could be tested by using additional cell death assays such as terminal deoxynucleotidyl transferase (TdT)-mediated dUTP nick end labeling (TUNEL) and fluoro-jade staining.

Cresyl violet stain has been widely used as a standard histological stain for neurons in the past. However this stain has limited specificity as it may stain other types of glia in addition to neurons. Instead, antibodies specific to various neuronal types could provide more insights on neuronal loss in the Aβ+Iron model. For example, markers for glutamatergic neurons or cholinergic neurons could be checked, which are reported to be affected in Alzheimer's disease (Ferreira-Vieira et al., 2016; Mufson et al., 2008; Wang and Reddy, 2017; Zhang et al., 2016),

NeuN antibody combined with Congo red stain or any other stain specific to β-amyloid could be helpful to see if neurons are affected in the vicinity of amyloid plaques. Additionally, as previously discussed in Chapter 3 (Section 3.4), the soluble forms of Aβ peptide are believed to be more toxic compared to the insoluble amyloid plaques (Haass and Selkoe, 2007; Sengupta et al., 2016; Tomic et al., 2009). While the soluble Aβ peptides were not studied within the timeframe of this thesis, it is likely that an increase in toxic Aβ peptides may have resulted in putative lipid peroxidation damage in the Aβ+Iron model. However, no significant reduction in neuron numbers was observed

in this model regardless of the relative toxicity of soluble and insoluble forms of Aβ, *in vivo*. This needs to be considered in the future analyses.

Limitations and future directions

As discussed above, there were several limitations of the analyses reported in this chapter. Although there was no evidence of colocalisation of iron-laden cells and Iba1-labelled microglia in Aβ+Iron mice and Aβ mice (Section 5.3.4), methodological artefacts of simultaneous labelling of more than one target remain to be investigated. Also immunolabelling with other microglial markers could not be checked within the timeframe of this thesis.

One marker that distinguishes microglia from macrophages is transmembrane protein 119 (TMEM119) (Bennett et al., 2016; Satoh et al., 2016). A combination of cluster of differentiation molecule 11B (CD11b) and cluster of differentiation 45 (CD45) is also described as distinguishing microglia from macrophages. Another important microglial marker which could be examined is triggering receptor expressed on myeloid cells 2 (TREM2) (Hopperton et al., 2017; Korzhevskii and Kirik, 2016).

Furthermore, the marker for Human Leukocyte Antigen – DR isotype (HLA-DR), the major histocompatibility complex II protein, has been widely used to identify activated microglia in human brains (Hendrickx et al., 2017; Walker and Lue, 2015). The marker for F5/80 is described for detecting resting microglia and macrophages (Wada et al., 2000; Yamasaki et al., 2014). Likewise, macrophages and activated microglia are reported to express cluster of differentiation 68 (CD68) protein at higher levels than resting microglia (Bodea et al., 2014; Hendrickx et al., 2017).

Additionally, detailed analyses on general microglial morphology, density and activation could be done by Sholl analysis, which would facilitate detection of possible microglial morphological changes in the Aβ+Iron model and the Aβ model (Kongsui et al., 2014; Norris et al., 2014).

As previously described in the General Introduction chapter (Section 1.4), it is likely that the Aβ+Iron model may display damage in the connectome (synapses and neuronal processes) although there was no clear evidence of neuronal loss. The investigation regarding whether the connectome is subjected to damage could not be completed within the timeframe of this thesis. To see if the Aβ+Iron model displays synaptic loss or synaptic pathology, follow-up studies could label brain sections with synaptophysin marker which is known to be an abundant membrane protein of synaptic vesicles (Clare et al., 2010; de Wilde et al., 2016; Eastwood et al., 1995; Gudi et al., 2017; Masliah et al., 1990).

Apart from the markers of oxidative damage used in this study, other markers for oxidative stress could be tested (e.g., universal markers for reactive oxygen species/reactive nitrogen species, 8-Nitroguanine, superoxide dismutase and others) to see if there is any damage due to oxidative stress in the Aβ+Iron model. Besides these, markers for ferroptosis (iron-dependent cell death, described in more detail in Chapter 6) could also be used for doing additional checks (Cao and Dixon, 2016; Lewerenz et al., 2018).

Conclusion

This chapter addressed the question of whether elevated brain iron may increase oxidative damage or neuronal death in response to Aβ. It provided preliminary evidence of possible oxidative damage in the brain of the Aβ+Iron model at 6 months of age, supplementing evidence reported in the previous chapter of labile (ferrous) iron accumulation in this model. If these preliminary observations are confirmed by follow-up studies, it could suggest the combination of increased brain iron and Aβ pathology may contribute to early neuronal damage or other degenerative changes in the Aβ+Iron model at this age. However ferrous iron accumulation and potential oxidative changes were generally not prominent in regions containing amyloid. Furthermore initial studies did not provide clear evidence of neuronal loss in the Aβ+Iron model compared to the Aβ model.

This may suggest that any toxicity resulting from increased iron and Aβ pathology is limited either because unregulated labile iron pools are insufficient to cause high levels of cell damage or because unknown protective mechanisms are successfully limiting damage at this age. Immune responses by microglial cells may be one possible protective mechanism. While there was no evidence that iron increased numbers of microglia around insoluble aggregates of Aβ in the Aβ+Iron model compared to the Aβ model, preliminary evidence suggested that the proportion of these microglia in or transiting to more active states may be considerably higher in the Aβ+Iron model. This suggests that microglia may be mounting additional immune responses in this model. Whether the net result of microgliosis is protective or inappropriately inflammatory remains to be determined as potential methodological artefacts remain to be clarified so clear evidence could not be obtained for the involvement of microglia in uptake and removal of excess iron. However taken together with the findings from the previous chapters that increased mouse brain iron levels did not contribute to exacerbation of amyloidosis at 6 months of age, these observations may suggest that microglial clearance of iron, amyloid or both may contribute to neuroprotection in the Aβ+Iron model.

6. General discussion

How or even whether brain iron abnormalities contribute to AD remains controversial (Section 1.6) and it is unclear whether excess brain iron is a causal factor for AD or whether it is a secondary consequence of AD (Bolognin et al., 2011; Boopathi and Kolandaivel, 2016; Collingwood et al., 2008; House et al., 2004b; Mantyh et al., 1993; Tahmasebinia and Emadi, 2017). One reason for this has been the absence of a suitable mouse model which manifests both chronic brain iron accumulation and pathological features of AD. To address this issue, this PhD project has used a recently developed 'Aβ+Iron' mouse model, unique to our group, that was generated by cross-breeding the *Hfe*$^{-/-}$*xTfr2*^{mut} mouse model of human iron overload disorder haemochromatosis ('Iron' model) with an APPswe/PS1ΔE9 mouse model ('Aβ' model), and backcrossing onto the AKR background to maximise iron loading (Section 2.1). The resulting mouse model displays chronic brain iron accumulation and cerebral amyloidosis.

Key questions investigated by this thesis

Key characteristics of the relationships between iron and Alzheimer's disease were explored in this thesis using the Aβ+Iron mouse (Fig 6.1). The fundamental questions which were addressed were as follows:

i) Does excess brain iron change the amyloid plaque load? (addressed in Hypothesis 1)
ii) Is there a relationship between patterns of iron and amyloid loading across different regions of the brain? (addressed in Hypothesis 2)
iii) What cell types show increased iron loading in healthy brain or in the vicinity of amyloid plaques? (addressed in Hypotheses 2 and 3)
iv) Does the combination of excess brain iron and amyloidosis increase oxidative damage or neuronal damage or death? (addressed in Hypothesis 3)

The broad hypothesis that high brain iron levels may exacerbate Alzheimer's amyloid pathology was not supported by the findings of this thesis. Overall, data obtained in this thesis suggest that instead, normal brain iron homeostatic and storage mechanisms involving myelin and myelin-associated cells or other unidentified glia may allow considerable increases in iron in this model without accelerating amyloidosis or neuronal loss. The thesis has provided new insights into the nature of the relationship between iron and amyloid that may be relevant to the treatment of patients with iron chelation therapy.

The three specific hypotheses tested in the different chapters of the thesis will now be discussed in more detail.

Hypothesis 1

The first hypothesis (Hypothesis 1) tested primarily in Chapter 3 and also further addressed in Chapter 4 was that (a) brain iron level is increased in the Aβ+Iron model as compared to the Aβ model; (b) excess brain iron may augment cerebral amyloidosis in the Aβ+Iron model as compared to the Aβ model; (c) excess brain iron may co-localise with insoluble Aβ pathology in the Aβ+Iron model.

As reported in Chapter 3, brain iron content measured by non-haem iron assay of homogenised brain hemispheres at 6 months of age showed substantial iron loading in the Aβ+Iron model compared to the age-, gender- and strain-matched Aβ model (fold change ≥ 1.8, $p<0.0001$, n ≥11 mice/group, with ≥4 per sex in each group). This was supported by the finding, reported in Chapter 4, that the relative intensity of 3,3'-diaminobenzidine-4HCl (DAB)-enhanced Perls' staining was significantly increased in the Aβ+Iron model compared to the Aβ model (fold change 1.7, $p<0.0001$, n=4 mice/group).

The data presented in Chapter 3 support the first and third parts of Hypothesis 1 as brain iron levels were increased in the Aβ+Iron model compared to the Aβ model both as measured by non-haem iron assay and as detected by DAB-enhanced Perls' histochemical staining and more plaques were found to be co-localised with iron in the Aβ+Iron model, as discussed in more detail below. However despite this, the second part of the hypothesis was not supported as there was no evidence of increased amyloid deposition in the Aβ+Iron model compared to the Aβ model.

Specifically there was no significant difference in the amyloid plaque count and other key features of amyloid deposits such as density in the six month old Aβ+Iron model compared to the Aβ model (n=4 mice/group, $p>0.05$, Section 3.3.1). This may suggest that increased brain iron alone does not contribute to the aggravation of cerebral amyloidosis, at least in the early stages of the disease.

It is considered unlikely that the failure to detect differences represented methodological limitations since to visualise deposits of insoluble non-amyloid Aβ peptide in addition to deposits that correspond to classical Aβ amyloid, three different methods were used: Congo red fluorescence, Congo red birefringence under polarised light (the 'gold standard' for amyloid detection) and antibody 4G8 labelling. While many studies only use Congo red fluorescence or antibodies to Aβ peptide, these sometimes label structures that are not positive for Congo red birefringence, which is

a required feature for structures to comply with the standard definition of 'amyloid' of the Nomenclature Committee of the International Society of Amyloidosis (Benson et al., 2018; Sipe et al., 2012; Westermark et al., 2005).

Although there was no evidence for increases in amyloid, there was a possible increase in iron binding to plaques since all amyloid plaques clearly contained iron in the Aβ+Iron model, as compared to the Aβ model where ~15-20% plaques did not contain sufficient iron to be visibly detectable by DAB-enhanced Perls' staining. This suggests more iron may be incorporated into plaques when brain iron levels are higher.

As previously discussed (Section 3.4), this observation may also relate to the concept of iron deposits on plaques acting as oxidative stress 'hotspots'. Some studies have proposed that the Aβ peptide facilitates the accumulation and reduction of ferric iron to the ferrous form within amyloid deposits (Everett et al., 2014a; Everett et al., 2014b; Khan et al., 2006). However, most of these studies are *in vitro* and do not take into account factors such as glial cells around plaques or proteins in the extracellular environment which may modify the valence state of amyloid-bound iron. In the present study, while Perls' stain can detect the potentially labile ferrous form of iron (Meguro et al., 2007), it primarily detects ferric iron, and plaques did not appear to be detected by Turnbull's stain, even using the more sensitive perfusion method (Section 4.3.2). Furthermore again, in the light of the findings of Section 3.3.3.3, there was no evidence of increased iron promoting amyloid deposition in the Aβ+Iron model compared to the Aβ model although iron co-localised with amyloid in both of these models.

It is therefore possible that the amount of amyloid is limited by the amount of Aβ. More exactly the rate of generation of amyloidogenic Aβ may be the main factor determining the amount and rate of amyloid production as long as there is some threshold level of iron available that is sufficient to initiate and/or sustain amyloid deposition, if indeed iron is required at all. Although this appears likely from *in vitro* observations such as those of House and colleagues that amyloidogenesis is impaired by iron chelation (House et al., 2004b), this has yet to be fully confirmed and it remains possible that other agents could also initiate amyloidogenesis *in vivo* in some circumstances.

As discussed in Section 4.4, there is currently little if any evidence that iron itself can increase generation of amyloidogenic Aβ directly, for example through actions on the IRE-IRP system, but this is difficult to assess without more complex mouse models than those presently available.

Regardless of the nature of the iron-amyloid relationship in AD pathogenesis, the clear co-localisation of iron with both amyloid and other insoluble forms of Aβ aggregates confirmed in the

present study supports the use of iron as a surrogate marker for the detection of disease pathology by neuroimaging of patients. Increased levels of iron in brain tissue are believed to aid in detecting changes in transverse relaxation (T2) and susceptibility of magnetic resonance imaging (MRI) in AD tissue. This has led many researchers to see the presence of elevated iron as a promising way of diagnosing AD long before other pathological symptoms become visible (Acosta-Cabronero et al., 2013; Antharam et al., 2012; El Tayara Nel et al., 2007; Jack et al., 2005; Meadowcroft et al., 2009; Meadowcroft et al., 2015b).

Hypothesis 2

The second hypothesis which was addressed by this thesis was that brain iron distribution in different cell types and structures is generally similar in the Aβ+Iron model and the *Hfe*$^{-/-}$*xTfr2*^{mut} model (the 'Iron model') with the important exception of iron associated with amyloid plaques and iron-associated cells in the vicinity of amyloid plaques in the Aβ+Iron model (plaques are not present in the 'Iron model').

The findings presented in Chapter 4 support Hypothesis 2 as considerable amounts of iron accumulated in the choroid plexus, myelin and myelin-associated cells whereas neurons and astrocytes showed little if any evidence of iron accumulation. This is consistent with the earlier findings from our lab for the Iron model (Heidari et al., 2016b).

Specifically, there was little evidence for abnormal iron loading in astrocytes or reactive astrogliosis even in areas of increased iron loading in either the Aβ model or the Aβ+Iron model (Section 4.3.7). Similarly, preliminary observations in the present study (data not shown) suggest that the unidentified iron-laden cells in the vicinity of amyloid plaques are not astrocytes, although this remains to be confirmed in ongoing studies in our lab.

There was also little if any evidence of iron accumulation in neurons in the hippocampus, the cortex or the midbrain of both the Aβ and the Aβ+Iron models. This suggests that there may be protective mechanisms which can prevent neuronal iron loading despite the presence of overall increased brain iron levels and amyloidosis with associated neurodegenerative changes in the Aβ+Iron model. Given the very low levels of iron detected in neurons it is also possible that neuronal intracellular iron insufficiency may compromise normal neuronal functions in Aβ+Iron model, as has been reported for mice deficient for the iron regulatory protein Irp2 (Jeong et al., 2011; Zumbrennen-Bullough et al., 2014).

Additionally, it was observed that the Aβ+Iron model contained various groups of unidentified iron-laden cells, including solitary or independent cells not clearly associated with myelin and cells associated with amyloid plaques. Yet interestingly, although most amyloid plaques contained iron in the Aβ+Iron model, overall there was an inverse relationship between plaque load and regional iron levels. More plaques were detected in areas with weak iron staining such as the cerebral cortex, hippocampus and entorhinal cortex whereas few if any plaques were observed in brain regions such as the thalamus and the basal ganglia which had relatively strong iron staining. This again suggests that high levels of iron alone may not be sufficient to increase amyloid deposition in the immediate vicinity as otherwise, if this were true, more amyloid plaques would be expected to be seen in the brain regions with most iron.

It was also noted, as discussed in Chapter 4 (Section 4.4), that although the level of iron staining associated with individual Aβ aggregates was high compared to the surrounding neuropil and other structures in the immediate vicinity, the total amount of iron associated with amyloid appears likely to be a tiny fraction of the total brain iron stored in myelin or cells having high levels of iron. This is one of the issues identified in the project which makes the probable success of any iron chelation therapy questionable.

Taken together, the findings from Chapter 3 and Chapter 4 suggest that although iron and amyloid co-aggregate, surplus iron does not inevitably lead to substantial aggravation of cerebral amyloidosis.

Hypothesis 3

The third hypothesis examined by this thesis had two components, that microglia surround amyloid plaques in the Aβ+Iron mouse model and may have increased intracellular iron content, and that increased brain iron levels may augment oxidative damage or neuronal loss in the mouse model of amyloidosis.

As reported in Chapters 4 and 5, Iba1 labelling identified microglia surrounding plaques in the Aβ+Iron model, although whether these contained iron could not be clearly ascertained. While there was preliminary evidence for labile ferrous iron (Section 4.3.2) and potential oxidative damage (Section 5.3.5) in some brain regions, these generally did not correspond with regions containing amyloid. Furthermore there was no evidence for increased neuronal loss in the Aβ+Iron model in the NeuN labelling studies reported here (Section 5.3.6). While these data remain to be confirmed, this suggests the existence of protective mechanisms possibly, although not necessarily, involving microglia.

These findings may suggest that by six months of age, even the lifelong exposure of the Aβ+Iron model to high brain iron levels is not sufficient to trigger additional neurodegenerative cell loss beyond that already occurring in the regular Aβ model. Some authors have proposed that the iron-amyloid interaction may even be neuroprotective if it results in redox-silencing of iron, although this has not been demonstrated for non-pharmacological iron increases *in vivo* (Bishop and Robinson, 2003; Bishop and Robinson, 2004; House et al., 2004a; Nakamura et al., 2007; Telling et al., 2017; Zou et al., 2002).

Ferroptosis

Recently, an iron-dependent cell death pathway called 'ferroptosis' has been put forward as a novel mechanism of how abnormal iron may be harmful. This pathway is proposed to involve iron-dependent accumulation of reactive oxygen species and depletion of plasma membrane polyunsaturated fatty acids (Bogdan et al., 2016; Cao and Dixon, 2016; Dixon et al., 2012).

As there was no clear evidence of neuronal loss in the Aβ+Iron model and so far no evidence has been found for ferroptosis in the brain of the Iron model (unpublished data, Johnstone, Heidari and colleagues), this was not prioritised for investigation within the timeframe of this thesis. Future studies could however include the study of ferroptosis-related transcripts in the Aβ+Iron model to see if this model has altered expression of these genes as compared to the Iron model as well as the Aβ model.

Possible protective roles of glia

The hypothesis that microglia surround amyloid plaques in the mouse models of amyloidosis was supported by the findings of this study. Although iron-laden cells were frequently observed in the vicinity of amyloid plaques, the combined labelling procedures for iron, amyloid and microglia could not verify that these cells were microglia, possibly due to technical issues when using more than one labelling protocol simultaneously.

As discussed in Section 5.1, it is well established that microglia cluster around amyloid plaques (Bolmont et al., 2008; Haga et al., 1989; Itagaki et al., 1989; Liebmann et al., 2016; Stalder et al., 1999; Wegiel and Wisniewski, 1990). One of the most potentially important findings of this thesis is that a far greater proportion of amyloid plaques was surrounded by cells with morphologies resembling activated or transitional microglia in the Aβ+Iron model than in the Aβ model, even though there was no difference in total microglial count around plaques based on Iba1-labelling. As activated microglia are reported to be able to clear more amyloid (Lee et al., 2013), it will be

important to investigate this in the Aβ+Iron model and examine how iron chelation might affect this. In addition, the illustrations of this thesis failed to disclose if amyloid was present in microglia or other cell types e.g. neurons. Follow-up studies could investigate this using higher resolution microscopy such as confocal microscopy.

Hepcidin-ferroportin interactions and neuronal protection

Thomsen and colleagues have noted that unless there is a large change in iron levels of the central nervous system, ferroportin expression appears to remain unchanged (Thomsen et al., 2015). The authors suggested this based on the reports of unaltered ferroportin levels in both iron deficient and iron excess conditions (Burdo et al., 2001; Wu et al., 2004). In the context of the present study, dysfunction of HFE and TFR2 is expected to result in very low levels of hepcidin transcripts in the Aβ+Iron model, similar to what was observed in the Iron model. Since hepcidin binding to ferroportin leads to its internalisation, low levels of hepcidin would in turn tend to preserve ferroportin on the neuronal cell surface, helping to safeguard neurons against excess iron accumulation (unpublished data, Johnstone, Heidari and colleagues). Follow-up analyses could examine hepcidin levels and ferroportin levels in the Aβ+Iron model.

Neuron-centric and holistic perspectives of AD

Strooper and Karran have commented that the traditional hypotheses of AD pathogenesis endeavour to explain neurodegeneration in terms of neuron-centric mechanisms. In these hypotheses, a single primary trigger such as β-amyloid is proposed to instigate the disease process, followed by subsequent downstream secondary phenomena such as oxidative damage, neuroinflammation, neuronal damage and ultimately dementia (De Strooper and Karran, 2016). However some clinical observations have not fully corroborated these hypotheses and the authors emphasize the need for more holistic perspectives which consider neuronal networks, oligodendrocytes, astrocyte, microglia and vasculature (De Strooper and Karran, 2016). In agreement with this view, the findings of the present study suggest more detailed investigations in the Aβ+Iron model may enable the elucidation of important pathways around iron, myelin, oligodendrocytes, other glia and vasculature and correlate these with neurons and neurodegeneration.

Protective mechanisms involving iron storage in myelin and myelin-associated cells

It is likely that the sequestration of iron in myelin and myelin-associated cells may help protect the brain of the Iron model against damaging effects of high iron concentrations (Heidari et al., 2016a; Heidari et al., 2016b). Consistent with observations reported previously by our group in the Iron model and discussed previously (Heidari et al., 2016a; Heidari et al., 2016b), iron in Aβ+Iron model

was also localised in myelin and myelin-associated cells whereas, little if any DAB-enhanced Perls' stainable iron was detected in neurons and astrocytes. Iron storage in myelin may help prevent excessive neuronal iron loading despite extra-neuronal increases in iron and this may potentially protect against neurodegeneration. Storage of iron in myelin might also protect microglia, astrocytes and other glial cells against detrimental effects of surplus iron. However, while the brain of the Aβ+Iron model may be able to handle excessive iron as long as the storage capacity of myelin is not exceeded, it cannot be ruled out that in AD patients white matter damage and subsequent release of potentially labile iron may occur if excess iron is deposited beyond the safe storage limits of myelin and myelin-associated cells.

A simple schematic summarising some of the key players in the complex relationship of iron and amyloid is presented in Fig 6.1 below. Some key questions that remain unanswered include the nature of the relationship, if any, between iron and amyloidogenesis, whether microglia are involved in the deposition or the clearance of amyloid plaques or both and what other mechanisms if any may contribute to possible neuroprotection in this model.

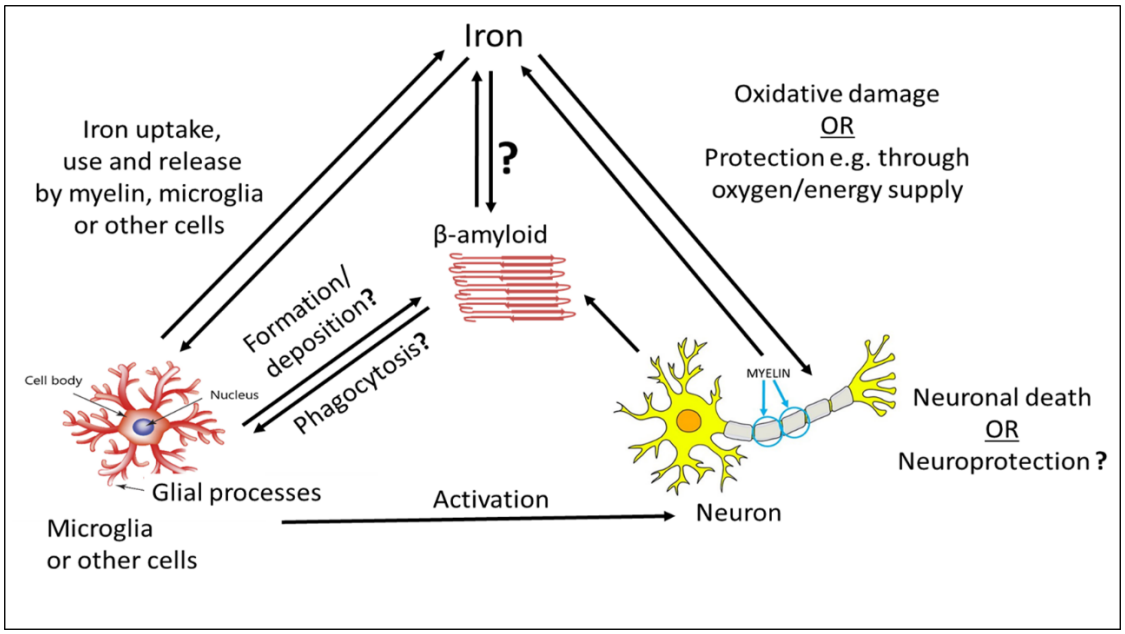

Fig. 6.1 Overview of some of the key players in the relationship of iron and amyloid. The figure summarises some key questions in the iron-amyloid relationship considered in this thesis.

Limitations and future directions

As the limitations of the individual studies in this thesis have already been discussed in the relevant chapters, the following section focuses on the requirements for addressing in the future how myelin damage, glial involvement and neuronal or synaptic changes may be relevant to the Aβ+Iron model.

i. Limitations of the mouse model

Ageing is the biggest risk factor for AD and Aβ+Iron mice may not have been old enough to manifest harmful consequences of excess iron. The AKR strain is a widely used background strain for generating mice with elevated iron levels due to its ability to maximize iron loading phenotype (Fleming et al., 2001) but it has a short lifespan (Festing and Blackmore, 1971; Yuan et al., 2009). Another major barrier of this study was slow breeding rates of Aβ+Iron mice. Due to these limitations, adequate number of mice could not be obtained to investigate effects of older age and gender on the parameters which were studied. Other members of the lab are examining older ages (9-12 months) in the present model and also studies of similar mice on other background strains and with other Alzheimer's-related pathologies are now commencing to see if the life expectancy of the mice can be extended (e.g. beyond 12 months) and also to investigate if there is any underlying strain-specific differences. For example, follow-up studies could look into the effects of cross-breeding the Iron model with other mouse models of AD, including mice which display tauopathy.

ii. Need for additional studies of neuronal function

In addition to using other methods besides NeuN to assess neuronal loss (discussed in more detail below), the possibility that neurons may survive but have functional deficits needs to be considered at the cellular and molecular levels as well as the level of the whole animal. As previously described in Chapter 5 (Section 5.4), it is possible that the Aβ+Iron model may display damage in the connectome (synapses and neuronal processes) even though there was no clear evidence of neuronal loss, although this could not be assessed within the timeframe of this thesis. To see if the Aβ+Iron model displays synaptic loss or pathology, follow-up studies could label brain sections for markers such as synaptophysin, an abundant membrane protein of synaptic vesicles.

Also functional effects need to be examined by behavioural and cognitive studies. This is being carried out by other members of our group (unpublished studies, Elvis Freeman-Acquah, Dan Johnstone and colleagues, in progress). It will be of paramount importance to investigate if the phenotype with the combination of both increased brain iron and amyloidosis shows altered

cognitive ability compared to phenotypes having either brain iron accumulation only or amyloidosis only. Considering the histochemical findings of this study, the likelihood of observing minimal if any cognitive deficits cannot be ruled out.

iii. Investigating mechanisms of neuronal damage or protection

As already discussed in Section 3.4, soluble forms of Aβ peptide are now widely believed to be more toxic than the insoluble amyloid plaques (Haass and Selkoe, 2007; Sengupta et al., 2016; Tomic et al., 2009). While the analysis on soluble Aβ peptides could not be completed within the timeframe of this thesis, it is possible that any increase in toxic Aβ peptides in the Aβ+Iron model may have contributed to putative oxidative damage. Experiments involving enzyme-linked immunosorbent assay (ELISA) method to measure the levels of soluble amyloid deposits are planned by other members in the lab however it is important to note that no significant reduction in relative neuronal counts per unit area was observed in this model, irrespective of the relative toxicities and levels of soluble and insoluble Aβ forms.

Additional assessment of neuronal loss or damage could be done by using additional cell death assays, e.g., terminal deoxynucleotidyl transferase (TdT)-mediated dUTP nick end labeling (TUNEL) and Fluorojade staining. Additionally, markers for specific neuronal types affected in AD could be tested, e.g. markers for cholinergic neurons or glutamatergic neurons (Ferreira-Vieira et al., 2016; Mufson et al., 2008; Wang and Reddy, 2017; Zhang et al., 2016). As noted above, another marker is synaptophysin, which could be used to check if the Aβ+Iron model has synaptic abnormalities (Clare et al., 2010; de Wilde et al., 2016; Eastwood et al., 1995; Gudi et al., 2017; Masliah et al., 1990).

iv. Additional investigations of relationships of iron and different glial cells

Generally, co-localisation of iron-laden cells with Iba1-labelled microglia was not observed in Aβ+Iron mice and Aβ mice (Section 5.3.4) but immunolabelling using other microglial markers such as TMEM119, CD11b and CD45 could be examined alone or in conjunction with iron or ferritin labelling to provide more information on whether microglia are involved in the phagocytosis or deposition of amyloid plaques in this model.

Changes in different myelin-related proteins and myelin abnormalities are known to contribute to AD associated cognitive decline (Bartzokis, 2004; O'Donnell et al., 1999; O'Sullivan et al., 2001; Peters and Sethares, 2002). Future studies could look at various features of myelin, for example myelin damage and abnormalities and changes in the expression of myelin-related genes in the Aβ+Iron model, as has been reported by our group for the Iron model (Heidari et al., 2016b).

As light microscopy could not reveal where exactly iron was loading in myelin, DAB-enhanced Perls' staining combined with electron microscopy could assess whether iron is in myelin or in the fluid between myelin and axon or within the axon itself. Connor and Menzies reported that iron was confined to astrocytes and microglia in a myelin-deficient rat model whereas oligodendrocytes contained most iron in the littermate controls (Connor and Menzies, 1990). As described previously (Section 4.4), placing Aβ+Iron mice on a cuprizone diet (Ludwin, 1978; Matsushima and Morell, 2001) or cross-breeding these mice with a myelin deficient model (Duncan et al., 2011) could help to see where iron would be loading if there was less myelin available for iron storage.

Dietary iron supplementation and iron chelation studies

The long-term usage of iron chelators are reported to result in deficiency of systemic iron and anaemia with several side-effects in older people with different health issues (Cuajungco et al., 2000; Guo et al., 2013). Iron chelators can also seize iron from ferritin and other compounds which are vital for maintaining the iron-dependent intrinsic physiology of body. Hence, various researchers demand careful attention toward distinction of iron specific compounds, which are involved in the disease progression and those which are required for normal brain functioning before treating patients with iron chelators (Collingwood et al., 2008; Raven et al., 2013).

As this study provided no evidence that surplus iron worsens amyloid pathology or neuronal loss in the six month old Aβ+Iron mice, iron chelation may not be beneficial to these mice. Nevertheless, follow-up investigations using mice of younger and older ages would be worth pursuing to study effects of iron chelators in the Aβ+Iron model and compare their efficacies at different time points.

Conclusion

Overall, the research reported here suggests that sequestration of iron in myelin and other protective mechanisms may permit substantial accumulation of iron in the brain without contributing to the exacerbation of cerebral amyloidosis or neuronal death. However the findings of this thesis have generated several additional questions.

If increased iron does not contribute to the aggravation of amyloidosis related pathology, does the complex of iron, amyloid and microglia or other glia serve to protect neurons from possible toxicity of increased iron and amyloid deposition?

What would be the effect of too much or too little systemic iron in the periphery, as compared to in the brain? For instance, if there is excess iron in the blood, this may enhance oxygen carriage by blood and could help support oxygen supply to the brain despite the presence of cerebrovascular disease. In this scenario, high levels of peripheral iron may have beneficial effects without necessarily entering the brain yet problems may arise if this iron is chelated in the large proportions of AD patients who have cerebrovasculopathy as this could reduce brain oxygen supply. It should also be noted that high blood levels do not necessarily imply that brain iron levels are dangerously high.

For example only a few patients with the iron overload disease haemochromatosis have been shown to have high brain iron accumulation (Berg et al., 2000; Nielsen et al., 1995). It is also not always clear if the patients being treated with iron chelators have high brain iron levels. A related concern is that even in patients with high brain levels of iron as detected by MRI, such iron may not be toxic if sequestered in myelin, making chelation at best unnecessary and potentially deleterious.

The justification for clinical trials of early iron chelation therapy in AD patients or people with mild cognitive impairment now appears questionable. Surplus iron is present throughout the life of the Aβ+Iron mouse and yet this does not seem to affect Alzheimer's amyloid related pathogenesis. Furthermore early administration of patients with iron chelators may deprive them of iron needed for proper cellular functioning. A very high degree of caution appears warranted in such circumstances. In any event, the findings from this thesis are expected to have direct translational consequences for AD and other neurodegenerative conditions and also possibly for patients with iron disorders such as haemochromatosis.

REFERENCES

Abbott, N.J. 2002. Astrocyte–endothelial interactions and blood–brain barrier permeability. Journal of Anatomy. 200:523-534.

Abbott, N.J. 2005. Dynamics of CNS barriers: evolution, differentiation, and modulation. Cell Mol Neurobiol. 25:5-23.

Abboud, S., and D.J. Haile. 2000. A novel mammalian iron-regulated protein involved in intracellular iron metabolism. Journal of Biological Chemistry. 275:19906-19912.

Abelein, A., A. Gräslund, and J. Danielsson. 2015. Zinc as chaperone-mimicking agent for retardation of amyloid β peptide fibril formation. Proceedings of the National Academy of Sciences. 112:5407-5412.

Acikyol, B., R. Graham, D. Trinder, M. House, J. Olynyk, R. Scott, E. Milward, and D. Johnstone. 2013. Brain transcriptome perturbations in the transferrin receptor 2 mutant mouse support the case for brain changes in iron loading disorders, including effects relating to long-term depression and long-term potentiation. Neuroscience. 235:119-128.

Acosta-Cabronero, J., G.B. Williams, A. Cardenas-Blanco, R.J. Arnold, V. Lupson, and P.J. Nestor. 2013. In vivo quantitative susceptibility mapping (QSM) in Alzheimer's disease. PloS One. 8:e81093.

Addess, K.J., J.P. Basilion, R.D. Klausner, T.A. Rouault, and A. Pardi. 1997. Structure and dynamics of the iron responsive element RNA: implications for binding of the RNA by iron regulatory binding proteins. Journal of Molecular Biology. 274:72-83.

Adlard, P.A., and A.I. Bush. 2006. Metals and Alzheimer's disease. Journal of Alzheimer's Disease: JAD. 10:145-163.

Adlard, P.A., and A.I. Bush. 2018. Metals and Alzheimer's Disease: How Far Have We Come in the Clinic? Journal of Alzheimer's Disease : JAD. 62:1369-1379.

Aguilar-Martinez, P. 2007. [Non-HFE-related hereditary iron overload]. Presse Med. 36:1279-1291.

Aisen, P., C. Enns, and M. Wessling-Resnick. 2001. Chemistry and biology of eukaryotic iron metabolism. The International Journal of Biochemistry and Cell Biology. 33:940-959.

Aisen, P., A. Leibman, and J. Zweier. 1978. Stoichiometric and site characteristics of the binding of iron to human transferrin. Journal of Biological Chemistry. 253:1930-1937.

Akatsu, H., A. Hori, T. Yamamoto, M. Yoshida, M. Mimuro, Y. Hashizume, I. Tooyama, and E.M. Yezdimer. 2012. Transition metal abnormalities in progressive dementias. Biometals. 25:337-350.

Albert, M.S., S.T. DeKosky, D. Dickson, B. Dubois, H.H. Feldman, N.C. Fox, A. Gamst, D.M. Holtzman, W.J. Jagust, and R.C. Petersen. 2011. The diagnosis of mild cognitive impairment due to Alzheimer’s disease: Recommendations from the National Institute on Aging-Alzheimer’s Association workgroups on diagnostic guidelines for Alzheimer's disease. Alzheimer's and Dementia. 7:270-279.

Aldred, A.R., P.W. Dickson, P.D. Marley, and G. Schreiber. 1987. Distribution of transferrin synthesis in brain and other tissues in the rat. The Journal of Biological Chemistry. 262:5293-5297.

Ali-Rahmani, F., C.-L. Schengrund, and J.R. Connor. 2014a. HFE gene variants, iron, and lipids: a novel connection in Alzheimer's disease. Frontiers in Pharmacology. 5.

Ali-Rahmani, F., C.L. Schengrund, and J.R. Connor. 2014b. HFE gene variants, iron, and lipids: a novel connection in Alzheimer's disease. Front Pharmacol. 5:165.

Allen, R., P. Barker, F. Wehrl, H. Song, and C. Earley. 2001. MRI measurement of brain iron in patients with restless legs syndrome. Neurology. 56:263-265.

Altamura, S., and M.U. Muckenthaler. 2008. Iron toxicity in diseases of aging: Alzheimer's disease, Parkinson's disease and atherosclerosis. Journal of Alzheimer's Disease: JAD. 16:879-895.

Altamura, S., and M.U. Muckenthaler. 2009. Iron toxicity in diseases of aging: Alzheimer's disease, Parkinson's disease and atherosclerosis. Journal of Alzheimer's Disease. 16:879-895.

Alzheimer's Association. 2013. 2013 Alzheimer's disease facts and figures. Alzheimer's and Dementia. 9:208-245.

Amit, T., O. Bar-Am, D. Mechlovich, L. Kupershmidt, M.B.H. Youdim, and O. Weinreb. 2017. The novel multitarget iron chelating and propargylamine drug M30 affects APP regulation and processing activities in Alzheimer's disease models. Neuropharmacology. 123:359-367.

Andersen, H.H., K.B. Johnsen, and T. Moos. 2014. Iron deposits in the chronically inflamed central nervous system and contributes to neurodegeneration. Cellular and Molecular Life Sciences. 71:1607-1622.

Andrews, N.C. 2000. Iron homeostasis: insights from genetics and animal models. Nature Reviews Genetics. 1:208-217.

Antharam, V., J.F. Collingwood, J.-P. Bullivant, M.R. Davidson, S. Chandra, A. Mikhaylova, M.E. Finnegan, C. Batich, J.R. Forder, and J. Dobson. 2012. High field magnetic resonance microscopy of the human hippocampus in Alzheimer's disease: quantitative imaging and correlation with iron. Neuroimage. 59:1249-1260.

Armstrong, D.M., W.C. Benzing, J. Evans, R.D. Terry, D. Shields, and L.A. Hansen. 1989. Substance P and somatostatin coexist within neuritic plaques: implications for the pathogenesis of Alzheimer's disease. Neuroscience. 31:663-671.

Arnold, S.E., N. Louneva, K. Cao, L.-S. Wang, L.-Y. Han, D.A. Wolk, S. Negash, S.E. Leurgans, J.A. Schneider, and A.S. Buchman. 2013. Cellular, synaptic, and biochemical features of resilient cognition in Alzheimer's disease. Neurobiology of Aging. 34:157-168.

Asai, M., C. Hattori, B. Szabó, N. Sasagawa, K. Maruyama, S.-i. Tanuma, and S. Ishiura. 2003. Putative function of ADAM9, ADAM10, and ADAM17 as APP α-secretase. Biochemical and Biophysical Research Communications. 301:231-235.

Avramovich-Tirosh, Y., T. Amit, O. Bar-Am, H. Zheng, M. Fridkin, and M.B. Youdim. 2007a. Therapeutic targets and potential of the novel brain- permeable multifunctional iron chelator-monoamine oxidase inhibitor drug, M-30, for the treatment of Alzheimer's disease. J Neurochem. 100:490-502.

Avramovich-Tirosh, Y., L. Reznichenko, T. Mit, H. Zheng, M. Fridkin, O. Weinreb, S. Mandel, and M.B. Youdim. 2007b. Neurorescue activity, APP regulation and amyloid-beta peptide reduction by novel multi-

functional brain permeable iron- chelating- antioxidants, M-30 and green tea polyphenol, EGCG. Curr Alzheimer Res. 4:403-411.

Ayonrinde, O.T., E.A. Milward, A.C. Chua, D. Trinder, and J.K. Olynyk. 2008. Clinical perspectives on hereditary hemochromatosis. Critical reviews in Clinical Laboratory Sciences. 45:451-484.

Ayton, S., N.G. Faux, A.I. Bush, and A.s.D.N. Initiative. 2015. Ferritin levels in the cerebrospinal fluid predict Alzheimer/'s disease outcomes and are regulated by APOE. Nature Communications. 6.

Ayton, S., Y. Wang, I. Diouf, J.A. Schneider, J. Brockman, M.C. Morris, and A.I. Bush. 2019. Brain iron is associated with accelerated cognitive decline in people with Alzheimer pathology. Molecular Psychiatry.

Bacon, B.R., L.W. Powell, P.C. Adams, T.F. Kresina, and J.H. Hoofnagle. 1999. Molecular medicine and hemochromatosis: at the crossroads. Gastroenterology. 116:193-207.

Bagnato, F., S. Hametner, B. Yao, P. van Gelderen, H. Merkle, F.K. Cantor, H. Lassmann, and J.H. Duyn. 2011. Tracking iron in multiple sclerosis: a combined imaging and histopathological study at 7 Tesla. Brain. 134:3602-3615.

Baik, S.H., S. Kang, S.M. Son, and I. Mook-Jung. 2016. Microglia contributes to plaque growth by cell death due to uptake of amyloid beta in the brain of Alzheimer's disease mouse model. Glia. 64:2274-2290.

Banati, R.B., J. Gehrmann, C. Czech, U. Monning, L.L. Jones, G. Konig, K. Beyreuther, and G.W. Kreutzberg. 1993a. Early and rapid de novo synthesis of Alzheimer beta A4-amyloid precursor protein (APP) in activated microglia. Glia. 9:199-210.

Banati, R.B., J. Gehrmann, P. Schubert, and G.W. Kreutzberg. 1993b. Cytotoxicity of microglia. Glia. 7:111-118.

Bandyopadhyay, S., X. Huang, H. Cho, N. Greig, M. Youdim, and J. Rogers. 2006. Metal specificity of an iron-responsive element in Alzheimer’s APP mRNA 5’ untranslated region, tolerance of SH-SY5Y and H4 neural cells to desferrioxamine, clioquinol, VK-28, and a piperazine chelator. Oxidative Stress and Neuroprotection. Springer. 237-247.

Banerjee, P., A. Sahoo, S. Anand, A. Bir, and S. Chakrabarti. 2016. The Oral Iron Chelator, Deferasirox, Reverses the Age-Dependent Alterations in Iron and Amyloid-beta Homeostasis in Rat Brain: Implications in the Therapy of Alzheimer's Disease. Journal of Alzheimer's Disease : JAD. 49:681-693.

Banks, W.A. 2016. From blood-brain barrier to blood-brain interface: new opportunities for CNS drug delivery. Nature Reviews. Drug discovery. 15:275-292.

Barger, S.W., and A.D. Harmon. 1997. Microglial activation by Alzheimer amyloid precursor protein and modulation by apolipoprotein E. Nature. 388:878.

Baron, O., A. Boudi, C. Dias, M. Schilling, A. Nolle, G. Vizcay-Barrena, I. Rattray, H. Jungbluth, W. Scheper, R.A. Fleck, G.P. Bates, and M. Fanto. 2017. Stall in Canonical Autophagy-Lysosome Pathways Prompts Nucleophagy-Based Nuclear Breakdown in Neurodegeneration. Current Biology : CB. 27:3626-3642.e3626.

Barton, J.C., and C.Q. Edwards. 2000. Hemochromatosis: genetics, pathophysiology, diagnosis and treatment. Cambridge University Press.

Barton, J.C., R. Sawada-Hirai, B.E. Rothenberg, and R.T. Acton. 1999. Two novel missense mutations of the HFE gene (I105T and G93R) and identification of the S65C mutation in Alabama hemochromatosis probands. Blood Cells, Molecules, and Diseases. 25:147-155.

Bartzokis, G. 2004. Age-related myelin breakdown: a developmental model of cognitive decline and Alzheimer's disease. Neurobiology of Aging. 25:5-18.

Bartzokis, G., M. Beckson, D.B. Hance, P. Marx, J.A. Foster, and S.R. Marder. 1997. MR evaluation of age-related increase of brain iron in young adult and older normal males. Magnetic Resonance Imaging. 15:29-35.

Bartzokis, G., P.H. Lu, and J. Mintz. 2007. Human brain myelination and amyloid beta deposition in Alzheimer's disease. Alzheimer's & Dementia. 3:122-125.

Bartzokis, G., D. Sultzer, P.H. Lu, K.H. Nuechterlein, J. Mintz, and J.L. Cummings. 2004a. Heterogeneous age-related breakdown of white matter structural integrity: implications for cortical "disconnection" in aging and Alzheimer's disease. Neurobiol Aging. 25:843-851.

Bartzokis, G., D. Sultzer, J. Mintz, L.E. Holt, P. Marx, C.K. Phelan, and S.R. Marder. 1994. In vivo evaluation of brain iron in Alzheimer's disease and normal subjects using MRI. Biological Psychiatry. 35:480-487.

Bartzokis, G., T.A. Tishler, I.S. Shin, P.H. Lu, and J.L. Cummings. 2004b. Brain ferritin iron as a risk factor for age at onset in neurodegenerative diseases. Annals of the New York Academy of Sciences. 1012:224-236.

Batra, J., and P. Seth. 2002. Effect of iron deficiency on developing rat brain. Indian Journal of Clinical Biochemistry. 17:108-114.

Baumann, N., and D. Pham-Dinh. 2001. Biology of oligodendrocyte and myelin in the mammalian central nervous system. Physiological Reviews. 81:871-927.

Beard, C.M., E. Kokmen, C. Sigler, G.E. Smith, T. Petterson, and P.C. O'Brien. 1996. Cause of death in Alzheimer's disease. Annals of Epidemiology. 6:195-200.

Bell, R.D., and B.V. Zlokovic. 2009. Neurovascular mechanisms and blood-brain barrier disorder in Alzheimer's disease. Acta Neuropathol. 118:103-113.

Belyaev, N.D., K.A. Kellett, C. Beckett, N.Z. Makova, T.J. Revett, N.N. Nalivaeva, N.M. Hooper, and A.J. Turner. 2010. The transcriptionally active amyloid precursor protein (APP) intracellular domain is preferentially produced from the 695 isoform of APP in a {beta}-secretase-dependent pathway. The Journal of Biological Chemistry. 285:41443-41454.

Bennett, B.D., P. Denis, M. Haniu, D.B. Teplow, S. Kahn, J.-C. Louis, M. Citron, and R. Vassar. 2000. A furin-like convertase mediates propeptide cleavage of BACE, the Alzheimer's β-secretase. Journal of Biological Chemistry. 275:37712-37717.

Bennett, M.L., F.C. Bennett, S.A. Liddelow, B. Ajami, J.L. Zamanian, N.B. Fernhoff, S.B. Mulinyawe, C.J. Bohlen, A. Adil, A. Tucker, I.L. Weissman, E.F. Chang, G. Li, G.A. Grant, M.G. Hayden Gephart, and B.A. Barres. 2016. New tools for studying microglia in the mouse and human CNS. Proceedings of the National Academy of Sciences of the United States of America. 113:E1738-1746.

Benson, M.D., J.N. Buxbaum, D.S. Eisenberg, G. Merlini, M.J.M. Saraiva, Y. Sekijima, J.D. Sipe, and P. Westermark. 2018. Amyloid nomenclature 2018: recommendations by the International Society of Amyloidosis (ISA) nomenclature committee. Amyloid : The international Journal of Experimental and Clinical Investigation. 25:215-219.

Berezovska, O., A. Lleo, L.D. Herl, M.P. Frosch, E.A. Stern, B.J. Bacskai, and B.T. Hyman. 2005. Familial Alzheimer's disease presenilin 1 mutations cause alterations in the conformation of presenilin and interactions with amyloid precursor protein. The Journal of Neuroscience. 25:3009-3017.

Berg, D., U. Hoggenmüller, E. Hofmann, R. Fischer, M. Kraus, M. Scheurlen, and G. Becker. 2000. The basal ganglia in haemochromatosis. Neuroradiology. 42:9-13.

Bertram, L., and R.E. Tanzi. 2004. Alzheimer's disease: one disorder, too many genes? Human Molecular Genetics. 13:R135-R141.

Beydoun, R., M.A. Hamood, D.M.G. Zubeita, and K.C. Kondapalli. 2017. Na+/H+ Exchanger 9 Regulates Iron Mobilization at the Blood Brain Barrier in Response to Iron Starvation. Journal of Biological Chemistry. M116. 769240.

Biron, K.E., D.L. Dickstein, R. Gopaul, and W.A. Jefferies. 2011. Amyloid triggers extensive cerebral angiogenesis causing blood brain barrier permeability and hypervascularity in Alzheimer's disease. PloS One. 6:e23789.

Bishop, G.M., T.N. Dang, R. Dringen, and S.R. Robinson. 2011. Accumulation of non-transferrin-bound iron by neurons, astrocytes, and microglia. Neurotox Res. 19:443-451.

Bishop, G.M., and S.R. Robinson. 2003. Human Abeta1-42 reduces iron-induced toxicity in rat cerebral cortex. Journal of neuroscience research. 73:316-323.

Bishop, G.M., and S.R. Robinson. 2004. The amyloid paradox: amyloid-beta-metal complexes can be neurotoxic and neuroprotective. Brain Pathol. 14:448-452.

Bishop, G.M., I.F. Scheiber, R. Dringen, and S.R. Robinson. 2010. Synergistic accumulation of iron and zinc by cultured astrocytes. J Neural Transm (Vienna). 117:809-817.

Bitting, L., A. Naidu, B. Cordell, and G.M. Murphy. 1996. β-amyloid peptide secretion by a microglial cell line is induced by β-amyloid-(25–35) and lipopolysaccharide. Journal of Biological Chemistry. 271:16084-16089.

Bodea, L.G., Y. Wang, B. Linnartz-Gerlach, J. Kopatz, L. Sinkkonen, R. Musgrove, T. Kaoma, A. Muller, L. Vallar, D.A. Di Monte, R. Balling, and H. Neumann. 2014. Neurodegeneration by activation of the microglial complement-phagosome pathway. The Journal of Neuroscience. 34:8546-8556.

Bogdan, A.R., M. Miyazawa, K. Hashimoto, and Y. Tsuji. 2016. Regulators of Iron Homeostasis: New Players in Metabolism, Cell Death, and Disease. Trends Biochem Sci. 41:274-286.

Bolmont, T., F. Haiss, D. Eicke, R. Radde, C.A. Mathis, W.E. Klunk, S. Kohsaka, M. Jucker, and M.E. Calhoun. 2008. Dynamics of the Microglial/Amyloid Interaction Indicate a Role in Plaque Maintenance. The Journal of Neuroscience. 28:4283-4292.

Bolognin, S., L. Messori, D. Drago, C. Gabbiani, L. Cendron, and P. Zatta. 2011. Aluminum, copper, iron and zinc differentially alter amyloid-Abeta(1-42) aggregation and toxicity. The international Journal of Biochemistry & Cell Biology. 43:877-885.

Boopathi, S., and P. Kolandaivel. 2016. Fe(2+) binding on amyloid beta-peptide promotes aggregation. Proteins. 84:1257-1274.

Booth, A.G., and M.J. Wilson. 1981. Human placental coated vesicles contain receptor-bound transferrin. Biochem. J. 196:355-362.

Borchelt, D.R., G. Thinakaran, C.B. Eckman, M.K. Lee, F. Davenport, T. Ratovitsky, C.-M. Prada, G. Kim, S. Seekins, and D. Yager. 1996. Familial Alzheimer's disease–linked presenilin 1 variants elevate Aβ1–42/1–40 ratio in vitro and in vivo. Neuron. 17:1005-1013.

Boserup, M.W., J. Lichota, D. Haile, and T. Moos. 2011. Heterogenous distribution of ferroportin-containing neurons in mouse brain. Biometals. 24:357-375.

Bourassa, M.W., A.C. Leskovjan, R.V. Tappero, E.R. Farquhar, C.A. Colton, W.E. Van Nostrand, and L.M. Miller. 2013. Elevated copper in the amyloid plaques and iron in the cortex are observed in mouse models of Alzheimer's disease that exhibit neurodegeneration. Biomedical Spectroscopy and Imaging. 2:129-139.

Boyd, D., C. Vecoli, D. Belcher, S. Jain, and J. Drysdale. 1985. Structural and functional relationships of human ferritin H and L chains deduced from cDNA clones. Journal of Biological Chemistry. 260:11755-11761.

Braak, H., and E. Braak. 1991. Neuropathological stageing of Alzheimer-related changes. Acta neuropathologica. 82:239-259.

Braak, H., E. Braak, D. Yilmazer, R.A. de Vos, E.N. Jansen, and J. Bohl. 1996. Pattern of brain destruction in Parkinson's and Alzheimer's diseases. J Neural Transm (Vienna). 103:455-490.

Braak, H., uuml, U. b, C. Schultz, and K.D. Tredici. 2006. Vulnerability of cortical neurons to Alzheimer's and Parkinson's diseases. Journal of Alzheimer's Disease. 9:35-44.

Bradbury, M. 1997. Transport of Iron in the Blood-Brain-Cerebrospinal Fluid System. Journal of Neurochemistry. 69:443-454.

Bramblett, G.T., M. Goedert, R. Jakes, S.E. Merrick, J.Q. Trojanowski, and V.M. Lee. 1993. Abnormal tau phosphorylation at Ser 396 in Alzheimer's disease recapitulates development and contributes to reduced microtubule binding. Neuron. 10:1089-1099.

Brasted, M., C.A. White, T.G. Kennedy, and L.A. Salamonsen. 2003. Mimicking the events of menstruation in the murine uterus. Biology of Reproduction. 69:1273-1280.

Brown, L., E. Hansnata, and H.A. La. 2017b. Economic Cost of Dementia in Australia. Alzheimer’s Australia, Canberra.

Bruni, A. 1997. Cloning of a gene bearing missense mutations in early onset familial Alzheimer's disease: a Calabrian study. Functional Neurology. 13:257-261.

Brunk, U.T., and A. Terman. 2002. Lipofuscin: mechanisms of age-related accumulation and influence on cell function. Free Radic Biol Med. 33:611-619.

Burdo, J.R., S.L. Menzies, I.A. Simpson, L.M. Garrick, M.D. Garrick, K.G. Dolan, D.J. Haile, J.L. Beard, and J.R. Connor. 2001. Distribution of divalent metal transporter 1 and metal transport protein 1 in the normal and Belgrade rat. Journal of Neuroscience Research. 66:1198-1207.

Burn, J., and P.F. Chinnery. 2006. Neuroferritinopathy. Seminars in Pediatric Neurology. Vol. 13. Elsevier. 176-181.

Burns, A., R. Jacoby, P. Luthert, and R. Levy. 1990. Cause of death in Alzheimer's disease. Age and Ageing. 19:341-344.

Bush, A.I. 2003. The metallobiology of Alzheimer's disease. Trends in Neurosciences. 26:207-214.

Bush, A.I., W.H. Pettingell, G. Multhaup, M. d Paradis, J.-P. Vonsattel, J.F. Gusella, K. Beyreuther, C.L. Masters, and R.E. Tanzi. 1994. Rapid induction of Alzheimer A beta amyloid formation by zinc. Science. 265:1464-1467.

Butterfield, D.A. 1997. β-Amyloid-associated free radical oxidative stress and neurotoxicity: implications for Alzheimer's disease. Chemical Research in Toxicology. 10:495-506.

Cai, H., Y. Wang, D. McCarthy, H. Wen, D.R. Borchelt, D.L. Price, and P.C. Wong. 2001. BACE1 is the major beta-secretase for generation of Abeta peptides by neurons. Nature Neuroscience. 4:233-234.

Camaschella, C. 2005. Understanding iron homeostasis through genetic analysis of hemochromatosis and related disorders. Blood. 106:3710-3717.

Camaschella, C., A. Roetto, A. Calì, M. De Gobbi, G. Garozzo, M. Carella, N. Majorano, A. Totaro, and P. Gasparini. 2000. The gene TFR2 is mutated in a new type of haemochromatosis mapping to 7q22. Nature Genetics. 25:14-15.

Cammermyer, J. 1947. Deposition of iron in paraventricular areas of the human brain in hemochromatosis. Journal of Neuropathology and Experimental Neurology. 6:111-127.

Campion, D., C. Dumanchin, D. Hannequin, B. Dubois, S. Belliard, M. Puel, C. Thomas-Anterion, A. Michon, C. Martin, and F. Charbonnier. 1999. Early-onset autosomal dominant Alzheimer disease: prevalence, genetic heterogeneity, and mutation spectrum. The American Journal of Human Genetics. 65:664-670.

Cao, J.Y., and S.J. Dixon. 2016. Mechanisms of ferroptosis. Cellular and Molecular Life Sciences. 73:2195-2209.

Cardoso, F.L., D. Brites, and M.A. Brito. 2010. Looking at the blood–brain barrier: molecular anatomy and possible investigation approaches. Brain Research Reviews. 64:328-363.

Cartwright, G.E., C.Q. Edwards, K. Kravitz, M. Skolnick, D.B. Amos, A. Johnson, and L. Buskjaer. 1979. Hereditary hemochromatosis: phenotypic expression of the disease. New England Journal of Medicine. 301:175-179.

Casey, J.L., M.W. Hentze, D.M. Koeller, S.W. Caughman, T.A. Rouault, R.D. Klausner, and J.B. Harford. 1988. Iron-responsive elements: regulatory RNA sequences that control mRNA levels and translation. Science. 240:924-928.

Castro, M.A., A. Hadziselimovic, and C.R. Sanders. 2019. The Vexing Complexity of the Amyloidogenic Pathway. Protein Science.

Chakrabarty, P., K. Jansen-West, A. Beccard, C. Ceballos-Diaz, Y. Levites, C. Verbeeck, A.C. Zubair, D. Dickson, T.E. Golde, and P. Das. 2010. Massive gliosis induced by interleukin-6 suppresses Aβ deposition in vivo: evidence against inflammation as a driving force for amyloid deposition. The FASEB Journal. 24:548-559.

Chamberlain, R., T. M Wengenack, J. F Poduslo, M. Garwood, and C. R Jack. 2011. Magnetic resonance imaging of amyloid plaques in transgenic mouse models of Alzheimer's disease. Current Medical Imaging Reviews. 7:3-7.

Chasteen, N.D., and P.M. Harrison. 1999. Mineralization in ferritin: an efficient means of iron storage. Journal of Structural Biology. 126:182-194.

Chasteen, N.D., and J. Williams. 1981. The influence of pH on the equilibrium distribution of iron between the metal-binding sites of human transferrin. Biochem. J. 193:717-727.

Cheepsunthorn, P., C. Palmer, and J.R. Connor. 1998. Cellular distribution of ferritin subunits in postnatal rat brain. Journal of Comparative Neurology. 400:73-86.

Cheepsunthorn, P., C. Palmer, S. Menzies, R.L. Roberts, and J.R. Connor. 2001. Hypoxic/ischemic insult alters ferritin expression and myelination in neonatal rat brains. Journal of Comparative Neurology. 431:382-396.

Chen, M., and B.A. Yankner. 1991. An antibody to β amyloid and the amyloid precursor protein inhibits cell-substratum adhesion in many mammalian cell types. Neuroscience Letters. 125:223-226.

Chen, T.T., L. Li, D.-H. Chung, C.D. Allen, S.V. Torti, F.M. Torti, J.G. Cyster, C.-Y. Chen, F.M. Brodsky, and E.C. Niemi. 2005. TIM-2 is expressed on B cells and in liver and kidney and is a receptor for H-ferritin endocytosis. The Journal of Experimental Medicine. 202:955-965.

Chen, X., D.B. Cho, and P.C. Yang. 2010. Double staining immunohistochemistry. North American Journal of Medical Sciences. 2:241-245.

Cherny, R.A., C.S. Atwood, M.E. Xilinas, D.N. Gray, W.D. Jones, C.A. McLean, K.J. Barnham, I. Volitakis, F.W. Fraser, and Y.-S. Kim. 2001. Treatment with a copper-zinc chelator markedly and rapidly inhibits β-amyloid accumulation in Alzheimer's disease transgenic mice. Neuron. 30:665-676.

Cherry, J.D., J.A. Olschowka, and M.K. O'Banion. 2014. Are "resting" microglia more "m2"? Frontiers in Immunology. 5:594.

Chua, A.C., R.D. Delima, E.H. Morgan, C.E. Herbison, J.E. Tirnitz-Parker, R.M. Graham, R.E. Fleming, R.S. Britton, B.R. Bacon, and J.K. Olynyk. 2010. Iron uptake from plasma transferrin by a transferrin receptor 2 mutant mouse model of haemochromatosis. Journal of Hepatology. 52:425-431.

Citron, M., T.S. Diehl, G. Gordon, A.L. Biere, P. Seubert, and D.J. Selkoe. 1996. Evidence that the 42-and 40-amino acid forms of amyloid β protein are generated from the β-amyloid precursor protein by different protease activities. Proceedings of the National Academy of Sciences. 93:13170-13175.

Clare, R., V.G. King, M. Wirenfeldt, and H.V. Vinters. 2010. Synapse loss in dementias. Journal of Neuroscience Research. 88:2083-2090.

Cleveland, D.W., S.-Y. Hwo, and M.W. Kirschner. 1977. Physical and chemical properties of purified tau factor and the role of tau in microtubule assembly. Journal of Molecular Biology. 116:227-247.

Codazzi, F., I. Pelizzoni, D. Zacchetti, and F. Grohovaz. 2015. Iron entry in neurons and astrocytes: a link with synaptic activity. Frontiers in Molecular Neuroscience. 8.

Cole, G., J. Neal, S. Singhrao, B. Jasani, and G. Newman. 1993. The distribution of amyloid plaques in the cerebellum and brain stem in Down's syndrome and Alzheimer's disease: a light microscopical analysis. Acta neuropathologica. 85:542-552.

Colette Daubner, S., J.I. Ehrlich, A.J. Ramsey, and P.F. Fitzpatrick. 1995. Identification of iron ligands in tyrosine hydroxylase by mutagenesis of conserved histidinyl residues. Protein Science. 4:2082-2086.

Collingwood, J.F., R.K. Chong, T. Kasama, L. Cervera-Gontard, R.E. Dunin-Borkowski, G. Perry, M. Pósfai, S.L. Siedlak, E.T. Simpson, and M.A. Smith. 2008. Three-dimensional tomographic imaging and characterization of iron compounds within Alzheimer's plaque core material. Journal of Alzheimer's Disease. 14:235-245.

Collingwood, J.F., A. Mikhaylova, M. Davidson, C. Batich, W.J. Streit, J. Terry, and J. Dobson. 2005. In situ characterization and mapping of iron compounds in Alzheimer's disease tissue. Journal of Alzheimer's disease : JAD. 7:267-272.

Condello, C., P. Yuan, A. Schain, and J. Grutzendler. 2015. Microglia constitute a barrier that prevents neurotoxic protofibrillar Abeta42 hotspots around plaques. Nat Commun. 6:6176.

Connor, J., and S. Menzies. 1990. Altered cellular distribution of iron in the central nervous system of myelin deficient rats. Neuroscience. 34:265-271.

Connor, J., S. Menzies, S. St Martin, and E. Mufson. 1990. Cellular distribution of transferrin, ferritin, and iron in normal and aged human brains. Journal of Neuroscience Research. 27:595-611.

Connor, J., S. Menzies, S. St Martin, and E. Mufson. 1992a. A histochemical study of iron, transferrin, and ferritin in Alzheimer's diseased brains. Journal of Neuroscience Research. 31:75-83.

Connor, J., E. Milward, S. Moalem, M. Sampietro, P. Boyer, M. Percy, C. Vergani, R. Scott, and M. Chorney. 2001. Is hemochromatosis a risk factor for Alzheimer's disease? Journal of Alzheimer's Disease: JAD. 3:471-477.

Connor, J., B. Snyder, J. Beard, R. Fine, and E. Mufson. 1992b. Regional distribution of iron and iron-regulatory proteins in the brain in aging and Alzheimer's disease. Journal of Neuroscience Research. 31:327-335.

Connor, J.R., and S.L. Menzies. 1995. Cellular management of iron in the brain. Journal of the Neurological Sciences. 134:33-44.

Connor, J.R., and S.L. Menzies. 1996. Relationship of iron to oligodendrocytes and myelination. Glia. 17:83-93.

Corder, E., A. Saunders, W. Strittmatter, D. Schmechel, P. Gaskell, G. Small, A. Roses, J. Haines, and M.A. Pericak-Vance. 1993. Gene dose of apolipoprotein E type 4 allele and the risk of Alzheimer's disease in late onset families. Science. 261:921-923.

Correas, I., J. Diaz-Nido, and J. Avila. 1992. Microtubule-associated protein tau is phosphorylated by protein kinase C on its tubulin binding domain. Journal of Biological Chemistry. 267:15721-15728.

Crapper, D., S. Krishnan, and A. Dalton. 1973. Brain aluminum distribution in Alzheimer's disease and experimental neurofibrillary degeneration. Science. 180:511-513.

Crapper McLachlan, D.R., A.J. Dalton, T.P. Kruck, M.Y. Bell, W.L. Smith, W. Kalow, and D.F. Andrews. 1991. Intramuscular desferrioxamine in patients with Alzheimer's disease. Lancet. 337:1304-1308.

Crews, F.T., and R.P. Vetreno. 2016. Mechanisms of neuroimmune gene induction in alcoholism. Psychopharmacology. 233:1543-1557.

Crichton, R.R., D.T. Dexter, and R.J. Ward. 2012. Brain iron metabolism and its perturbation in neurological diseases. Springer.

Crowe, A., and E.H. Morgan. 1992. Iron and transferrin uptake by brain and cerebrospinal fluid in the rat. Brain Res. 592:8-16.

Cruts, M., C.M. van Duijn, H. Backhovens, M. Van den Broeck, A. Wehnert, S. Serneels, R. Sherrington, M. Hutton, J. Hardy, and P.H. St George-Hyslop. 1998. Estimation of the genetic contribution of presenilin-1 and-2 mutations in a population-based study of presenile Alzheimer disease. Human Molecular Genetics. 7:43-51.

Cuajungco, M.P., K.Y. Faget, X. Huang, R.E. Tanzi, and A.I. Bush. 2000. Metal chelation as a potential therapy for Alzheimer's disease. Annals of the New York Academy of Sciences. 920:292-304.

Cullen, K.M., Z. Kócsi, and J. Stone. 2005. Pericapillary haem-rich deposits: evidence for microhaemorrhages in aging human cerebral cortex. Journal of Cerebral Blood Flow & Metabolism. 25:1656-1667.

Cullen, K.M., Z. Kócsi, and J. Stone. 2006. Microvascular pathology in the aging human brain: evidence that senile plaques are sites of microhaemorrhages. Neurobiology of Aging. 27:1786-1796.

DaSilva, K.A., J.E. Shaw, and J. McLaurin. 2010. Amyloid-β fibrillogenesis: structural insight and therapeutic intervention. Experimental Neurology. 223:311-321.

Dautry-Varsat, A. 1986. Receptor-mediated endocytosis: the intracellular journey of transferrin and its receptor. Biochimie. 68:375-381.

Dautry-Varsat, A., A. Ciechanover, and H.F. Lodish. 1983. pH and the recycling of transferrin during receptor-mediated endocytosis. Proceedings of the National Academy of Sciences. 80:2258-2262.

Davis, B.M., M. Salinas-Navarro, M.F. Cordeiro, L. Moons, and L. De Groef. 2017. Characterizing microglia activation: a spatial statistics approach to maximize information extraction. Scientific Reports. 7:1576.

Davis, D., F. Schmitt, D. Wekstein, and W. Markesbery. 1999. Alzheimer neuropathologic alterations in aged cognitively normal subjects. Journal of Neuropathology & Experimental Neurology. 58:376-388.

Davoli, M.A., J. Fourtounis, J. Tam, S. Xanthoudakis, D. Nicholson, G.S. Robertson, G.Y. Ng, and D. Xu. 2002. Immunohistochemical and biochemical assessment of caspase-3 activation and DNA fragmentation following transient focal ischemia in the rat. Neuroscience. 115:125-136.

De Domenico, I., E. Lo, D.M. Ward, and J. Kaplan. 2009. Hepcidin-induced internalization of ferroportin requires binding and cooperative interaction with Jak2. Proceedings of the National Academy of Sciences. 106:3800-3805.

De Domenico, I., D.M. Ward, M.C.B. di Patti, S.Y. Jeong, S. David, G. Musci, and J. Kaplan. 2007a. Ferroxidase activity is required for the stability of cell surface ferroportin in cells expressing GPI-ceruloplasmin. The EMBO Journal. 26:2823-2831.

De Domenico, I., D.M. Ward, C. Langelier, M.B. Vaughn, E. Nemeth, W.I. Sundquist, T. Ganz, G. Musci, and J. Kaplan. 2007b. The molecular mechanism of hepcidin-mediated ferroportin down-regulation. Molecular Biology of the Cell. 18:2569-2578.

de Silva, H.R., A. Jen, C. Wickenden, L.-S. Jen, S.L. Wilkinson, and A.J. Patel. 1997. Cell-specific expression of β-amyloid precursor protein isoform mRNAs and proteins in neurons and astrocytes. Molecular Brain Research. 47:147-156.

De Strooper, B., and E. Karran. 2016. The cellular phase of Alzheimer's disease. Cell. 164:603-615.

de Villiers, J.N.P., R. Hillermann, L. Loubser, and M.J. Kotze. 1999. Spectrum of mutations in the HFE gene implicated in haemochromatosis and porphyria. Human Molecular Genetics. 8:1517-1522.

de Wilde, M.C., C.R. Overk, J.W. Sijben, and E. Masliah. 2016. Meta-analysis of synaptic pathology in Alzheimer's disease reveals selective molecular vesicular machinery vulnerability. Alzheimer's and Dementia. 12:633-644.

Deane, R., W. Zheng, and B.V. Zlokovic. 2004. Brain capillary endothelium and choroid plexus epithelium regulate transport of transferrin-bound and free iron into the rat brain. Journal of Neurochemistry. 88:813-820.

Del Zoppo, G. 2010. The neurovascular unit in the setting of stroke. Journal of Internal Medicine. 267:156-171.

Delima, R.D., A.C. Chua, J.E. Tirnitz-Parker, E.K. Gan, K.D. Croft, R.M. Graham, J.K. Olynyk, and D. Trinder. 2012. Disruption of hemochromatosis protein and transferrin receptor 2 causes iron-induced liver injury in mice. Hepatology. 56:585-593.

Dementia Australia. 2017.

Dementia Australia. 2018. Dementia Prevalence Data 2018-2058, commissioned research undertaken by NATSEM, University of Canberra.

Demougeot, C., D. Methy, A. Prigent-Tessier, P. Garnier, N. Bertrand, J. Guilland, A. Beley, and C. Marie. 2003a. Effects of a direct injection of liposoluble iron into rat striatum. Importance of the rate of iron delivery to cells. Free Radical Research. 37:59-67.

Demougeot, C., D. Methy, A. Prigent-Tessier, P. Garnier, N. Bertrand, J.C. Guilland, A. Beley, and C. Marie. 2003b. Effects of a direct injection of liposoluble iron into rat striatum. Importance of the rate of iron delivery to cells. Free Radic Res. 37:59-67.

Dickinson, T.K., and J.R. Connor. 1995. Cellular distribution of iron, transferrin, and ferritin in the hypotransferrinemic (Hp) mouse brain. J Comp Neurol. 355:67-80.

Dickson, P.W., A.R. Aldred, P.D. Marley, G.F. Tu, G.J. Howlett, and G. Schreiber. 1985. High prealbumin and transferrin mRNA levels in the choroid plexus of rat brain. Biochem Biophys Res Commun. 127:890-895.

Dixon, S.J., K.M. Lemberg, M.R. Lamprecht, R. Skouta, E.M. Zaitsev, C.E. Gleason, D.N. Patel, A.J. Bauer, A.M. Cantley, W.S. Yang, B. Morrison, 3rd, and B.R. Stockwell. 2012. Ferroptosis: an iron-dependent form of nonapoptotic cell death. Cell. 149:1060-1072.

Dong, J., J.E. Shokes, R.A. Scott, and D.G. Lynn. 2006. Modulating amyloid self-assembly and fibril morphology with Zn (II). Journal of the American Chemical Society. 128:3540-3542.

Donovan, A., A. Brownlie, Y. Zhou, J. Shepard, S.J. Pratt, J. Moynihan, B.H. Paw, A. Drejer, B. Barut, and A. Zapata. 2000. Positional cloning of zebrafish ferroportin1 identifies a conserved vertebrate iron exporter. Nature. 403:776-781.

Donovan, V., C. Kim, A.K. Anugerah, J.S. Coats, U. Oyoyo, A.C. Pardo, and A. Obenaus. 2014. Repeated mild traumatic brain injury results in long-term white-matter disruption. Journal of Cerebral Blood Flow and Metabolism. 34:715-723.

Dörner, M., J. Salfeld, H. Will, E.A. Leibold, J. Vass, and H. Munro. 1985. Structure of human ferritin light subunit messenger RNA: comparison with heavy subunit message and functional implications. Proceedings of the National Academy of Sciences. 82:3139-3143.

Drayer, B., P. Burger, R. Darwin, S. Riederer, R. Herfkens, and G. Johnson. 1986a. MRI of brain iron. American Journal of Roentgenology. 147:103-110.

Dringen, R., G.M. Bishop, M. Koeppe, T.N. Dang, and S.R. Robinson. 2007. The pivotal role of astrocytes in the metabolism of iron in the brain. Neurochemical Research. 32:1884-1890.

Duce, J.A., A. Tsatsanis, M.A. Cater, S.A. James, E. Robb, K. Wikhe, S.L. Leong, K. Perez, T. Johanssen, and M.A. Greenough. 2010. Iron-export ferroxidase activity of β-amyloid precursor protein is inhibited by zinc in Alzheimer's disease. Cell. 142:857-867.

Dudeffant, C., M. Vandesquille, K. Herbert, C.M. Garin, S. Alves, V. Blanchard, E.E. Comoy, F. Petit, and M. Dhenain. 2017. Contrast-enhanced MR microscopy of amyloid plaques in five mouse models of amyloidosis and in human Alzheimer’s disease brains. Scientific Reports. 7:4955.

Duncan, I.D., Y. Kondo, and S.C. Zhang. 2011. The myelin mutants as models to study myelin repair in the leukodystrophies. Neurotherapeutics. 8:607-624.

Dusek, P., S.A. Schneider, and J. Aaseth. 2016. Iron chelation in the treatment of neurodegenerative diseases. Journal of Trace Elements in Medicine and Biology.

Easterling, C.S., and E. Robbins. 2008. Dementia and dysphagia. Geriatric Nursing. 29:275-285.

Eastwood, S.L., P.W. Burnet, and P.J. Harrison. 1995. Altered synaptophysin expression as a marker of synaptic pathology in schizophrenia. Neuroscience. 66:309-319.

Ebrahimi, K.H., C. Dienemann, S. Hoefgen, M.E. Than, P.-L. Hagedoorn, and W.R. Hagen. 2013a. The amyloid precursor protein (APP) does not have a ferroxidase site in its E2 domain. PloS One. 8:e72177.

Ebrahimi, K.H., P.-L. Hagedoorn, and W.R. Hagen. 2012. A synthetic peptide with the putative iron binding motif of amyloid precursor protein (APP) does not catalytically oxidize iron. PloS One. 7:e40287-e40287.

Ebrahimi, K.H., P.-L. Hagedoorn, and W.R. Hagen. 2013b. Phosphate accelerates displacement of Fe (III) by Fe (II) in the ferroxidase center of Pyrococcus furiosus ferritin. FEBS letters. 587:220-225.

El Tannir El Tayara, N., B. Delatour, C. Le Cudennec, M. Guegan, A. Volk, and M. Dhenain. 2006. Age-related evolution of amyloid burden, iron load, and MR relaxation times in a transgenic mouse model of Alzheimer's disease. Neurobiology of Disease. 22:199-208.

El Tayara Nel, T., A. Volk, M. Dhenain, and B. Delatour. 2007. Transverse relaxation time reflects brain amyloidosis in young APP/PS1 transgenic mice. Magn Reson Med. 58:179-184.

El Tayara, N.E.T., B. Delatour, C. Le Cudennec, M. Guégan, A. Volk, and M. Dhenain. 2006. Age-related evolution of amyloid burden, iron load, and MR relaxation times in a transgenic mouse model of Alzheimer's disease. Neurobiology of Disease. 22:199-208.

Ellervik, C., H. Birgens, A. Tybjærg-Hansen, and B.G. Nordestgaard. 2007. Hemochromatosis genotypes and risk of 31 disease endpoints: Meta-analyses including 66,000 cases and 226,000 controls. Hepatology. 46:1071-1080.

Emera, D., R. Romero, and G. Wagner. 2012. The evolution of menstruation: a new model for genetic assimilation: explaining molecular origins of maternal responses to fetal invasiveness. BioEssays. 34:26-35.

Emerit, J., C. Beaumont, and F. Trivin. 2001. Iron metabolism, free radicals, and oxidative injury. Biomedicine and Pharmacotherapy. 55:333-339.

érald Le Gac, G., F.-Y. Dupradeau, C. Mura, S. Jacolot, V. Scotet, G. Esnault, A.-Y. Mercier, J. Rochette, and C. Férec. 2003. Phenotypic expression of the C282Y/Q283P compound heterozygosity in HFE and molecular modeling of the Q283P mutation effect. Blood Cells, Molecules, and Diseases. 30:231-237.

Erb, G.L., D.L. Osterbur, and S.M. LeVine. 1996. The distribution of iron in the brain: A phylogenetic analysis using iron histochemistry. Developmental Brain Research. 93:120-128.

Evans, C.A., M.S. Harbuz, T. Ostenfeld, A. Norrish, and J.M. Blackwell. 2001. Nramp1 is expressed in neurons and is associated with behavioural and immune responses to stress. Neurogenetics. 3:69-78.

Everett, J., E. Céspedes, L.R. Shelford, C. Exley, J.F. Collingwood, J. Dobson, G. van der Laan, C.A. Jenkins, E. Arenholz, and N.D. Telling. 2014a. Ferrous iron formation following the co-aggregation of ferric iron and the Alzheimer's disease peptide β-amyloid (1–42). Journal of The Royal Society Interface. 11:20140165.

Everett, J., E. Céspedes, L.R. Shelford, C. Exley, J.F. Collingwood, J. Dobson, G. van der Laan, C.A. Jenkins, E. Arenholz, and N.D. Telling. 2014b. Evidence of redox-active iron formation following aggregation of ferrihydrite and the Alzheimer’s disease peptide β-amyloid. Inorganic Chemistry. 53:2803-2809.

Falangola, M.F., S.P. Lee, R.A. Nixon, K. Duff, and J.A. Helpern. 2005. Histological co-localization of iron in Abeta plaques of PS/APP transgenic mice. Neurochem Res. 30:201-205.

Farrer, L.A., L.A. Cupples, J.L. Haines, B. Hyman, W.A. Kukull, R. Mayeux, R.H. Myers, M.A. Pericak-Vance, N. Risch, and C.M. van Duijn. 1997. Effects of age, sex, and ethnicity on the association between apolipoprotein E genotype and Alzheimer disease. A meta-analysis. APOE and Alzheimer Disease Meta Analysis Consortium. JAMA. 278:1349-1356.

Faux, N.G., A. Rembach, J. Wiley, K.A. Ellis, D. Ames, C.J. Fowler, R.N. Martins, K.K. Pertile, R.L. Rumble, B. Trounson, C.L. Masters, and A.I. Bush. 2014. An anemia of Alzheimer's disease. Molecular Psychiatry. 19:1227-1234.

Feder, J., A. Gnirke, W. Thomas, Z. Tsuchihashi, D. Ruddy, A. Basava, F. Dormishian, R. Domingo, M. Ellis, and A. Fullan. 1996. A novel MHC class I-like gene is mutated in patients with hereditary haemochromatosis. Nature Genetics. 13:399-408.

Feder, J.N., D.M. Penny, A. Irrinki, V.K. Lee, J.A. Lebron, N. Watson, Z. Tsuchihashi, E. Sigal, P.J. Bjorkman, and R.C. Schatzman. 1998a. The hemochromatosis gene product complexes with the transferrin receptor and lowers its affinity for ligand binding. Proceedings of the National Academy of Sciences USA. 95:1472-1477.

Feder, J.N., D.M. Penny, A. Irrinki, V.K. Lee, J.A. Lebrón, N. Watson, Z. Tsuchihashi, E. Sigal, P.J. Bjorkman, and R.C. Schatzman. 1998b. The hemochromatosis gene product complexes with the transferrin receptor and lowers its affinity for ligand binding. Proceedings of the National Academy of Sciences USA. 95:1472-1477.

Ferreira-Vieira, T.H., I.M. Guimaraes, F.R. Silva, and F.M. Ribeiro. 2016. Alzheimer's disease: Targeting the Cholinergic System. Current Neuropharmacology. 14:101-115.

Festing, M.F., and D.K. Blackmore. 1971. Life span of specified-pathogen-free (MRC category 4) mice and rats. Lab Anim. 5:179-192.

Fillebeen, C., L. Descamps, M.-P. Dehouck, L. Fenart, M. Benaïssa, G. Spik, R. Cecchelli, and A. Pierce. 1999. Receptor-mediated transcytosis of lactoferrin through the blood-brain barrier. Journal of Biological Chemistry. 274:7011-7017.

Finch, C. 1994. Regulators of iron balance in humans. Blood. 84:1697-1702.

Fischbach, F.A., D.W. Gregory, P.M. Harrison, T.G. Hoy, and J.M. Williams. 1971. On the structure of hemosiderin and its relationship to ferritin. Journal of Ultrastructure Research. 37:495-503.

Fleming, M.D., M.A. Romano, M.A. Su, L.M. Garrick, M.D. Garrick, and N.C. Andrews. 1998. Nramp2 is mutated in the anemic Belgrade (b) rat: evidence of a role for Nramp2 in endosomal iron transport. Proceedings of the National Academy of Sciences. 95:1148-1153.

Fleming, R.E., and B.R. Bacon. 2005. Orchestration of iron homeostasis. N Engl J Med. 352:1741-1744.

Fleming, R.E., C.C. Holden, S. Tomatsu, A. Waheed, E.M. Brunt, R.S. Britton, B.R. Bacon, D.C. Roopenian, and W.S. Sly. 2001. Mouse strain differences determine severity of iron accumulation in Hfe knockout model of hereditary hemochromatosis. Proceedings of the National Academy of Sciences. 98:2707-2711.

Fleming, R.E., M.C. Migas, C.C. Holden, A. Waheed, R.S. Britton, S. Tomatsu, B.R. Bacon, and W.S. Sly. 2000. Transferrin receptor 2: continued expression in mouse liver in the face of iron overload and in hereditary hemochromatosis. Proceedings of the National Academy of Sciences USA. 97:2214-2219.

Frackowiak, J., H.M. Wisniewski, J. Wegiel, G.S. Merz, K. Iqbal, and K.C. Wang. 1992. Ultrastructure of the microglia that phagocytose amyloid and the microglia that produce beta-amyloid fibrils. Acta Neuropathol. 84:225-233.

Franco, R., and D. Fernandez-Suarez. 2015. Alternatively activated microglia and macrophages in the central nervous system. Progress in Neurobiology. 131:65-86.

Fraser, P.E., D.-S. Yang, G. Yu, L. Lévesque, M. Nishimura, S. Arawaka, L.C. Serpell, E. Rogaeva, and P. St George-Hyslop. 2000. Presenilin structure, function and role in Alzheimer disease. Biochimica et Biophysica Acta (BBA)-Molecular Basis of Disease. 1502:1-15.

Fredriksson, A., N. Schröder, P. Eriksson, I. Izquierdo, and T. Archer. 1999. Neonatal iron exposure induces neurobehavioural dysfunctions in adult mice. Toxicology and Applied Pharmacology. 159:25-30.

Frey, W.H., J. Liu, X. Chen, R.G. Thorne, J.R. Fawcett, T.A. Ala, and Y.-E. Rahman. 1997. Delivery of 125I-NGF to the brain via the olfactory route. Drug Delivery. 4:87-92.

Fu, H., J. Hardy, and K.E. Duff. 2018. Selective vulnerability in neurodegenerative diseases. Nature Neuroscience. 21:1350-1358.

Gallagher, J.J., M.E. Finnegan, B. Grehan, J. Dobson, J.F. Collingwood, and M.A. Lynch. 2012. Modest amyloid deposition is associated with iron dysregulation, microglial activation, and oxidative stress. Journal of Alzheimer's Disease. 28:147-161.

Gallagher, J.J., A.M. Minogue, and M.A. Lynch. 2013. Impaired performance of female APP/PS1 mice in the Morris water maze is coupled with increased Abeta accumulation and microglial activation. Neuro-degenerative Diseases. 11:33-41.

Gallyas, F., and I. Merchenthaler. 1988. Copper-H2O2 oxidation strikingly improves silver intensification of the nickel-diaminobenzidine (Ni-DAB) end-product of the peroxidase reaction. The Journal of Histochemistry and Cytochemistry. 36:807-810.

Ganz, T., and E. Nemeth. 2016. Iron Balance and the Role of Hepcidin in Chronic Kidney Disease. Semin Nephrol. 36:87-93.

Gao, J., J. Chen, M. Kramer, H. Tsukamoto, A.-S. Zhang, and C.A. Enns. 2009. Interaction of the hereditary hemochromatosis protein HFE with transferrin receptor 2 is required for transferrin-induced hepcidin expression. Cell Metabolism. 9:217-227.

Garbuzova-Davis, S., E. Haller, S. Saporta, I. Kolomey, S.V. Nicosia, and P.R. Sanberg. 2007. Ultrastructure of blood–brain barrier and blood–spinal cord barrier in SOD1 mice modeling ALS. Brain Research. 1157:126-137.

Garcia-Alloza, M., E.M. Robbins, S.X. Zhang-Nunes, S.M. Purcell, R.A. Betensky, S. Raju, C. Prada, S.M. Greenberg, B.J. Bacskai, and M.P. Frosch. 2006. Characterization of amyloid deposition in the APPswe/PS1dE9 mouse model of Alzheimer disease. Neurobiology of Disease. 24:516-524.

Gehring, N.H., M.W. Hentze, and K. Pantopoulos. 1999. Inactivation of both RNA binding and aconitase activities of iron regulatory protein-1 by quinone-induced oxidative stress. Journal of Biological Chemistry. 274:6219-6225.

Ghasemlou, N., S.Y. Jeong, S. Lacroix, and S. David. 2007. T cells contribute to lysophosphatidylcholine-induced macrophage activation and demyelination in the CNS. Glia. 55:294-302.

Ghebranious, N., L. Ivacic, J. Mallum, and C. Dokken. 2005. Detection of ApoE E2, E3 and E4 alleles using MALDI-TOF mass spectrometry and the homogeneous mass-extend technology. Nucleic Acids Res. 33:e149.

Giannetti, A.M., and P.J. Björkman. 2004. HFE and transferrin directly compete for transferrin receptor in solution and at the cell surface. Journal of Biological Chemistry. 279:25866-25875.

Gillen, K.M., M. Mubarak, T.D. Nguyen, and D. Pitt. 2018. Significance and In Vivo Detection of Iron-Laden Microglia in White Matter Multiple Sclerosis Lesions. Frontiers in Immunology. 9:255.

Giometto, B., F. Bozza, V. Argentiero, P. Gallo, S. Pagni, M.G. Piccinno, and B. Tavolato. 1990. Transferrin receptors in rat central nervous system: An immunocytochemical study. Journal of the Neurological Sciences. 98:81-90.

Giulian, D. 1987. Ameboid microglia as effectors of inflammation in the central nervous system. Journal of Neuroscience Research. 18:155-171, 132-153.

Glenner, G.G., and C.W. Wong. 1984a. Alzheimer's disease and Down's syndrome: sharing of a unique cerebrovascular amyloid fibril protein. Biochem Biophys Res Commun. 122:1131-1135.

Glenner, G.G., and C.W. Wong. 1984b. Alzheimer's disease: initial report of the purification and characterization of a novel cerebrovascular amyloid protein. Biochem Biophys Res Commun. 120:885-890.

Goate, A., M.-C. Chartier-Harlin, M. Mullan, J. Brown, F. Crawford, L. Fidani, L. Giuffra, A. Haynes, N. Irving, and L. James. 1991. Segregation of a missense mutation in the amyloid precursor protein gene with familial Alzheimer's disease. Nature. 349:704-706.

Gochee, P.A., L.W. Powell, D.J. Cullen, D. Du Sart, E. Rossi, and J.K. Olynyk. 2002. A population-based study of the biochemical and clinical expression of the H63D hemochromatosis mutation. Gastroenterology. 122:646-651.

Goedert, M., M. Hasegawa, R. Jakes, S. Lawler, A. Cuenda, and P. Cohen. 1997. Phosphorylation of microtubule-associated protein tau by stress-activated protein kinases. FEBS letters. 409:57-62.

Goedert, M., and R. Jakes. 1990. Expression of separate isoforms of human tau protein: correlation with the tau pattern in brain and effects on tubulin polymerization. The EMBO Journal. 9:4225.

Goedert, M., A. Klug, and R.A. Crowther. 2006. Tau protein, the paired helical filament and Alzheimer's disease. Journal of Alzheimer's Disease. 9:195-208.

Goedert, M., M. Spillantini, R. Jakes, D. Rutherford, and R. Crowther. 1989. Multiple isoforms of human microtubule-associated protein tau: sequences and localization in neurofibrillary tangles of Alzheimer's disease. Neuron. 3:519-526.

Golub, M.S., S.L. Germann, R.S. Araiza, J.R. Reader, S.M. Griffey, and K. Kent Lloyd. 2005. Movement disorders in the Hfe knockout mouse. Nutritional neuroscience. 8:239-244.

Gomes-Leal, W. 2012. Microglial physiopathology: how to explain the dual role of microglia after acute neural disorders? Brain and Behavior. 2:345-356.

Good, P.F., D.P. Perl, L.M. Bierer, and J. Schmeidler. 1992. Selective accumulation of aluminum and iron in the neurofibrillary tangles of Alzheimer's disease: a laser microprobe (LAMMA) study. Annals of Neurology. 31:286-292.

Good, P.F., P. Werner, A. Hsu, C.W. Olanow, and D.P. Perl. 1996. Evidence of neuronal oxidative damage in Alzheimer's disease. The American Journal of Pathology. 149:21.

Goodman, L. 1953. Alzheimer's disease: a clinico-pathologic analysis of twenty-three cases with a theory on pathogenesis. The Journal of Nervous and Mental Disease. 118:97-130.

Goodwill, K.E., C. Sabatier, C. Marks, R. Raag, P.F. Fitzpatrick, and R.C. Stevens. 1997. Crystal structure of tyrosine hydroxylase at 2.3 Å and its implications for inherited neurodegenerative diseases. Nature Structural and Molecular Biology. 4:578-585.

Graham, R.M., A.C. Chua, K.W. Carter, R.D. Delima, D. Johnstone, C.E. Herbison, M.J. Firth, R. O'Leary, E.A. Milward, and J.K. Olynyk. 2010a. Hepatic iron loading in mice increases cholesterol biosynthesis. Hepatology. 52:462-471.

Graham, R.M., A.C. Chua, K.W. Carter, R.D. Delima, D. Johnstone, C.E. Herbison, M.J. Firth, R. O'Leary, E.A. Milward, J.K. Olynyk, and D. Trinder. 2010b. Hepatic iron loading in mice increases cholesterol biosynthesis. Hepatology. 52:462-471.

Graham, S.F., M.B. Nasaruddin, M. Carey, C. Holscher, B. McGuinness, P.G. Kehoe, S. Love, P. Passmore, C.T. Elliott, A.A. Meharg, and B.D. Green. 2014. Age-associated changes of brain copper, iron, and zinc in Alzheimer's disease and dementia with Lewy bodies. Journal of Alzheimer's Disease : JAD. 42:1407-1413.

Granzotto, A., and P. Zatta. 2012. Metal ions and beta amyloid: conformational modifications and biological aspects. Springer.

Green, R., R. Charlton, H. Seftel, T. Bothwell, F. Mayet, B. Adams, C. Finch, and M. Layrisse. 1968. Body iron excretion in man: a collaborative study. The American Journal of Medicine. 45:336-353.

Greenberg, G.R., and M.M. Wintrobe. 1946. A labile iron pool. Journal of Biological Chemistry. 165:397-398.

Greenberg, S.M., and J.-P.G. Vonsattel. 1997. Diagnosis of cerebral amyloid angiopathy sensitivity and specificity of cortical biopsy. Stroke. 28:1418-1422.

Gruenheid, S., M. Cellier, S. Vidal, and P. Gros. 1995. Identification and characterization of a second mouse Nramp gene. Genomics. 25:514-525.

Grundke-Iqbal, I., J. Fleming, Y.-C. Tung, H. Lassmann, K. Iqbal, and J. Joshi. 1990. Ferritin is a component of the neuritic (senile) plaque in Alzheimer dementia. Acta Neuropathologica. 81:105-110.

Grundke-Iqbal, I., K. Iqbal, M. Quinlan, Y.-C. Tung, M.S. Zaidi, and H.M. Wisniewski. 1986a. Microtubule-associated protein tau. A component of Alzheimer paired helical filaments. Journal of Biological Chemistry. 261:6084-6089.

Grundke-Iqbal, I., K. Iqbal, Y.-C. Tung, M. Quinlan, H.M. Wisniewski, and L.I. Binder. 1986b. Abnormal phosphorylation of the microtubule-associated protein tau (tau) in Alzheimer cytoskeletal pathology. Proceedings of the National Academy of Sciences USA. 83:4913-4917.

Grutzendler, J., K. Helmin, J. Tsai, and W.B. Gan. 2007. Various dendritic abnormalities are associated with fibrillar amyloid deposits in Alzheimer's disease. Annals of the New York Academy of Sciences. 1097:30-39.

Gudi, V., L. Gai, V. Herder, L.S. Tejedor, M. Kipp, S. Amor, K.W. Suhs, F. Hansmann, A. Beineke, W. Baumgartner, M. Stangel, and T. Skripuletz. 2017. Synaptophysin Is a Reliable Marker for Axonal Damage. Journal of Neuropathology and Experimental Neurology.

Gunshin, H., B. Mackenzie, U.V. Berger, Y. Gunshin, M.F. Romero, W.F. Boron, S. Nussberger, J.L. Gollan, and M.A. Hediger. 1997. Cloning and characterization of a mammalian proton-coupled metal-ion transporter. Nature. 388:482-488.

Guo, C., T. Wang, W. Zheng, Z.-Y. Shan, W.-P. Teng, and Z.-Y. Wang. 2013. Intranasal deferoxamine reverses iron-induced memory deficits and inhibits amyloidogenic APP processing in a transgenic mouse model of Alzheimer's disease. Neurobiology of Aging. 34:562-575.

Gusel'nikova, V.V., and D.E. Korzhevskiy. 2015. NeuN As a Neuronal Nuclear Antigen and Neuron Differentiation Marker. Acta Naturae. 7:42-47.

Gutierrez, J.A., J. Yu, S. Rivera, and M. Wessling-Resnick. 1997. Functional expression cloning and characterization of SFT, a stimulator of Fe transport. The Journal of Cell Biology. 139:895-905.

Gyoneva, S., S.A. Swanger, J. Zhang, D. Weinshenker, and S.F. Traynelis. 2016. Altered motility of plaque-associated microglia in a model of Alzheimer’s disease. Neuroscience. 330:410-420.

Haass, C., A.Y. Hung, and D.J. Selkoe. 1991. Processing of beta-amyloid precursor protein in microglia and astrocytes favors an internal localization over constitutive secretion. Journal of Neuroscience. 11:3783-3793.

Haass, C., C.A. Lemere, A. Capell, M. Citron, P. Seubert, D. Schenk, L. Lannfelt, and D.J. Selkoe. 1995. The Swedish mutation causes early-onset Alzheimer's disease by β-secretase cleavage within the secretory pathway. Nature Medicine. 1:1291-1296.

Haass, C., and D.J. Selkoe. 2007. Soluble protein oligomers in neurodegeneration: lessons from the Alzheimer's amyloid beta-peptide. Nat Rev Mol Cell Biol. 8:101-112.

Haga, S., K. Akai, and T. Ishii. 1989. Demonstration of microglial cells in and around senile (neuritic) plaques in the Alzheimer brain. An immunohistochemical study using a novel monoclonal antibody. Acta Neuropathol. 77:569-575.

Halliwell, B., and J.M. Gutteridge. 2015. Free radicals in biology and medicine. Oxford University Press, USA.

Hamos, J.E., L.J. DeGennaro, and D.A. Drachman. 1989a. Synaptic loss in Alzheimer's disease and other dementias. Neurology. 39:355-361.

Hamos, J.E., L.J. DeGennaro, and D.A. Drachman. 1989b. Synaptic loss in Alzheimer's disease and other dementias. Neurology. 39:355-355.

Han, J., W.E. Seaman, X. Di, W. Wang, M. Willingham, F.M. Torti, and S.V. Torti. 2011. Iron uptake mediated by binding of H-ferritin to the TIM-2 receptor in mouse cells. PloS One. 6:e23800-e23800.

Hänninen, M.M., J. Haapasalo, H. Haapasalo, R.E. Fleming, R.S. Britton, B.R. Bacon, and S. Parkkila. 2009. Expression of iron-related genes in human brain and brain tumors. BMC Neuroscience. 10:36.

Hardy, P.A., D. Gash, R. Yokel, A. Andersen, Y. Ai, and Z. Zhang. 2005. Correlation of R2 with total iron concentration in the brains of rhesus monkeys. Journal of Magnetic Resonance Imaging. 21:118-127.

Hare, D.J., J.D. Doecke, N.G. Faux, A. Rembach, I. Volitakis, C.J. Fowler, R. Grimm, P.A. Doble, R.A. Cherny, C.L. Masters, A.I. Bush, and B.R. Roberts. 2015. Decreased plasma iron in Alzheimer's disease is due to transferrin desaturation. ACS Chem Neurosci. 6:398-402.

Hare, D.J., E.P. Raven, B.R. Roberts, M. Bogeski, S.D. Portbury, C.A. McLean, C.L. Masters, J.R. Connor, A.I. Bush, P.J. Crouch, and P.A. Doble. 2016. Laser ablation-inductively coupled plasma-mass spectrometry imaging of white and gray matter iron distribution in Alzheimer's disease frontal cortex. Neuroimage. 137:124-131.

Harold, D., R. Abraham, P. Hollingworth, R. Sims, A. Gerrish, M.L. Hamshere, J.S. Pahwa, V. Moskvina, K. Dowzell, A. Williams, N. Jones, C. Thomas, A. Stretton, A.R. Morgan, S. Lovestone, J. Powell, P. Proitsi, M.K. Lupton, C. Brayne, D.C. Rubinsztein, M. Gill, B. Lawlor, A. Lynch, K. Morgan, K.S. Brown, P.A. Passmore, D. Craig, B. McGuinness, S. Todd, C. Holmes, D. Mann, A.D. Smith, S. Love, P.G. Kehoe, J. Hardy, S. Mead, N. Fox, M. Rossor, J. Collinge, W. Maier, F. Jessen, B. Schurmann, R. Heun, H. van den Bussche, I. Heuser, J. Kornhuber, J. Wiltfang, M. Dichgans, L. Frolich, H. Hampel, M. Hull, D. Rujescu, A.M. Goate, J.S. Kauwe, C. Cruchaga, P. Nowotny, J.C. Morris, K. Mayo, K. Sleegers, K. Bettens, S. Engelborghs, P.P. De Deyn, C. Van Broeckhoven, G. Livingston, N.J. Bass, H. Gurling, A. McQuillin, R. Gwilliam, P. Deloukas, A. Al-Chalabi, C.E. Shaw, M. Tsolaki, A.B. Singleton, R. Guerreiro, T.W. Muhleisen, M.M. Nothen, S. Moebus, K.H. Jockel, N. Klopp, H.E. Wichmann, M.M. Carrasquillo, V.S. Pankratz, S.G. Younkin, P.A. Holmans, M. O'Donovan, M.J. Owen, and J. Williams. 2009. Genome-wide association study identifies variants at CLU and PICALM associated with Alzheimer's disease. Nat Genet. 41:1088-1093.

Harris, Z.L., Y. Takahashi, H. Miyajima, M. Serizawa, R. MacGillivray, and J.D. Gitlin. 1995. Aceruloplasminemia: molecular characterization of this disorder of iron metabolism. Proceedings of the National Academy of Sciences USA. 92:2539-2543.

Harrison-Findik, D.D. 2010. Gender-related variations in iron metabolism and liver diseases. World Journal of Hepatology. 2:302-310.

Harrison, P.M., and P. Arosio. 1996. The ferritins: molecular properties, iron storage function and cellular regulation. Biochimica et Biophysica Acta (BBA)-Bioenergetics. 1275:161-203.

Hautot, D., Q. Pankhurst, N. Khan, and J. Dobson. 2003. Preliminary evaluation of nanoscale biogenic magnetite in Alzheimer's disease brain tissue. Proceedings of the Royal Society of London B: Biological Sciences. 270:S62-S64.

Heidari, M., S.H. Gerami, B. Bassett, R.M. Graham, A.C. Chua, R. Aryal, M.J. House, J.F. Collingwood, C. Bettencourt, H. Houlden, M. Ryten, J.K. Olynyk, D. Trinder, D.M. Johnstone, and E.A. Milward. 2016a. Pathological relationships involving iron and myelin may constitute a shared mechanism linking various rare and common brain diseases. Rare diseases. 4:e1198458.

Heidari, M., D.M. Johnstone, B. Bassett, R. Graham, A. Chua, M. House, J.F. Collingwood, C. Bettencourt, H. Houlden, and M. Ryten. 2016b. Brain iron accumulation affects myelin-related molecular systems implicated in a rare neurogenetic disease family with neuropsychiatric features. Molecular Psychiatry.

Hendrickx, D.A.E., C.G. van Eden, K.G. Schuurman, J. Hamann, and I. Huitinga. 2017. Staining of HLA-DR, Iba1 and CD68 in human microglia reveals partially overlapping expression depending on cellular morphology and pathology. Journal of Neuroimmunology. 309:12-22.

Heneka, M.T., M.J. Carson, J. El Khoury, G.E. Landreth, F. Brosseron, D.L. Feinstein, A.H. Jacobs, T. Wyss-Coray, J. Vitorica, R.M. Ransohoff, K. Herrup, S.A. Frautschy, B. Finsen, G.C. Brown, A. Verkhratsky, K. Yamanaka, J. Koistinaho, E. Latz, A. Halle, G.C. Petzold, T. Town, D. Morgan, M.L. Shinohara, V.H. Perry, C. Holmes, N.G. Bazan, D.J. Brooks, S. Hunot, B. Joseph, N. Deigendesch, O. Garaschuk, E. Boddeke, C.A. Dinarello, J.C. Breitner, G.M. Cole, D.T. Golenbock, and M.P. Kummer. 2015. Neuroinflammation in Alzheimer's disease. Lancet Neurol. 14:388-405.

Hentze, M.W., M.U. Muckenthaler, and N.C. Andrews. 2004. Balancing acts: molecular control of mammalian iron metabolism. Cell. 117:285-297.

Hentze, M.W., M.U. Muckenthaler, B. Galy, and C. Camaschella. 2010. Two to tango: regulation of Mammalian iron metabolism. Cell. 142:24-38.

Herbison, C.E., K. Thorstensen, A.C. Chua, R.M. Graham, P. Leedman, J.K. Olynyk, and D. Trinder. 2009. The role of transferrin receptor 1 and 2 in transferrin-bound iron uptake in human hepatoma cells. American Journal of Physiology-Cell Physiology. 297:C1567-C1575.

Hickman, S.E. 2008. Microglial dysfunction and defective β-amyloid clearance pathways in aging Alzheimer’s disease mice. J Neurosci 28:8354-8360.

Hironishi, M., E. Ueyama, and E. Senba. 1999. Systematic expression of immediate early genes and intensive astrocyte activation induced by intrastriatal ferrous iron injection. Brain Res. 828:145-153.

Hixson, J.E., and D.T. Vernier. 1990. Restriction isotyping of human apolipoprotein E by gene amplification and cleavage with HhaI. J Lipid Res. 31:545-548.

Hooper, N., and A. Turner. 2002. The search for α-secretase and its potential as a therapeutic approach to Alzheimer's disease. Current Medicinal Chemistry. 9:1107-1119.

Hopperton, K.E., D. Mohammad, M.O. Trépanier, V. Giuliano, and R.P. Bazinet. 2017. Markers of microglia in post-mortem brain samples from patients with Alzheimer’s disease: a systematic review. Molecular Psychiatry. 23:177.

House, E., J. Collingwood, A. Khan, O. Korchazkina, G. Berthon, and C. Exley. 2004a. Aluminium, iron, zinc and copper influence the in vitro formation of amyloid fibrils of Abeta42 in a manner which may have consequences for metal chelation therapy in Alzheimer's disease. Journal of Alzheimer's Disease : JAD. 6:291-301.

House, E., J. Collingwood, A. Khan, O. Korchazkina, G. Berthon, and C. Exley. 2004b. Aluminium, iron, zinc and copper influence the in vitro formation of amyloid fibrils of Aβ 42 in a manner which may have consequences for metal chelation therapy in Alzheimer's disease. Journal of Alzheimer's Disease. 6:291-301.

Hristovska, I., and O. Pascual. 2015. Deciphering Resting Microglial Morphology and Process Motility from a Synaptic Prospect. Frontiers in Integrative Neuroscience. 9:73.

Huang, X., C.S. Atwood, R.D. Moir, M.A. Hartshorn, J.-P. Vonsattel, R.E. Tanzi, and A.I. Bush. 1997. Zinc-induced Alzheimer’s Aβ1–40 aggregation is mediated by conformational factors. Journal of Biological Chemistry. 272:26464-26470.

Hulet, S.W., E.J. Hess, W. Debinski, P. Arosio, K. Bruce, S. Powers, and J.R. Connor. 1999a. Characterization and distribution of ferritin binding sites in the adult mouse brain. J Neurochem. 72:868-874.

Hulet, S.W., S.O. Heyliger, S. Powers, and J.R. Connor. 2000. Oligodendrocyte progenitor cells internalize ferritin via clathrin-dependent receptor mediated endocytosis. Journal of Neuroscience Research. 61:52-60.

Hulet, S.W., S. Powers, and J.R. Connor. 1999b. Distribution of transferrin and ferritin binding in normal and multiple sclerotic human brains. J Neurol Sci. 165:48-55.

Hurrell, R., and I. Egli. 2010. Iron bioavailability and dietary reference values. The American journal of Clinical Nutrition. 91:1461S-1467S.

Iacono, D., S.M. Resnick, R. O'Brien, A.B. Zonderman, Y. An, O. Pletnikova, G. Rudow, B. Crain, and J.C. Troncoso. 2014. Mild cognitive impairment and asymptomatic Alzheimer disease subjects: equivalent β-amyloid and tau loads with divergent cognitive outcomes. Journal of Neuropathology and Experimental Neurology. 73:295-304.

Igarashi, T., T.T. Huang, and L.J. Noble. 2001. Regional vulnerability after traumatic brain injury: gender differences in mice that overexpress human copper, zinc superoxide dismutase. Exp Neurol. 172:332-341.

Itagaki, S., P.L. McGeer, H. Akiyama, S. Zhu, and D. Selkoe. 1989. Relationship of microglia and astrocytes to amyloid deposits of Alzheimer disease. Journal of Neuroimmunology. 24:173-182.

Iwai, K., S.K. Drake, N.B. Wehr, A.M. Weissman, T. LaVaute, N. Minato, R.D. Klausner, R.L. Levine, and T.A. Rouault. 1998. Iron-dependent oxidation, ubiquitination, and degradation of iron regulatory protein 2: implications for degradation of oxidized proteins. Proceedings of the National Academy of Sciences. 95:4924-4928.

Izawa, T., J. Yamate, R.J. Franklin, and M. Kuwamura. 2010. Abnormal iron accumulation is involved in the pathogenesis of the demyelinating dmy rat but not in the hypomyelinating mv rat. Brain Res. 1349:105-114.

Jack, C.R., M. Garwood, T.M. Wengenack, B. Borowski, G.L. Curran, J. Lin, G. Adriany, O.H. Gröhn, R. Grimm, and J.F. Poduslo. 2004. In vivo visualization of Alzheimer's amyloid plaques by magnetic resonance imaging in transgenic mice without a contrast agent. Magnetic Resonance in Medicine. 52:1263-1271.

Jack, C.R., Jr., T.M. Wengenack, D.A. Reyes, M. Garwood, G.L. Curran, B.J. Borowski, J. Lin, G.M. Preboske, S.S. Holasek, G. Adriany, and J.F. Poduslo. 2005. In vivo magnetic resonance microimaging of individual amyloid plaques in Alzheimer's transgenic mice. The Journal of Neuroscience. 25:10041-10048.

Jacobs, A. 1977. An intracellular transit iron pool. In Ciba Foundation Symposium 51-Iron Metabolism. Wiley Online Library. 91-106.

Jankowsky, J.L., D.J. Fadale, J. Anderson, G.M. Xu, V. Gonzales, N.A. Jenkins, N.G. Copeland, M.K. Lee, L.H. Younkin, and S.L. Wagner. 2004. Mutant presenilins specifically elevate the levels of the 42 residue β-amyloid peptide in vivo: evidence for augmentation of a 42-specific γ secretase. Human Molecular Genetics. 13:159-170.

Jellinger, K., W. Paulus, I. Grundke-Iqbal, P. Riederer, and M.B. Youdim. 1990. Brain iron and ferritin in Parkinson's and Alzheimer's diseases. J Neural Transm Park Dis Dement Sect. 2:327-340.

Jeong, S.Y., D.R. Crooks, H. Wilson-Ollivierre, M.C. Ghosh, R. Sougrat, J. Lee, S. Cooperman, J.B. Mitchell, C. Beaumont, and T.A. Rouault. 2011. Iron insufficiency compromises motor neurons and their mitochondrial function in Irp2-null mice. PloS One. 6:e25404.

Jeong, S.Y., and S. David. 2003. Glycosylphosphatidylinositol-anchored ceruloplasmin is required for iron efflux from cells in the central nervous system. Journal of Biological Chemistry. 278:27144-27148.

Jeong, S.Y., and S. David. 2006. Age-related changes in iron homeostasis and cell death in the cerebellum of ceruloplasmin-deficient mice. The Journal of Neuroscience. 26:9810-9819.

Ji, C., and D.J. Kosman. 2015. Molecular mechanisms of non-transferrin-bound and transferring-bound iron uptake in primary hippocampal neurons. J Neurochem. 133:668-683.

Jin, L.-W. 2012. Microglia in Alzheimer’s Disease. International Journal of Alzheimer's Disease. 2012:2.

Johnstone, D. 2010. Microarray studies of genome-wide changes in brain and heart gene expression in mouse models of iron overload| NOVA. The University of Newcastle's Digital Repository.

Johnstone, D., R.M. Graham, D. Trinder, R.D. Delima, C. Riveros, J.K. Olynyk, R.J. Scott, P. Moscato, and E.A. Milward. 2012a. Brain transcriptome perturbations in the Hfe−/− mouse model of genetic iron loading. Brain Research. 1448:144-152.

Johnstone, D., R.M. Graham, D. Trinder, R.D. Delima, C. Riveros, J.K. Olynyk, R.J. Scott, P. Moscato, and E.A. Milward. 2012b. Brain transcriptome perturbations in the Hfe(-/-) mouse model of genetic iron loading. Brain Res. 1448:144-152.

Johnstone, D., and E.A. Milward. 2010a. Genome-wide microarray analysis of brain gene expression in mice on a short-term high iron diet. Neurochem Int. 56:856-863.

Johnstone, D., and E.A. Milward. 2010b. Genome-wide microarray analysis of brain gene expression in mice on a short-term high iron diet. Neurochemistry International. 56:856-863.

Johnstone, D., and E.A. Milward. 2010c. Molecular genetic approaches to understanding the roles and regulation of iron in brain health and disease. Journal of Neurochemistry. 113:1387-1402.

Johnstone, D., and E.A. Milward. 2010d. Molecular genetic approaches to understanding the roles and regulation of iron in brain health and disease. J Neurochem. 113:1387-1402.

Johnstone, D.M., R.M. Graham, D. Trinder, C. Riveros, J.K. Olynyk, R.J. Scott, P. Moscato, and E.A. Milward. 2012c. Changes in brain transcripts related to Alzheimer's disease in a model of HFE hemochromatosis are not consistent with increased Alzheimer's disease risk. Journal of Alzheimer's Disease: JAD. 30:791-803.

Jorgenson, L.A., J.D. Wobken, and M.K. Georgieff. 2003. Perinatal iron deficiency alters apical dendritic growth in hippocampal CA1 pyramidal neurons. Developmental Neuroscience. 25:412-420.

Kakhlon, O., and Z.I. Cabantchik. 2002. The labile iron pool: characterization, measurement, and participation in cellular processes. Free Radical Biology and Medicine. 33:1037-1046.

Kaldor, I. 1954. STUDIES ON INTERMEDIARY IRON METABOLISM. Australian Journal of Experimental Biology & Medical Science. 32.

Kamalinia, G., F. Khodagholi, F. Atyabi, M. Amini, F. Shaerzadeh, M. Sharifzadeh, and R. Dinarvand. 2013. Enhanced brain delivery of deferasirox-lactoferrin conjugates for iron chelation therapy in neurodegenerative disorders: in vitro and in vivo studies. Mol Pharm. 10:4418-4431.

Kamman, R.L., K.G. Go, W. Brouwer, and H.J. Berendsen. 1988. Nuclear magnetic resonance relaxation in experimental brain edema: effects of water concentration, protein concentration, and temperature. Magn Reson Med. 6:265-274.

Kanekiyo, T., and G. Bu. 2014. The low-density lipoprotein receptor-related protein 1 and amyloid-beta clearance in Alzheimer's disease. Frontiers in Aging Neuroscience. 6:93.

Kanekiyo, T., H. Xu, and G. Bu. 2014. ApoE and Aβ in Alzheimer's disease: Accidental encounters or partners? Neuron. 81:740-754.

Karperien, A., H. Jelinek, and A. Buchan. 2008. Box-counting analysis of microglia form in schizophrenia, Alzheimer's disease and affective disorder. Fractals. 16:103-107.

Karr, J.W., L.J. Kaupp, and V.A. Szalai. 2004. Amyloid-β binds Cu2+ in a mononuclear metal ion binding site. Journal of the American Chemical Society. 126:13534-13538.

Katz, M.L., and W.G. Robison. 2002. What is lipofuscin? Defining characteristics and differentiation from other autofluorescent lysosomal storage bodies. Archives of Gerontology and Geriatrics. 34:169-184.

Katz, M.L., H.J. Stientjes, C.L. Gao, and J.S. Christianson. 1993. Iron-induced accumulation of lipofuscin-like fluorescent pigment in the retinal pigment epithelium. Invest Ophthalmol Vis Sci. 34:3161-3171.

Kawabata, H., R.E. Fleming, D. Gui, S.Y. Moon, T. Saitoh, J. O'Kelly, Y. Umehara, Y. Wano, J.W. Said, and H.P. Koeffler. 2005. Expression of hepcidin is down-regulated in TfR2 mutant mice manifesting a phenotype of hereditary hemochromatosis. Blood. 105:376-381.

Kawabata, H., R.S. Germain, P.T. Vuong, T. Nakamaki, J.W. Said, and H.P. Koeffler. 2000. Transferrin receptor 2-α supports cell growth both in iron-chelated cultured cells and in vivo. Journal of Biological Chemistry. 275:16618-16625.

Kawabata, H., R. Yang, T. Hirama, P.T. Vuong, S. Kawano, A.F. Gombart, and H.P. Koeffler. 1999. Molecular cloning of transferrin receptor 2 A new member of the transferrin receptor-like family. Journal of Biological Chemistry. 274:20826-20832.

Ke, Y., Y.Z. Chang, X.L. Duan, J.R. Du, L. Zhu, K. Wang, X. Da Yang, K.P. Ho, and Z.-m. Qian. 2005. Age-dependent and iron-independent expression of two mRNA isoforms of divalent metal transporter 1 in rat brain. Neurobiology of Aging. 26:739-748.

Kehrer, J.P. 2000. The Haber–Weiss reaction and mechanisms of toxicity. Toxicology. 149:43-50.

Keren-Shaul, H., A. Spinrad, A. Weiner, O. Matcovitch-Natan, R. Dvir-Szternfeld, T.K. Ulland, E. David, K. Baruch, D. Lara-Astaiso, B. Toth, S. Itzkovitz, M. Colonna, M. Schwartz, and I. Amit. 2017. A Unique Microglia Type Associated with Restricting Development of Alzheimer's Disease. Cell. 169:1276-1290.e1217.

Khan, A., J.P. Dobson, and C. Exley. 2006. Redox cycling of iron by Abeta42. Free Radic Biol Med. 40:557-569.

Khurana, R., V.N. Uversky, L. Nielsen, and A.L. Fink. 2001. Is Congo red an amyloid-specific dye? The Journal of Biological Chemistry. 276:22715-22721.

Kim, H.Y., T. LaVaute, K. Iwai, R.D. Klausner, and T.A. Rouault. 1996. Identification of a conserved and functional iron-responsive element in the 5'-untranslated region of mammalian mitochondrial aconitase. The Journal of Biological Chemistry. 271:24226-24230.

Kim, S.U., and J. de Vellis. 2005. Microglia in health and disease. Journal of Neuroscience Research. 81:302-313.

Kirschvink, J.L., A. Kobayashi-Kirschvink, and B.J. Woodford. 1992. Magnetite biomineralization in the human brain. Proceedings of the National Academy of Sciences USA. 89:7683-7687.

Kitazume, S., A. Yoshihisa, T. Yamaki, M. Oikawa, Y. Tachida, K. Ogawa, R. Imamaki, Y. Hagiwara, N. Kinoshita, Y. Takeishi, K. Furukawa, N. Tomita, H. Arai, N. Iwata, T. Saido, N. Yamamoto, and N. Taniguchi. 2012. Soluble amyloid precursor protein 770 is released from inflamed endothelial cells and activated platelets: a novel biomarker for acute coronary syndrome. The Journal of Biological Chemistry. 287:40817-40825.

Klafki, H.-W., D. Abramowski, R. Swoboda, P. Paganetti, and M. Staufenbiel. 1996. The carboxyl termini of β-amyloid peptides 1-40 and 1-42 are generated by distinct γ-secretase activities. Journal of Biological Chemistry. 271:28655-28659.

Klausner, R.D., G. Ashwell, J. Van Renswoude, J.B. Harford, and K.R. Bridges. 1983. Binding of apotransferrin to K562 cells: explanation of the transferrin cycle. Proceedings of the National Academy of Sciences. 80:2263-2266.

Klomp, L.W., Z.S. Farhangrazi, L.L. Dugan, and J.D. Gitlin. 1996. Ceruloplasmin gene expression in the murine central nervous system. J Clin Invest. 98:207-215.

Knutson, M.D., J.E. Levy, N.C. Andrews, and M. Wessling-Resnick. 2001. Expression of stimulator of Fe transport is not enhanced in Hfe knockout mice. The Journal of Nutrition. 131:1459-1464.

Koeller, D.M., J.L. Casey, M.W. Hentze, E.M. Gerhardt, L. Chan, R.D. Klausner, and J.B. Harford. 1989. A cytosolic protein binds to structural elements within the iron regulatory region of the transferrin receptor mRNA. Proceedings of the National Academy of Sciences USA. 86:3574-3578.

Koenigsknecht, J., and G. Landreth. 2004. Microglial phagocytosis of fibrillar beta-amyloid through a beta1 integrin-dependent mechanism. The Journal of Neuroscience. 24:9838-9846.

Koeppen, A.H. 1995. The history of iron in the brain. Journal of the Neurological Sciences. 134:1-9.

Koeppen, A.H., S.C. Michael, D. Li, Z. Chen, M.J. Cusack, W.M. Gibson, S.V. Petrocine, and J. Qian. 2008. The pathology of superficial siderosis of the central nervous system. Acta neuropathologica. 116:371-382.

Koffie, R.M., M. Meyer-Luehmann, T. Hashimoto, K.W. Adams, M.L. Mielke, M. Garcia-Alloza, K.D. Micheva, S.J. Smith, M.L. Kim, V.M. Lee, B.T. Hyman, and T.L. Spires-Jones. 2009. Oligomeric amyloid beta associates with postsynaptic densities and correlates with excitatory synapse loss near senile plaques. Proceedings of the National Academy of Sciences USA. 106:4012-4017.

Koh, C.J., and M. Lee. 2006. Structural analysis of amyloid aggregates by multifunctional fluorescence nanoscopy. Current Applied Physics. 6:e257-e260.

Kohgo, Y., K. Ikuta, T. Ohtake, Y. Torimoto, and J. Kato. 2008. Body iron metabolism and pathophysiology of iron overload. International Journal of Hematology. 88:7-15.

Kojro, E., and F. Fahrenholz. 2005. The non-amyloidogenic pathway: structure and function of α-secretases. In Alzheimer's Disease. Springer. 105-127.

Kongsui, R., S.B. Beynon, S.J. Johnson, and F.R. Walker. 2014. Quantitative assessment of microglial morphology and density reveals remarkable consistency in the distribution and morphology of cells within the healthy prefrontal cortex of the rat. Journal of Neuroinflammation. 11:182.

Korzhevskii, D.E., and O.V. Kirik. 2016. Brain Microglia and Microglial Markers. Neuroscience and Behavioral Physiology. 46:284-290.

Kreutzberg, G.W. 1996. Microglia: a sensor for pathological events in the CNS. Trends in Neurosciences. 19:312-318.

Kupershmidt, L., T. Amit, O. Bar-Am, M.B. Youdim, and O. Weinreb. 2012. The novel multi-target iron chelating-radical scavenging compound M30 possesses beneficial effects on major hallmarks of Alzheimer's disease. Antioxid Redox Signal. 17:860-877.

Kurt, M.A., D.C. Davies, M. Kidd, K. Duff, S.C. Rolph, K.H. Jennings, and D.R. Howlett. 2001. Neurodegenerative changes associated with beta-amyloid deposition in the brains of mice carrying mutant amyloid precursor protein and mutant presenilin-1 transgenes. Exp Neurol. 171:59-71.

Kurz, T., A. Terman, B. Gustafsson, and U.T. Brunk. 2008. Lysosomes in iron metabolism, ageing and apoptosis. Histochemistry and Cell Biology. 129:389-406.

LaFerla, F.M., K.N. Green, and S. Oddo. 2007. Intracellular amyloid-[beta] in Alzheimer's disease. Nature Reviews. Neuroscience. 8:499.

LaFerla, F.M., and S. Oddo. 2005. Alzheimer's disease: Aβ, tau and synaptic dysfunction. Trends in Molecular Medicine. 11:170-176.

Lalonde, R., H. Kim, J. Maxwell, and K. Fukuchi. 2005. Exploratory activity and spatial learning in 12-month-old APP 695 SWE/co+PS1/ΔE9 mice with amyloid plaques. Neuroscience Letters. 390:87-92.

Lambe, T., R.J. Simpson, S. Dawson, T. Bouriez-Jones, T.L. Crockford, M. Lepherd, G.O. Latunde-Dada, H. Robinson, K.B. Raja, and D.R. Campagna. 2009. Identification of a Steap3 endosomal targeting motif essential for normal iron metabolism. Blood. 113:1805-1808.

Lammich, S., E. Kojro, R. Postina, S. Gilbert, R. Pfeiffer, M. Jasionowski, C. Haass, and F. Fahrenholz. 1999. Constitutive and regulated α-secretase cleavage of Alzheimer's amyloid precursor protein by a disintegrin metalloprotease. Proceedings of the National Academy of Sciences. 96:3922-3927.

Lannfelt, L., H. Basun, L.-O. Wahlund, B.A. Rowe, and S.L. Wagner. 1995. Decreased α-secretase-cleaved amyloid precursor protein as a diagnostic marker for Alzheimer's diseas. Nature Medicine. 1:829-832.

Lassmann, H., C. Bancher, H. Breitschopf, J. Wegiel, M. Bobinski, K. Jellinger, and H.M. Wisniewski. 1995. Cell death in Alzheimer's disease evaluated by DNA fragmentation in situ. Acta Neuropathologica. 89:35-41.

Lawson, D.M., P.J. Artymiuk, S.J. Yewdall, J.M. Smith, J.C. Livingstone, A. Treffry, A. Luzzago, S. Levi, P. Arosio, G. Cesareni, and et al. 1991. Solving the structure of human H ferritin by genetically engineering intermolecular crystal contacts. Nature. 349:541-544.

Lebron, J.A., M.J. Bennett, D.E. Vaughn, A.J. Chirino, P.M. Snow, G.A. Mintier, J.N. Feder, and P.J. Bjorkman. 1998. Crystal structure of the hemochromatosis protein HFE and characterization of its interaction with transferrin receptor. Cell. 93:111-123.

Lebrón, J.A., A.P. West, and P.J. Bjorkman. 1999. The hemochromatosis protein HFE competes with transferrin for binding to the transferrin receptor. Journal of Molecular Biology. 294:239-245.

Lee, D.C., J. Rizer, J.B. Hunt, M.L. Selenica, M.N. Gordon, and D. Morgan. 2013. Review: experimental manipulations of microglia in mouse models of Alzheimer's pathology: activation reduces amyloid but hastens tau pathology. Neuropathology and Applied Neurobiology. 39:69-85.

Lee, G., N. Cowan, and M. Kirschner. 1988. The primary structure and heterogeneity of tau protein from mouse brain. Science. 239:285-288.

Lee, G.R., S. Nacht, J.N. Lukens, and G. Cartwright. 1968. Iron metabolism in copper-deficient swine. Journal of Clinical Investigation. 47:2058.

Lee, J.H., J. Ryan, C. Andreescu, H. Aizenstein, and H.K. Lim. 2015. Brainstem morphological changes in Alzheimer’s disease. Neuroreport. 26:411.

Leitner, D.F., B. Todorich, X. Zhang, and J.R. Connor. 2015. Semaphorin4A Is Cytotoxic to Oligodendrocytes and Is Elevated in Microglia and Multiple Sclerosis. ASN Neuro. 7.

Lestas, A. 1976. The Effect of pH upon Human Transferrin: Selective Labelling of the Two Iron-binding Sites. British Journal of Haematology. 32:341-350.

LeVine, S.M. 1997. Iron deposits in multiple sclerosis and Alzheimer's disease brains. Brain Res. 760:298-303.

Levy-Lahad, E., W. Wasco, P. Poorkaj, D.M. Romano, J. Oshima, W.H. Pettingell, C.-e. Yu, P.D. Jondro, S.D. Schmidt, and K. Wang. 1995. Candidate gene for the chromosome 1 familial Alzheimer's disease locus. Science. 269:973-977.

Lewerenz, J., G. Ates, A. Methner, M. Conrad, and P. Maher. 2018. Oxytosis/Ferroptosis-(Re-) Emerging Roles for Oxidative Stress-Dependent Non-apoptotic Cell Death in Diseases of the Central Nervous System. Frontiers in Neuroscience. 12:214.

Li, J.Y., N. Paragas, R.M. Ned, A. Qiu, M. Viltard, T. Leete, I.R. Drexler, X. Chen, S. Sanna-Cherchi, and F. Mohammed. 2009. Scara5 is a ferritin receptor mediating non-transferrin iron delivery. Developmental Cell. 16:35-46.

Liddelow, S.A., K.A. Guttenplan, L.E. Clarke, F.C. Bennett, C.J. Bohlen, L. Schirmer, M.L. Bennett, A.E. Munch, W.S. Chung, T.C. Peterson, D.K. Wilton, A. Frouin, B.A. Napier, N. Panicker, M. Kumar, M.S. Buckwalter, D.H. Rowitch, V.L. Dawson, T.M. Dawson, B. Stevens, and B.A. Barres. 2017. Neurotoxic reactive astrocytes are induced by activated microglia. Nature. 541:481-487.

Liebmann, T., N. Renier, K. Bettayeb, P. Greengard, M. Tessier-Lavigne, and M. Flajolet. 2016. Three-Dimensional Study of Alzheimer's Disease Hallmarks Using the iDISCO Clearing Method. Cell Reports. 16:1138-1152.

Lin, M.T., and M.F. Beal. 2006. Mitochondrial dysfunction and oxidative stress in neurodegenerative diseases. Nature. 443:787.

Ling, E.A., and W.C. Wong. 1993. The origin and nature of ramified and amoeboid microglia: a historical review and current concepts. Glia. 7:9-18.

Linke, R.P. 2006. Congo red staining of amyloid: improvements and practical guide for a more precise diagnosis of amyloid and the different amyloidoses. In Protein misfolding, aggregation, and conformational diseases. Springer. 239-276.

Liu, C.C., T. Kanekiyo, H. Xu, and G. Bu. 2013. Apolipoprotein E and Alzheimer disease: risk, mechanisms and therapy. Nat Rev Neurol. 9:106-118.

Liu, F., T. Zaidi, K. Iqbal, I. Grundke-Iqbal, and C.-X. Gong. 2002. Aberrant glycosylation modulates phosphorylation of tau by protein kinase A and dephosphorylation of tau by protein phosphatase 2A and 5. Neuroscience. 115:829-837.

Liu, Z., C. Condello, A. Schain, R. Harb, and J. Grutzendler. 2010. CX3CR1 in microglia regulates brain amyloid deposition through selective protofibrillar amyloid-beta phagocytosis. The Journal of neuroscience. 30:17091-17101.

Lodygensky, G.A., J.P. Marques, R. Maddage, E. Perroud, S.V. Sizonenko, P.S. Hüppi, and R. Gruetter. 2012. In vivo assessment of myelination by phase imaging at high magnetic field. NeuroImage. 59:1979-1987.

Lopes da Silva, S., B. Vellas, S. Elemans, J. Luchsinger, P. Kamphuis, K. Yaffe, J. Sijben, M. Groenendijk, and T. Stijnen. 2014. Plasma nutrient status of patients with Alzheimer's disease: Systematic review and meta-analysis. Alzheimer's and Dementia. 10:485-502.

Lopes, K.O., D.L. Sparks, and W.J. Streit. 2008. Microglial dystrophy in the aged and Alzheimer's disease brain is associated with ferritin immunoreactivity. Glia. 56:1048-1060.

López, O.L., and S.T. DeKosky. 2008. Clinical symptoms in Alzheimer's disease. Handbook of Clinical Neurology. 89:207-216.

Lou, L.X., B. Geng, Y. Chen, F. Yu, J. Zhao, and C.S. Tang. 2009. ENDOPLASMIC RETICULUM STRESS INVOLVED IN HEART AND LIVER INJURY IN IRON-LOADED RATS. Clinical and Experimental Pharmacology and Physiology. 36:612-618.

Lovell, M., J. Robertson, W. Teesdale, J. Campbell, and W. Markesbery. 1998. Copper, iron and zinc in Alzheimer's disease senile plaques. Journal of the Neurological Sciences. 158:47-52.

Ludwin, S.K. 1978. Central nervous system demyelination and remyelination in the mouse: an ultrastructural study of cuprizone toxicity. Lab Invest. 39:597-612.

Lue, L.F., D.G. Walker, L. Brachova, T.G. Beach, J. Rogers, A.M. Schmidt, D.M. Stern, and S.D. Yan. 2001. Involvement of microglial receptor for advanced glycation endproducts (RAGE) in Alzheimer's disease: identification of a cellular activation mechanism. Exp Neurol. 171:29-45.

Lutz, B.M., and J. Peng. 2018. Deep Profiling of the Aggregated Proteome in Alzheimer's Disease: From Pathology to Disease Mechanisms. Proteomes. 6.

Lymboussaki, A., E. Pignatti, G. Montosi, C. Garuti, D.J. Haile, and A. Pietrangelo. 2003. The role of the iron responsive element in the control of ferroportin1/IREG1/MTP1 gene expression. Journal of Hepatology. 39:710-715.

Lyon, E., and E.L. Frank. 2001. Hereditary hemochromatosis since discovery of the HFE gene. Clin Chem. 47:1147-1156.

Maaroufi, K., M. Ammari, M. Jeljeli, V. Roy, M. Sakly, and H. Abdelmelek. 2009. Impairment of emotional behavior and spatial learning in adult Wistar rats by ferrous sulfate. Physiology and Behavior. 96:343-349.

Madsen, J.B., J. Folke, and B. Pakkenberg. 2018. Stereological Quantification of Plaques and Tangles in Neocortex from Alzheimer’s Disease Patients. Journal of Alzheimer’s Disease 1-12 pp.

Magaki, S., R. Raghavan, C. Mueller, K.C. Oberg, H.V. Vinters, and W.M. Kirsch. 2007. Iron, copper, and iron regulatory protein 2 in Alzheimer's disease and related dementias. Neuroscience Letters. 418:72-76.

Mandrekar, S., Q. Jiang, C.Y. Lee, J. Koenigsknecht-Talboo, D.M. Holtzman, and G.E. Landreth. 2009. Microglia mediate the clearance of soluble Abeta through fluid phase macropinocytosis. The Journal of Neuroscience. 29:4252-4262.

Mann, D.M., B. Marcyniuk, P.O. Yates, D. Neary, and J.S. Snowden. 1988. The progression of the pathological changes of Alzheimer's disease in frontal and temporal neocortex examined both at biopsy and at autopsy. Neuropathology and Applied Neurobiology. 14:177-195.

Mantyh, P.W., J.R. Ghilardi, S. Rogers, E. DeMaster, C.J. Allen, E.R. Stimson, and J.E. Maggio. 1993. Aluminum, Iron, and Zinc Ions Promote Aggregation of Physiological Concentrations of β-Amyloid Peptide. Journal of Neurochemistry. 61:1171-1174.

Markesbery, W.R. 1997. Oxidative stress hypothesis in Alzheimer's disease. Free Radical Biology and Medicine. 23:134-147.

Marques, F., J.C. Sousa, G. Coppola, F. Gao, R. Puga, H. Brentani, D.H. Geschwind, N. Sousa, M. Correia-Neves, and J.A. Palha. 2011. Transcriptome signature of the adult mouse choroid plexus. Fluids and Barriers of the CNS. 8:10-10.

Masliah, E., R.D. Terry, M. Alford, and R. DeTeresa. 1990. Quantitative immunohistochemistry of synaptophysin in human neocortex: an alternative method to estimate density of presynaptic terminals in paraffin sections. The journal of Histochemistry and Cytochemistry. 38:837-844.

Masters, C.L., G. Simms, N.A. Weinman, G. Multhaup, B.L. McDonald, and K. Beyreuther. 1985. Amyloid plaque core protein in Alzheimer disease and Down syndrome. Proceedings of the National Academy of Sciences. 82:4245-4249.

Mathiisen, T.M., K.P. Lehre, N.C. Danbolt, and O.P. Ottersen. 2010. The perivascular astroglial sheath provides a complete covering of the brain microvessels: an electron microscopic 3D reconstruction. Glia. 58:1094-1103.

Matsushima, G.K., and P. Morell. 2001. The neurotoxicant, cuprizone, as a model to study demyelination and remyelination in the central nervous system. Brain Pathol. 11:107-116.

Mattson, M.P. 2004. Pathways Towards and Away from Alzheimer's Disease. Nature. 430:631-639.

Mawuenyega, K.G., W. Sigurdson, V. Ovod, L. Munsell, T. Kasten, J.C. Morris, K.E. Yarasheski, and R.J. Bateman. 2010. Decreased clearance of CNS beta-amyloid in Alzheimer's disease. Science. 330:1774.

Maynard, C.J., R. Cappai, I. Volitakis, R.A. Cherny, A.R. White, K. Beyreuther, C.L. Masters, A.I. Bush, and Q.-X. Li. 2002. Overexpression of Alzheimer's disease amyloid-β opposes the age-dependent elevations of brain copper and iron. Journal of Biological Chemistry. 277:44670-44676.

McCarthy, R.C., and D.J. Kosman. 2015. Iron transport across the blood–brain barrier: development, neurovascular regulation and cerebral amyloid angiopathy. Cellular and molecular life sciences. 72:709-727.

McCarthy, R.C., Y.H. Park, and D.J. Kosman. 2014. sAPP modulates iron efflux from brain microvascular endothelial cells by stabilizing the ferrous iron exporter ferroportin. EMBO Rep. 15:809-815.

McCarthy, R.C., J.C. Sosa, A.M. Gardeck, A.S. Baez, C.-H. Lee, and M. Wessling-Resnick. 2018a. Inflammation-induced iron transport and metabolism by brain microglia. Journal of Biological Chemistry. 293:7853-7863.

McCarthy, R.C., J.C. Sosa, A.M. Gardeck, A.S. Baez, C.H. Lee, and M. Wessling-Resnick. 2018b. Inflammation-induced iron transport and metabolism by brain microglia. The Journal of Biological Chemistry. 293:7853-7863.

McKhann, G.M., D.S. Knopman, H. Chertkow, B.T. Hyman, C.R. Jack, C.H. Kawas, W.E. Klunk, W.J. Koroshetz, J.J. Manly, and R. Mayeux. 2011. The diagnosis of dementia due to Alzheimer's disease: Recommendations from the National Institute on Aging-Alzheimer's Association workgroups on diagnostic guidelines for Alzheimer's disease. Alzheimer's and Dementia. 7:263-269.

McKie, A.T., and D.J. Barlow. 2004. The SLC40 basolateral iron transporter family (IREG1/ferroportin/MTP1). Pflügers Archiv. 447:801-806.

McKie, A.T., D. Barrow, G.O. Latunde-Dada, A. Rolfs, G. Sager, E. Mudaly, M. Mudaly, C. Richardson, D. Barlow, and A. Bomford. 2001. An iron-regulated ferric reductase associated with the absorption of dietary iron. Science. 291:1755-1759.

McKie, A.T., P. Marciani, A. Rolfs, K. Brennan, K. Wehr, D. Barrow, S. Miret, A. Bomford, T.J. Peters, and F. Farzaneh. 2000. A novel duodenal iron-regulated transporter, IREG1, implicated in the basolateral transfer of iron to the circulation. Molecular Cell. 5:299-309.

McLachlan, S., S.-M. Lee, T.M. Steele, P.L. Hawthorne, M.A. Zapala, E. Eskin, N.J. Schork, G.J. Anderson, and C.D. Vulpe. 2010. In silico QTL mapping of basal liver iron levels in inbred mouse strains. Physiological Genomics.

Meadowcroft, M.D., J.R. Connor, M.B. Smith, and Q.X. Yang. 2009. MRI and histological analysis of beta-amyloid plaques in both human Alzheimer's disease and APP/PS1 transgenic mice. Journal of Magnetic Resonance Imaging. 29:997-1007.

Meadowcroft, M.D., J.R. Connor, and Q.X. Yang. 2015a. Cortical iron regulation and inflammatory response in Alzheimer's disease and APPSWE/PS1ΔE9 mice: a histological perspective. Frontiers in Neuroscience. 9.

Meadowcroft, M.D., D.G. Peters, R.P. Dewal, J.R. Connor, and Q.X. Yang. 2015b. The effect of iron in MRI and transverse relaxation of amyloid-beta plaques in Alzheimer's disease. NMR Biomed. 28:297-305.

Mechlovich, D., T. Amit, O. Bar-Am, S. Mandel, M.B. Youdim, and O. Weinreb. 2014. The novel multi-target iron chelator, M30 modulates HIF-1alpha-related glycolytic genes and insulin signaling pathway in the frontal cortex of APP/PS1 Alzheimer's disease mice. Curr Alzheimer Res. 11:119-127.

Mecocci, P., U. MacGarvey, and M.F. Beal. 1994. Oxidative damage to mitochondrial DNA is increased in Alzheimer's disease. Annals of Neurology. 36:747-751.

Meguro, R., Y. Asano, H. Iwatsuki, and K. Shoumura. 2003. Perfusion-Perls and-Turnbull methods supplemented by DAB intensification for nonheme iron histochemistry: demonstration of the superior sensitivity of the methods in the liver, spleen, and stomach of the rat. Histochemistry and Cell Biology. 120:73-82.

Meguro, R., Y. Asano, S. Odagiri, C. Li, H. Iwatsuki, and K. Shoumura. 2007. Nonheme-iron histochemistry for light and electron microscopy: a historical, theoretical and technical review. Archives of Histology and Cytology. 70:1-19.

Meguro, R., Y. Asano, S. Odagiri, C. Li, and K. Shoumura. 2008. Cellular and subcellular localizations of nonheme ferric and ferrous iron in the rat brain: a light and electron microscopic study by the perfusion-Perls and-Turnbull methods. Archives of Histology and Cytology. 71:205-222.

Meyer, E., M.A. Kurian, and S.J. Hayflick. 2015. Neurodegeneration with brain iron accumulation: genetic diversity and pathophysiological mechanisms. Annual Review of Genomics and Human Genetics. 16:257-279.

Miller, E.M. 2016. The reproductive ecology of iron in women. American journal of Physical Anthropology. 159:S172-195.

Miller, Y., B. Ma, and R. Nussinov. 2010. Zinc ions promote Alzheimer Aβ aggregation via population shift of polymorphic states. Proceedings of the National Academy of Sciences. 107:9490-9495.

Mills, E., X.-p. Dong, F. Wang, and H. Xu. 2010. Mechanisms of brain iron transport: insight into neurodegeneration and CNS disorders. Future Medicinal Chemistry. 2:51-64.

Milstone, L.M., R.-H. Hu, J.D. Dziura, and J. Zhou. 2012. Impact of epidermal desquamation on tissue stores of iron. Journal of Dermatological Science. 67:9-14.

Milward, E.A., D.G. Bruce, M.W. Knuiman, M.L. Divitini, M. Cole, C.A. Inderjeeth, R.M. Clarnette, G. Maier, A. Jablensky, and J.K. Olynyk. 2010. A cross-sectional community study of serum iron measures and cognitive status in older adults. Journal of Alzheimer's Disease : JAD. 20:617-623.

Miret, S., R.J. Simpson, and A.T. McKie. 2003. Physiology and molecular biology of dietary iron absorption. Annual Review of Nutrition. 23:283-301.

Miyajima, H., Y. Takahashi, T. Kamata, H. Shimizu, N. Sakai, and J.D. Gitlin. 1997. Use of desferrioxamine in the treatment of aceruloplasminemia. Annals of Neurology. 41:404-407.

Moos, T. 1995. Developmental profile of non-heme iron distribution in the rat brain during ontogenesis. Developmental Brain Research. 87:203-213.

Moos, T., and K. Mollgard. 1993. A sensitive post-DAB enhancement technique for demonstration of iron in the central nervous system. Histochemistry. 99:471-475.

Moos, T., and E.H. Morgan. 1998. Evidence for low molecular weight, non-transferrin-bound iron in rat brain and cerebrospinal fluid. Journal of Neuroscience Research. 54:486-494.

Moos, T., and E.H. Morgan. 2004a. The metabolism of neuronal iron and its pathogenic role in neurological disease: review. Annals of the New York Academy of Sciences. 1012:14-26.

Moos, T., and E.H. Morgan. 2004c. The significance of the mutated divalent metal transporter (DMT1) on iron transport into the Belgrade rat brain. J Neurochem. 88:233-245.

Moos, T., and T.R. Nielsen. 2006. Ferroportin in the postnatal rat brain: implications for axonal transport and neuronal export of iron. In Seminars in pediatric neurology. Vol. 13. Elsevier. 149-157.

Moos, T., T.R. Nielsen, T. Skjørringe, and E.H. Morgan. 2007. Iron trafficking inside the brain. Journal of Neurochemistry. 103:1730-1740.

Moos, T., and T. Rosengren Nielsen. 2006. Ferroportin in the postnatal rat brain: implications for axonal transport and neuronal export of iron. Semin Pediatr Neurol. 13:149-157.

Moos, T., T. Skjoerringe, S. Gosk, and E.H. Morgan. 2006. Brain capillary endothelial cells mediate iron transport into the brain by segregating iron from transferrin without the involvement of divalent metal transporter 1. Journal of Neurochemistry. 98:1946-1958.

Moos, T., D. Trinder, and E. Morgan. 2000. Cellular distribution of ferric iron, ferritin, transferrin and divalent metal transporter 1 (DMT1) in substantia nigra and basal ganglia of normal and beta2-microglobulin deficient mouse brain. Cellular and Molecular Biology. 46:549-561.

Morishima-Kawashima, M., M. Hasegawa, K. Takio, M. Suzuki, H. Yoshida, K. Titani, and Y. Ihara. 1995. Proline-directed and non-proline-directed phosphorylation of PHF-tau. Journal of Biological Chemistry. 270:823-829.

Mourad, F.H., A.V. Hoffbrand, M. Sheikh-Taha, S. Koussa, A.I. Khoriaty, and A. Taher. 2003. Comparison between desferrioxamine and combined therapy with desferrioxamine and deferiprone in iron overloaded thalassaemia patients. British journal of Haematology. 121:187-189.

Muckenthaler, M.U. 2014. How mutant HFE causes hereditary hemochromatosis. Blood. 124:1212-1213.

Mufson, E.J., S.E. Counts, S.E. Perez, and S.D. Ginsberg. 2008. Cholinergic system during the progression of Alzheimer's disease: therapeutic implications. Expert Review of Neurotherapeutics. 8:1703-1718.

Mullen, R.J., C.R. Buck, and A.M. Smith. 1992. NeuN, a neuronal specific nuclear protein in vertebrates. Development. 116:201-211.

Müllner, E.W., and L.C. Kühn. 1988. A stem-loop in the 3’ untranslated region mediates iron-dependent regulation of transferrin receptor mRNA stability in the cytoplasm. Cell. 53:815-825.

Multhaup, G., A. Schlicksupp, L. Hesse, D. Beher, T. Ruppert, C.L. Masters, and K. Beyreuther. 1996. The amyloid precursor protein of Alzheimer's disease in the reduction of copper (II) to copper (I). Science. 271:1406-1409.

Nakamura, M., N. Shishido, A. Nunomura, M.A. Smith, G. Perry, Y. Hayashi, K. Nakayama, and T. Hayashi. 2007. Three histidine residues of amyloid-beta peptide control the redox activity of copper and iron. Biochemistry. 46:12737-12743.

Neher, J.J., U. Neniskyte, J.-W. Zhao, A. Bal-Price, A.M. Tolkovsky, and G.C. Brown. 2011. Inhibition of microglial phagocytosis is sufficient to prevent inflammatory neuronal death. The Journal of Immunology. 186:4973-4983.

Nelson, P.T., L.A. Soma, and E. Lavi. 2002. Microglia in diseases of the central nervous system. Ann Med. 34:491-500.

Nemeth, E., G.C. Preza, C.-L. Jung, J. Kaplan, A.J. Waring, and T. Ganz. 2006. The N-terminus of hepcidin is essential for its interaction with ferroportin: structure-function study. Blood. 107:328-333.

Nemeth, E., M.S. Tuttle, J. Powelson, M.B. Vaughn, A. Donovan, D.M. Ward, T. Ganz, and J. Kaplan. 2004. Hepcidin regulates cellular iron efflux by binding to ferroportin and inducing its internalization. Science. 306:2090-2093.

Nguyen-Legros, J., J. Bizot, M. Bolesse, and J. Pulicani. 1979. [" Diaminobenzidine black" as a new histochemical demonstration of exogenous iron (author's transl)]. Histochemistry. 66:239-244.

Nicolas, G., L. Viatte, M. Bennoun, C. Beaumont, A. Kahn, and S. Vaulont. 2002. Hepcidin, a new iron regulatory peptide. Blood Cells, Molecules, and Diseases. 29:327-335.

Nielsen, J., L.N. Jensen, and K. Krabbe. 1995. Hereditary haemochromatosis: a case of iron accumulation in the basal ganglia associated with a parkinsonian syndrome. Journal of Neurology, Neurosurgery & Psychiatry. 59:318-321.

Nimmerjahn, A., F. Kirchhoff, and F. Helmchen. 2005a. Resting microglial cells are highly dynamic surveillants of brain parenchyma in vivo. Science. 308:1314-1318.

Nimmerjahn, A., F. Kirchhoff, and F. Helmchen. 2005b. Resting microglial cells are highly dynamic surveillants of brain parenchyma in vivo. Science. 308:1314-1318.

Ninomiya, H., J.M. Roch, M.P. Sundsmo, D.A. Otero, and T. Saitoh. 1993. Amino acid sequence RERMS represents the active domain of amyloid beta/A4 protein precursor that promotes fibroblast growth. J Cell Biol. 121:879-886.

Nnah, I.C., and M. Wessling-Resnick. 2018. Brain Iron Homeostasis: A Focus on Microglial Iron. Pharmaceuticals. 11.

Norris, G., N. Derecki, and J. Kipnis. 2014. Microglial Sholl Analysis.

O'Donnell, K.A., P.R. Rapp, and P.R. Hof. 1999. Preservation of prefrontal cortical volume in behaviorally characterized aged macaque monkeys. Experimental Neurology. 160:300-310.

O'Sullivan, M., D.K. Jones, P. Summers, R. Morris, S. Williams, and H. Markus. 2001. Evidence for cortical "disconnection" as a mechanism of age-related cognitive decline. Neurology. 57:632-638.

Oakley, H., S.L. Cole, S. Logan, E. Maus, P. Shao, J. Craft, A. Guillozet-Bongaarts, M. Ohno, J. Disterhoft, and L. Van Eldik. 2006. Intraneuronal β-amyloid aggregates, neurodegeneration, and neuron loss in transgenic mice with five familial Alzheimer's disease mutations: potential factors in amyloid plaque formation. Journal of Neuroscience. 26:10129-10140.

Ohgami, R.S., D.R. Campagna, A. McDonald, and M.D. Fleming. 2006. The Steap proteins are metalloreductases. Blood. 108:1388-1394.

Omara, F.O., B.R. Blakley, and D.L. Hamilton. 1992. Effect of dietary iron supplementation on the body burden of iron in mice. Nutrition Research. 12:1245-1252.

Orihuela, R., C.A. McPherson, and G.J. Harry. 2016. Microglial M1/M2 polarization and metabolic states. British Journal of Pharmacology. 173:649-665.

Osaki, S., D.A. Johnson, and E. Frieden. 1966. The possible significance of the ferrous oxidase activity of ceruloplasmin in normal human serum. Journal of Biological Chemistry. 241:2746-2751.

Pankhurst, Q., D. Hautot, N. Khan, and J. Dobson. 2008. Increased levels of magnetic iron compounds in Alzheimer's disease. Journal of Alzheimer's Disease. 13:49-52.

Papanikolaou, G., and K. Pantopoulos. 2005. Iron metabolism and toxicity. Toxicology and Applied Pharmacology. 202:199-211.

Papanikolaou, G., M.E. Samuels, E.H. Ludwig, M.L. MacDonald, P.L. Franchini, M.P. Dube, L. Andres, J. MacFarlane, N. Sakellaropoulos, M. Politou, E. Nemeth, J. Thompson, J.K. Risler, C. Zaborowska, R. Babakaiff, C.C. Radomski, T.D. Pape, O. Davidas, J. Christakis, P. Brissot, G. Lockitch, T. Ganz, M.R. Hayden, and Y.P. Goldberg. 2004. Mutations in HFE2 cause iron overload in chromosome 1q-linked juvenile hemochromatosis. Nat Genet. 36:77-82.

Paresce, D.M., R.N. Ghosh, and F.R. Maxfield. 1996. Microglial cells internalize aggregates of the Alzheimer's disease amyloid beta-protein via a scavenger receptor. Neuron. 17:553-565.

Parikh, I., D.W. Fardo, and S. Estus. 2014. Genetics of PICALM expression and Alzheimer's disease. PloS One. 9:e91242.

Patel, B.N., R.J. Dunn, S.Y. Jeong, Q. Zhu, J.-P. Julien, and S. David. 2002. Ceruloplasmin regulates iron levels in the CNS and prevents free radical injury. The Journal of Neuroscience. 22:6578-6586.

Paterson, S., N. Armstrong, B. Iacopetta, H. McArdle, and E. Morgan. 1984. Intravesicular pH and iron uptake by immature erythroid cells. Journal of Cellular Physiology. 120:225-232.

Paula, V.d.J.R.d., F.M. Guimarães, B.S. Diniz, and O.V. Forlenza. 2009. Neurobiological pathways to Alzheimers disease: Amyloid-beta, Tau protein or both? Dement. Neuropsychol. 3.

Paxinos, G. 2013. Paxinos and Franklin's the mouse brain in stereotaxic coordinates. Academic Press.

Pearse, B. 1982. Coated vesicles from human placenta carry ferritin, transferrin, and immunoglobulin G. Proceedings of the National Academy of Sciences. 79:451-455.

Pelizzoni, I., D. Zacchetti, A. Campanella, F. Grohovaz, and F. Codazzi. 2013. Iron uptake in quiescent and inflammation-activated astrocytes: a potentially neuroprotective control of iron burden. Biochim Biophys Acta. 1832:1326-1333.

Pericak-Vance, M., J. Bebout, P. Gaskell, L. Yamaoka, W.-Y. Hung, M. Alberts, A. Walker, R. Bartlett, C. Haynes, and K. Welsh. 1991. Linkage studies in familial Alzheimer disease: evidence for chromosome 19 linkage. American journal of Human Genetics. 48:1034.

Perl, D.P., and A.R. Brody. 1980. Alzheimer's disease: X-ray spectrometric evidence of aluminum accumulation in neurofibrillary tangle-bearing neurons. Science. 208:297-299.

Perlmutter, L.S., E. Barron, and H.C. Chui. 1990. Morphologic association between microglia and senile plaque amyloid in Alzheimer's disease. Neurosci Lett. 119:32-36.

Persidsky, Y., S.H. Ramirez, J. Haorah, and G.D. Kanmogne. 2006. Blood-brain barrier: structural components and function under physiologic and pathologic conditions. J Neuroimmune Pharmacol. 1:223-236.

Peters, A., and C. Sethares. 2002. Aging and the myelinated fibers in prefrontal cortex and corpus callosum of the monkey. Journal of Comparative Neurology. 442:277-291.

Peters, A., and C. Sethares. 2004. Oligodendrocytes, their progenitors and other neuroglial cells in the aging primate cerebral cortex. Cerebral Cortex. 14:995-1007.

Peters, D.G., J.R. Connor, and M.D. Meadowcroft. 2015. The relationship between iron dyshomeostasis and amyloidogenesis in Alzheimer's disease: Two sides of the same coin. Neurobiology of Disease. 81:49-65.

Petkova, A.T., Y. Ishii, J.J. Balbach, O.N. Antzutkin, R.D. Leapman, F. Delaglio, and R. Tycko. 2002. A structural model for Alzheimer's beta -amyloid fibrils based on experimental constraints from solid state NMR. Proceedings of the National Academy of Sciences USA. 99:16742-16747.

Piccinelli, P., and T. Samuelsson. 2007. Evolution of the iron-responsive element. RNA. 13:952-966.

Pickett, E.K., R.M. Koffie, S. Wegmann, C.M. Henstridge, A.G. Herrmann, M. Colom-Cadena, A. Lleo, K.R. Kay, M. Vaught, R. Soberman, D.M. Walsh, B.T. Hyman, and T.L. Spires-Jones. 2016. Non-Fibrillar Oligomeric Amyloid-beta within Synapses. Journal of Alzheimer's Disease : JAD. 53:787-800.

Pietrangelo, A. 2005. Non-HFE hemochromatosis. Semin Liver Dis. 25:450-460.

Pietrangelo, A. 2010. Hereditary hemochromatosis: pathogenesis, diagnosis, and treatment. Gastroenterology. 139:393-408, 408.e391-392.

Pinkston, J.B. 1999. Dementia, aging, and intellectual disabilities: a handbook-By Matthew P. Janicki & Arthur J. Dalton (eds.). Philadelphia: Brunner/Mazel, 1999. 488 pp. ISBN 0-87630-916-3. Research in Developmental Disabilities. 6:449-450.

Plemel, J.R., N.J. Michaels, N. Weishaupt, A.V. Caprariello, M.B. Keough, J.A. Rogers, A. Yukseloglu, J. Lim, V.V. Patel, K.S. Rawji, S.K. Jensen, W. Teo, B. Heyne, S.N. Whitehead, P.K. Stys, and V.W. Yong. 2018. Mechanisms of lysophosphatidylcholine-induced demyelination: A primary lipid disrupting myelinopathy. Glia. 66:327-347.

Poirier, J. 2000. Apolipoprotein E and Alzheimer's disease a role in amyloid catabolism. Annals of the New York Academy of Sciences. 924:81-90.

Ponte, P., P.G. DeWhitt, J. Schilling, J. Miller, D. Hsu, B. Greenberg, K. Davis, W. Wallace, I. Lieberburg, and F. Fuller. 1988. A new A4 amyloid mRNA contains a domain homologous to serine proteinase inhibitors. Nature. 331:525-527.

Portelius, E., E. Price, G. Brinkmalm, M. Stiteler, M. Olsson, R. Persson, A. Westman-Brinkmalm, H. Zetterberg, A.J. Simon, and K. Blennow. 2011. A novel pathway for amyloid precursor protein processing. Neurobiology of Aging. 32:1090-1098.

Preibisch, S., S. Saalfeld, and P. Tomancak. 2009a. Globally optimal stitching of tiled 3D microscopic image acquisitions. Bioinformatics. 25:1463-1465.

Preibisch, S., S. Saalfeld, and P. Tomancak. 2009b. Globally optimal stitching of tiled 3D microscopic image acquisitions. Bioinformatics. 25:1463-1465.

Priller, C., T. Bauer, G. Mitteregger, B. Krebs, H.A. Kretzschmar, and J. Herms. 2006. Synapse formation and function is modulated by the amyloid precursor protein. The Journal of neuroscience. 26:7212-7221.

Puchtler, H., F. Sweat, and M. Levine. 1962. On the binding of Congo red by amyloid. Journal of Histochemistry & Cytochemistry. 10:355-364.

Puzzo, D., and O. Arancio. 2013. Amyloid-beta peptide: Dr. Jekyll or Mr. Hyde? Journal of Alzheimer's Disease : JAD. 33 Suppl 1:S111-120.

Qian, Z.M., H. Li, H. Sun, and K. Ho. 2002. Targeted drug delivery via the transferrin receptor-mediated endocytosis pathway. Pharmacological Reviews. 54:561-587.

Radanovic, M., F.R. Pereira, F. Stella, I. Aprahamian, L.K. Ferreira, O.V. Forlenza, and G.F. Busatto. 2013. White matter abnormalities associated with Alzheimer's disease and mild cognitive impairment: a critical review of MRI studies. Expert Review of Neurotherapeutics. 13:483-493.

Raffin, S.B., C.H. Woo, K.T. Roost, D.C. Price, and R. Schmid. 1974. Intestinal absorption of hemoglobin iron-heme cleavage by mucosal heme oxygenase. Journal of Clinical Investigation. 54:1344.

Raha, A.A., R.A. Vaishnav, R.P. Friedland, A. Bomford, and R. Raha-Chowdhury. 2013. The systemic iron-regulatory proteins hepcidin and ferroportin are reduced in the brain in Alzheimer’s disease. Acta Neuropathol Commun

Rajamohamedsait, H.B., and E.M. Sigurdsson. 2012. Histological staining of amyloid and pre-amyloid peptides and proteins in mouse tissue. Methods Mol Biol. 849:411-424.

Rajendran, L., and R.C. Paolicelli. 2018. Microglia-Mediated Synapse Loss in Alzheimer's Disease. The Journal of Neuroscience. 38:2911-2919.

Ramanathan, A., A.R. Nelson, A.P. Sagare, and B.V. Zlokovic. 2015. Impaired vascular-mediated clearance of brain amyloid beta in Alzheimer's disease: the role, regulation and restoration of LRP1. Frontiers in Aging Neuroscience. 7:136.

Ramos-Vara, J.A. 2005. Technical aspects of immunohistochemistry. Veterinary Pathology. 42:405-426.

Ranganathan, P.N., Y. Lu, B.K. Fuqua, and J.F. Collins. 2012. Immunoreactive hephaestin and ferroxidase activity are present in the cytosolic fraction of rat enterocytes. Biometals. 25:687-695.

Rao, R., I. Tkac, E.L. Townsend, R. Gruetter, and M.K. Georgieff. 2003. Perinatal iron deficiency alters the neurochemical profile of the developing rat hippocampus. The Journal of Nutrition. 133:3215-3221.

Raven, E.P., P.H. Lu, T.A. Tishler, P. Heydari, and G. Bartzokis. 2013. Increased iron levels and decreased tissue integrity in hippocampus of Alzheimer's disease detected in vivo with magnetic resonance imaging. Journal of Alzheimer's Disease: JAD. 37:127-136.

Reedy, C.J., and B.R. Gibney. 2004. Heme protein assemblies. Chemical Reviews. 104:617-650.

Reeves, P.G., F.H. Nielsen, and G.C. Fahey Jr. 1993. AIN-93 purified diets for laboratory rodents: final report of the American Institute of Nutrition ad hoc writing committee on the reformulation of the AIN-76A rodent diet. J Nutr. 123:1939-1951.

Religa, D., D. Strozyk, R. Cherny, I. Volitakis, V. Haroutunian, B. Winblad, J. Naslund, and A. Bush. 2006. Elevated cortical zinc in Alzheimer disease. Neurology. 67:69-75.

Richardson, S.J., R.C. Wijayagunaratne, D.G. D'Souza, V.M. Darras, and S.L. Van Herck. 2015. Transport of thyroid hormones via the choroid plexus into the brain: the roles of transthyretin and thyroid hormone transmembrane transporters. Frontiers in Neuroscience. 9:66.

Richter, G.W. 1958. Electron microscopy of hemosiderin: Presence of ferritin and occurrence of crystalline lattices in hemosiderin deposits. The Journal of Cell Biology. 4:55-58.

Ries, M., and M. Sastre. 2016. Mechanisms of Aβ Clearance and Degradation by Glial Cells. Frontiers in Aging Neuroscience. 8:160.

Roberts, S.B., J.A. Ripellino, K.M. Ingalls, N.K. Robakis, and K.M. Felsenstein. 1994. Non-amyloidogenic cleavage of the beta-amyloid precursor protein by an integral membrane metalloendopeptidase. Journal of Biological Chemistry. 269:3111-3116.

Rogers, J.T., A.I. Bush, H.H. Cho, D.H. Smith, A.M. Thomson, A.L. Friedlich, D.K. Lahiri, P.J. Leedman, X. Huang, and C.M. Cahill. 2008. Iron and the translation of the amyloid precursor protein (APP) and ferritin mRNAs: riboregulation against neural oxidative damage in Alzheimer's disease. Biochem Soc Trans. 36:1282-1287.

Rogers, J.T., J.D. Randall, C.M. Cahill, P.S. Eder, X. Huang, H. Gunshin, L. Leiter, J. McPhee, S.S. Sarang, and T. Utsuki. 2002. An iron-responsive element type II in the 5'-untranslated region of the Alzheimer's amyloid precursor protein transcript. Journal of Biological Chemistry. 277:45518-45528.

Roher, A.E., T.A. Kokjohn, S.G. Clarke, M.R. Sierks, C.L. Maarouf, G.E. Serrano, M.S. Sabbagh, and T.G. Beach. 2017. APP/Aβ structural diversity and Alzheimer's disease pathogenesis. Neurochemistry International. 110:1-13.

Rosenberg, G.A. 2012. Neurological diseases in relation to the blood–brain barrier. Journal of Cerebral Blood Flow & Metabolism. 32:1139-1151.

Rossi, M., H. Ruottinen, S. Soimakallio, I. Elovaara, and P. Dastidar. 2013. Clinical MRI for iron detection in Parkinson's disease. Clin Imaging. 37:631-636.

Rothenberger, S., M.R. Food, R. Gabathuler, M.L. Kennard, T. Yamada, O. Yasuhara, P.L. McGeer, and W.A. Jefferies. 1996. Coincident expression and distribution of melanotransferrin and transferrin receptor in human brain capillary endothelium. Brain Research. 712:117-121.

Rouault, T.A. 2006. The role of iron regulatory proteins in mammalian iron homeostasis and disease. Nature Chemical Biology. 2:406-414.

Rouault, T.A. 2013. Iron metabolism in the CNS: implications for neurodegenerative diseases. Nature Reviews Neuroscience. 14:551-564.

Rouault, T.A., and S. Cooperman. 2006. Brain iron metabolism. Seminars in Pediatric Neurology. Vol. 13. Elsevier. 142-148.

Rouault, T.A., M.W. Hentze, S.W. Caughman, J.B. Harford, and R.D. Klausner. 1988. Binding of a cytosolic protein to the iron-responsive element of human ferritin messenger RNA. Science. 241:1207-1210.

Rouault, T.A., D.-L. Zhang, and S.Y. Jeong. 2009. Brain iron homeostasis, the choroid plexus, and localization of iron transport proteins. Metabolic Brain Disease. 24:673-684.

Rozemuller, J.M., P. Eikelenboom, and F.C. Stam. 1986. Role of microglia in plaque formation in senile dementia of the Alzheimer type. An immunohistochemical study. Virchows Arch B Cell Pathol Incl Mol Pathol. 51:247-254.

Russo, N., M. Edwards, T. Andrews, M. O'Brien, and K.P. Bhatia. 2004. Hereditary haemochromatosis is unlikely to cause movement disorders--a critical review. J Neurol. 251:849-852.

Rutgers, M., A. Pielen, and M. Gille. 2007. Chronic cerebellar ataxia and hereditary hemochromatosis: causal or coincidental association? Journal of Neurology. 254:1296-1297.

Rutledge, J.N., S.K. Hilal, A.J. Silver, R. Defendini, and S. Fahn. 1987. Study of movement disorders and brain iron by MR. American Journal of Roentgenology. 149:365-379.

Saadoun, S., M.J. Tait, A. Reza, D.C. Davies, B.A. Bell, A.S. Verkman, and M.C. Papadopoulos. 2009. AQP4 gene deletion in mice does not alter blood-brain barrier integrity or brain morphology. Neuroscience. 161:764-772.

Sadigh-Eteghad, S., M. Talebi, and M. Farhoudi. 2012. Association of apolipoprotein E epsilon 4 allele with sporadic late onset Alzheimer`s disease. A meta-analysis. Neurosciences (Riyadh). 17:321-326.

Samaniego, F., J. Chin, K. Iwai, T.A. Rouault, and R.D. Klausner. 1994. Molecular characterization of a second iron-responsive element binding protein, iron regulatory protein 2. Structure, function, and post-translational regulation. Journal of Biological Chemistry. 269:30904-30910.

Sampietro, M., L. Caputo, A. Casatta, M. Meregalli, A. Pellagatti, J. Tagliabue, G. Annoni, and C. Vergani. 2001. The hemochromatosis gene affects the age of onset of sporadic Alzheimer's disease. Neurobiol Aging. 22:563-568.

Sanchez, M., B. Galy, B. Schwanhaeusser, J. Blake, T. Bahr-Ivacevic, V. Benes, M. Selbach, M.U. Muckenthaler, and M.W. Hentze. 2011. Iron regulatory protein-1 and -2: transcriptome-wide definition of binding mRNAs and shaping of the cellular proteome by iron regulatory proteins. Blood. 118:e168-179.

Santiago, C., A. Ballesteros, C. Tami, L. Martínez-Muñoz, G.G. Kaplan, and J.M. Casasnovas. 2007. Structures of T Cell Immunoglobulin Mucin Receptors 1 and 2 Reveal Mechanisms for Regulation of Immune Responses by the TIM Receptor Family. Immunity. 26:299-310.

Santos, P., C.L. Dinardo, R.D. Cançado, I.T. Schettert, J.E. Krieger, and A.C. Pereira. 2012. Non-HFE hemochromatosis. Rev Bras Hematol Hemoter. 34:311-316.

Sanvisens, N., M.C. Bañó, M. Huang, and S. Puig. 2011. Regulation of ribonucleotide reductase in response to iron deficiency. Molecular Cell. 44:759-769.

Sarlus, H., and M.T. Heneka. 2017. Microglia in Alzheimer's disease. Journal of Clinical investigation. 127:3240-3249.

Satoh, J., Y. Kino, N. Asahina, M. Takitani, J. Miyoshi, T. Ishida, and Y. Saito. 2016. TMEM119 marks a subset of microglia in the human brain. Neuropathology. 36:39-49.

Satoh, J.i. 2018. Gene expression profiles of M1 and M2 microglia characterized by comparative analysis of public datasets. Clinical and Experimental Neuroimmunology. 9:124-138.

Saunders, A., W. Strittmatter, D. Schmechel, P.S. George-Hyslop, M. Pericak-Vance, S. Joo, B. Rosi, J. Gusella, D. Crapper-MacLachlan, and M. Alberts. 1993. Association of apolipoprotein E allele ϵ4 with late-onset familial and sporadic Alzheimer's disease. Neurology. 43:1467-1467.

Scheltens, P., F. Barkhof, D. Leys, E.C. Wolters, R. Ravid, and W. Kamphorst. 1995. Histopathologic correlates of white matter changes on MRI in Alzheimer's disease and normal aging. Neurology. 45:883-888.

Schenker, C., D. Meier, W. Wichmann, P. Boesiger, and A. Valavanis. 1993. Age distribution and iron dependency of the T2 relaxation time in the globus pallidus and putamen. Neuroradiology. 35:119-124.

Scherrmann, J.-M. 2010. Neurovascular Unit. In Encyclopedia of Psychopharmacology. I.P. Stolerman, editor. Springer Berlin Heidelberg. p877-877.

Schindelin, J., I. Arganda-Carreras, E. Frise, V. Kaynig, M. Longair, T. Pietzsch, S. Preibisch, C. Rueden, S. Saalfeld, and B. Schmid. 2012. Fiji: an open-source platform for biological-image analysis. Nature Methods. 9:676-682.

Schmidt, P.J., P.T. Toran, A.M. Giannetti, P.J. Bjorkman, and N.C. Andrews. 2008. The transferrin receptor modulates Hfe-dependent regulation of hepcidin expression. Cell Metab. 7:205-214.

Schrag, M., A. Crofton, M. Zabel, A. Jiffry, D. Kirsch, A. Dickson, X.W. Mao, H.V. Vinters, D.W. Domaille, and C.J. Chang. 2011a. Effect of cerebral amyloid angiopathy on brain iron, copper, and zinc in Alzheimer's disease. Journal of Alzheimer's Disease. 24:137-149.

Schrag, M., G. McAuley, J. Pomakian, A. Jiffry, S. Tung, C. Mueller, H.V. Vinters, E.M. Haacke, B. Holshouser, and D. Kido. 2010. Correlation of hypointensities in susceptibility-weighted images to tissue histology in dementia patients with cerebral amyloid angiopathy: a postmortem MRI study. Acta Neuropathologica. 119:291-302.

Schrag, M., C. Mueller, U. Oyoyo, M.A. Smith, and W.M. Kirsch. 2011b. Iron, zinc and copper in the Alzheimer's disease brain: a quantitative meta-analysis. Some insight on the influence of citation bias on scientific opinion. Progress in Neurobiology. 94:296-306.

Schulz, K., A. Kroner, and S. David. 2012. Iron efflux from astrocytes plays a role in remyelination. Journal of Neuroscience. 32:4841-4847.

Seabrook, G., D. Smith, B. Bowery, A. Easter, T. Reynolds, S. Fitzjohn, R. Morton, H. Zheng, G. Dawson, and D. Sirinathsinghji. 1999. Mechanisms contributing to the deficits in hippocampal synaptic plasticity in mice lacking amyloid precursor protein. Neuropharmacology. 38:349-359.

Selkoe, D., T. Yamazaki, M. Citron, M. Podlisny, E. Koo, D. Teplow, and C. Haass. 1996. The Role of APP Processing and Trafficking Pathways in the Formation of Amyloid β-Proteina. Annals of the New York Academy of Sciences. 777:57-64.

Selkoe, D.J. 2001. Presenilin, Notch, and the genesis and treatment of Alzheimer's disease. Proceedings of the National Academy of Sciences USA. 98:11039-11041.

Sengupta, U., A.N. Nilson, and R. Kayed. 2016. The Role of Amyloid-β Oligomers in Toxicity, Propagation, and Immunotherapy. EBioMedicine. 6:42-49.

Sheng, J.G., R.E. Mrak, and W.S.T. Griffin. 1997. Neuritic plaque evolution in Alzheimer's disease is accompanied by transition of activated microglia from primed to enlarged to phagocytic forms. Acta Neuropathologica. 94:1-5.

Siddappa, A.J.M., R.B. Rao, J.D. Wobken, E.A. Leibold, J.R. Connor, and M.K. Georgieff. 2002. Developmental changes in the expression of iron regulatory proteins and iron transport proteins in the perinatal rat brain. Journal of Neuroscience Research. 68:761-775.

Silvestri, L., and C. Camaschella. 2008. A potential pathogenetic role of iron in Alzheimer's Disease. Journal of Cellular and Molecular Medicine. 12:1548-1550.

Sinha, S., J.P. Anderson, R. Barbour, G.S. Basi, R. Caccavello, D. Davis, M. Doan, H.F. Dovey, N. Frigon, J. Hong, K. Jacobson-Croak, N. Jewett, P. Keim, J. Knops, I. Lieberburg, M. Power, H. Tan, G. Tatsuno, J. Tung, D. Schenk, P. Seubert, S.M. Suomensaari, S. Wang, D. Walker, J. Zhao, L. McConlogue, and V. John. 1999. Purification and cloning of amyloid precursor protein beta-secretase from human brain. Nature. 402:537-540.

Sipe, J.D., M.D. Benson, J.N. Buxbaum, S. Ikeda, G. Merlini, M.J. Saraiva, and P. Westermark. 2012. Amyloid fibril protein nomenclature: 2012 recommendations from the Nomenclature Committee of the International Society of Amyloidosis. Amyloid. 19:167-170.

Sisodia, S.S. 1992. Beta-amyloid precursor protein cleavage by a membrane-bound protease. Proceedings of the National Academy of Sciences USA. 89:6075-6079.

Smith, D.P., D.G. Smith, C.C. Curtain, J.F. Boas, J.R. Pilbrow, G.D. Ciccotosto, T.-L. Lau, D.J. Tew, K. Perez, and J.D. Wade. 2006. Copper-mediated amyloid-β toxicity is associated with an intermolecular histidine bridge. Journal of Biological Chemistry. 281:15145-15154.

Smith, M.A., P.L. Harris, L.M. Sayre, and G. Perry. 1997. Iron accumulation in Alzheimer disease is a source of redox-generated free radicals. Proceedings of the National Academy of Sciences USA. 94:9866-9868.

Smith, M.A., K. Wehr, P.L. Harris, S.L. Siedlak, J.R. Connor, and G. Perry. 1998. Abnormal localization of iron regulatory protein in Alzheimer's disease. Brain research. 788:232-236.

Sobotka, T., P. Whittaker, J. Sobotka, R. Brodie, D. Wander, M. Robl, M. Bryant, and C. Barton. 1996. Neurobehavioral dysfunctions associated with dietary iron overload. Physiology and Behavior. 59:213-219.

Soriano, S., D.C. Lu, S. Chandra, C.U. Pietrzik, and E.H. Koo. 2001. The amyloidogenic pathway of amyloid precursor protein (APP) is independent of its cleavage by caspases. Journal of Biological Chemistry. 276:29045-29050.

Sperling, R.A., P.S. Aisen, L.A. Beckett, D.A. Bennett, S. Craft, A.M. Fagan, T. Iwatsubo, C.R. Jack, J. Kaye, and T.J. Montine. 2011. Toward defining the preclinical stages of Alzheimer's disease: Recommendations from the National Institute on Aging-Alzheimer's Association workgroups on diagnostic guidelines for Alzheimer's disease. Alzheimer's and Dementia. 7:280-292.

St George-Hyslop, P.H., R.E. Tanzi, R.J. Polinsky, J.L. Haines, L. Nee, P.C. Watkins, R.H. Myers, R.G. Feldman, D. Pollen, D. Drachman, and et al. 1987. The genetic defect causing familial Alzheimer's disease maps on chromosome 21. Science. 235:885-890.

Stalder, M., A. Phinney, A. Probst, B. Sommer, M. Staufenbiel, and M. Jucker. 1999. Association of microglia with amyloid plaques in brains of APP23 transgenic mice. American Journal of Pathology. 154:1673-1684.

Stein, J., F. Hartmann, and A.U. Dignass. 2010. Diagnosis and management of iron deficiency anemia in patients with IBD. Nature Reviews Gastroenterology and Hepatology. 7:599-610.

Stokin, G.B., C. Lillo, T.L. Falzone, R.G. Brusch, E. Rockenstein, S.L. Mount, R. Raman, P. Davies, E. Masliah, and D.S. Williams. 2005. Axonopathy and transport deficits early in the pathogenesis of Alzheimer's disease. Science. 307:1282-1288.

Sweeney, M.D., Z. Zhao, A. Montagne, A.R. Nelson, and B.V. Zlokovic. 2019. Blood-Brain Barrier: From Physiology to Disease and Back. Physiological Reviews. 99:21-78.

Tahmasebinia, F., and S. Emadi. 2017. Effect of metal chelators on the aggregation of beta-amyloid peptides in the presence of copper and iron. Biometals. 30:285-293.

Tam, W.Y., N.P. Au, and C.H. Ma. 2016. The association between laminin and microglial morphology in vitro. Scientific Reports. 6:28580.

Tampellini, D. 2015. Synaptic activity and Alzheimer's disease: a critical update. Frontiers in Neuroscience. 9:423.

Tang, Y., and W. Le. 2016. Differential Roles of M1 and M2 Microglia in Neurodegenerative Diseases. Molecular Neurobiology. 53:1181-1194.

Tanzi, R.E., A.I. McClatchey, E.D. Lamperti, L. Villa-Komaroff, J.F. Gusella, and R.L. Neve. 1988. Protease inhibitor domain encoded by an amyloid protein precursor mRNA associated with Alzheimer's disease. Nature. 331(6156):528-30

Taylor, E.M., and E.H. Morgan. 1990. Developmental changes in transferrin and iron uptake by the brain in the rat. Developmental Brain Research. 55:35-42.

Telling, N.D., J. Everett, J.F. Collingwood, J. Dobson, G. van der Laan, J.J. Gallagher, J. Wang, and A.P. Hitchcock. 2017. Iron Biochemistry is Correlated with Amyloid Plaque Morphology in an Established Mouse Model of Alzheimer's Disease. Cell Chemical Biology. 24:1205-1215. e1203.

Terman, A., and U.T. Brunk. 2004. Lipofuscin. The International Journal of Biochemistry and Cell Biology. 36:1400-1404.

Terry, R.D., E. Masliah, D.P. Salmon, N. Butters, R. DeTeresa, R. Hill, L.A. Hansen, and R. Katzman. 1991a. Physical basis of cognitive alterations in Alzheimer's disease: synapse loss is the major correlate of cognitive impairment. Annals of Neurology. 30:572-580.

Terry, R.D., E. Masliah, D.P. Salmon, N. Butters, R. DeTeresa, R. Hill, L.A. Hansen, and R. Katzman. 1991b. Physical basis of cognitive alterations in Alzheimer's disease: synapse loss is the major correlate of cognitive impairment. Annals of Neurology. 30:572-580.

Thal, D.R., U. Rüb, M. Orantes, and H. Braak. 2002. Phases of Aβ-deposition in the human brain and its relevance for the development of AD. Neurology. 58:1791-1800.

Thomsen, M.S., M.V. Andersen, P.R. Christoffersen, M.D. Jensen, J. Lichota, and T. Moos. 2015. Neurodegeneration with inflammation is accompanied by accumulation of iron and ferritin in microglia and neurons. Neurobiology of Disease. 81:108-118.

Tian, J., J. Shi, and D.M. Mann. 2004. Cerebral amyloid angiopathy and dementia. Panminerva Med. 46:253-264.

Tjernberg, L.O., A. Pramanik, S. Bjorling, P. Thyberg, J. Thyberg, C. Nordstedt, K.D. Berndt, L. Terenius, and R. Rigler. 1999. Amyloid beta-peptide polymerization studied using fluorescence correlation spectroscopy. Chem Biol. 6:53-62.

Todorich, B., J.M. Pasquini, C.I. Garcia, P.M. Paez, and J.R. Connor. 2009a. Oligodendrocytes and myelination: the role of iron. Glia. 57:467-478.

Todorich, B., J.M. Pasquini, C.I. Garcia, P.M. Paez, and J.R. Connor. 2009b. Oligodendrocytes and myelination: the role of iron. Glia. 57:467-478.

Todorich, B., X. Zhang, and J. Connor. 2011. H-ferritin is the Major Source of Iron for Oligodendrocytes. Glia. 927-935 pp.

Todorich, B., X. Zhang, B. Slagle-Webb, W.E. Seaman, and J.R. Connor. 2008a. Tim-2 is the receptor for H-ferritin on oligodendrocytes. J Neurochem. 107:1495-1505.

Todorich, B., X. Zhang, B. Slagle-Webb, W.E. Seaman, and J.R. Connor. 2008b. Tim-2 is the receptor for H-ferritin on oligodendrocytes. Journal of neurochemistry. 107:1495-1505.

Tomic, J.L., A. Pensalfini, E. Head, and C.G. Glabe. 2009. Soluble fibrillar oligomer levels are elevated in Alzheimer's disease brain and correlate with cognitive dysfunction. Neurobiology of Disease. 35:352-358.

Toussaint, L., L. Bertrand, L. Hue, R.R. Crichton, and J.P. Declercq. 2007. High-resolution X-ray structures of human apoferritin H-chain mutants correlated with their activity and metal-binding sites. J Mol Biol. 365:440-452.

Trapp, G.A., G. Miner, R. Zimmerman, A. Mastri, and L. Heston. 1978. Aluminum levels in brain in Alzheimer's disease. Biological Psychiatry.

Trinder, D., and E. Baker. 2003. Transferrin receptor 2: a new molecule in iron metabolism. The International Journal of Biochemistry and Cell Biology. 35:292-296.

Tsai, J., J. Grutzendler, K. Duff, and W.B. Gan. 2004. Fibrillar amyloid deposition leads to local synaptic abnormalities and breakage of neuronal branches. Nature Neuroscience. 7:1181-1183.

Tu, G.F., M.G. Achen, A.R. Aldred, B.R. Southwell, and G. Schreiber. 1991. The distribution of cerebral expression of the transferrin gene is species specific. Journal of Biological Chemistry. 266:6201-6208.

Turner, P.R., K. O'Connor, W.P. Tate, and W.C. Abraham. 2003. Roles of amyloid precursor protein and its fragments in regulating neural activity, plasticity and memory. Progress in Neurobiology. 70:1-32.

Ueda, F., K.B. Raja, R.J. Simpson, I.S. Trowbridge, and M.W. Bradbury. 1993. Rate of 59Fe uptake into brain and cerebrospinal fluid and the influence thereon of antibodies against the transferrin receptor. J Neurochem. 60:106-113.

Uematsu, M., A. Nakamura, M. Ebashi, K. Hirokawa, R. Takahashi, and T. Uchihara. 2018. Brainstem tau pathology in Alzheimer’s disease is characterized by increase of three repeat tau and independent of amyloid β. Acta Neuropathologica Communications. 6:1.

Unal-Cevik, I., M. Kilinc, Y. Gursoy-Ozdemir, G. Gurer, and T. Dalkara. 2004. Loss of NeuN immunoreactivity after cerebral ischemia does not indicate neuronal cell loss: a cautionary note. Brain Res. 1015:169-174.

Urrutia, P., P. Aguirre, A. Esparza, V. Tapia, N.P. Mena, M. Arredondo, C. González-Billault, and M.T. Núñez. 2013. Inflammation alters the expression of DMT1, FPN1 and hepcidin, and it causes iron accumulation in central nervous system cells. Journal of Neurochemistry. 126:541-549.

Valko, M., H. Morris, and M. Cronin. 2005. Metals, toxicity and oxidative stress. Current Medicinal Chemistry. 12:1161-1208.

Van Bergen, J., X. Li, J. Hua, S. Schreiner, S. Steininger, F. Quevenco, M. Wyss, A. Gietl, V. Treyer, and S. Leh. 2016. Colocalization of cerebral iron with amyloid beta in mild cognitive impairment. Scientific Reports. 6.

van Duijn, S., M. Bulk, S.G. van Duinen, R.J. Nabuurs, M.A. van Buchem, L. van der Weerd, and R. Natté. 2017. Cortical Iron Reflects Severity of Alzheimer’s Disease. Journal of Alzheimer's Disease. 60:1533-1545.

van Groen, T., A.J. Kiliaan, and I. Kadish. 2006. Deposition of mouse amyloid beta in human APP/PS1 double and single AD model transgenic mice. Neurobiology of Disease. 23:653-662.

Van Rooden, S., N.T. Doan, M.J. Versluis, J.D. Goos, A.G. Webb, A.M. Oleksik, W.M. van der Flier, P. Scheltens, F. Barkhof, and A.W. Weverling–Rynsburger. 2015. 7T T 2∗-weighted magnetic resonance imaging reveals cortical phase differences between early-and late-onset Alzheimer's disease. Neurobiology of Aging. 36:20-26.

Vassar, R., B.D. Bennett, S. Babu-Khan, S. Kahn, E.A. Mendiaz, P. Denis, D.B. Teplow, S. Ross, P. Amarante, R. Loeloff, Y. Luo, S. Fisher, J. Fuller, S. Edenson, J. Lile, M.A. Jarosinski, A.L. Biere, E. Curran, T. Burgess, J.C. Louis, F. Collins, J. Treanor, G. Rogers, and M. Citron. 1999. Beta-secretase cleavage of Alzheimer's amyloid precursor protein by the transmembrane aspartic protease BACE. Science. 286:735-741.

Venegas, C., S. Kumar, B.S. Franklin, T. Dierkes, R. Brinkschulte, D. Tejera, A. Vieira-Saecker, S. Schwartz, F. Santarelli, and M.P. Kummer. 2017. Microglia-derived ASC specks cross-seed amyloid-β in Alzheimer's disease. Nature. 552:355.

Verghese, P.B., J.M. Castellano, K. Garai, Y. Wang, H. Jiang, A. Shah, G. Bu, C. Frieden, and D.M. Holtzman. 2013. ApoE influences amyloid-β (Aβ) clearance despite minimal apoE/Aβ association in physiological conditions. Proceedings of the National Academy of Sciences USA. 110:E1807-E1816.

Vina, J., and A. Lloret. 2010. Why women have more Alzheimer's disease than men: gender and mitochondrial toxicity of amyloid-beta peptide. Journal of Alzheimer's disease : Journal of Alzheimer's Disease. 20 Suppl 2:S527-533.

Vinters, H.V. 1987. Cerebral amyloid angiopathy. A critical review. Stroke. 18:311-324.

Volianskis, A., R. Køstner, M. Mølgaard, S. Hass, and M.S. Jensen. 2010. Episodic memory deficits are not related to altered glutamatergic synaptic transmission and plasticity in the CA1 hippocampus of the APPswe/PS1δE9-deleted transgenic mice model of β-amyloidosis. Neurobiology of Aging. 31:1173-1187.

Vulpe, C.D., Y.-M. Kuo, T.L. Murphy, L. Cowley, C. Askwith, N. Libina, J. Gitschier, and G.J. Anderson. 1999. Hephaestin, a ceruloplasmin homologue implicated in intestinal iron transport, is defective in the sla mouse. Nature genetics. 21:195-199.

Vymazal, J., D. Urgosik, and J.W. Bulte. 2000. Differentiation between hemosiderin- and ferritin-bound brain iron using nuclear magnetic resonance and magnetic resonance imaging. Cell Mol Biol (Noisy-le-grand). 46:835-842.

Wada, R., C.J. Tifft, and R.L. Proia. 2000. Microglial activation precedes acute neurodegeneration in Sandhoff disease and is suppressed by bone marrow transplantation. Proceedings of the National Academy of Sciences of the United States of America USA. 97:10954-10959.

Wadghiri, Y.Z., D.M. Hoang, T. Wisniewski, and E.M. Sigurdsson. 2012. In vivo magnetic resonance imaging of amyloid-β plaques in mice. Amyloid Proteins: Methods and Protocols:435-451.

Waheed, A., S. Parkkila, X.Y. Zhou, S. Tomatsu, Z. Tsuchihashi, J.N. Feder, R.C. Schatzman, R.S. Britton, B.R. Bacon, and W.S. Sly. 1997. Hereditary hemochromatosis: effects of C282Y and H63D mutations on association with β2-microglobulin, intracellular processing, and cell surface expression of the HFE protein in COS-7 cells. Proceedings of the National Academy of Sciences USA. 94:12384-12389.

Walker, D.G., and L.F. Lue. 2015. Immune phenotypes of microglia in human neurodegenerative disease: challenges to detecting microglial polarization in human brains. Alzheimer's Research and Therapy. 7:56.

Wallace, D., L. Summerville, P. Lusby, and V. Subramaniam. 2005. First phenotypic description of transferrin receptor 2 knockout mouse, and the role of hepcidin. Gut. 54:980-986.

Wallace, D.F., and V.N. Subramaniam. 2007. Non-HFE haemochromatosis. World J Gastroenterol. 13:4690-4698.

Wallace, D.F., L. Summerville, E.M. Crampton, and V.N. Subramaniam. 2008. Defective trafficking and localization of mutated transferrin receptor 2: implications for type 3 hereditary hemochromatosis. American Journal of Physiology-Cell Physiology. 294:C383-C390.

Walton, J. 2006. Aluminum in hippocampal neurons from humans with Alzheimer's disease. Neurotoxicology. 27:385-394.

Wang, J., H. Tanila, J. Puoliväli, I. Kadish, and T. Groen. 2004a. Gender differences in the amount and deposition of amyloid in APPswe and PS1 double transgenic mice. 318-327 pp.

Wang, Q., M.J. Rowan, and R. Anwyl. 2004b. Beta-amyloid-mediated inhibition of NMDA receptor-dependent long-term potentiation induction involves activation of microglia and stimulation of inducible nitric oxide synthase and superoxide. The Journal of Neuroscience. 24:6049-6056.

Wang, R., and P.H. Reddy. 2017. Role of Glutamate and NMDA Receptors in Alzheimer's Disease. Journal of Alzheimer's disease : JAD. 57:1041-1048.

Wang, X.S., W.Y. Ong, and J.R. Connor. 2001. A light and electron microscopic study of the iron transporter protein DMT-1 in the monkey cerebral neocortex and hippocampus. J Neurocytol. 30:353-360.

Wang, Y., and Y. Ha. 2004. The X-ray structure of an antiparallel dimer of the human amyloid precursor protein E2 domain. Molecular Cell. 15:343-353.

Wang, Y., T.K. Ulland, J.D. Ulrich, W. Song, J.A. Tzaferis, J.T. Hole, P. Yuan, T.E. Mahan, Y. Shi, and S. Gilfillan. 2016. TREM2-mediated early microglial response limits diffusion and toxicity of amyloid plaques. Journal of Experimental Medicine. 20151948.

Wasco, W., K. Bupp, M. Magendantz, J.F. Gusella, R.E. Tanzi, and F. Solomon. 1992. Identification of a mouse brain cDNA that encodes a protein related to the Alzheimer disease-associated amyloid beta protein precursor. Proceedings of the National Academy of Sciences USA. 89:10758-10762.

Wasco, W., S. Gurubhagavatula, M. d Paradis, D.M. Romano, S.S. Sisodia, B.T. Hyman, R.L. Neve, and R.E. Tanzi. 1993. Isolation and characterization of APLP2 encoding a homologue of the Alzheimer's associated amyloid β protein precursor. Nature Genetics. 5:95-100.

Wayne Martin, W., F.Q. Ye, and P.S. Allen. 1998. Increasing striatal iron content associated with normal aging. Movement Disorders. 13:281-286.

Wegiel, J., and H. Wisniewski. 1990. The complex of microglial cells and amyloid star in three-dimensional reconstruction. Acta Neuropathologica. 81:116-124.

Weingarten, M.D., A.H. Lockwood, S.-Y. Hwo, and M.W. Kirschner. 1975. A protein factor essential for microtubule assembly. Proceedings of the National Academy of Sciences USA. 72:1858-1862.

Wengenack, T.M., D.A. Reyes, G.L. Curran, B.J. Borowski, J. Lin, G.M. Preboske, S.S. Holasek, E.J. Gilles, R. Chamberlain, M. Marjanska, C.R. Jack, Jr., M. Garwood, and J.F. Poduslo. 2011. Regional differences in MRI detection of amyloid plaques in AD transgenic mouse brain. Neuroimage. 54:113-122.

West, A.P., M.J. Bennett, V.M. Sellers, N.C. Andrews, C.A. Enns, and P.J. Bjorkman. 2000. Comparison of the interactions of transferrin receptor and transferrin receptor 2 with transferrin and the hereditary hemochromatosis protein HFE. Journal of Biological Chemistry. 275:38135-38138.

West, M.J., P.D. Coleman, D.G. Flood, and J.C. Troncoso. 1994. Differences in the pattern of hippocampal neuronal loss in normal ageing and Alzheimer's disease. The Lancet. 344:769-772.

Westermark, P., M.D. Benson, J.N. Buxbaum, A.S. Cohen, B. Frangione, S. Ikeda, C.L. Masters, G. Merlini, M.J. Saraiva, and J.D. Sipe. 2005. Amyloid: toward terminology clarification. Report from the Nomenclature Committee of the International Society of Amyloidosis. Amyloid. 12:1-4.

Wetzel, R. 2006. Kinetics and thermodynamics of amyloid fibril assembly. Accounts of Chemical Research. 39:671-679.

White, A.R., R. Reyes, J.F. Mercer, J. Camakaris, H. Zheng, A.I. Bush, G. Multhaup, K. Beyreuther, C.L. Masters, and R. Cappai. 1999. Copper levels are increased in the cerebral cortex and liver of APP and APLP2 knockout mice. Brain Research. 842:439-444.

Whitehouse, P.J., D.L. Price, R.G. Struble, A.W. Clark, J.T. Coyle, and M.R. Delon. 1982. Alzheimer's disease and senile dementia: loss of neurons in the basal forebrain. Science. 215:1237-1239.

Williamson, J., J. Goldman, and K.S. Marder. 2009. Genetic aspects of Alzheimer disease. The Neurologist. 15:80.

Wisniewski, H.M., A.W. Vorbrodt, J. Wegiel, J. Morys, and A.S. Lossinsky. 1990. Ultrastructure of the cells forming amyloid fibers in Alzheimer disease and scrapie. Am J Med Genet Suppl. 7:287-297.

Wisniewski, H.M., G.Y. Wen, and K.S. Kim. 1989. Comparison of four staining methods on the detection of neuritic plaques. Acta Neuropathol. 78:22-27.

Wolf, H.K., R. Buslei, R. Schmidt-Kastner, P.K. Schmidt-Kastner, T. Pietsch, O.D. Wiestler, and I. Blumcke. 1996. NeuN: a useful neuronal marker for diagnostic histopathology. The journal of Histochemistry and Cytochemistry. 44:1167-1171.

Wong, B.X., A. Tsatsanis, L.Q. Lim, P.A. Adlard, A.I. Bush, and J.A. Duce. 2014. β-Amyloid precursor protein does not possess ferroxidase activity but does stabilize the cell surface ferrous iron exporter ferroportin. PloS One. 9:e114174.

Wong, E., P. Sheehan, and C. Lieber. 1997. Observation of metastable abeta amyloid protofibrils by atomic force microscopy. Science. 277:1971-1975.

Wood, H. 2015. Alzheimer disease: Iron--the missing link between ApoE and Alzheimer disease? Nat Rev Neurol. 11:369.

Wood, H. 2017. Twin peaks of microglial activation observed in Alzheimer disease. Nature Reviews Neurology. 13:129.

Wu, K.L., Y.Q. Li, A. Tabassum, W.Y. Lu, I. Aubert, and C.S. Wong. 2010. Loss of neuronal protein expression in mouse hippocampus after irradiation. Journal of Neuropathology and Experimental Neurology. 69:272-280.

Wu, L.J.-c., A.M. Leenders, S. Cooperman, E. Meyron-Holtz, S. Smith, W. Land, R.Y. Tsai, U.V. Berger, Z.-H. Sheng, and T.A. Rouault. 2004. Expression of the iron transporter ferroportin in synaptic vesicles and the blood–brain barrier. Brain Research. 1001:108-117.

Wyss-Coray, T. 2006a. Inflammation in Alzheimer disease: driving force, bystander or beneficial response? Nature Medicine. 12:1005.

Wyss-Coray, T. 2006b. Inflammation in Alzheimer disease: driving force, bystander or beneficial response? Nature Medicine. 12:1005-1015.

Xie, S., J. Xiao, G. Gong, Y. Zang, Y. Wang, H. Wu, and X. Jiang. 2006. Voxel-based detection of white matter abnormalities in mild Alzheimer disease. Neurology. 66:1845-1849.

Xiong, F., W. Ge, and C. Ma. 2019. Quantitative proteomics reveals distinct composition of amyloid plaques in Alzheimer's disease. Alzheimer's and Dementia. 15:429-440.

Xiong, H., D. Callaghan, J. Wodzinska, J. Xu, M. Premyslova, Q.-Y. Liu, J. Connelly, and W. Zhang. 2011. Biochemical and behavioral characterization of the double transgenic mouse model (APPswe/PS1dE9) of Alzheimer's disease. Neuroscience Bulletin. 27:221-232.

Xu, G., Y. Ran, S.E. Fromholt, C. Fu, A.T. Yachnis, T.E. Golde, and D.R. Borchelt. 2015. Murine Abeta over-production produces diffuse and compact Alzheimer-type amyloid deposits. Acta Neuropathologica Communications. 3:72.

Xu, G.P., K.R. Dave, R. Vivero, R. Schmidt-Kastner, T.J. Sick, and M.A. Perez-Pinzon. 2002. Improvement in neuronal survival after ischemic preconditioning in hippocampal slice cultures. Brain Res. 952:153-158.

Yamada, M. 2015. Cerebral amyloid angiopathy: emerging concepts. Journal of Stroke. 17:17-30.

Yamasaki, R., H. Lu, O. Butovsky, N. Ohno, A.M. Rietsch, R. Cialic, P.M. Wu, C.E. Doykan, J. Lin, A.C. Cotleur, G. Kidd, M.M. Zorlu, N. Sun, W. Hu, L. Liu, J.C. Lee, S.E. Taylor, L. Uehlein, D. Dixon, J. Gu, C.M. Floruta, M. Zhu, I.F. Charo, H.L. Weiner, and R.M. Ransohoff. 2014. Differential roles of microglia and monocytes in the inflamed central nervous system. The Journal of Experimental Medicine. 211:1533-1549.

Yan, P., A.W. Bero, J.R. Cirrito, Q. Xiao, X. Hu, Y. Wang, E. Gonzales, D.M. Holtzman, and J.-M. Lee. 2009. Characterizing the appearance and growth of amyloid plaques in APP/PS1 mice. The Journal of Neuroscience. 29:10706-10714.

Yan, R., M.J. Bienkowski, M.E. Shuck, H. Miao, M.C. Tory, A.M. Pauley, J.R. Brashier, N.C. Stratman, W.R. Mathews, A.E. Buhl, D.B. Carter, A.G. Tomasselli, L.A. Parodi, R.L. Heinrikson, and M.E. Gurney. 1999. Membrane-anchored aspartyl protease with Alzheimer's disease beta-secretase activity. Nature. 402:533-537.

Yan, S.D., X. Chen, J. Fu, M. Chen, H. Zhu, A. Roher, T. Slattery, L. Zhao, M. Nagashima, J. Morser, A. Migheli, P. Nawroth, D. Stern, and A.M. Schmidt. 1996. RAGE and amyloid-beta peptide neurotoxicity in Alzheimer's disease. Nature. 382:685-691.

Yang, M., and D.B. Teplow. 2008. Amyloid β-protein monomer folding: free-energy surfaces reveal alloform-specific differences. Journal of Molecular Biology. 384:450-464.

Yang, Y., L. Martin, F. Cuzin, M.-G. Mattei, and M. Rassoulzadegan. 1996. Genomic structure and chromosomal localization of the mouse CDEI-binding protein CDEBP (APLP2) gene and promoter sequences. Genomics. 35:24-29.

Youdim, M., M. Fridkin, and H. Zheng. 2004. Novel bifunctional drugs targeting monoamine oxidase inhibition and iron chelation as an approach to neuroprotection in Parkinson's disease and other neurodegenerative diseases. Journal of Neural Transmission. 111:1455-1471.

Youn, J.C., D.Y. Lee, J.H. Jhoo, K.W. Kim, I.H. Choo, and J.I. Woo. 2011. Prevalence of neuropsychiatric syndromes in Alzheimer's disease (AD). Archives of Gerontology and Geriatrics. 52:258-263.

Yu, L., S. Wang, X. Chen, H. Yang, X. Li, Y. Xu, and X. Zhu. 2015. Orientin alleviates cognitive deficits and oxidative stress in Aβ 1–42-induced mouse model of Alzheimer's disease. Life Siences. 121:104-109.

Yuan, P., C. Condello, C.D. Keene, Y. Wang, T.D. Bird, S.M. Paul, W. Luo, M. Colonna, D. Baddeley, and J. Grutzendler. 2016. TREM2 Haplodeficiency in Mice and Humans Impairs the Microglia Barrier Function Leading to Decreased Amyloid Compaction and Severe Axonal Dystrophy. Neuron. 90:724-739.

Yuan, R., S.W. Tsaih, S.B. Petkova, C. Marin de Evsikova, S. Xing, M.A. Marion, M.A. Bogue, K.D. Mills, L.L. Peters, C.J. Bult, C.J. Rosen, J.P. Sundberg, D.E. Harrison, G.A. Churchill, and B. Paigen. 2009. Aging in inbred strains of mice: study design and interim report on median lifespans and circulating IGF1 levels. Aging Cell. 8:277-287.

Zecca, L., M. Gallorini, V. SchuÈnemann, A.X. Trautwein, M. Gerlach, P. Riederer, P. Vezzoni, and D. Tampellini. 2001. Iron, neuromelanin and ferritin content in the substantia nigra of normal subjects at different ages: consequences for iron storage and neurodegenerative processes. Journal of Neurochemistry. 76:1766-1773.

Zecca, L., M.B. Youdim, P. Riederer, J.R. Connor, and R.R. Crichton. 2004. Iron, brain ageing and neurodegenerative disorders. Nat Rev Neurosci. 5:863-873.

Zechel, S., K. Huber-Wittmer, and O. von Bohlen und Halbach. 2006. Distribution of the iron-regulating protein hepcidin in the murine central nervous system. Journal of Neuroscience Research. 84:790-800.

Zeineh, M.M., Y. Chen, H.H. Kitzler, R. Hammond, H. Vogel, and B.K. Rutt. 2015. Activated iron-containing microglia in the human hippocampus identified by magnetic resonance imaging in Alzheimer disease. Neurobiology of Aging. 36:2483-2500.

Zhang, S., M.B. Tang, H.Y. Luo, C.H. Shi, and Y.M. Xu. 2017. Necroptosis in neurodegenerative diseases: a potential therapeutic target. Cell Death and Disease. 8:e2905.

Zhang, Y.-w., R. Thompson, H. Zhang, and H. Xu. 2011. APP processing in Alzheimer's disease. Molecular Brain. 4:3.

Zhang, Y., P. Li, J. Feng, and M. Wu. 2016. Dysfunction of NMDA receptors in Alzheimer's disease. Neurological Sciences. 37:1039-1047.

Zhao, G., J. Tan, G. Mao, M.Z. Cui, and X. Xu. 2007. The same γ-secretase accounts for the multiple intramembrane cleavages of APP. Journal of Neurochemistry. 100:1234-1246.

Zhao, R., W. Hu, J. Tsai, W. Li, and W.B. Gan. 2017. Microglia limit the expansion of β-amyloid plaques in a mouse model of Alzheimer’s disease. Mol Neurodegener. 12.

Zheng, H., M. Jiang, M.E. Trumbauer, D.J. Sirinathsinghji, R. Hopkins, D.W. Smith, R.P. Heavens, G.R. Dawson, S. Boyce, M.W. Conner, K.A. Stevens, H.H. Slunt, S.S. Sisoda, H.Y. Chen, and L.H. Van der Ploeg. 1995. beta-Amyloid precursor protein-deficient mice show reactive gliosis and decreased locomotor activity. Cell. 81:525-531.

Zheng, H., and E.H. Koo. 2006. The amyloid precursor protein: beyond amyloid. Mol Neurodegener. 1:5.

Zhong, S., K. Wu, I.B. Black, and D.G. Schaar. 1996. Characterization of the genomic structure of the mouse APLP1 gene. Genomics. 32:159-162.

Zhou, T., Z. Huang, X. Sun, X. Zhu, L. Zhou, M. Li, B. Cheng, X. Liu, and C. He. 2017. Microglia polarization with M1/M2 phenotype changes in rd1 mouse model of retinal degeneration. Frontiers in Neuroanatomy. 11:77.

Zhou, X.Y., S. Tomatsu, R.E. Fleming, S. Parkkila, A. Waheed, J. Jiang, Y. Fei, E.M. Brunt, D.A. Ruddy, and C.E. Prass. 1998. HFE gene knockout produces mouse model of hereditary hemochromatosis. Proceedings of the National Academy of Sciences. 95:2492-2497.

Zhu, X., S.S. Kalirai, A.P. Hitchcock, and D.A. Bazylinski. 2015. What is the correct Fe L 23 X-ray absorption spectrum of magnetite? Journal of Electron Spectroscopy and Related Phenomena. 199:19-26.

Ziebell, J.M., P.D. Adelson, and J. Lifshitz. 2015. Microglia: dismantling and rebuilding circuits after acute neurological injury. Metabolic Brain Disease. 30:393-400.

Zou, K., J.S. Gong, K. Yanagisawa, and M. Michikawa. 2002. A novel function of monomeric amyloid beta-protein serving as an antioxidant molecule against metal-induced oxidative damage. The Journal of Neuroscience. 22:4833-4841.

Zucca, F.A., C. Bellei, S. Giannelli, M.R. Terreni, M. Gallorini, E. Rizzio, G. Pezzoli, A. Albertini, and L. Zecca. 2006. Neuromelanin and iron in human locus coeruleus and substantia nigra during aging: consequences for neuronal vulnerability. J Neural Transm. 113:757-767.

Zumbrennen-Bullough, K.B., L. Becker, L. Garrett, S.M. Hölter, J. Calzada-Wack, I. Mossbrugger, L. Quintanilla-Fend, I. Racz, B. Rathkolb, T. Klopstock, W. Wurst, A. Zimmer, E. Wolf, H. Fuchs, V. Gailus-Durner, M.H. de Angelis, S.J. Romney, and E.A. Leibold. 2014. Abnormal brain iron metabolism in Irp2 deficient mice is associated with mild neurological and behavioral impairments. PloS One. 9:e98072.